PDF-XChange Editor
KOUPIT plnou verzi!
www.pdfxchange.cz

Cellular/Molecular

Preferential Inhibition of Tonically over Phasically Activated NMDA Receptors by Pregnane Derivatives

Vojtech Vyklicky,[1]* Tereza Smejkalova,[1]* Barbora Krausova,[1] Ales Balik,[1] Miloslav Korinek,[1] Jirina Borovska,[1] Martin Horak,[1] Marketa Chvojkova,[1] Lenka Kleteckova,[1] Karel Vales,[1] Jiri Cerny,[1] Michaela Nekardova,[2,3] Hana Chodounska,[2] Eva Kudova,[2] and Ladislav Vyklicky[1]

[1]Institute of Physiology, Czech Academy of Sciences, 142 20 Prague 4, Czech Republic, [2]Institute of Organic Chemistry and Biochemistry, Czech Academy of Sciences, 166 10 Prague 2, Czech Republic, and [3]Faculty of Mathematics and Physics, Charles University in Prague, 121 16 Prague 2, Czech Republic

Postsynaptic *N*-methyl-D-aspartate receptors (NMDARs) phasically activated by presynaptically released glutamate are critical for synaptic transmission and plasticity. However, under pathological conditions, excessive activation of NMDARs by tonically increased ambient glutamate contributes to excitotoxicity associated with various acute and chronic neurological disorders. Here, using heterologously expressed GluN1/GluN2A and GluN1/GluN2B receptors and rat autaptic hippocampal microisland cultures, we show that pregnanolone sulfate inhibits NMDAR currents induced by a prolonged glutamate application with a higher potency than the NMDAR component of EPSCs. For synthetic pregnanolone derivatives substituted with a carboxylic acid moiety at the end of an aliphatic chain of varying length and attached to the steroid skeleton at C3, the difference in potency between tonic and phasic inhibition increased with the length of the residue. The steroid with the longest substituent, pregnanolone hemipimelate, had no effect on phasically activated receptors while inhibiting tonically activated receptors. In behavioral tests, pregnanolone hemipimelate showed neuroprotective activity without psychomimetic symptoms. These results provide insight into the influence of steroids on neuronal function and stress their potential use in the development of novel therapeutics with neuroprotective action.

Key words: memantine; neuroprotection; neurosteroid; NMDA receptor; pregnanolone sulfate; synaptic transmission

Significance Statement

Synaptic activation of *N*-methyl-D-aspartate receptors (NMDARs) plays a key role in synaptic plasticity, but excessive tonic NMDAR activation mediates excitotoxicity associated with many neurological disorders. Therefore, there is much interest in pharmacological agents capable of selectively blocking tonically activated NMDARs while leaving synaptically activated NMDARs intact. Here, we show that an endogenous neurosteroid pregnanolone sulfate is more potent at inhibiting tonically than synaptically activated NMDARs. Further, we report that a novel synthetic analog of pregnanolone sulfate, pregnanolone hemipimelate, inhibits tonic NMDAR currents without inhibiting the NMDAR component of the EPSC and shows neuroprotective activity *in vivo* without inducing psychomimetic side effects. These results suggest steroids may have a clinical advantage over other known classes of NMDAR inhibitors.

Introduction

N-methyl-D-aspartate receptors (NMDARs) are a subtype of ionotropic glutamate receptors that are highly permeable to calcium and expressed by virtually all neurons in the mammalian CNS. They are localized at a high density at postsynaptic regions, but are also present in extrasynaptic membrane (Petralia, 2012).

Received Aug. 25, 2015; revised Dec. 11, 2015; accepted Jan. 4, 2016.

Author contributions: V.V., T.S., K.V., J.C., H.C., E.K., and L.V. designed research; V.V., T.S., B.K., A.B., M.K., J.B., M.H., M.C., L.K., M.N., H.C., and E.K. performed research; V.V., T.S., B.K., A.B., M.K., J.B., M.H., M.C., L.K., K.V., J.C., M.N., H.C., E.K., and L.V. analyzed data; V.V., T.S., K.V., J.C., H.C., E.K., and L.V. wrote the paper.

This work was supported by the Czech Science Foundation (Grants 303/12/1464 and P304/12/G069), the Technology Agency of the Czech Republic (Grant TE01020028), the Grant Agency of Charles University (Grant 1520-243-253483; 800313/2012/2.LF, Research Project of the CAS (Grant RVO: 67985823, the Center of Biomedical Research (CZ.1.07/2.3.00/30.0025 project supported by the European Science Foundation), Biotechnology and Biomedicine Center of the Academy of Sciences and Charles University in Vestec (CZ.1.05/1.1.00/02.0109 project supported by the European Regional Development Fund). The computational study by M.N. was supported by the Czech Science Foundation (Grant P208/12/G016) and Research Project RVO: 61388963 of the Institute of Organic Chemistry and Biochemistry, CAS. Molecular graphics and analyses were performed with the University of California–San Francisco Chimera package, developed by the Resource for Biocomputing, Visualization, and Informatics (supported by National Institute of General Medical Sciences Grant P41-GM103311). We thank M. Kuntosova for excellent technical assistance and Grygoryi Tsenov for fruitful consultations.

The authors hold U.S. Patent No.: US8575376: "Steroid Anionic Compounds: Method of Their Production, Usage, and Pharmaceutical Preparation Involving Them," without direct corporate involvement at this time.

*V.V. and T.S. contributed equally to this work.

Correspondence should be addressed to Dr. Ladislav Vyklicky, Jr, Institute of Physiology CAS, Videnska 1083, 142 20 Prague 4, Czech Republic. E-mail: vyklicky@biomed.cas.cz.

DOI:10.1523/JNEUROSCI.3181-15.2016

Copyright © 2016 the authors 0270-6474/16/362161-15$15.00/0

PDF-XChange Editor
KOUPIT plnou verzi!
www.pdfxchange.cz

At excitatory synapses, glutamate is phasically released from presynaptic terminals, producing a glutamate concentration transient with an estimated peak of ~1 mM and a decay time constant of 1–2 ms (Clements et al., 1992). Synaptically activated NMDARs are vital for synaptogenesis, synaptic plasticity, learning, and memory (Lynch, 2004; Traynelis et al., 2010; Huganir and Nicoll, 2013). Further, phasic/synaptic NMDAR activation may promote cell survival under some conditions (Hardingham et al., 2002; Léveillé et al., 2008; Papadia et al., 2008; but see Wroge et al., 2012).

Tonic NMDAR activation, conversely, mediates excitotoxicity. Glutamate transporters normally maintain glutamate concentration in the extracellular space at low levels. Estimates of the "physiological" ambient glutamate concentration vary from as low as 25 nM to 1–4 μM (Sah et al., 1989; Wahl et al., 1994; Cavelier et al., 2005; Herman and Jahr, 2007). Under pathological conditions, however, ambient glutamate concentration increases, resulting in tonic receptor activation that results in excitotoxicity (Olney, 1969). This form of neuronal death is dependent on calcium influx through NMDARs (Choi, 1987) and is implicated in a variety of neurological conditions (Parsons and Raymond, 2014).

Given the different outcomes of tonic versus phasic/synaptic NMDAR signaling, there is much interest in NMDAR inhibitors capable of selectively blocking tonically activated NMDARs while leaving phasically/synaptically activated NMDARs intact. Inhibitors of NMDARs have shown some promise in models of human neurodegenerative diseases (Choi and Rothman, 1990), but their broader use is limited by their side effects that typically include psychomimetic symptoms, presumably due to the inhibition of normal synaptic transmission (Lipton, 1993; Rogawski, 1993; Rogawski and Wenk, 2003; Manahan-Vaughan et al., 2008). Memantine, an NMDAR antagonist used in Alzheimer's disease therapy, has been suggested to block preferentially tonically activated extrasynaptic NMDARs rather than phasically activated synaptic NMDARs, with a 2-fold difference in the IC_{50} values (Xia et al., 2010), although other studies found a smaller difference (Emnett et al., 2013). Theoretical considerations predict that, although NMDAR inhibitors with use-dependent onset and offset of inhibition ("trapping" blockers), exemplified by memantine, would show some preference for tonically versus phasically activated NMDARs, the strongest selectivity would be achieved by use-dependent inhibitors with slow onset and use-independent offset of inhibition ("foot-in-the-door" block; Vyklicky et al., 2014). Because an endogenous neurosteroid, 20-oxo-5β-pregnan-3α-yl sulfate (PA-S; 3α,5β-pregnanolone sulfate), is an NMDAR inhibitor with a foot-in-the-door mechanism of block (Petrovic et al., 2005; Vyklicky et al., 2015), we have explored the effect of PA-S and novel synthetic PA-S analogs on synaptically activated NMDARs and on receptors activated by sustained glutamate applications.

The results of our experiments, in agreement with the prediction, demonstrate that PA-S has a higher preference for tonically activated NMDARs than for NMDARs activated during synaptic transmission. All of the six structural analogs of PA-S tested exhibited a higher preference for tonically activated receptors. The most selective PA-S analog, pregnanolone hemipimelate (PA-hPim), showed no inhibition of phasically and synaptically activated receptors while inhibiting tonically activated receptors. Behavioral tests demonstrate that PA-hPim has neuroprotective activity without inducing psychomimetic symptoms. Overall, our results provide a unique opportunity for the development of new therapeutic neurosteroid-based ligands to treat diseases associated with the dysfunction of the glutamate system.

Materials and Methods

Cell culture

HEK293 cells. Human embryonic kidney 293 (HEK293) cells were maintained in Opti-MEM I (Invitrogen) supplemented with 5% fetal bovine serum (PAN Biotech) at 37°C in 5% CO_2. Cells were plated at a density of 10^5 cells/cm^2 and 24 h later transiently transfected with expression vectors containing the rat glutamate receptor subunits GluN1–1a (GenBank accession no. U08261) and GluN2A (GenBank accession no. D13211) or GluN2B (GenBank accession no. M91562) using Matra-A reagent (IBA) (Borovska et al., 2012). Equal amounts (300 μg) of cDNAs encoding for GluN1, GluN2A or GluN2B, and GFP (pQBI 25; Takara) were used. After trypsinization, the cells were resuspended in Opti-MEM I containing 1% fetal bovine serum supplemented with 20 mM $MgCl_2$, 1 mM D,L-2-amino-5-phosphonopentanoic acid (D,L-AP5), and 3 mM kynurenic acid to prevent excitotoxicity.

Micro-island cultures. Micro-island cultures were prepared as described previously (Burgalossi et al., 2012). Glass coverslips were coated with 0.15% agarose (Serva) and stamped with an array of microdots (~200 μm in diameter, spaced ~200 μm apart) of permissive substrate containing 0.1 mg/ml poly-D-lysine and 0.2 mg/ml collagen (Serva). Primary cortical astrocyte cultures were prepared from postnatal day 1 male Wistar rat pups and grown for 1–2 weeks in DMEM with GlutaMax (Invitrogen), 10% fetal bovine serum (Invitrogen) and pen/strep before being plated on the microdot-stamped coverslips at 5000 cells/cm^2. Hippocampal neurons were isolated from postnatal day 1 male Wistar rat pups and plated on top of the astrocyte microislands at 3000 cells/cm^2 in Neurobasal A medium with B27 Supplement (Invitrogen), GlutaMax, and pen/strep. This protocol yields a large proportion of islands containing a solitary hippocampal neuron forming autapses.

Electrophysiology

HEK293 cells were used for electrophysiological recordings 24–48 h after transfection. Whole-cell voltage-clamp recordings were made at room temperature at a holding potential of −60 mV, with capacitance and series resistance (<10 MΩ) compensation of 80–90%. Data were acquired with an Axopatch 200B amplifier, sampled at 10 kHz, and filtered at 2 kHz. Patch pipettes (3–5 MΩ) were filled with a solution containing the following (in mM): 120 gluconic acid, 15 CsCl, 10 BAPTA, 10 HEPES, 3 $MgCl_2$, 1 $CaCl_2$, and 2 ATP-Mg salt, pH adjusted to 7.2 with CsOH. Extracellular solution contained the following (in mM): 160 NaCl, 2.5 KCl, 10 HEPES, 10 glucose, 0.2 EDTA, and 0.7 $CaCl_2$, pH adjusted to 7.3 with NaOH. Glycine (10 μM) was present in the control and test solutions. Drug applications were made with a microprocessor-controlled multibarrel fast perfusion system. The solution exchange rate was ~10 ms.

Whole-cell voltage-clamp recordings of autaptic EPSCs were obtained at room temperature at a holding potential of −70 mV from solitary excitatory hippocampal neurons at 11–16 d *in vitro*. Intracellular solution contained the following (in mM): 125 gluconic acid, 15 KCl, 10 HEPES, 5 EGTA, 0.5 $CaCl_2$, 2 ATP-Mg salt, 0.3 GTP-Na salt, and 10 creatine phosphate, pH adjusted to 7.2 with KOH. Autaptic EPSCs were evoked by 1 ms depolarization to 0 mV every 15 s. Evoked dual AMPA and NMDA EPSCs were recorded in extracellular solution containing the following (in mM): 160 NaCl, 2.5 KCl, 10 glucose, 10 HEPES, 2 $CaCl_2$, 0.01 glycine, and 0.01 bicuculline methochloride, pH adjusted to 7.3 with NaOH. To assess presynaptic effects of steroids, 50 μM D-AP5 was added to the above extracellular solution to isolate AMPA EPSCs and paired-pulse stimulation with 50 ms interpulse interval was used to evoke a pair of EPSCs every 15 s. To isolate AMPA mEPSCs, 0.5 μM TTX was added to the extracellular solution. Solutions were applied using a gravity-fed fast perfusion system with a manifold connecting to a single solution outlet. During the recordings of evoked EPSCs (but not miniature EPSCs) series resistance (<20 MΩ) was 80% compensated. Data were acquired with an Axopatch 200B amplifier, sampled at 20 kHz, filtered at 2 kHz, and analyzed with pClamp software. The AMPA component of the dual EPSC was estimated as the peak of the response. The NMDA component

PDF-XChange Editor
KOUPIT plnou verzi!
www.pdfxchange.cz

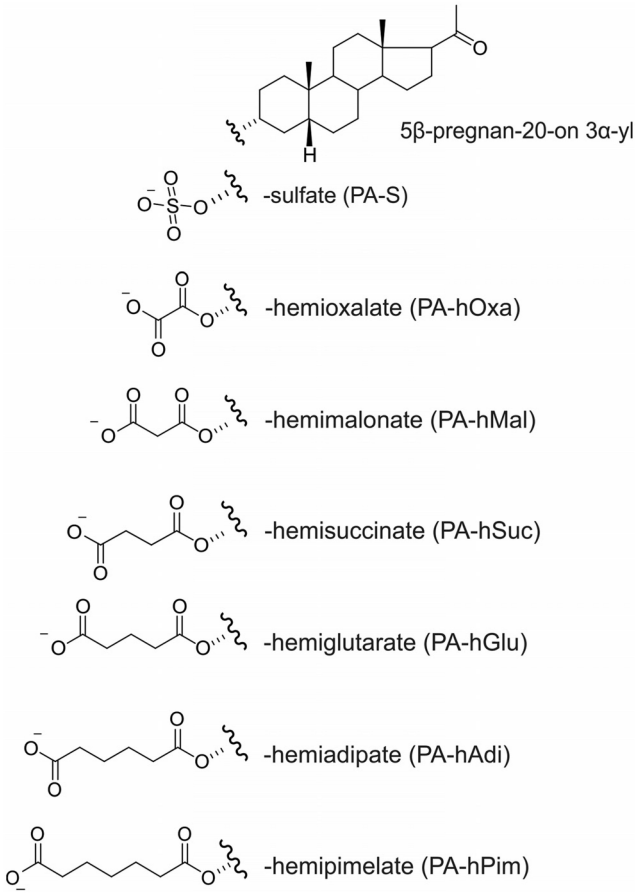


Figure 1. Chemical structures of steroids tested for their biological activity at NMDARs. The structure of PA and the residues substituted in position α of carbon C3 are shown.

of the dual EPSC was estimated from the double-exponential fit to the decay of the later portion of the EPSC (starting at 40 ms after stimulation, after the AMPA component had decayed to baseline) and extrapolated to the expected time of NMDA EPSC peak (14 ms after stimulation, as determined from control NMDA EPSCs recorded in the presence of 10 μM CNQX).

Steroids were dissolved in DMSO and added to the extracellular solution at the indicated concentrations, with the final DMSO concentration of 1%. An equivalent amount of DMSO was present in control solutions. All drugs, unless otherwise stated, were purchased from Sigma-Aldrich.

Data analysis

IC_{50} was determined from a fit to the following logistic equation:

$$I = \frac{100}{1 + \left(\frac{IC_{50}}{[steroid]}\right)^{h}}$$

or from a single dose of steroid using the following formula:

$$IC_{50} = [steroid] \times \sqrt[h]{\frac{100 - I}{I}}$$

Where I is the relative degree of inhibition in %, [*steroid*] is the steroid concentration used and h fixed at 1.0 for peak and 1.2 for steady state, based on the dose–response curves for PA-S (see Fig. 2*B*). Calculations of IC_{50} were made assuming 100% inhibition at a saturating steroid concentration.

Steroid synthesis

3α,5β-pregnanolone (PA-OH; Steraloids) was the starting material for the preparation of the majority of the steroids studied (Fig. 1). Pyridine sulfur trioxide complex with pregnanolone afforded PA-S (Stastna et al., 2009). Then, PA-OH treated with oxalic acid dichloride gave hemioxalate (PA-hOxa). Treatment by 2,2-dimethyl-1,3-dioxane-4,6-dione (Meldrum's acid) gave hemimalonate (PA-hMal). Reactions of PA-OH with succinic or glutaric anhydrides afforded-hemisuccinate (PA-hSuc; Stastna et al., 2009) and -hemiglutarate (PA-hGlu), respectively. Selective monoesterification of PA-OH with adipic or pimelic acids catalyzed by *N*,*N*′-dicyclohexylcarbodiimide and *N*,*N*-dimethyl-4-aminopyridine yielded steroid-hemiadipate (PA-hAdi) and -hemipimelate (PA-hPim), respectively (see below).

Melting points (Mp) were determined on a micro-melting point apparatus (Helmut Hund) and are uncorrected. Optical rotations were measured in chloroform using an Autopol IV (Rudolf Research Analytical). $[\alpha]_D$ values are given in degrees (10^{-1} deg cm^2 g^{-1}). IR spectra were recorded on a Bruker IFS 55 spectrometer (wave numbers in cm^{-1}). Proton and carbon NMR spectra were measured on an FT NMR spectrometer Bruker AVANCE-400 (400 MHz, 101 MHz) in $CDCl_3$ with tetramethylsilane as the internal standard (unless otherwise stated). Chemical shifts are given in parts per million (delta scale). Coupling constants (J) and width of multiplets (W) are given in Hertz. Mass spectra were obtained with spectrometers ZAB-EQ (at 70 eV) or LCQ Classic (Thermo-Finnigan). Thin-layer chromatography (TLC) was performed on silica gel (ICN Biochemicals). Preparative TLC (prep-TLC) was performed on 200 mm × 200 mm plates coated with a 0.4-mm-thick layer of the same material. For column chromatography, neutral silica gel 60 μm (Merck) was used. Analytical samples were dried over phosphorus pentoxide at 50°C/100 Pa. Anhydrous THF was prepared by distillation with benzophenone/Na immediately before use.

PA-S. For details of PA-S preparation, please see Stastna et al. (2009).

PA-hOxa. A mixture of PA-OH (320 mg, 1 mmol), dry dichloromethane (4 ml), triethylamine (0.14 ml), and 1 drop of previously prepared solution (2 ml of dry dichloromethane and 1 drop dimethylformamide) was added to a cooled (0°C) mixture of dichloromethane (2 ml) and oxalic acid dichloride (0.26 ml, 3 mmol). The mixture was allowed to attain 10°C and then stirred for 2 h under these conditions. Then, 20 ml of water was added to decompose excess of the reagent and the mixture was stirred for 30 min at room temperature. The organic layer was separated and ethyl acetate (20 ml) was added to the dichloromethane extract. Then, aqueous solution of potassium carbonate was added (10%, 50 ml), the organic layer with undesired by-products was separated and, subsequently, aqueous solution of HCl (1 N, to pH ~4) was cautiously added to the aqueous layer. The crude product was obtained by extraction with ethyl acetate (2 × 25 ml) and dried. Crystallization from acetone/*n*-heptane gave 230 mg (59%) of hemioxalate (PA-hOxa): Mp 112–114°C. $[\alpha]_D$ +110 (*c* 0.37, $CHCl_3$). ^{1}H NMR: δ 0.60 (^{3}H, *s*, H-18), 0.96 (^{3}H, *s*, H-19), 2.14 (^{3}H, *s*, H-21), 2.55 (^{1}H, *t*, J = 8.8, H-17), 4.96 (^{1}H, m, H-3). ^{13}C NMR: δ 211.0 (C-20), 157.9 (COOH), 157.8 (CO-O), 79.0 (C-3), 64.0 (C-17), 56.9, 44.69, 42.0, 40.5, 39.3, 35.9, 35.0, 34.8, 31.9, 31.6, 27.0, 26.4, 26.3, 24.6, 23.3, 23.1, 21.0, 13.6. IR ($CHCl_3$): 2938, 2873, 1735, 1699, 1238, 1231, 1194. MS: ESI m/z 317.3 (100%, M-COCOOH), 389.3 (25%, M-1). HR-MS (ESI) m/z for $C_{23}H_{33}O_5$ [M-1] calculated 389.2334, found 389.2334.

PA-hMal. PA-OH (320 mg, 1 mmol) in dry toluene was added to a dry reaction vessel with 2,2-dimethyl-4,6-dioxo-1,3-dioxolane (Meldrum's acid, 160 mg, 1.1 mmol). The reaction mixture was stirred and heated to reflux for 4 h. Solvent was evaporated under reduced pressure. Chromatography of the crude product (422 mg) on a small (10 g) silica gel column (10% acetone in petroleum ether) gave 230 mg of oily product, which after crystallization (ether/petroleum ether) afforded (PA-hMal) as white crystals 190 mg (47%): Mp 118–120°C. $[\alpha]_D$ +116 (*c* 0.23, $CHCl_3$). ^{1}H NMR: δ 0.60 (^{3}H, s, H-18), 0.95 (^{3}H, s, H-19), 2.11 (^{3}H, s, H-21), 2.53 (^{1}H, *t*, J = 8.8, H-17), 3.41 (^{2}H, s, H-2′), 4.84 (^{1}H, m, H-3). ^{13}C NMR: δ 209.8 (C-20), 178.0 (COOH), 173.0 (COO), 73.8 (C-3), 64.0 (C-17), 56.8, 44.5, 42.0, 40.6, 39.3, 35.9, 35.1, 34.83, 32.2, 31.7, 26.9, 26.6, 26.4, 24.6, 23.4, 23.1, 21.0, 13.6. IR ($CHCl_3$): 3509, 3090, 2701 (OH); 1735, 1700 (C=O, carboxyl); 1718 (C=O, 20-ketone), 1194, 1156 (C-O). MS: ESI m/z 427.2 (100%, M + Na). HR-MS (ESI) m/z for $C_{24}H_{36}O_5Na$ (M + Na) calculated 427.2455, found 427.2455. For $C_{24}H_{36}O_5$ (404.5) calculated: 71.26% C, 8.97% H; found: 71.30% C, 9.10% H. As a side

PDF-XChange Editor
KOUPIT plnou verzi!
www.pdfxchange.cz

product (132 mg, 40%) was isolated less polar dipregnanolone malonyl ester.

PA-hSuc. For details of PA-hSuc preparation, please see Stastna et al. (2009).

PA-hGlu. A mixture of PA-OH (320 mg, 1 mmol) and glutaric acid anhydride (573 mg, 5 mmol) was dried overnight at 50°C. Dry pyridine (6 ml) and 4-(dimethylamino)pyridine (184 mg, 1.5 mmol) were added. The mixture was refluxed for 36 h. The reaction mixture was poured into water and extracted with chloroform (3 × 20 ml), combined organic extracts were washed with brine and dried. Solvents were evaporated and the brown residue was purified by column chromatography (10% of acetone in petroleum ether) to afford white solids. Crystallization from ethyl acetate/acetone/petroleum ether gave 178 mg (48%) of the desired hemiester (PA-hGlu): Mp 128−130°C. $[\alpha]_D$ +100 (*c* 0.27, $CHCl_3$). ^{1}H NMR: δ 0.60 (^{3}H, s, H-18), 0.94 (^{3}H, s, H-19), 1.96 (2H, *p*, *J* = 14.6, H-3′), 2.12 (^{3}H, s, H-21), 2.38 (^{2}H, *t*, *J* = 7.3, H-2′), 2.44 (^{2}H, *t*, *J* = 7.3, H-4′), 2.54 (^{1}H, *t*, *J*, 8.8, H-17), 4.75 (^{1}H, m, H-3). ^{13}C NMR: δ 209.8 (C-20), 178.4 (COOH), 172.5 (COO), 74.6 (C-3), 64.1 (C-17), 56.9, 44.5, 42.0, 40.6, 39.4, 36.0, 35.2, 34.8, 33.8, 33.1, 32.4, 31.7, 27.1, 26.8, 26.5, 24.6, 23.4, 23.1, 21.0, 20.1, 13.6. IR ($CHCl_3$): 3516 (OH); 1711 (C=O), 593 (CH_3CO). MS: ESI m/z 455.3 (100%, M + Na), 477.3 (35%, M + Na + H). For $C_{26}H_{40}O_5$ (432.3) calculated: 72.19% C, 9.32% H; found: 72.14% C, 9.45% H.

PA-hAdi. N,N′-Dicyclohexylcarbodiimide (410 mg, 2 mmol) in dry benzene (10 ml) was added into a solution of adipic acid (300 mg, 2 mmol) in dry THF (10 ml) under inert atmosphere and the mixture was stirred for 1 h. Then, a solution of PA-OH (320 mg, 1 mmol) and 4-(dimethylamino)pyridine (10 mg, 0.08 mmol) in dry benzene (10 ml) was added dropwise over 15 min. This reaction mixture was stirred at room temperature for 16 h and then the solvents were evaporated. The residue was purified on a column of silica gel (petroleum ether/ether, 9:1) to afford noncrystalizing hemiester (350 mg, 78%): $[\alpha]_D$ + 89 (c 0.49, $CHCl_3$). ^{1}H-NMR: δ 0.60 (*s*, ^{3}H (H-18); 0.92 (*s*, ^{3}H, H-19); 2.11 (*s*, ^{3}H, H-21); 2.30 (m, ^{2}H, W∼20, H-adipate); 2.37 (m, ^{2}H, W∼20, H-adipate); 2.53 (*t*, ^{1}H, *J* = 9, H-17); 4.73 (m, 1H, W = 35, H-3). IR ($CHCl_3$): 1727, 1706 (C=O); 1358 (CH_3C=O); 1233, 1193, 1183 (C-O). For $C_{27}H_{42}O_5$ (446.6) calculated: 72.61% C; 9.48% H; found: 72.13% C; 9.53% H.

PA-hPim. The same procedure as for PA-hAdi was used. Instead of adipic acid, pimelic acid (heptanedioic acid) was used to produce PA-hPim. Oily, $[\alpha]_D$ + 72.3 (c 0.33, $CHCl_3$). ^{1}H-NMR: δ 0.60 (*s*, ^{3}H, H-18); 0.93 (*s*, ^{3}H, H-19); 2.11 (*s*, ^{3}H, H-21); 2.30 (m, 2H, W∼20, H-pimelate); 2.37 (m, 2H, W∼20, H-pimelate); 2.53 (*t*, 1H, *J* = 8.8); 4.74 (m, 1H, W = 35, H-3). ^{13}C NMR (MeOD): δ 209.6 (C-20), 178.6 (COO), 173.2 (COO-), 74.1, 63.9, 56.7, 44.8, 44.3, 41.9, 40.4, 39.2, 35.8, 35.1, 34.6, 34.6, 32.3, 31.5, 28.7, 26.9, 26.7, 26.3, 24.74, 24.70, 24.4, 23.3, 22.9, 20.9, 13.4 (C-18). IR ($CHCl_3$): 3516 (COOH, monomer), 1725 (C=O, ester), 1705 (C=O, $COCH_3$), 1261 (C-O, ester). MS: (ESI): 460 (4%, M). HR-MS (+ESI) calculated for $C_{28}H_{44}O_5Na$ [M+Na] 483.3081, found 483.3080.

Computational methods

The relevant physicochemical properties of neuroactive steroids were calculated by quantum mechanics computational methods and by physicochemical properties predictor.

Preparation of structures. The geometries of steroids were obtained by the modeling of the ligand taken from the x-ray structure (3CAV PDB code; Faucher et al., 2008) using PyMOL program (version 1.5.0.4; Schrödinger) and were optimized by the RI-DFT/B-LYP/SVP method with the Turbomole program (Ahlrichs et al., 1989). The empirical dispersion correction (*D*; Jurecka et al., 2007) and COSMO continuum solvation model (Klamt and Schuurmann, 1993) were used on the gradient optimization. The most stable local minima of the steroids were generated by the quenched molecular dynamics simulation with Amber 14 (Salomon-Ferrer et al., 2013) in explicit water solvent (the simulation was run for 30 ns; the constant temperature was 303 K). The parameters were obtained from the GAFF force field. The charges were calculated using the RESP procedure at the HF/6–31G* level (Bayly et al., 1993). The resulting geometries were minimized by the RI-DFT-D/B-LYP/SVP//COSMO method and their single-point energies were calculated at the RI-DFT-D3/B-LYP/TZVPP level (Grimme et al., 2010).

Docking. Docking with AutoDock was used to sample the conformational variability of steroid molecules in the confined space within the NMDAR. AutoDock 4.2.3 calculations were prepared and analyzed in AutoDockTools (ADT) 1.5.6rc3 (Sanner, 1999). Protein and ligand charges were assigned by ADT using Gasteiger charges. To assess the relative rate of the steroid inhibition onset (the steroid distribution in the channel vestibule), genetic algorithm runs of 50 steps were used within an 80 × 80 × 60 grid (1 Å spacing) surrounding the extracellular mouth of the model of NMDAR in its activated state (Vyklicky et al., 2015). Combined results of 30 runs (resulting in 675–1400 poses after clustering) were analyzed for each steroid molecule. The electrostatic potential of NMDAR was calculated using the APBS program (Baker et al., 2001) and visualized with the UCSF Chimera package (Pettersen et al., 2004).

Predictions of thermodynamic properties. The solvation free energy (δG_{solv}) of steroids was calculated in the SMD continuum solvation model (the transfer from vacuum to water and from *n*-octanol to water) at the HF/6-31G* level with Gaussian software. The partition-coefficients (logP) of water/n-octanol phase were calculated at the M06-2X/6-31G* level in SMD with Gaussian as the difference between the total energies in water and in n-octanol. The distribution coefficients (logD) of water/n-octanol phase were predicted by the MarvinSketch program (Marvin 15.1.19, 2015; ChemAxon).

Behavioral methods

Animals. Experiments were performed on adult albino male Wistar rats (250–350 g) bred by the Institute of Physiology at the Czech Academy of Sciences (CAS). Rats were housed in a controlled environment (temperature 22 ± 1°C, humidity 50–60%, lights on 06:00–18:00 h) with free access to food and water. Experiments were conducted in accordance with the guidelines of the European Union directive 2010/63/EU and approved by the Animal Care and Use Committee of the Institute of Physiology CAS and by The Central Committee of the CAS. The Institute of Physiology possesses the National Institutes of Health Statement of Compliance with Standards for Humane Care and Use of Laboratory Animals.

Open-field test. Spontaneous locomotor activity was recorded in a soundproof MultiConditioning System arena (45 cm × 45 cm; TSE Systems), and expressed as the total distance traveled during 30 min. PA-hPim at a dose of 1 or 10 mg/kg was dissolved in 1 ml of 88 mM hydroxypropyl-β-cyclodextrine (β-CDX), pH 7.4. MK-801 was dissolved in PBS and given at a dose of 0.1, 0.2, or 0.3 mg/kg. The drugs were applied intraperitoneally 40 min before behavioral observations; control animals were injected with a corresponding volume of β-CDX or saline, respectively.

Passive avoidance. The passive avoidance apparatus (45 cm × 45 cm) consisted of two equally large compartments divided by a sliding door (Multi Conditioning system; TSE Systems). The rats were treated intraperitoneally with saline, β-CDX, PA-hPim (at 1 or 10 mg/kg), or MK-801 (at 0.1, 0.2, or 0.3 mg/kg) 30 min before a habituation session. At the beginning of each session, the rat was placed into the highly illuminated compartment and could avoid this aversive stimulus by crossing to the dark compartment. During the habituation session, the sliding door was lifted and the rat could move freely between the compartments for 5 min. Thirty minutes later, the rat was placed into the arena again for a training session. This time, after crossing to the dark compartment, the sliding door fell down and the rat received a mild electric foot shock (1.5 mA, 5 s duration) through the stainless steel grid floor. A testing session took place 1 h after the training session and was conducted in the same way except that the footshock was not activated. The latency to cross into the dark compartment was analyzed.

Spontaneous alternation task in a Y-maze. The maze was constructed from Plexiglas with three arms of the same length (40 cm × 11 cm) interconnected at a 120° angle. Each rat was placed at the center of the maze at the beginning of the experiment and allowed to explore the maze freely for 10 min. An alternation was defined as sequentially entering all three arms without reentry into a previously visited arm. Percentage alternation was calculated as follows: (alternations/total entries − 2) ×

PDF-XChange Editor
KOUPIT plnou verzi!
www.pdfxchange.cz

100. Thirty minutes before experimental testing, rats were treated intraperitoneally with saline, β-CDX, PA-hPim (at the doses of 1 or 10 mg/kg), or MK-801 (at the doses of 0.1, 0.2, or 0.3 mg/kg). At the dose of 0.3 mg/kg, MK-801 induced stereotypical behavior precluding data evaluation.

Neuroprotection. Intrahippocampal lesion was induced by a bilateral infusion of 1 μl of 25 mM NMDA (Abcam) dissolved in PBS into the dorsal hippocampus (AP = 4; L = 2.5; DV = 4.8 mm). The infusions were performed with a syringe pump (model 540310 plus; TSE Systems) at a constant flow rate of 0.25 μl/min. Control animals were either intact, or received an intrahippocampal infusion of 1 μl of PBS. Because the two control groups were not statistically different in terms of their performance, they were pooled for subsequent analysis. PA-hPim (1 mg/kg in 1 ml of 88 mM β-CDX) was injected intraperitoneally 5 min after the NMDA infusion. NMDA-infused animals received either the corresponding volume of intraperitoneal β-CDX or no treatment; because these two groups were not statistically different, they were pooled for analysis. The animals recovered for 1 week before starting the Morris water maze (MWM) procedures. All drugs, unless otherwise stated, were purchased from Sigma-Aldrich.

MWM experiments were performed as described previously (Mikulecká et al., 2014). The maze was a black-painted circular plastic pool (210 cm in diameter, 40 cm high) filled with water (21°C). Rats were released from one of eight compass points (NW, NE, SE, W, S, N, SW, and E, in this order) at the periphery of the pool and allowed to swim until they found a transparent circular platform (10 cm in diameter submerged 1 cm below the water surface in the center of an arbitrarily chosen quadrant of the pool, SW) or until 60 s elapsed. Training consisted of 8 trials a day for 4 d. The position of the platform was stable throughout the experiment. Training was recorded by a camera placed above the center of the MWM. The videos were analyzed offline by Ethovision XT10 software (Noldus).

Statistical methods

In electrophysiology experiments, statistical comparisons of groups were performed using Student's *t* test ($p < 0.05$ was used to determine significance). Cumulative distributions of mEPSC amplitudes and interevent intervals were compared using Kolmogorov–Smirnov (K-S) test using a conservative value of $p < 0.001$ to determine significance. For behavioral experiments, one-way ANOVA followed by Holms-Sidak *post hoc* comparisons versus control group or two-way ANOVA followed by Student-Newman–Keuls *post hoc* tests were used. The results are presented as means ± SEM, with *n* indicating the number of cells (electrophysiology experiments) or animals (behavioral experiments).

Results

Recombinant receptors

NMDARs are activated phasically by synaptically released glutamate or tonically by extracellular glutamate elevated under pathological conditions. Kinetic simulations indicate that, based on the pharmacological mode of inhibitor action at the NMDAR, a different ratio of phasic over tonic inhibition is expected. Compounds such as PA-S with use-dependent and voltage-independent block and use-independent unblock are likely to preferentially inhibit tonically over phasically activated NMDAR and therefore may have a desirable therapeutic profile (Vyklicky et al., 2014). First, we tested the simulation predictions for PA-S at recombinant GluN1/GluN2B receptors expressed in HEK293 cells and activated by fast agonist application. Figure 2*A* shows an experiment in which we compared the ability of PA-S (50 μM) to inhibit the peak (phasic) response induced by fast 1 mM glutamate application (solution exchange rate ~10 ms) versus the steady-state response after glutamate application for 5 s. A dose–response analysis indicates that PA-S inhibited the peak responses less than the steady-state responses, with a 2-fold difference in potency (Fig. 2 *B*, *C*; peak $IC_{50} = 46 \pm 3$ μM; $n = 4$; steady-state $IC_{50} = 23 \pm 2$ μM; $n = 4$; $p < 0.001$). We have also tested recombinant GluN1/GluN2A receptors and found an even stronger (~6-fold) selectivity of PA-S for steady-state over peak inhibition (Fig. 2*C*; peak $IC_{50} = 296 \pm 34$ μM; steady-state $IC_{50} = 53 \pm 7$ μM; $n = 6$; $p < 0.001$). In an effort to identify novel steroid NMDAR inhibitors with desirable pharmacological properties, we have synthesized a series of 20-oxo-5β-pregnanes substituted in the position α of carbon C3 by carboxyl acids of increasing length (Fig. 1). We then tested these compounds for their ability to inhibit the peak versus the steady-state NMDAR response. Figure 2*D* illustrates an experiment in which PA-hPim (30 μM) was tested for its potency to inhibit peak and steady-state responses of GluN1/GluN2B receptors. Although the steady-state response to glutamate (1 mM) was inhibited by 66 ± 4%, the peak response was virtually unaffected (+0.02 ± 1.76%; $n = 8$) in the continuous presence of PA-hPim. The inhibitory effect was fully reversible within seconds of the steroid wash-out and the degree of the steroid-induced peak inhibition was the same for the first and the subsequent responses made in the presence of the steroid. Remarkably, the IC_{50} values for the steady-state response inhibition decreased with the length of the substituent aliphatic chain from PA-hOxa to PA-hPim (Fig. 2*E*), whereas the values of the IC_{50} for the peak response inhibition remained high. In fact, in the case of PA-hPim, peak response inhibition was so weak, the peak IC_{50} could not be determined accurately (Fig. 2, legend). The strong selectivity of PA-hPim for steady-state over peak responses was also observed for recombinant GluN1/GluN2A receptors (Fig. 2*E*).

It was of interest to compare the action of steroid inhibitors with that of memantine, which is approved for the treatment of Alzheimer's disease. Even though both memantine and steroids are use-dependent inhibitors, they differ in the voltage dependency of block and in the trapping versus foot-in-the-door mechanism of action (Blanpied et al., 1997; Petrovic et al., 2005; Vyklicky et al., 2015). Figure 3*A* shows that both memantine (10 μM) and PA-S (300 μM) inhibited steady-state GluN1/GluN2B receptor responses and exhibited pharmacodynamic similarities characterized by a slow offset of inhibition. Importantly, their actions differed when glutamate responses were induced in the continuous presence of the inhibitor to simulate the situation *in vivo*. In contrast to PA-S (Fig. 2*A*), the peak responses to glutamate made in the presence of memantine (10 μM) were progressively more inhibited with each glutamate application. This eventually eliminated the difference between the IC_{50} values for the peak versus the steady-state inhibition by memantine (peak $IC_{50} = 3.1 \pm 0.5$ μM; steady-state $IC_{50} = 2.7 \pm 0.4$ μM; $p = 0.125$; $n = 4$), with the ratio of the IC_{50} values being 1.14 ± 0.04 (Fig. 3*B*), confirming the advantage of steroid NMDAR inhibitors over memantine.

Structure–function relationship of the steroid inhibition of NMDAR

The complex process of steroid access to the NMDAR can be divided into three steps: (1) the micelles that occur in the extracellular liquid fuse with the membrane, (2) single molecules leave the membrane, and (3) molecules enter into the channel vestibule (Vyklicky et al., 2015). The physicochemical properties relevant to single molecules in water and in the membrane environment are listed in Table 1. As expected, we found a correlation between binding free energies δG_{exp} calculated from the experimentally determined steady-state IC_{50} values (Fig. 2*E*) and the length of the aliphatic chain. We also found a correlation between δG_{exp} and solvation energies δG_{solv} in the case of the transfer of the steroid molecule from vacuum to water and between δG_{exp}

PDF-XChange Editor
KOUPIT plnou verzi!
www.pdfxchange.cz

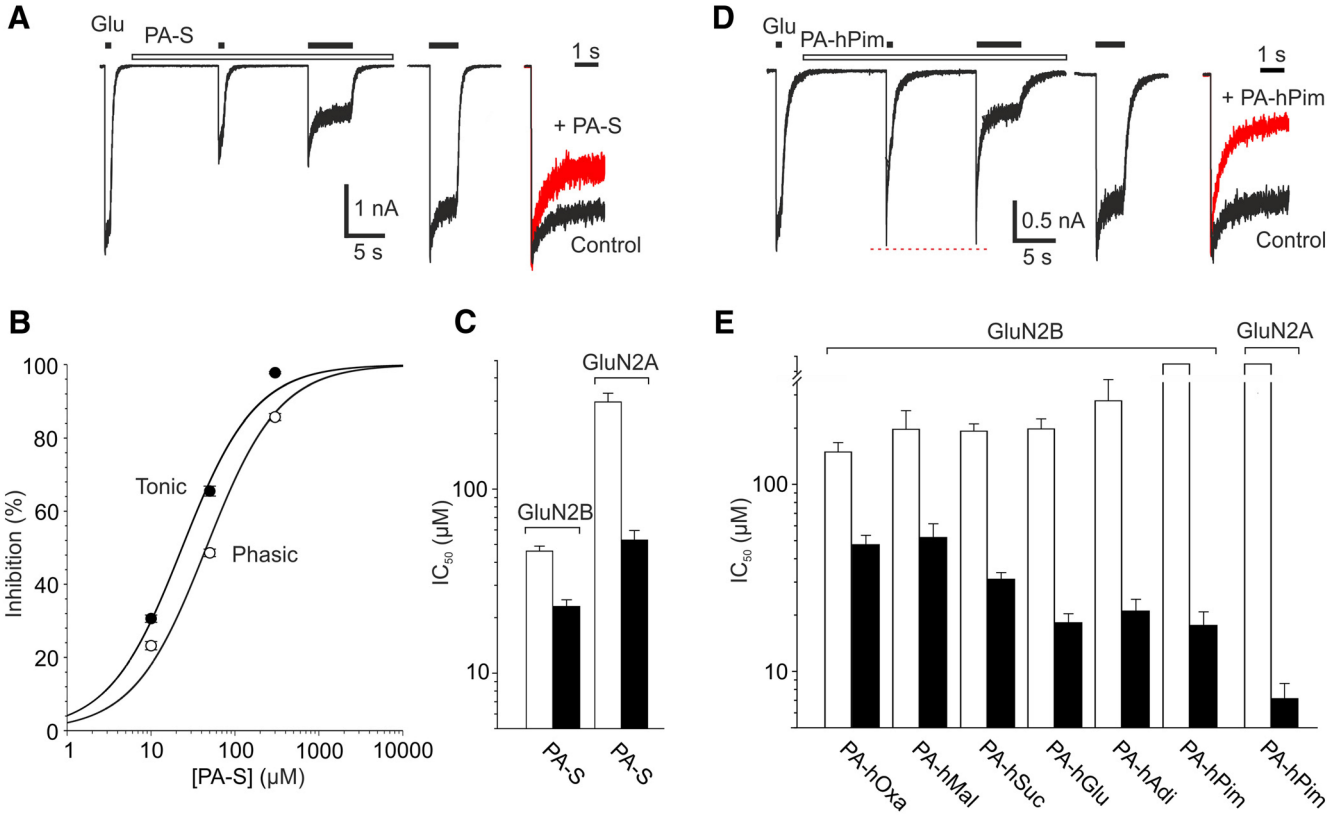


Figure 2. PA-S and its ester analogs are more potent at inhibiting steady-state than peak responses mediated by GluN1/GluN2B or GluN1/GluN2A receptors. ***A***, Responses evoked in a HEK293 cell expressing GluN1/GluN2B receptors by fast application of glutamate (1 mM) for 0.5 and 5 s in the absence and in the continuous presence of PA-S (50 μM). The duration of glutamate and steroid applications is indicated by filled and open bars, respectively. Right, Control response to glutamate (black) and a response made in the presence of PA-S (red) are shown overlaid and normalized with respect to their peak amplitude. ***B***, Dose–response curves for PA-S (10, 50, or 300 μM) inhibition of peak NMDAR responses (open symbols) and steady-state NMDAR responses (filled symbols). Data were fitted to Equation 1 and the smooth curves were calculated from the mean IC_{50} values. ***C***, Mean ± SEM of the IC_{50} values determined using Equation 2 for PA-S inhibition of the peak responses (open bars) and the steady-state responses (filled bars) of GluN1/GluN2A and GluN1/GluN2B receptors. ***D***, Responses induced by glutamate (1 mM) in the absence and in the continuous presence of PA-hPim (30 μM). The duration of glutamate and steroid applications is indicated by filled and open bars, respectively. Right, Control response (black) and a response recorded in the presence of PA-hPim (red) are shown normalized with respect to their peak and overlaid. ***E***, Mean ± SEM of the IC_{50} values determined using Equation 2 for each hemiester-PA analog from the relative steroid inhibition of the peak responses (open bars) and the steady-state responses (filled bars). The IC_{50} values for peak inhibition by PA-hPim were calculated from cells in which the steroid induced inhibition (5/8 for GluN1/GluN2B receptors and 5/6 for GluN1/GluN2A receptors).

and logD. δG_{solv} is probably influenced by a change of the conformation during the transfer of the steroids from n-octanol to water, which is not possible to describe accurately because of a large numbers of conformers (local minima). Together, these results indicate the importance of solvation energy and lipophilicity (Kudova et al., 2015) for steady-state inhibition.

Two major reasons contribute to the weaker inhibitory effect of steroids at phasically than at tonically activated NMDARs: the first is the use-dependent mechanism of steroid action (binding can start only after receptor activation), shared by all steroids in this study; the second is the slow onset of steroid-induced inhibition, which varies for different steroids (tens to hundreds of miliseconds). We wanted to explore in more detail how steroid structure may influence the rate of the onset of inhibition. The behavior of the steroids inside the NMDAR was modeled by their docking into the NMDAR channel (see Materials and Methods for details). We have used the model of the agonist-induced conformation of the channel vestibule based on our previous analysis of the role of Thr in the SYTAN motif combining experimental and modeling approaches (Vyklicky et al., 2015). The full model of the NMDAR was prepared by homology modeling based on the available crystal structures of AMPA and NMDARs (Sobolevsky et al., 2009; Karakas and Furukawa, 2014; Lee et al., 2014) using the MODELLER 9v6 software suite (Sali and Blundell, 1993). The opening of the channel was modeled by elongating the distance between the pairs of the corresponding Cα atoms of the topmost residues within the pore-forming helices of the GluN1 and GluN2B M3 domains. For the docking study, we selected PA-hOxa and PA-hPim, representing the steroids with the smallest and the largest difference in the peak versus the steady-state IC_{50}, respectively (Fig. 2*E*). Our modeling results suggest that the cumulative distribution near the Thr ring, the narrowest portion of the channel vestibule and likely the site of inhibitory steroid action (Vyklicky et al., 2015), is higher for PA-hOxa than for PA-hPim (Fig. 4*B*). Modeling suggests several factors affecting the cumulative distribution (which, as calculated, is indicative of the rate of the steroid inhibition onset). Both hemiester-PA derivatives interact with the whole nonpolar (Fig. 4*A*,*B*) inner surface of the NMDAR channel, mostly through van der Waals interactions. These interactions are influenced by partial desolvation in the place of the interaction, the character of the charged and polar parts of the steroid in the nonpolar surroundings (Barratt et al., 2006), and changes of the steroid conformation. Overall, these interactions result in slowing the rate of steroid access to the site of inhibitory action, particularly for the steroids with longer aliphatic chains, reducing their peak NMDAR current inhibition. To better understand the behavior of steroids inside of the NMDAR channel vestibule, we have investigated the flexibil-

PDF-XChange Editor
KOUPIT plnou verzi!
www.pdfxchange.cz

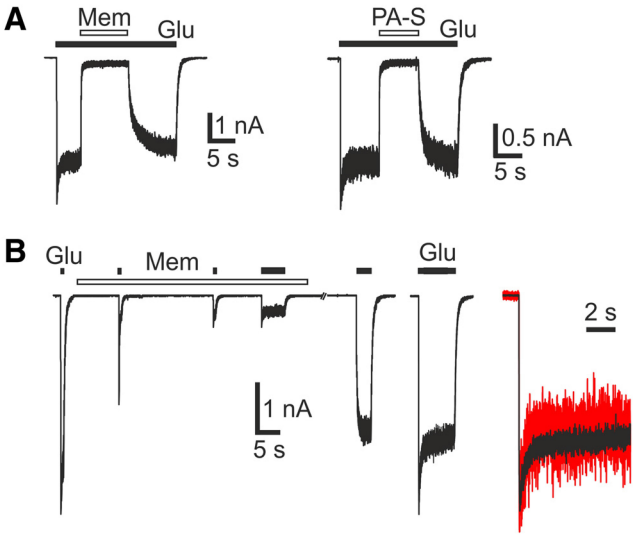


Figure 3. Memantine is only weakly selective for inhibiting tonically over phasically activated GluN1/GluN2B receptors. ***A***, Responses evoked by long glutamate (1 mM) applications in HEK293 cells expressing GluN1/GluN2B receptors. Memantine (10 μM) or PA-S (300 μM) were coapplied with glutamate as indicated. ***B***, Responses evoked by fast applications of glutamate (1 mM) for 0.5 and 5 s in the absence and in the continuous presence of memantine (10 μM). Right, Control response to glutamate (black) and a response made in the presence of memantine (red) are shown overlaid and normalized with respect to their peak amplitude.

ity and conformer stability of steroids in the NMDAR channel and in the water phase. We present changes of the conformation of the single molecule of PA-hPim and of PA-hOxa obtained using a quenched MD simulation in the explicit water phase (Fig. 4*C*). The deformation energy is expressed as the difference of the single point energies between the global minimum (extended form of the steroid; Fig. 4*C*) and the local minimum (compact conformer inside the NMDAR). For PA-hPim, the deformation energy is 5.87 kcal/mol for permittivity $\varepsilon = 78.4$, but only 3.91 kcal/mol for $\varepsilon = 4$, and 5.16 kcal/mol for $\varepsilon = 10$ (the ε values characterize the permittivity of implicit solvents; the first describes the water phase and the other two are commonly used for protein interior). The cumulative distribution of the compact local minimum is ~5% in the explicit water phase and ~30% inside the NMDAR channel for PA-hPim (Fig. 4*C*). These data indicate that PA-hPim is flexible and tends to adopt a more compact conformation inside the NMDAR through an intramolecular interaction of the aliphatic chain to the steroid skeleton. This intramolecular interaction has an adverse energy effect, but facilitates steroid passage to the gating Thr residues (Beck et al., 1999; Sobolevsky et al., 2002; Vyklicky et al., 2015). In contrast, the conformation of PA-hOxa inside the channel vestibule remains mostly extended (Fig. 4*C*). Together, our results suggest that interactions of steroids with the longer aliphatic chains with the nonpolar receptor interior, together with their flexibility, influence their rate of access to the site of their inhibitory action.

Native receptors

Next, we tested the effects of steroids on native NMDARs activated during synaptic transmission. We recorded autaptic EPSCs from solitary hippocampal neurons grown on micro-islands. To facilitate comparisons with recombinant receptor experiments, we conducted synaptic experiments at room temperature. In the presence of 2 mM Ca^{2+} and no added Mg^{2+}, we detected both the AMPAR and the NMDAR components of EPSCs. PA-S (100 μM) applied for 1.5 min increased the amplitude of the AMPAR component of the EPSC by 51 ± 5% ($p = 0.001$; $n = 8$) while decreasing the amplitude of the NMDAR component of the EPSC by 26 ± 5% ($p = 0.002$; $n = 8$) compared with baseline (Fig. 5*A*). The time course of deactivation of the NMDAR component of the EPSC was typically best fit by a double exponential function, from which we calculated τ_w. Consistent with its use-dependent NMDAR block, PA-S (100 μM) significantly decreased τ_w from 177 ± 16 ms to 156 ± 13 ms ($p = 0.014$; $n = 8$). This was largely due to a decrease in τ_s ($p = 0.040$); there was no significant effect on τ_f ($p = 0.071$) or the relative proportion of τ_f ($p = 0.413$).

We wanted to determine whether the mechanism underlying the potentiation of the AMPA EPSC amplitude was presynaptic or postsynaptic. To examine steroid effects on release probability, we examined the paired-pulse ratio of pharmacologically isolated, AMPAR-mediated evoked EPSCs. The amplitude of pure AMPAR EPSCs increased during 100 μM PA-S application to the same extent as was observed for the AMPAR component of the dual EPSCs (Fig. 5*B*, 66 ± 11%; $p = 0.219$ for the comparison between the potentiation of AMPAR component of the dual EPSC vs pure AMPAR EPSC). The paired-pulse ratio of AMPAR EPSCs was 0.81 ± 0.06 before steroid application and declined to 0.48 ± 0.05 ($p = 0.001$; $n = 5$) after 1.5 min PA-S (100 μM) application, suggesting that PA-S potentiates AMPAR EPSCs through a presynaptic mechanism. To confirm this, we recorded AMPA mEPSCs in the presence of TTX (Fig. 5*C*,*D*). In agreement with the decrease in the paired-pulse ratio (indicating a presynaptic effect), the frequency of AMPA mEPSCs was significantly increased by 100 μM PA-S (by 194 ± 41% of baseline; $p = 0.006$; $n = 6$). K-S tests confirmed that PA-S significantly shortened interevent intervals in 5/6 cells (Fig. 5*D*). In contrast, PA-S had no effect on AMPA mEPSC amplitude (−0.8 ± 5.3%; $p = 0.662$; $n = 6$). Cumulative distribution of AMPA mEPSC amplitudes was significantly altered in only 1/6 cells (Fig. 5*D*). The lack of a postsynaptic effect of PA-S on AMPARs was confirmed by examining responses induced by AMPA (5 μM) application to cultured hippocampal neurons. Responses to AMPA recorded in the presence of cyclothiazide (10 μM) were inhibited by PA-S (100 μM) by only 7.2 ± 1.0% of control ($n = 6$; Fig. 5*E*).

Next, we compared the inhibition of tonically versus synaptically activated native NMDARs by PA-S. PA-S (100 μM) strongly inhibited tonic currents evoked by 300 μM NMDA (Fig. 5*F*), on average by 81 ± 1% ($n = 14$; red symbol in Fig. 5*G*). These data were used to determine the PA-S IC_{50} for tonic inhibition of native NMDARs (30 ± 1 μM; $n = 14$). Given our result that PA-S potentiates glutamate release without affecting AMPARs postsynaptically, the ratio of the NMDAR/AMPAR component of the dual EPSC can be used as an indicator of the steroid effect at postsynaptic NMDARs (independent of its presynaptic effect). Figure 5*G* shows that the normalized amplitude of NMDAR EPSC decreased in the presence of 100 μM PA-S by 51 ± 3% ($p < 0.001$; $n = 8$). This was significantly different from the degree of the tonic current inhibition (Fig. 5*F* and red symbol in Fig. 5*G*; $p < 0.001$). We used the degree of NMDAR EPSC inhibition by 100 μM PA-S (Eq. 2) to calculate the PA-S IC_{50} at postsynaptic NMDARs (100 ± 10 μM; $n = 8$). These results demonstrate that PA-S is ~3-fold more potent at inhibiting tonically over synaptically activated NMDARs. We also examined PA-S inhibition of tonic currents evoked by 10 μM NMDA (data not shown) because the degree of inhibition is expected to depend on agonist concentration. PA-S (100 μM) inhibited tonic currents evoked by 10 μM NMDA by 71 ± 3% ($n = 9$), so a more conservative estimate of the PA-S IC_{50} for tonic current inhibition is 50 ± 7 μM, still 2-fold lower than the IC_{50} for PA-S inhibition of NMDAR EPSCs.

PDF-XChange Editor
KOUPIT plnou verzi!
www.pdfxchange.cz

Table 1. Quantitative characteristics of PA analogs

		$\Delta\alpha G_{solv}$ (kcal/mol SMD) transfer:						
		Vacuum to water		n-octanol to water				
Steroid	ΔG_{exp} (kcal/mol)	Neutral	Charged	Neutral	Charged	LogP	LogD	Steroid length (Å)
PA-hOxa	−5.92	−16.17	−75.48	3.57	−4.59	5.15	1.12	2.9
PA-hMal	−5.87	−20.80	−81.07	3.33	−5.19	4.96	1.27	4.5
PA-hSuc	−6.18	−24.67	−84.72	3.23	−5.11	4.95	1.16	6.3
PA-hGlu	−6.49	−26.56	−87.64	3.34	−5.12	5.25	1.68	7.6
PA-hAdi	−6.41	−25.91	−87.65	4.18	−4.28	5.96	2.12	8.9
PA-hPim	−6.51	−26.50	−88.25	4.62	−3.84	6.44	2.49	10.2
Correlation coefficient; *p*		(0.9; 0.020)	(0.9; 0.015)	(−0.5; >0.050)	(−0.5; >0.050)	(−0.7; >0.050)	(−0.8; 0.0488)	(−0.9; 0.011)

The experimental binding free energies (ΔG_{exp}) expressed from the IC_{50} values via the equation $\delta G_{exp} = RT\ln(IC_{50})$ were compared with the calculated values of ΔG_{solv}, LogP, and LogD. The negative values of ΔG_{solv} indicate the energy gained and the positive values indicate the energy required during the transfer from the first phase to the second phase. Linear regression was used for the correlation between ΔG_{exp} and the calculated data. The Pearson correlation coefficient was used to determine how well the calculated data approximate the experimental data; the values of *r* and *p* are given in parentheses. Steroid length indicates the distance spanning the carboxyl moiety and the C3 carbon.

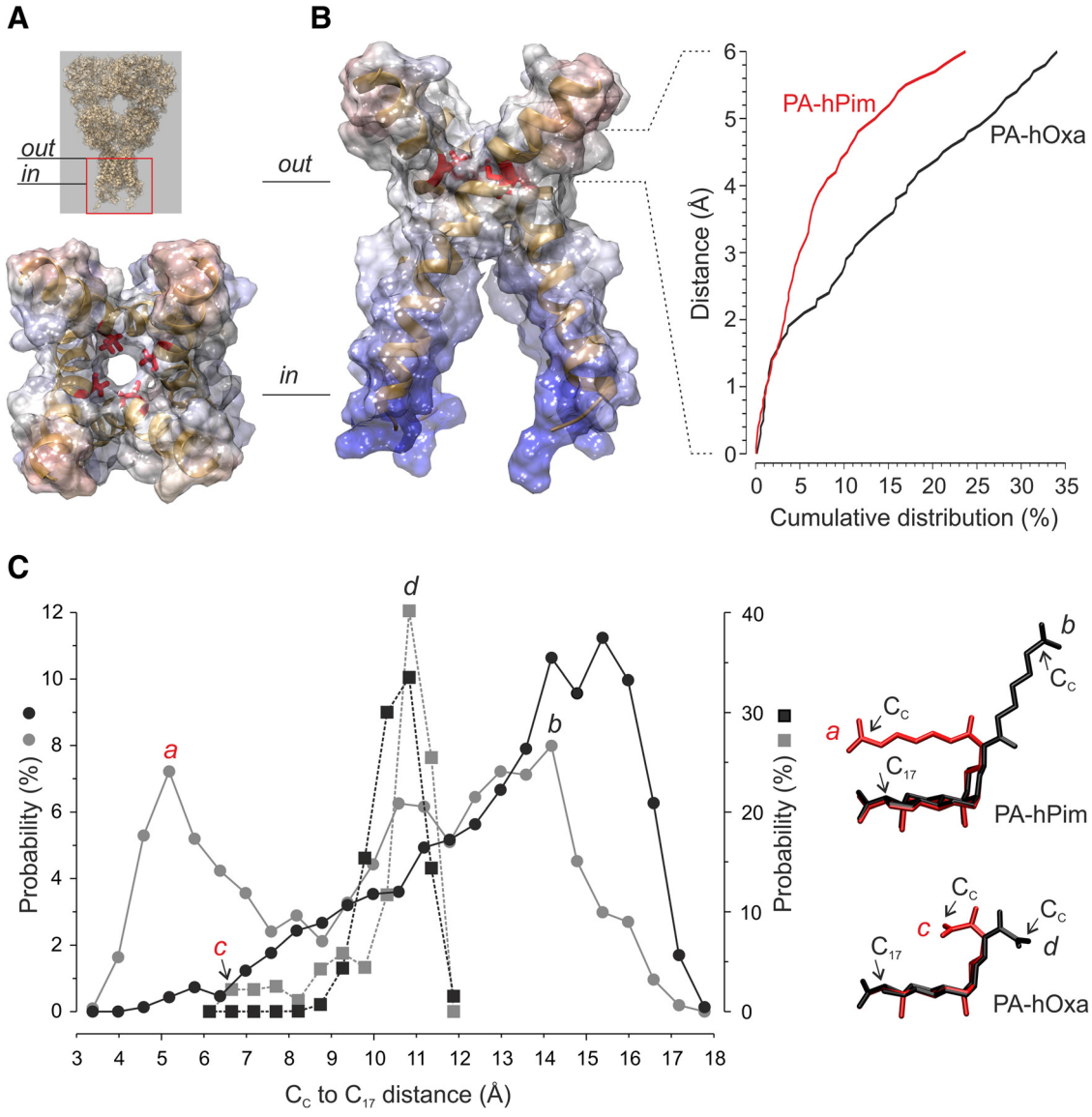


Figure 4. Interaction of steroids with the model of the activated state of the NMDAR. ***A***, M3 helices in the model of the activated state of NMDAR. Gating Thr residues are shown as red sticks. The surface is colored according to the electrostatic potential (blue/white/red as positive/neutral/negative). ***B***, Results of a docking analysis showing the probability of finding PA-hOxa and PA-hPim derivatives within the channel vestibule. It was assessed as the vertical distance between the nearest steroid atom to the plane defined by the Cα of the threonines (648/647). The position of Thr residues is marked with the bottom dashed line. ***C***, Difference between the distribution of PA-hPim conformers in the water environment (obtained from the MD quench, black curve) compared with the interior of the activated channel (from the docking, gray curve) shown as the distance from the terminal carboxyl group to the C17 carbon of the steroid skeleton.

PDF-XChange Editor
KOUPIT plnou verzi!
www.pdfxchange.cz

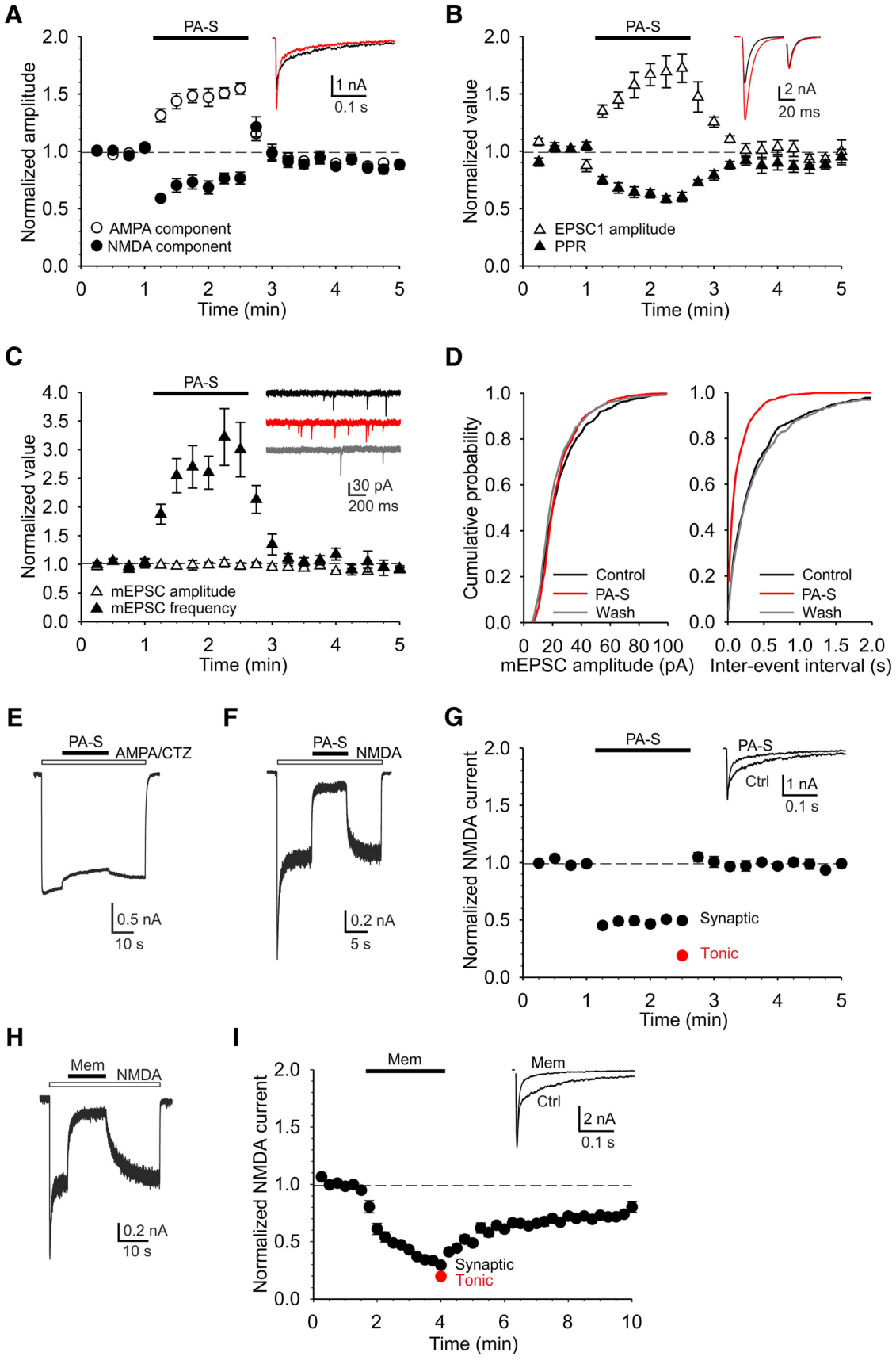


Figure 5. Effects of PA-S on native receptors and synaptic transmission. ***A***, Plot of the normalized amplitude of the AMPAR and the NMDAR component of dual EPSCs recorded before, during, and after 100 μM PA-S application. Inset, Sample dual EPSC traces recorded in control (black) and in the presence of 100 μM PA-S (red). ***B***, Plot of the normalized amplitude and paired-pulse ratio of pharmacologically isolated AMPAR EPSCs recorded before, during, and after PA-S (100 μM) application. Inset, Sample AMPAR EPSC traces recorded in control (black) and in the presence of 100 μM PA-S (red). ***C***, Plot of the normalized AMPA mEPSC amplitude and frequency recorded before, during, and after PA-S (100 μM) application. Inset, Sample traces (*Figure legend continues.*)

PDF-XChange Editor
KOUPIT plnou verzi!
www.pdfxchange.cz

The degree of PA-S selectivity for tonic over synaptic inhibition is similar to or higher than that reported for memantine (Xia et al., 2010; Emnett et al., 2013) and we wanted to confirm this in our system. Memantine (5 μM) inhibited tonic currents evoked in cultured hippocampal neurons by 300 μM NMDA by 80 ± 2% (Fig. 5*H*; $n = 6$), so the resulting memantine IC_{50} for tonic inhibition was 1.6 ± 0.2 μM. To examine synaptic effects of memantine, we again recorded dual EPSCs. The AMPAR component of the dual EPSC (data not shown) was unaffected by memantine (5 μM) applied for 2.5 min (+2.4 ± 1.3%; $n = 6$) and remained stable throughout the 10 min recording. In contrast, memantine inhibited the NMDAR component of the dual EPSC by 67 ± 2% ($p < 0.001$; $n = 6$). This effect had a slow onset and was only partially reversible in the time of the experiment. The degree of the NMDAR EPSC inhibition by memantine (Fig. 5*I*) was used to calculate the memantine IC_{50} at postsynaptic NMDARs (2.5 ± 0.1 μM; $n = 6$). Therefore, under our conditions, memantine is ~1.5-fold more potent at inhibiting tonic over synaptic NMDAR currents.

We tested the most promising PA-S analog, PA-hPim, at native NMDARs activated phasically during synaptic transmission versus tonically by prolonged agonist application. After PA-hPim (15 μM) application for 1.5 min, the amplitude of both components of the dual EPSC increased slightly relative to baseline (by 9.3 ± 9.0% for AMPA and by 21 ± 10% for NMDA; $n = 10$; Fig. 6*A*). At the same time, PA-hPim significantly decreased τ_w of the NMDAR component of the dual EPSC from 213 ± 5 ms to 170 ± 13 ms ($p = 0.007$; $n = 10$). This was due to a decrease in τ_s ($p = 0.006$) and τ_f ($p = 0.002$), without a change in the relative proportion of τ_f ($p = 0.876$). To distinguish presynaptic and postsynaptic effects of PA-hPim, we again examined pharmacologically isolated AMPAR EPSCs. The amplitude of AMPAR EPSCs increased during 15 μM PA-hPim application (Fig. 6*B*, by 30 ± 11%; $p = 0.201$ for the comparison between the potentiation of AMPAR component of the dual EPSC vs pure AMPAR EPSC). The paired-pulse ratio of AMPAR EPSCs was 0.67 ± 0.05 before steroid application and tended to decrease to 0.61 ± 0.06 ($p = 0.084$; $n = 7$) after 1.5 min of PA-hPim application. In agreement with the tendency to decrease the paired-pulse ratio, PA-hPim increased the frequency of AMPAR mEPSCs by 206 ± 90% of baseline ($p = 0.031$; $n = 6$; Fig. 6*C*), with a minimal effect on AMPAR mEPSC amplitude (+5.4 ± 2.0%, $p = 0.065$; $n = 6$). The analysis of the cumulative distribution of interevent intervals by the K-S test showed a significant shift toward lower values in the presence of PA-hPim in 5/6 cells. In contrast, the cumulative distribution of mEPSC amplitudes was altered in only 2/6 cells tested (Fig. 6*D*). Together, these data indicate that PA-hPim, like PA-S, potentiates AMPAR EPSCs largely through a presynaptic mechanism. Accordingly, responses to AMPA (5 μM) recorded in the presence of cyclothiazide (10 μM) were inhibited by PA-hPim (15 μM) by only 3.7 ± 1.0% of control ($n = 6$; Fig. 6*E*).

Next, we compared the inhibition of tonically versus synaptically activated native NMDARs by PA-hPim. PA-hPim (15 μM) robustly inhibited tonic 300 μM NMDA-evoked currents (Fig. 6*F*), on average by 70 ± 2% ($n = 6$; red symbol in Fig. 6*G*). These data were used to determine the PA-hPim IC_{50} for tonic inhibition of native NMDARs (7.4 ± 0.6 μM; $n = 6$). A more conservative estimate, determined from PA-hPim (15 μM) inhibition of tonic currents evoked by 10 μM NMDA, was 12 ± 1 μM ($n = 6$). To examine the effect of PA-hPim on synaptically activated NMDARs, we again used the ratio of the NMDAR/AMPAR component of the dual EPSC as an indicator of the steroid effect at postsynaptic NMDARs. Similarly to experiments on recombinant receptors, PA-hPim did not inhibit synaptically activated NMDARs (Fig. 6*G*). In fact, the normalized amplitude of NMDAR EPSCs increased slightly in the presence of 15 μM PA-hPim, by 12 ± 4% ($p = 0.011$; $n = 10$). It was therefore not possible to calculate the IC_{50} for PA-hPim inhibition of synaptically activated NMDARs, further emphasizing the remarkable selectivity of this novel synthetic steroid for inhibiting tonically activated NMDARs.

Behavioral experiments

Neuroprotective effects have been described for different classes of NMDAR antagonists, but their systemic application often leads to serious side effects ranging from motor impairment to the induction of schizophrenic-like psychosis (Krystal et al., 1994; Newcomer and Krystal, 2001). Therefore, we examined behavioral effects of systemic PA-hPim administration with the aim of testing its psychomimetic and neuroprotective activity. Psychomimetic symptoms were assessed first by monitoring locomotor activity in the open field (Bubser et al., 1992). Systemic PA-hPim administration (1 mg/kg or 10 mg/kg) did not induce hyperlocomotion (Fig. 7*A*). The higher dose tended to decrease the total distance traveled (ANOVA: $p = 0.022$), but the *post hoc* comparisons of PA-hPim versus β-CDX detected no significant differences. In contrast, the administration of MK-801 (0.2 and 0.3 mg/kg) caused a robust increase in locomotion (Fig. 7*A*; ANOVA: $p = 0.023$). Potential cognitive side effects of PA-hPim were assessed by testing spatial cognition in a step-through passive avoidance task and by testing working memory in a spontaneous alternation task in the Y-maze (Parada-Turska and Turski, 1990). The administration of PA-hPim (1 or 10 mg/kg) had no effect on performance in the step-through passive avoidance test (Fig. 7*B*; ANOVA: $p = 0.057$). In contrast, MK-801 completely disrupted learning in the passive avoidance task at all doses tested (Fig. 7*B*; ANOVA: $p < 0.001$). Similarly, PA-hPim (1 mg/kg or 10 mg/kg) had no effect on spontaneous alternation in the Y-maze (Fig. 7*C*; ANOVA: $p = 0.067$), whereas MK-801 reduced performance (Fig. 7*C*; ANOVA: $p = 0.015$). Together, these tests confirm the lack of undesirable psychomimetic and cognitive side effects of PA-hPim, in contrast to the NMDAR channel blocker MK-801, which causes significant hyperlocomotion and cognitive impairment.

We tested PA-hPim neuroprotective potential in a model of NMDA-induced hippocampal lesion. We tested spatial learning in the MWM for three groups of animals (see Materials and Methods): controls, animals with an intrahippocampal infusion

←

(*Figure legend continued.*) recorded in control (black), in the presence of 100 μM PA-S (red), and after PA-S washout (gray). ***D***, Mean cumulative probability plots of AMPA mEPSC amplitudes and interevent intervals. ***E***, Response of a cultured hippocampal neuron to AMPA (5 μM, in the presence of 10 μM CTZ), illustrating the small steady-state AMPAR current inhibition by PA-S (100 μM). ***F***, Response of a cultured hippocampal neuron to NMDA (300 μM) illustrating the robust steady-state NMDAR current inhibition by PA-S (100 μM). ***G***, Plot of the normalized ratio of the NMDAR/AMPAR EPSC amplitude calculated from data shown in ***A*** (synaptic NMDAR currents, black symbols). Mean ± SEM of the normalized steady-state NMDA-evoked current in the presence of 100 μM PA-S obtained from experiments illustrated in ***F*** (tonic NMDAR currents, red symbol). Inset shows dual EPSC traces in control and in the presence of PA-S (100 μM) normalized to the control peak (AMPA) EPSC amplitude. ***H***, Response of a cultured hippocampal neuron to NMDA (300 μM) illustrating the steady-state current inhibition by memantine (5 μM). ***I***, Plot of the normalized ratio of the NMDAR/AMPAR EPSC amplitude (synaptic NMDAR currents, black symbols). Also shown is the mean ± SEM of the normalized steady-state NMDA-evoked current in the presence of 5 μM memantine obtained from experiments illustrated in ***H*** (tonic NMDAR currents, red symbol). Inset, Dual EPSC traces in control and in the presence of memantine (5 μM) normalized to the control peak (AMPA) EPSC amplitude.

PDF-XChange Editor
KOUPIT plnou verzi!
www.pdfxchange.cz

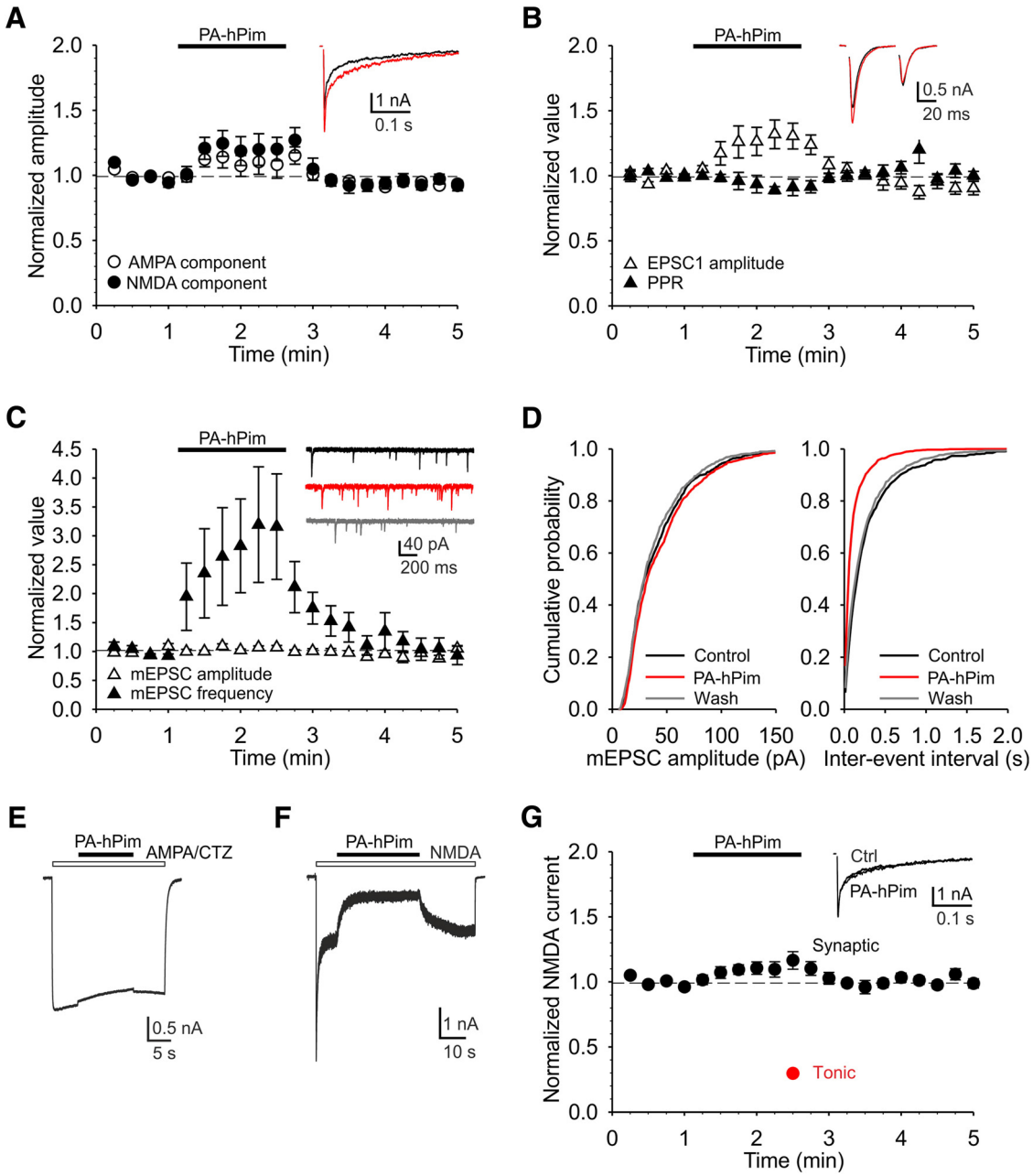


Figure 6. Effects of PA-hPim on native receptors and synaptic transmission. ***A***, Plot of the normalized amplitude of the AMPAR and the NMDAR component of the dual EPSCs recorded before, during, and after 15 μM PA-hPim application. Inset, Sample dual EPSC traces recorded in control (black) and in the presence of 15 μM PA-hPim (red). ***B***, Plot of the normalized AMPAR EPSC amplitude and paired-pulse ratio recorded before, during, and after PA-hPim (15 μM) application. Inset, Sample AMPAR EPSC traces recorded in control (black) and in the presence of 15 μM PA-hPim (red). ***C***, Plot of the normalized AMPAR mEPSC amplitude and frequency recorded before, during, and after PA-hPim (15 μM) application. Inset, Sample traces recorded in control (black), in the presence of 15 μM PA-hPim (red), and after PA-hPim washout (gray). ***D***, Mean cumulative probability plots of AMPAR mEPSC amplitudes and interevent intervals. ***E***, Response of a cultured hippocampal neuron to AMPA (5 μM, in the presence of 10 μM CTZ) illustrating the small steady-state AMPAR current inhibition by PA-hPim (15 μM). ***F***, Response of a cultured hippocampal neuron to NMDA (300 μM) illustrating the robust steady-state NMDAR current inhibition by PA-hPim (15 μM). ***G***, Plot of the normalized ratio of the NMDAR/AMPAR EPSC amplitude calculated from data shown in ***A*** (synaptic NMDAR currents, black symbols). Also shown is the mean ± SEM of the normalized steady-state NMDA-evoked current in the presence of 15 μM PA-hPim obtained from experiments illustrated in ***F*** (tonic NMDAR currents, red symbol). Inset, Dual EPSC traces in control and in the presence of PA-hPim (15 μM) normalized to the control peak (AMPA) EPSC amplitude.

of NMDA, and animals with an intrahippocampal infusion of NMDA followed by a systemic administration of 1 mg/kg PA-hPim (Fig. 7*D*). Our results indicate that all groups successfully learned to navigate to the hidden goal in the MWM, but the NMDA-lesioned group showed slower learning and this was especially apparent on day 2 of the training. Systemic administration of PA-hPim (1 mg/kg) after the NMDA infusion eliminated this learning deficit (Fig. 7*D*; two-way RM ANOVA: effect of training day $p < 0.001$; effect of group $p = 0.113$; interaction $p = 0.004$). Together, our behavioral results show that PA-hPim has neuroprotective properties without psychomimetic side effects.

Discussion

Our study demonstrates that endogenous neurosteroid PA-S and its analogs are effective antagonists of tonically activated NMDARs with a smaller or no effect on the amplitude of NMDAR EPSCs. Further, we show that steroids have a neuroprotective effect against cognitive deficits induced by NMDA infu-

PDF-XChange Editor
KOUPIT plnou verzi!
www.pdfxchange.cz

sion into the hippocampus, but, in contrast to MK-801, they do not induce psychomimetic symptoms in experimental animals.

Steroid inhibition of tonically and phasically activated NMDARs

We find that PA-S and its synthetic analogs inhibit tonically activated GluN1/GluN2A or GluN1/GluN2B receptors with a higher potency than phasically activated receptors. For GluN1/GluN2B receptors, this difference in potency was ~2-fold for the endogenous steroid PA-S and ~3-fold for synthetic steroids with a short substituent, such as PA-hOxa. Remarkably, PA-hPim, the synthetic derivative with the longest substituent, exhibited no effect at phasically activated receptors while inhibiting tonically activated receptors. To avoid the effect of slow steroid diffusion to the site of action at the NMDAR (Borovska et al., 2012; Vyklicky et al., 2015), the inhibition of tonically and phasically activated NMDAR was estimated from responses made in the continuous presence of the steroid. Due to the nature of the steroid–receptor interaction, the onset of inhibition is slow (hundreds of milliseconds) compared with the relatively fast onset of the NMDAR responses induced by 1 mM glutamate (tens of milliseconds). This difference, together with the fact that PA-S binding to the NMDAR can occur only in the presence of the agonist (i.e., it is use dependent; Petrovic et al., 2005; Kussius et al., 2009; Vyklicky et al., 2015), underlie the lower sensitivity of the peak versus the steady-state NMDAR response to inhibitory steroids.

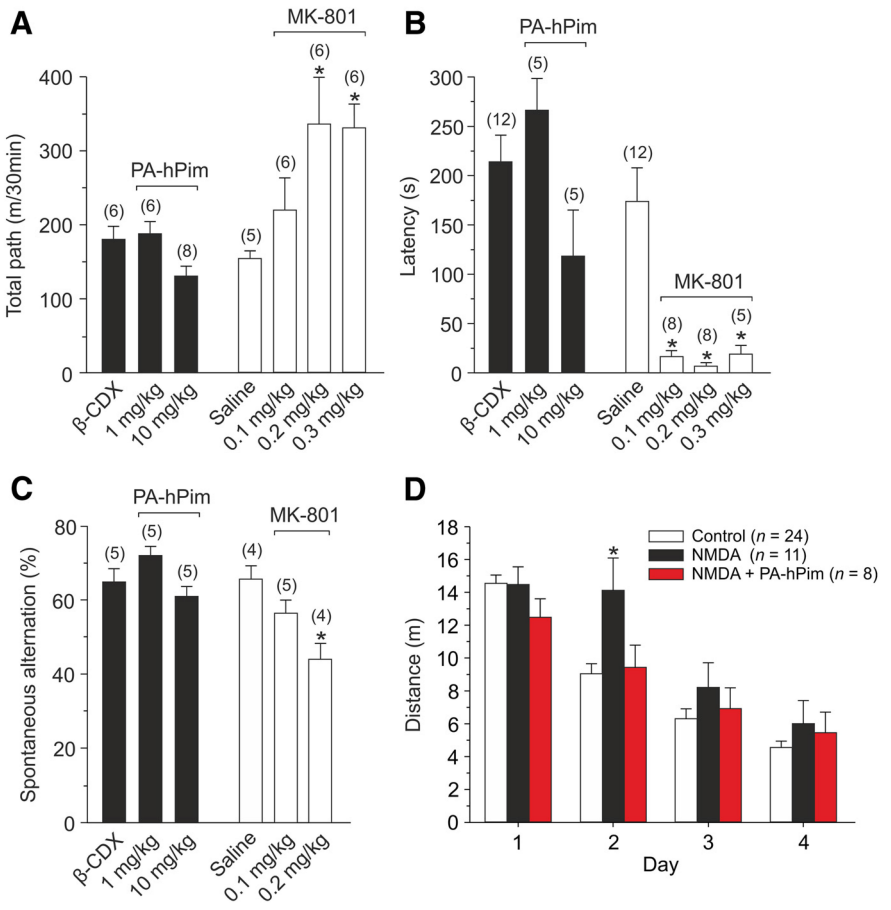


Figure 7. PA-hPim does not induce psychomimetic-like behavior, but reverses the learning deficit induced by intrahippocampal NMDA infusion. ***A***, Effect of PA-hPim (1 and 10 mg/kg) and MK-801 (0.1, 0.2, and 0.3 mg/kg) on locomotor activity in a novel environment in an open-field test. ***B***, Effect of PA-hPim (1 and 10 mg/kg) and MK-801 (0.1, 0.2, and 0.3 mg/kg) on step-through passive avoidance. ***C***, Effect of PA-hPim (1 and 10 mg/kg) and MK-801 (0.1 and 0.2 mg/kg) on spontaneous alternation in a Y-maze. ***D***, Effect of intrahippocampal NMDA infusion with or without subsequent systemic PA-hPim (1 mg/kg) treatment on spatial learning in the MWM. Plot shows the total path traveled to find the hidden platform. On day 2, NMDA infusion deteriorated spatial learning and PA-hPim prevented this learning deficit. One-way ANOVA was used to compare data in ***A***–***C*** and two-way ANOVA was used in ***D***. *Significant difference detected with a *post hoc* test.

PA derivatives with longer aliphatic chains show slower onset of inhibition compared with PA-S, which is important for their strong selectivity for steady-state over peak NMDAR responses. Our computational study suggests that steroids have a nonspecific affinity to the whole inner surface of the NMDAR channel vestibule. These nonpolar steroid–receptor interactions are accompanied by an induced change of the conformation of the steroids in the channel vestibule. The inhibitor with the longest chain (PA-hPim) forms intramolecular interactions between the steroid skeleton and the aliphatic chain, which enables it to attain a more compact conformation. The character of the inhibition (Fig. 2*D*) can be explained by the balance between the effect of the conformation change and the increase of the interaction energy due to the growing number of the interacting atoms. This process is slow because of a series of successive associations and dissociations and causes the slow onset of the steroid inhibition.

There are two additional pharmacodynamic properties of steroid-induced NMDAR inhibition that are likely to be clinically relevant. First, the peak amplitude and the ratio of the steady-state/peak were not significantly changed for the first and the subsequent NMDAR response made in the presence of steroid. This indicates that, in contrast to the onset of inhibition, which requires NMDAR activation, steroid dissociation proceeds at the same rate independently of receptor activation (Petrovic et al., 2005). This foot-in-the-door mechanism of inhibition (Sobolevskii and Khodorov, 2002; Vyklicky et al., 2014, 2015) is critical for the ability of steroids to inhibit steady-state responses while leaving the peak relatively intact. In contrast, trapping blockers such as memantine cannot dissociate from the receptor in the absence of the agonist, progressively inhibiting peak responses more strongly with repeated receptor activation. The second useful property of steroid-induced NMDAR inhibition is its voltage independence (Petrovic et al., 2005), which ensures that steroids would remain effective even in pathologically depolarized cells. In contrast, NMDAR inhibition by memantine becomes weaker at depolarized potentials (Chen et al., 1992).

Steroid modulation of synaptic transmission

We show that steroids (PA-S and PA-hPim) have multiple effects on synaptic transmission. Consistent with the results obtained on recombinant receptors, the postsynaptic effects were characterized by a lower degree of inhibition of NMDAR EPSCs than of tonic NMDA currents, with no postsynaptic effect on the AMPA EPSC. The decrease in the paired-pulse ratio and the increase in the frequency of AMPA mEPSC are consistent with a presynaptic

PDF-XChange Editor
KOUPIT plnou verzi!
www.pdfxchange.cz

increase in the probability of glutamate release by PA-S and its synthetic analogs. A similar presynaptic potentiation has been described in various preparations for pregnenolone sulfate, a positive NMDAR modulator (Meyer et al., 2002; Mameli et al., 2005; Zamudio-Bulcock and Valenzuela, 2011), but the cellular mechanisms of steroid presynaptic actions are not well understood. Interestingly, the presynaptic potentiation further amplifies the selectivity of NMDAR inhibitory steroids for tonically over synaptically activated NMDARs and may contribute to their lack of undesirable side effects. It is not clear how the presynaptic potentiation may influence steroid neuroprotective properties. The potentiation of synaptic glutamate release could contribute to extracellular glutamate accumulation under pathological conditions (Wroge et al., 2012) and thus reduce steroid neuroprotective potential. Conversely, synaptic NMDAR stimulation via the presynaptic mechanism, combined with the selective inhibition of tonic NMDAR signaling, may be particularly effective at shifting the balance of synaptic versus extrasynaptic NMDAR signaling toward promoting cell survival (Hardingham and Bading, 2010). Potential advantages or disadvantages of presynaptic modulation by steroids will thus be an important issue to address in future studies.

We find that the endogenous neurosteroid PA-S inhibits tonically activated native NMDARs with ~3-fold higher potency than synaptically activated NMDARs. This difference in potency is at least as good as that reported previously (Xia et al., 2010) for therapeutic doses of memantine, which was suggested to underlie the tolerability of this clinically approved drug in patients suffering from Alzheimer's disease. However, others (Emnett et al., 2013) show that, in the continuous presence of memantine, synaptic NMDAR responses to repeated stimulation become progressively more inhibited, eventually resulting in minimal memantine selectivity for tonically over synaptically activated receptors. Our own results are more in agreement with Emnett et al. (2013) and confirm that PA-S is more selective than memantine for tonically over synaptically activated NMDARs. Further, our data show that the synthetic PA-S analog PA-hPim with the highest selectivity for inhibiting tonically over phasically activated recombinant receptors does not inhibit synaptically activated native NMDARs at all and in fact slightly potentiates their responses. Steroids thus represent a very promising therapeutic agent for excitotoxicity associated with acute and chronic NMDAR overstimulation.

Steroid neuroprotective action *in vivo*

Application of drugs inhibiting the NMDAR often shows a protective effect on the behavioral consequences of excitatory damage. However, many such drugs are excluded from the search for potential human neuroprotectants due to their significant side effects ranging from sensory and motor disturbances to the induction of schizophrenia-like symptoms such as hyperlocomotion and cognitive deficit. In fact, acute administration of noncompetitive NMDAR antagonists, such as dizocilpine (MK-801), to laboratory rodents is a commonly used and extensively validated animal model of schizophrenia (Young et al., 2010; Micale et al., 2013). Memantine appears to be well tolerated clinically, but in animal studies, the neuroprotective dose of 20 mg/kg memantine (Chen et al., 1992) does cause hyperlocomotion (Bubser et al., 1992) and even lower doses induce cognitive impairments (Dix et al., 2010). After systemic administration of PA-hPim at 2 doses (1 mg/kg or 10 mg/kg), we found no evidence of hyperlocomotion in the open field and no cognitive impairment in the passive avoidance task or in the spontaneous alternation test in the Y-maze. In contrast, MK-801, which is neuroprotective in the dose range 0.1–1 mg/kg (McDonald et al., 1990), caused severe cognitive impairment at doses ≥0.1 mg/kg and induced hyperlocomotion at doses ≥0.2 mg/kg. We evaluated the neuroprotective effect of PA-hPim (1 mg/kg) on spatial learning performance in rats with NMDA-induced bilateral lesion of the hippocampus, a model of excitotoxic neurodegeneration (Wang et al., 1991). The performance of NMDA-lesioned animals treated with PA-hPim was significantly better than the performance of animals with the NMDA lesion and no different from the performance of control animals. The neuroprotective effect of PA-hPim is consistent with several reports of neuroprotective properties of other neuroactive steroid derivatives such as preganolone hemisuccinate (Weaver et al., 1997; Lapchak, 2004, 2006), pregnanolone glutamate (Rambousek et al., 2011), or pregnanolone valinate (MacNevin et al., 2009).

In summary, we show that PA-S and its synthetic analogs inhibit tonically activated NMDARs with a higher potency than excitatory neurotransmission and that steroid neuroprotective activity in behavioral tests is devoid of psychomimetic side effects. Our results provide valuable insights into the influence of neurosteroids on neuronal function and emphasize their potential use in the development of novel therapeutics with neuroprotective action.

References

Ahlrichs R, Bar M, Haser M, Horn H, Kolmel C (1989) Electronic-structure calculations on workstation computers–the program system turbomole. Chemical Physics Letters 162:165–169. CrossRef

Baker NA, Sept D, Joseph S, Holst MJ, McCammon JA (2001) Electrostatics of nanosystems: application to microtubules and the ribosome. Proc Natl Acad Sci U S A 98:10037–10041. CrossRef Medline

Barratt E, Bronowska A, Vondrásek J, Cerný J, Bingham R, Phillips S, Homans SW (2006) Thermodynamic penalty arising from burial of a ligand polar group within a hydrophobic pocket of a protein receptor. J Mol Biol 362:994–1003. CrossRef Medline

Bayly CI, Cieplak P, Cornell WD, Kollman PA (1993) A well-behaved electrostatic potential based method using charge restraints for deriving atomic charges–the resp model. J Phys Chem 97:10269–10280. CrossRef

Beck C, Wollmuth LP, Seeburg PH, Sakmann B, Kuner T (1999) NMDAR channel segments forming the extracellular vestibule inferred from the accessibility of substituted cysteines. Neuron 22:559–570. CrossRef Medline

Blanpied TA, Boeckman FA, Aizenman E, Johnson JW (1997) Trapping channel block of NMDA-activated responses by amantadine and memantine. J Neurophysiol 77:309–323. Medline

Borovska J, Vyklicky V, Stastna E, Kapras V, Slavikova B, Horak M, Chodounska H, Vyklicky L Jr (2012) Access of inhibitory neurosteroids to the NMDA receptor. Br J Pharmacol 166:1069–1083. CrossRef Medline

Bubser M, Keseberg U, Notz PK, Schmidt WJ (1992) Differential behavioural and neurochemical effects of competitive and non-competitive NMDA receptor antagonists in rats. Eur J Pharmacol 229:75–82. CrossRef Medline

Burgalossi A, Jung S, Man KN, Nair R, Jockusch WJ, Wojcik SM, Brose N, Rhee JS (2012) Analysis of neurotransmitter release mechanisms by photolysis of caged Ca2+ in an autaptic neuron culture system. Nat Protoc 7:1351–1365. CrossRef Medline

Cavelier P, Hamann M, Rossi D, Mobbs P, Attwell D (2005) Tonic excitation and inhibition of neurons: ambient transmitter sources and computational consequences. Prog Biophys Mol Biol 87:3–16. CrossRef Medline

Chen HS, Pellegrini JW, Aggarwal SK, Lei SZ, Warach S, Jensen FE, Lipton SA (1992) Open-channel block of N-methyl-D-aspartate (NMDA) responses by memantine: therapeutic advantage against NMDA receptor-mediated neurotoxicity. J Neurosci 12:4427–4436. Medline

Choi DW (1987) Ionic dependence of glutamate neurotoxicity. J Neurosci 7:369–379. Medline

Choi DW, Rothman SM (1990) The role of glutamate neurotoxicity in hypoxic-ischemic neuronal death. Annu Rev Neurosci 13:171–182. CrossRef Medline

PDF-XChange Editor
KOUPIT plnou verzi!
www.pdfxchange.cz

Clements JD, Lester RA, Tong G, Jahr CE, Westbrook GL (1992) The time course of glutamate in the synaptic cleft. Science 258:1498–1501. CrossRef Medline

Dix S, Gilmour G, Potts S, Smith JW, Tricklebank M (2010) A within-subject cognitive battery in the rat: differential effects of NMDA receptor antagonists. Psychopharmacology 212:227–242. CrossRef Medline

Emnett CM, Eisenman LN, Taylor AM, Izumi Y, Zorumski CF, Mennerick S (2013) Indistinguishable synaptic pharmacodynamics of the N-methyl-D-aspartate receptor channel blockers memantine and ketamine. Mol Pharmacol 84:935–947. CrossRef Medline

Faucher F, Cantin L, Luu-The V, Labrie F, Breton R (2008) The crystal structure of human Delta4–3-ketosteroid 5beta-reductase defines the functional role of the residues of the catalytic tetrad in the steroid double bond reduction mechanism. Biochemistry 47:8261–8270. CrossRef Medline

Grimme S, Antony J, Ehrlich S, Krieg H (2010) A consistent and accurate ab initio parametrization of density functional dispersion correction (DFT-D) for the 94 elements H-Pu. J Chem Phys 132:154104. CrossRef Medline

Hardingham GE, Bading H (2010) Synaptic versus extrasynaptic NMDA receptor signalling: implications for neurodegenerative disorders. Nat Rev Neurosci 11:682–696. CrossRef Medline

Hardingham GE, Fukunaga Y, Bading H (2002) Extrasynaptic NMDARs oppose synaptic NMDARs by triggering CREB shut-off and cell death pathways. Nat Neurosci 5:405–414. Medline

Herman MA, Jahr CE (2007) Extracellular glutamate concentration in hippocampal slice. J Neurosci 27:9736–9741. CrossRef Medline

Huganir RL, Nicoll RA (2013) AMPARs and synaptic plasticity: the last 25 years. Neuron 80:704–717. CrossRef Medline

Jurecka P, Cerný J, Hobza P, Salahub DR (2007) Density functional theory augmented with an empirical dispersion term. Interaction energies and geometries of 80 noncovalent complexes compared with ab initio quantum mechanics calculations. J Comput Chem 28:555–569. CrossRef Medline

Karakas E, Furukawa H (2014) Crystal structure of a heterotetrameric NMDA receptor ion channel. Science 344:992–997. CrossRef Medline

Klamt A, Schuurmann G (1993) Cosmo–a new approach to dielectric screening in solvents with explicit expressions for the screening energy and its gradient. J Chem Soc Perk T 2:799–805.

Krystal JH, Karper LP, Seibyl JP, Freeman GK, Delaney R, Bremner JD, Heninger GR, Bowers MB Jr, Charney DS (1994) Subanesthetic effects of the noncompetitive NMDA antagonist, ketamine, in humans: psychotomimetic, perceptual, cognitive, and neuroendocrine responses. Archives of General Psychiatry 51:199–214. CrossRef Medline

Kudova E, Chodounska H, Slavikova B, Budesinsky M, Nekardova M, Vyklicky V, Krausova B, Svehla P, Vyklicky L (2015) A new class of potent N-methyl-D-aspartate receptor inhibitors: sulfated neuroactive steroids with lipophilic D-ring modifications. J Med Chem 58:5950–5966. CrossRef Medline

Kussius CL, Kaur N, Popescu GK (2009) Pregnanolone sulfate promotes desensitization of activated NMDA receptors. J Neurosci 29:6819–6827. CrossRef Medline

Lapchak PA (2004) The neuroactive steroid 3-alpha-ol-5-beta-pregnan-20-one hemisuccinate, a selective NMDA receptor antagonist improves behavioral performance following spinal cord ischemia. Brain Res 997:152–158. CrossRef Medline

Lapchak PA (2006) 3alpha-OL-5-beta-pregnan-20-one hemisuccinate, a steroidal low-affinity NMDA receptor antagonist improves clinical rating scores in a rabbit multiple infarct ischemia model: synergism with tissue plasminogen activator. Exp Neurol 197:531–537. CrossRef Medline

Lee CH, Lü W, Michel JC, Goehring A, Du J, Song X, Gouaux E (2014) NMDA receptor structures reveal subunit arrangement and pore architecture. Nature 511:191–197. CrossRef Medline

Léveillé F, El Gaamouch F, Gouix E, Lecocq M, Lobner D, Nicole O, Buisson A (2008) Neuronal viability is controlled by a functional relation between synaptic and extrasynaptic NMDA receptors. FASEB J 22:4258–4271. CrossRef Medline

Lipton SA (1993) Prospects for clinically tolerated NMDA antagonists: open-channel blockers and alternative redox states of nitric oxide. Trends Neurosci 16:527–532. CrossRef Medline

Lynch MA (2004) Long-term potentiation and memory. Physiol Rev 84:87–136. CrossRef Medline

MacNevin CJ, Atif F, Sayeed I, Stein DG, Liotta DC (2009) Development and screening of water-soluble analogs of progesterone and allopregnanolone in models of brain injury. J Med Chem 52:6012–6023. CrossRef Medline

Mameli M, Carta M, Partridge LD, Valenzuela CF (2005) Neurosteroid-induced plasticity of immature synapses via retrograde modulation of presynaptic NMDA receptors. J Neurosci 25:2285–2294. CrossRef Medline

Manahan-Vaughan D, von Haebler D, Winter C, Juckel G, Heinemann U (2008) A single application of MK801 causes symptoms of acute psychosis, deficits in spatial memory, and impairment of synaptic plasticity in rats. Hippocampus 18:125–134. CrossRef Medline

McDonald JW, Silverstein FS, Cardona D, Hudson C, Chen R, Johnston MV (1990) Systemic administration of MK-801 protects against N-methyl-D-aspartate- and quisqualate-mediated neurotoxicity in perinatal rats. Neuroscience 36:589–599. CrossRef Medline

Meyer DA, Carta M, Partridge LD, Covey DF, Valenzuela CF (2002) Neurosteroids enhance spontaneous glutamate release in hippocampal neurons. J Biol Chem 277:28725–28732. CrossRef Medline

Micale V, Kucerova J, Sulcova A (2013) Leading compounds for the validation of animal models of psychopathology. Cell Tissue Res 354:309–330. CrossRef Medline

Mikulecká A, Subrt M, Stuchlík A, Kubová H (2014) Consequences of early postnatal benzodiazepines exposure in rats. I. Cognitive-like behavior. Front Behav Neurosci 8:101. Medline

Newcomer JW, Krystal JH (2001) NMDA receptor regulation of memory and behavior in humans. Hippocampus 11:529–542. Medline

Olney JW (1969) Brain lesions, obesity, and other disturbances in mice treated with monosodium glutamate. Science 164:719–721. CrossRef Medline

Papadia S, Soriano FX, Léveillé F, Martel MA, Dakin KA, Hansen HH, Kaindl A, Sifringer M, Fowler J, Stefovska V, McKenzie G, Craigon M, Corriveau R, Ghazal P, Horsburgh K, Yankner BA, Wyllie DJ, Ikonomidou C, Hardingham GE (2008) Synaptic NMDA receptor activity boosts intrinsic antioxidant defenses. Nat Neurosci 11:476–487. CrossRef Medline

Parada-Turska J, Turski WA (1990) Excitatory amino acid antagonists and memory: effect of drugs acting at N-methyl-D-aspartate receptors in learning and memory tasks. Neuropharmacology 29:1111–1116. CrossRef Medline

Parsons MP, Raymond LA (2014) Extrasynaptic NMDA receptor involvement in central nervous system disorders. Neuron 82:279–293. CrossRef Medline

Petralia RS (2012) Distribution of extrasynaptic NMDA receptors on neurons. ScientificWorldJournal 2012:267120. CrossRef Medline

Petrovic M, Sedlacek M, Horak M, Chodounska H, Vyklický L Jr (2005) 20-oxo-5beta-pregnan-3alpha-yl sulfate is a use-dependent NMDA receptor inhibitor. J Neurosci 25:8439–8450. CrossRef Medline

Pettersen EF, Goddard TD, Huang CC, Couch GS, Greenblatt DM, Meng EC, Ferrin TE (2004) UCSF Chimera–a visualization system for exploratory research and analysis. J Comput Chem 25:1605–1612. CrossRef Medline

Rambousek L, Bubenikova-Valesova V, Kacer P, Syslova K, Kenney J, Holubova K, Najmanova V, Zach P, Svoboda J, Stuchlík A, Chodounska H, Kapras V, Adamusova E, Borovska J, Vyklicky L, Vales K (2011) Cellular and behavioural effects of a new steroidal inhibitor of the N-methyl-D-aspartate receptor 3alpha5beta-pregnanolone glutamate. Neuropharmacology 61:61–68. CrossRef Medline

Rogawski MA (1993) Therapeutic potential of excitatory amino acid antagonists: channel blockers and 2,3-benzodiazepines. Trends Pharmacol Sci 14:325–331. CrossRef Medline

Rogawski MA, Wenk GL (2003) The neuropharmacological basis for the use of memantine in the treatment of Alzheimer's disease. CNS Drug Rev 9:275–308. Medline

Sah P, Hestrin S, Nicoll RA (1989) Tonic activation of NMDA receptors by ambient glutamate enhances excitability of neurons. Science 246:815–818. CrossRef Medline

Sali A, Blundell TL (1993) Comparative protein modelling by satisfaction of spatial restraints. J Mol Biol 234:779–815. CrossRef Medline

Salomon-Ferrer R, Case DA, Walker RC (2013) An overview of the Amber biomolecular simulation package. WIREs Comput Mol Sci 3:198–210. CrossRef

Sanner MF (1999) Python: a programming language for software integra-

PDF-XChange Editor
KOUPIT plnou verzi!
www.pdfxchange.cz

tion and development. Journal of molecular graphics and modelling 17: 57–61. Medline

Sobolevskii AI, Khodorov BI (2002) Blocker studies of the functional architecture of the NMDA receptor channel. Neurosci Behav Physiol 32: 157–171. CrossRef Medline

Sobolevsky AI, Beck C, Wollmuth LP (2002) Molecular rearrangements of the extracellular vestibule in NMDAR channels during gating. Neuron 33:75–85. CrossRef Medline

Sobolevsky AI, Rosconi MP, Gouaux E (2009) X-ray structure, symmetry and mechanism of an AMPA-subtype glutamate receptor. Nature 462: 745–756. CrossRef Medline

Stastna E, Chodounska H, Pouzar V, Kapras V, Borovska J, Cais O, Vyklicky L Jr (2009) Synthesis of C3, C5, and C7 pregnane derivatives and their effect on NMDA receptor responses in cultured rat hippocampal neurons. Steroids 74:256–263. CrossRef Medline

Traynelis SF, Wollmuth LP, McBain CJ, Menniti FS, Vance KM, Ogden KK, Hansen KB, Yuan H, Myers SJ, Dingledine R (2010) Glutamate receptor ion channels: structure, regulation, and function. Pharmacol Rev 62: 405–496. CrossRef Medline

Vyklicky V, Korinek M, Smejkalova T, Balik A, Krausova B, Kaniakova M, Lichnerova K, Cerný J, Krusek J, Dittert I, Horak M, Vyklicky L (2014) Structure, function, and pharmacology of NMDA receptor channels. Physiol Res 63:S191–S203. Medline

Vyklicky V, Krausova B, Cerný J, Balik A, Zapotocky M, Novotny M, Lichnerova K, Smejkalova T, Kaniakova M, Korinek M, Petrovic M, Kacer P, Horak M, Chodounska H, Vyklicky L (2015) Block of NMDA receptor channels by endogenous neurosteroids: implications for the agonist induced conformational states of the channel vestibule. Sci Rep 5:10935. CrossRef Medline

Wahl F, Obrenovitch TP, Hardy AM, Plotkine M, Boulu R, Symon L (1994) Extracellular glutamate during focal cerebral ischaemia in rats: time course and calcium dependency. J Neurochem 63:1003–1011. Medline

Wang S, Lees GJ, Rosengren LE, Karlsson JE, Stigbrand T, Hamberger A, Haglid KG (1991) The effect of an N-methyl-D-aspartate lesion in the hippocampus on glial and neuronal marker proteins. Brain Res 541: 334–341. CrossRef Medline

Weaver CE Jr, Marek P, Park-Chung M, Tam SW, Farb DH (1997) Neuroprotective activity of a new class of steroidal inhibitors of the N-methyl-D-aspartate receptor. Proc Natl Acad Sci U S A 94:10450–10454. CrossRef Medline

Wroge CM, Hogins J, Eisenman L, Mennerick S (2012) Synaptic NMDA receptors mediate hypoxic excitotoxic death. J Neurosci 32:6732–6742. CrossRef Medline

Xia P, Chen HS, Zhang D, Lipton SA (2010) Memantine preferentially blocks extrasynaptic over synaptic NMDA receptor currents in hippocampal autapses. J Neurosci 30:11246–11250. CrossRef Medline

Young JW, Zhou X, Geyer MA (2010) Animal models of schizophrenia. Curr Top Behav Neurosci 4:391–433. CrossRef Medline

Zamudio-Bulcock PA, Valenzuela CF (2011) Pregnenolone sulfate increases glutamate release at neonatal climbing fiber-to-Purkinje cell synapses. Neuroscience 175:24–36. CrossRef Medline

PDF-XChange Editor
KOUPIT plnou verzi!
www.pdfxchange.cz

Journal of Medicinal Chemistry

Article

pubs.acs.org/jmc

A New Class of Potent *N*-Methyl-D-Aspartate Receptor Inhibitors: Sulfated Neuroactive Steroids with Lipophilic D-Ring Modifications

Eva Kudova,[*,†] Hana Chodounska,[†] Barbora Slavikova,[†] Milos Budesinsky,[†] Michaela Nekardova,[†,§,∥] Vojtech Vyklicky,[‡] Barbora Krausova,[‡] Pavel Svehla,[‡] and Ladislav Vyklicky[‡]

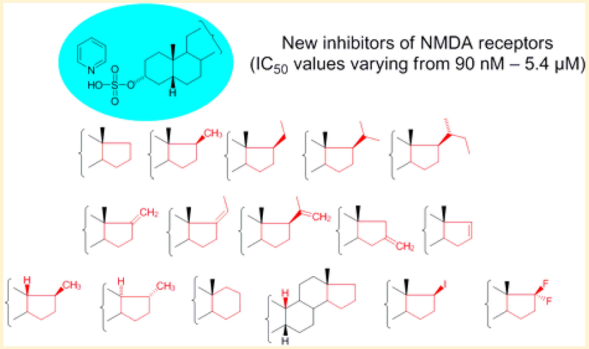
[†]Institute of Organic Chemistry and Biochemistry, Academy of Sciences of the Czech Republic v.v.i., Flemingovo nam 2, Prague 6−Dejvice, 16610, Czech Republic

[‡]Institute of Physiology, Academy of Sciences of the Czech Republic v.v.i., Videnska 1083, Prague 4, 14220, Czech Republic

[§]Faculty of Mathematics and Physics, Charles University in Prague, Ke Karlovu 3, Prague 2, 12116, Czech Republic

Supporting Information

ABSTRACT: *N*-Methyl-D-aspartate receptors (NMDARs) are glutamate-gated ion channels that play a crucial role in excitatory synaptic transmission. However, the overactivation of NMDARs can lead to excitotoxic cell damage/death, and as such, they play a role in numerous neuropathological conditions. The activity of NMDARs is known to be influenced by a wide variety of allosteric modulators, including neurosteroids, which in turn makes them promising therapeutic targets. In this study, we describe a new class of neurosteroid analogues which possess structural modifications in the steroid D-ring region. These analogues were tested on recombinant GluN1/GluN2B receptors to evaluate the structure−activity relationship. Our results demonstrate that there is a strong correlation between this new structural feature and the in vitro activity, as all tested compounds were evaluated as more potent inhibitors of NMDA-induced currents (IC_{50} values varying from 90 nM to 5.4 μM) than the known endogeneous neurosteroid−pregnanolone sulfate (IC_{50} = 24.6 μM).



INTRODUCTION

N-Methyl-D-aspartate receptors (NMDARs) are glutamate-gated calcium permeable ion channels involved in excitatory synaptic transmission and synaptic plasticity.[1] However, their overactivation leads to excitotoxicity, a specific form of neuronal cell death that is thought to underlie various forms of neurodegeneration, such as Alzheimer's disease, ischemia, or traumatic brain injury.[2−5] The activity of NMDARs can be influenced by several allosteric modulators, including neurosteroids, neuroactive compounds synthesized in the nervous tissue from cholesterol, or steroidal precursors from peripheral sources.[6,7] Neurosteroids have both positive and negative effects on NMDARs, and such modulatory effects play a role in many physiological processes, including learning and development and certain neuropsychiatric disorders.[8,9]

20-Oxo-5β-pregnan-3α-yl sulfate (pregnanolone sulfate; 3α5βS, Figure 1) is an endogenous neurosteroid that inhibits responses of NMDARs.[10] Similarly to the open channel blockers, 3α5βS acts in a use-dependent manner (requiring receptor activation by agonists), but unlike them, its effect is voltage-independent.[10,11] Kinetic properties of steroid binding and inhibition are slow and not typical of a simple receptor−ligand interaction in an aqueous solution.[12] This indirectly suggests the importance of the plasma membrane as a compartment where the steroid accumulates to reach its binding site on NMDARs.

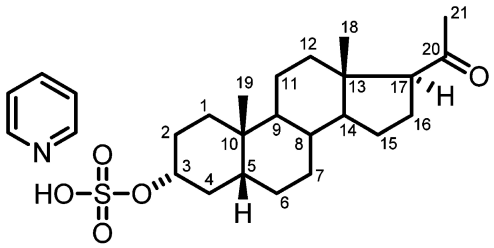


Figure 1. Structure of pregnanolone sulfate with steroid ring numbering system.

The inhibitory effect of neurosteroids on NMDARs is dependent upon the bent steroid ring structure that is associated with a 5β-stereochemistry, whereas the more planar arrangement of 5α-pregnanes favors potentiation.[13] In addition, the stereochemistry at position C-3 is also crucial to the inhibitory effect. As such, steroids having the combined 3α5β configuration were demonstrated as potent inhibitors of

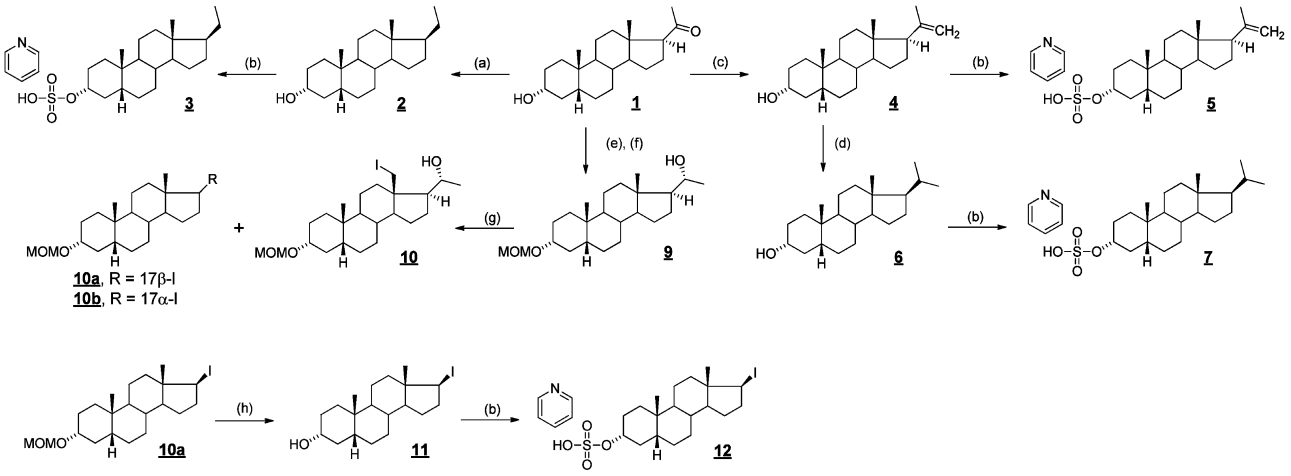
Received: April 11, 2015
Published: July 14, 2015

 © 2015 American Chemical Society

DOI: 10.1021/acs.jmedchem.5b00570
J. Med. Chem. 2015, 58, 5950−5966

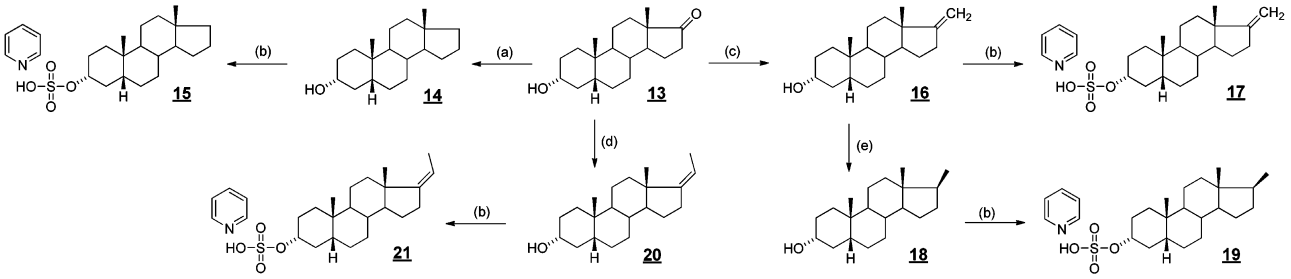
PDF-XChange Editor
KOUPIT plnou verzi!
www.pdfxchange.cz

Scheme 1. Synthesis of D-Modified Compounds 3, 5, 7, and 12 Derived from Pregnanolone[a]



[a]Reagents and conditions: (a) diethylene glycol, NaOH, hydrazine hydrate; (b) py·SO_3, $CHCl_3$, pyridine; (c) $CH_3P(C_6H_5)_3I$, *n*-BuLi, THF; (d) H_2, Pd/$CaCO_3$, EtOAc, EtOH; (e) MOMCl, DIPEA, THF, reflux; (f) $NaBH_4$, MeOH, 0 °C; (g) $PhI(OAc)_2$, I_2, DCM, 500 W; (h) HCl, MeOH, H_2O.

Scheme 2. Synthesis of D-Modified Compounds 15, 17, 19, and 21[a]



[a]Reagents and conditions: (a) Zn, TMSCl, MeOH, DCM; (b) py·SO_3, $CHCl_3$, pyridine; (c) $CH_3P(C_6H_5)_3Br$, NaH, DMSO; (d) $CH_3CH_2P(C_6H_5)_3Br$, K^{t}OBu, THF; (e) H_2, Pd/$CaCO_3$, EtOAc, EtOH.

NMDA-induced currents.[13,14] To elucidate the effect of charge and chain length on modulatory action, a series of sulfate, hemiesters, permethylated amines, and carboxylic acids were synthesized (it has been established that C-3 substituent must bear charge to maintain the biological activity, while uncharged derivatives have no significant effect on NMDA modulation).[12,13] Our previous study on the structure−activity relationship of 3α5βS analogues also demonstrated that analogues having various substituents at the C-7 carbon may participate in steroid binding on the NMDA receptor[15] as well. The following paper describes the structure−activity relationship study of pregnanolone sulfate analogues with structural modifications on the steroidal D-ring that has not been previously reported. To elucidate the structure−activity relationship of the acetyl moiety of the pregnane skeleton and the relevance of the 20-oxo group, a series of nonpolar 3α5βS analogues were synthesized and their biological activity was evaluated on human embryonic kidney cells (HEK293) transfected with plasmids encoding GluN1-a/GluN2B/GFP genes. In addition, we have evaluated the action on recombinant (GluN1/Glu2A-D), native NMDA receptors expressed in hippocampal neurons, native AMPA/kainate, and native GABA receptors. A detailed understanding of the structure−activity relationships between neurosteroids and NMDA receptors is important for the development of drugs with potential therapeutic use. It has already been shown that a synthetic analogue of 3α5βS pregnanolone hemisuccinate ester has neuroprotective activity in both in vitro and in vivo models of neurodegeneration.[16−18]

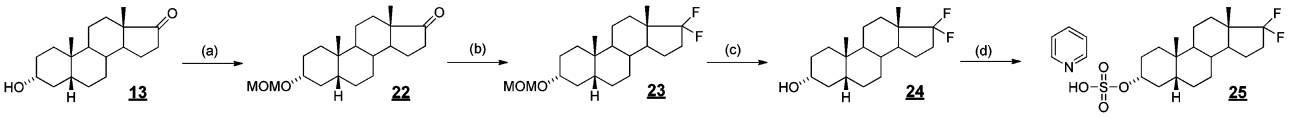
RESULTS AND DISCUSSION

Chemistry. Compounds **3**, **5**, **7**, and **12** (Scheme 1) were prepared from the commercially available pregnanolone (**1**). 17-Ethyl-androstane sulfate **3** was prepared by a two-step reaction sequence: Huang−Minlon modification of Wolff−Kischner reduction,[19] followed by the treatment of the 3α-hydroxy derivative (**2**) with a sulfur trioxide pyridine complex in $CHCl_3$ to afford derivative **3** (57% yield). Compound **4** (20-exomethylene derivative) was prepared from pregnanolone (**1**) by Wittig reaction using methyltriphenylphosphonium iodide with *n*-BuLi in 76% yield. Then, sulfate **5** was prepared by sulfation (py·SO_3 complex in $CHCl_3$) in 78% yield. Compound **7** (17β-methyl derivative) was prepared from the previously described 20-methylene derivative (**4**): the double bond was reduced using Pd/$CaCO_3$ catalyzed hydrogenation in EtOAc and EtOH to give 20-methyl-5β-pregnane derivative **6** (76% yield). The 3α-hydroxy group was then transformed into the sulfate by sulfur trioxide pyridine complex in $CHCl_3$ and pyridine to afford 17-*iso*-propyl derivative **7** (93% yield). Compound **12** (17β-iodo-androstane) was prepared by a five-step sequence: compound **1** was first converted to MOM-derivative **8** (98%). Then, the 20-keto group was reduced by

DOI: 10.1021/acs.jmedchem.5b00570
J. Med. Chem. 2015, 58, 5950−5966

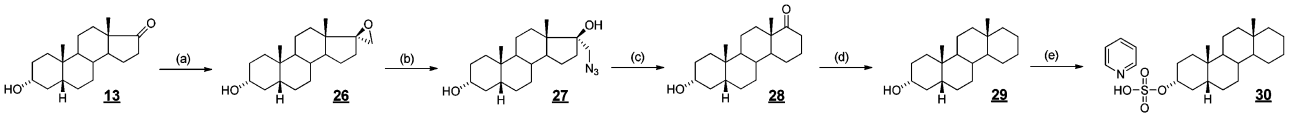
PDF-XChange Editor
KOUPIT plnou verzi!
www.pdfxchange.cz

Scheme 3. Synthesis of D-Modified Compound 25[a]



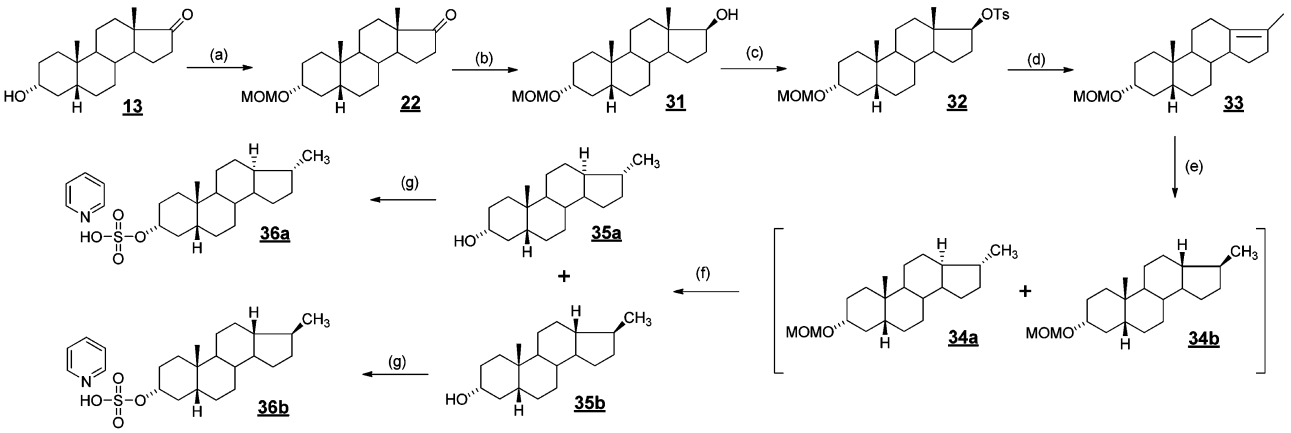
[a]Reagents and conditions: (a) MOMCl, DIPEA, DCM; (b) Bis(2-methoxyethyl)aminosulfur trifluoride, THF, 80 °C; (c) HCl, MeOH, H_2O; (d) py·SO_3, $CHCl_3$, pyridine.

Scheme 4. Synthesis of D-Modified Compound 30[a]



[a]Reagents and conditions: (a) $(CH_3)_3SI$, K^{t}OBu, DMF; (b) NaN_3, NH_4Cl, EtOH, H_2O, 90 °C; (c) NaI, TMSCl, acetonitrile; (d) Zn, TMSCl, MeOH, DCM; (e) py·SO_3, $CHCl_3$, pyridine.

Scheme 5. Synthesis of D-Modified Compounds 36a,36b[a]



[a]Reagents and conditions: (a) MOMCl, DIPEA, DCM; (b) $NaBH_4$, EtOH; (c) *p*-TsCl, DMAP, pyridine; (d) MeMgBr, 100 °C, toluene; (e) H_2, Pd/C, EtOAc, EtOH; (f) CH_3COCl, MeOH, benzene; (g) py·SO_3, $CHCl_3$, pyridine.

sodium borohydride to afford 20*R*-alcohol **9** as the major product (86% yield). Subsequently, compound **9** was treated with diacetoxyiodobenzene and iodine, and the reaction mixture was irradiated by halogen floodlight (500W). Compound **10**, having an iodine at position C-18, was isolated as the major product (58%). A mixture of compounds **10a** and **10b** was isolated as the byproduct. Attempts to isolate and purify compound **10b** on prep-TLC (30% ether in petroleum ether) failed due to the extreme similarity of R_f factors of compounds **10a** and **10b**. Therefore, only compound **10a** was isolated as a pure solid. Compound **10b** was isolated as a mixture with compound **10a**. Detailed spectroscopic data was obtained after acid hydrolysis of the MOM-protecting group, which afforded compound **11** (84% yield). The 3α-hydroxy group was then transformed into the sulfate by sulfur trioxide pyridine complex in $CHCl_3$ to afford derivative **12** (72% yield).

Compounds **15**, **17**, **19**, **21**, **25**, **30**, **36a**, **36b**, **43**, and **45** were prepared from 3α-hydroxy-5β-androstan-17-one (**13**). Compound **15** was prepared by a two-step reaction sequence (Scheme 2): Zn/TMSCl mediated Clemmensen reduction[20] of the 17-oxo group (79% yield), followed by treatment of 3α-hydroxy derivative **14** with a sulfur trioxide pyridine complex in $CHCl_3$ and pyridine to afford derivative **15** (67% yield). Compound **16** was prepared from compound **13** by Wittig reaction, using methyltriphenylphosphonium bromide with NaH, in 90% yield. 17-Exomethylene sulfate **17** (Scheme 2) was prepared by sulfation of **16** (py·SO_3 complex) in 81% yield. 17-Methylene derivative **16** was used for the synthesis of 17-methyl sulfate **19** (Scheme 2); catalytic hydrogenation using Pd/$CaCO_3$ gave 17-methyl derivative **18** (75% yield), which was converted into sulfate **19** (py·SO_3 complex, 78% yield). 17-Ethylidene-androstane sulfate **21** was prepared from compound **13** by a two-step reaction sequence: a Wittig reaction using ethyltriphenylphosphonium bromide,[21] followed by sulfation (py.SO_3 complex) to afford sulfate **21** (63% yield, Scheme 2).

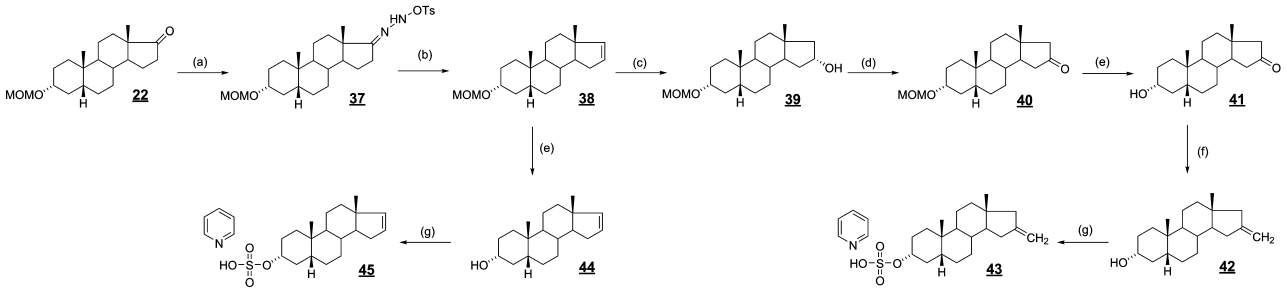
17-Difluoro-androstane sulfate **25** (Scheme 3) was prepared by a four-step sequence: the 3α-hydroxy group of starting material **13** was protected as MOM-ether **22** in 93% yield. Then, the 17-ketone was treated with bis(2-methoxyethyl)-aminosulfur trifluoride in a sealed glass tube under an inert atmosphere, to afford difluoro derivative **23** (27%). The MOM group was removed under acidic conditions using HCl in MeOH in 91% yield. Sulfate **25** was prepared by treatment with sulfur trioxide pyridine complex (73% yield).

D-Homoandrostane sulfate **30** (Scheme 4) was prepared by modified Möller procedure for the conversion of a five-membered D-ring into a D-homo moiety:[22] the reaction of compound **13** with trimethylsulfonium iodide and potassium

DOI: 10.1021/acs.jmedchem.5b00570
J. Med. Chem. 2015, 58, 5950−5966

PDF-XChange Editor
KOUPIT plnou verzi!
www.pdfxchange.cz

Scheme 6. Synthesis of D-Modified Compounds 43 and 45[a]



[a]Reagents and conditions: (a) $CH_3C_6H_4SO_2NHNH_2$, MeOH, reflux; (b) MeI, THF; (c) 9-BBN, THF, 0 °C; (d) PCC, DCM, pyridine; (e) HCl, MeOH, H_2O; (f) $CH_3P(C_6H_5)_3Br$, NaH, DMSO; (g) py·SO_3, $CHCl_3$, pyridine.

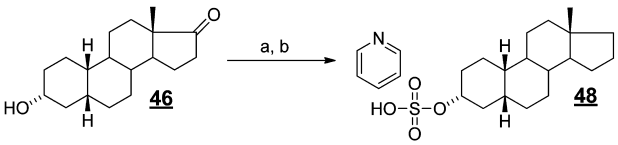
tert-butoxide in DMF afforded oxirane derivative **26** (78%), which was opened with sodium azide and ammonium chloride in an aqueous EtOH (**27**, 78% yield) and then cyclized with sodium iodide and trimethylsilyl iodide to afford D-homo derivative **28** in 73% yield. Finally, Zn/TMSCl modified Clemmensen reduction[20] of the 17a-oxo group (**29**, 65% yield), followed by treatment of the 3α-hydroxy group with a sulfur trioxide pyridine complex in $CHCl_3$ and pyridine, gave sulfate **30** (93% yield).

For the synthesis of isomeric 18-nor sulfates **36a** and **36b** (Scheme 5), we used our previously reported[23] methodology, utilizing the Kägi–Miescher rearrangement (1,2 shift of the C-18 methyl group): treatment of compound **13** with MOMCl in the presence of DIPEA gave derivative **22** in 93% yield. Reduction using $NaBH_4$ in EtOH gave 17β-alcohol derivative **31** in 94% yield. Compound **31** was then treated with *p*-toluenesulfonyl chloride in the presence of DMAP in pyridine to give 17β-tosylate **32** in 81% yield. The Kägi–Miescher rearrangement (1,2 shift of the C-18 methyl group-already described two sentences prior) was accomplished by refluxing 17β-tosylate **32** in toluene with methylmagnesium bromide to afford the desired $\Delta^{13(17)}$-ene derivative (**33**) in 63% yield. Reduction of the double bond using catalytic hydrogenation with Pd/C in EtOAc and EtOH gave a mixture of stereoisomers (**34a** and **34b**, 83%, stereoisomers were not separated). Acidic deprotection of the MOM group afforded a mixture of stereoisomers **35a** and **35b** (86%). HPLC separation gave compound **35a** and **35b** as a pure material. The homonuclear 2D-H,H-COSY, 2D-H,H-ROESY and heteronuclear 2D-H,C-HSQC and 2D-H,C-HMBC spectra were used for the structural assignment of the carbon and proton signals of compounds **35a** and **35b** (for details, see Supporting Information Table S1). Sulfates **36a** and **36b** were prepared by treatment with sulfur trioxide pyridine complex in 85% and 96% yield, respectively.

16-Exomethylene-androstane sulfate **43** and androst-16,17-ene sulfate **45** (Scheme 6) were prepared from common intermediate **38**: compound **13** was protected as MOM-ether **22** and then treated with tosylhydrazide in methanol under reflux to afford hydrazone **37** in 67% yield. Shapiro reaction of tosylhydrazone **37** with *n*-BuLi gave Δ^{16}-ene derivative **38** in 98% yield. Hydroxylation of the double bond of compound **38** using 9-BBN afforded 16-hydroxy derivative **39** (60% yield); position C-16 was functionalized by hydroboration. Preliminary experiments with borane in tetrahydrofuran afforded a mixture of 16- and 17-OH derivatives. Hydroboration with the bulkier hydroborating agent 9-borabicyclo(3.3.1)nonane (9-BBN) gave almost exclusively the 16α-derivative. Compound **39** was then oxidized by PCC in pyridine to afford 16-ketone derivative **40** in 95% yield. Deprotection of the MOM group using HCl in MeOH (**41**, 93% yield), Wittig reaction with methyltriphenylphosphonium bromide (**42**, 95% yield), and further treatment with pyridine sulfur trioxide pyridine complex gave sulfate **43** (56% yield). Direct deprotection of the MOM group of compound **38** using HCl in MeOH (**44**, 63% yield) and sulfation (py.SO_3 complex) gave sulfate **45** in 52% yield.

19-Nor-androstane derivative **47** (96% yield) was prepared by Zn/TMSCl modified Clemmensen reduction[20] of the 17-oxo group of compound **46**, which was prepared according to the literature.[24] Then, sulfate **48** was prepared by treatment of the 3α-hydroxy group with a sulfur trioxide pyridine complex in $CHCl_3$ and pyridine (35% yield, Scheme 7).

Scheme 7. Synthesis of D-Modified Compound 48 Derived from 3α-Hydroxy-5β-estran-17-one[a]

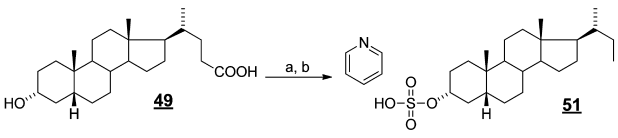


[a]Reagents and conditions: (a) Zn, TMSCl, MeOH, DCM; (b) py·SO_3, $CHCl_3$, pyridine.

Decarboxylation of commertially available lithocholic acid (**49**) with silver nitrate in DMSO afforded the desired 24-nor-5β-cholestane derivative (**50**) in 36% yield. Physical data were identical with literature.[25] Then, the 3α-hydroxy group was converted into sulfate **51** by treatment with a sulfur trioxide pyridine complex in $CHCl_3$ and pyridine in 83% yield (Scheme 8).

Biological Activity. To investigate the activity of pregnanolone sulfate and its analogues on NMDA receptors, cDNA encoding for the GluN1 and GluN2B subunits were

Scheme 8. Synthesis of D-Modified Compound 51 Derived from Lithocholic Acid[a]



[a]Reagents and conditions: (a) $AgNO_3$, DMSO, 80 °C; (c) py.SO_3, $CHCl_3$, pyridine.

DOI: 10.1021/acs.jmedchem.5b00570
J. Med. Chem. 2015, 58, 5950–5966

PDF-XChange Editor
KOUPIT plnou verzi!
www.pdfxchange.cz

cotransfected into HEK293 cells. Figure 2 shows control responses of the transfected cells to a fast application of

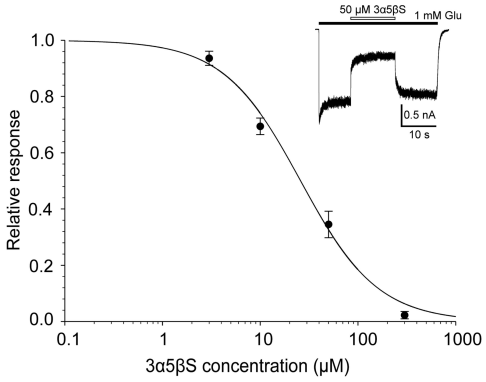


Figure 2. Effect of 3α5βS at GluN1/Glu2B receptors. Concentration–response curve for the 3α5βS effect at GluN1/Glu2B receptors. Data points are averaged values of normalized responses from five HEK293 cells. Error bars represent SD. The relative glutamate induced responses (I) recorded in the presence of 3α5βS (3–300 μM) and determined in individual cells were fit to the following logistic equation: $I = 1/(1 + ([3\alpha5\beta S]/IC_{50})^h)$, where IC_{50} is the concentration of 3α5βS that produces a 50% inhibition of agonist-evoked current, [3α5βS] is the 3α5βS concentration, and h is the apparent Hill coefficient. Inset show example of trace obtained from HEK293 cells transfected with cDNAs encoding GluN1/Glu2B receptors. 3α5βS (50 μM) was applied simultaneously with 1 mM glutamate (duration of 3α5βS and glutamate application is indicated by filled and open bars, respectively).

glutamate (1 mM) recorded in the presence of 10 μM glycine and no added Mg^{2+} from a cell voltage-clamped at a holding potential of −60 mV. The responses to a coapplication of 100 μM 3α5βS and glutamate made after the onset of the response to glutamate were inhibited in a dose-dependent manner. The results of the dose–response analysis indicate 100% inhibition at saturating steroid concentration with IC_{50} = 23.4 ± 1.6 μM and Hill coefficient 1.2 ± 0.1 (n = 5).

We have recently shown that the action of 3α5βS at the NMDA receptors involve several steps such as interaction of the steroid in its agglomerate form (the dominant form present in the water solution) with the cytoplasmic membrane and its subsequent binding in its single molecular form at the extracellular mouth of the channel vestibule to inhibit the NMDAR.[26] The value of IC_{50} therefore reflects total steroid concentration (sum of the single and agglomerate form) with predicted complex relation to the single molecular form present at the surface of the cytoplasmic membrane[26] (for details see Supporting Information). The amphipathic character of the D-modified steroids predicts that they may form solution similarly to 3α5βS. We have used light scattering analysis of compound **19** (as a model molecule) to infer on the form it exists in the water solution. The results show that compound **19** at concentrations ranging from 0.1 to 30 μM is present in the extracellular solution in three particle sizes (see Supporting Information, Figure S1; 3α5βS at a concentration relevant for NMDAR inhibition exists in two particle sizes (~2.5 and ~500 nm)).[26] At high steroid concentrations, the dose–response curve for some newly synthesized steroids deviated from that predicted by the logistic equation. We suspect that this was due to a greater proportion of the steroid being present in the form of large particle size(s) at higher steroid concentrations and the relatively lower contribution of the large particles to the steroid inhibitory effect. To avoid misinterpretation of the data, the IC_{50} for the newly synthesized steroids was determined from a single dose of the steroid using the following formula:

$$IC_{50} = [\text{compound}] \times \sqrt[h]{\frac{1 - I_I}{I_I}}$$

where I_I is the relative degree of inhibition, [compound] is the steroid concentration used, and h (fixed at 1.2). The IC_{50} value was determined for minimum of two steroid doses differing 3-fold in the concentration range. If the difference in the IC_{50} values was <10%, than the mean steroid IC_{50} was calculated from the steroid concentration most proximal to that inducing 50% inhibition. If the difference in the IC_{50} values determined for two steroid doses was >10%, then the dose–response analysis was determined at lower steroid concentrations to reach the formal criterion. In accordance with previous results, calculations of IC_{50} were made by assuming 100% inhibition at saturating steroid concentration[10,12] (see also Figure 2). Table 1 summarizes the IC_{50} determined for D-modified pregnanolone analogues.

Table 1. Effects of Pregnanolone Sulfate and its D-Modified Analogues on Responses of GluN1/GluN2B Receptors in HEK293 Cells to Glutamate

compound[a]	IC_{50} (μM) (h = 1.2), (n)	steroid concentration (μM)
pregnanolone sulfate[b]	24.6 ± 5.3 (n = 5)	100
3 (17β-CH_2CH_3)	0.4 ± 0.1 (n = 4)	1
5 (C_{20}=CH_2)	0.5 ± 0.1 (n = 5)	1
7 (17β-$CH(CH_3)_2$)	0.17 ± 0.03 (n = 3)	0.3
12 (17β-I)	0.6 ± 0.1 (n = 3)	0.3
15 (17β-H,17α-H)	1.2 ± 0.2 (n = 11)	3
17 (C_{17}=CH_2)	1.6 ± 0.3 (n = 6)	3
19 (17β-CH_3)	0.6 ± 0.1 (n = 5)	1
21 (C_{17}=$CHCH_3$)	0.8 ± 0.1 (n = 4)	1
25 (17β-F,17α-F)	7.0 ± 1.6 (n = 5)	10
30 (D-homo)	1.1 ± 0.3 (n = 4)	1
36a (17α-CH_3,18α-H)	0.9 ± 0.1 (n = 6)	3
36b (17β-CH_3,18β-H)	0.7 ± 0.1 (n = 4)	0.3
43 (C_{16}=CH_2)	2.2 ± 0.3 (n = 5)	3
45[c] ($\Delta^{16,17}$)	N/A	1, 3, 10, 50
48 (17α-H,17β-H,19β-H)	5.4 ± 1.5 (n = 6)	10
51 (17β-$CH(CH_3)CH_2CH_3$)	0.09 ± 0.01 (n = 3)	0.3

[a]The abbreviation of modification on the D-ring is added in the parentheses. [b]See the ref 12. [c]No effect at 1, 3, 10 μM, not soluble at 50 μM.

Effect of Pregnane 20-Oxo Group/Acetyl Moiety on Modulation of NMDARs. Comparison of the IC_{50} values of pregnanolone sulfate (IC_{50} = 24.6 ± 5.3 μM) with the deoxygenated analogue (compound **3**, IC_{50} = 0.4 ± 0.1 μM) shows more than a 60-fold decrease in the IC_{50} value, indicating that the 20-oxo group on the acetyl pregnane moiety can be removed while maintaining the ability of the neurosteroid to inhibit the NMDA induced currents. Additionally, changing the 20-oxo group to a methylene group (compound **5**) showed a ~50-fold decrease in IC_{50} values, in favor of steroid **5** (IC_{50} = 0.5 ± 0.1 μM). Moreover, interchange of the 20-methylene group (compound **5**) with a 20-methyl group (compound **7**) gave a ~3-fold decrease of IC_{50} values (IC_{50} = 0.16 ± 0.02 μM)

DOI: 10.1021/acs.jmedchem.5b00570
J. Med. Chem. 2015, 58, 5950–5966

PDF-XChange Editor
KOUPIT plnou verzi!
www.pdfxchange.cz

in favor of compound 7. Therefrom, we conclude that the 20-oxo group/acetyl moiety of pregnanolone sulfate (3α5βs) is not crucial for the ability of the neurosteroid to inhibit NMDA-induced currents.

Effect of Chain Length of Substituent at C-17 on Modulation of NMDARs. Comparison of alkyl modification on the D-ring of compounds **3**, 7, **19**, and **51** with acetyl moiety of pregnanolone sulfate shows that such structural modification leads to significant decrease of IC_{50} values as compared with 3α5βS: the replacement of the 17-acetyl moiety of pregnanolone sulfate with hydrogens resulted in more potent NMDAR inhibitor (compound **15**, IC_{50} = 1.2 ± 0.21 μM). Compounds **3**, 7, **19**, and **51** have alkyl substituents of increasing length on C-17. Comparison of the IC_{50} values of compound **19** (C-17-methyl, IC_{50} = 0.6 ± 0.1 μM), compound **3** (C-17-ethyl, IC_{50} = 0.4 ± 0.1 μM), compound 7 (C-17-*i*-propyl, IC_{50} = 0.16 ± 0.02 μM), and compound **51** (C-17-*i*-butyl, IC_{50} = 0.09 ± 0.01 μM) display anywhere from a 41- to a ~273-fold decrease in IC_{50} values, with respect to pregnanolone sulfate. These results clearly indicate that the replacement of the pregnanolone acetyl moiety with an alkyl substituent has a positive effect on the ability of the neurosteroid to inhibit NMDA-induced currents.

Steroids **36a** and **36b** are close structural analogues of steroid **15** (the 18-methyl group on C-13 is substituted by hydrogen), however, the conformation at C-13 and C-17 is identical for compound **36b**. Conversely, the conformation of C-13 and C-17 on compound **36a** is isomeric to **36b**. Comparison of the IC_{50} of steroids **36a** and **36b** (IC_{50} = 0.9 ± 0.1 and 0.7 ± 0.1 μM, respectively) with compound **15** (IC_{50} = 1.2 ± 0.2 μM) indicates that methyl group at C-13 does not have a large effect on the ability of the neurosteroid to inhibit NMDA-induced currents. Surprisingly, 19-nor derivative **48** shows a ~7-fold increase in its IC_{50} value as compared with compounds **36a** and **36b**.

Effect of D-Ring on Modulation of NMDARs. Comparing the IC_{50} of five-membered D-ring steroid **15** with six-membered steroid **30** (IC_{50}= 1.2 ± 0.2 and 1.1 ± 0.3 μM, respectively) indicates that expansion of the ring and the presence of the 17a-carbon does not affect the IC_{50} value.

Effect of Double Bond on Modulation of NMDARs. Three compounds bearing a methylene double bond were prepared: a 16-methylene (**43**, IC_{50} = 2.2 ± 0.3 μM), 17-methylene (**17**, IC_{50} = 1.6 ± 0.3 μM), and 20-methylene (**5**, IC_{50} = 0.5 ± 0.1 μM) derivative. Comparison of the IC_{50} values of these compounds indicates that the position of methylene moiety does affect the IC_{50} value, displaying a preference for location in place of the former carbonyl moiety. This was also found to be the case with the similarly located double bond of compound **21** (IC_{50} = 0.8 ± 0.08 μM), which gave a comparable IC_{50} value to that of compound **5**. Surprisingly, compound **45**, wherein the Δ^{16}-double bond was located within the ring, had no effect on NMDA-induced currents.

Effect of Halogen on Modulation of NMDARs. Comparison of the IC_{50} values of steroids **12** (IC_{50} = 0.6 ± 0.2 μM) and **15** (IC_{50} = 1.2 ± 0.2 μM) indicates that substitution of the C-17 hydrogen with an iodine has a pronounced effect on inhibition; compound **12** showing a 2-fold decrease in IC_{50} value in favor of the halogenated analogue. Conversely, substitution of both hydrogen atoms at C-17 by fluorine leads to an increase in the IC_{50} value (steroid **25**, IC_{50} = 7.0 ± 1.6 μM).

Effect of 17-Methyl-5β-Androstane 3-Sulfate (Compound 19) on Native and Recombinant Ionotropic Receptors. To investigate the influence of the subunit composition of the NMDA receptor on the effect of compound **19**, cDNAs encoding for the GluN1 and GluN2A-D subunits were cotransfected into HEK293 cells. Comparison of the IC_{50} values of the steroid **19** at GluN1/GluN2A-D show no significant differences (ANOVA; P = 0.215) and indicate that the action of the steroid is not dependent on the receptor subunit composition (Figure 3 and Table 2). Similarly no

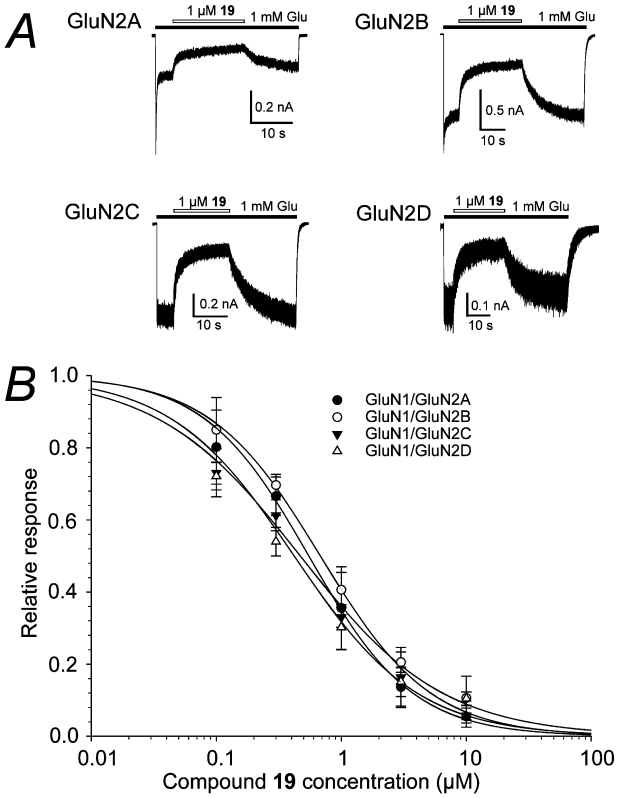


Figure 3. Effect of compound **19** at GluN1/Glu2A-D receptors. (A) Example of trace obtained from HEK293 cells transfected with cDNAs encoding GluN1/Glu2A (GluN2A), GluN1/Glu2B (GluN2B), GluN1/Glu2C (GluN2C), and GluN1/Glu2D (GluN2D) receptors. Compound **19** (1 μM) was applied simultaneously with 1 mM glutamate (duration of steroid and glutamate application is indicated by filled and open bars, respectively). (B) Concentration−response curves for the compound **19** effect at GluN1/Glu2A-D receptors. Data points are averaged values of normalized responses from five HEK293 cells. Error bars represent SD. The relative glutamate induced responses (I) recorded in the presence of the steroid (0.1−10 μM) and determined in individual cells were fit to the following logistic equation: $I = 1/(1 + ([\text{steroid}]/IC_{50})^h)$, where IC_{50} is the concentration of compound **19** that produces a 50% inhibition of agonist-evoked current, [steroid] is the compound **19** concentration, and h is the apparent Hill coefficient.

significant differences were found between native NMDA receptors expressed in cultured hippocampal neurons and recombinant GluN1/GluN2A-B receptors expected to be expressed in these cells.[27] In contrast to NMDA receptor response, the responses induced by 5 μM α-amino-3-hydroxy-5-methyl-4-isoxazolepropionic acid (AMPA) recorded in the presence of 10 μM cyclothiazide to block the receptor

DOI: 10.1021/acs.jmedchem.5b00570
J. Med. Chem. 2015, 58, 5950−5966

PDF-XChange Editor
KOUPIT plnou verzi!
www.pdfxchange.cz

Table 2. Effect of Compound 19 on Responses of Induced in GluN1/GluN2A-D Receptors in HEK293 Cells to Glutamate

	IC_{50} ± SD (μM)	h ± SD	n
GluN1/GluN2A	0.6 ± 0.2	1.0 ± 0.3	5
GluN1/GluN2B	0.7 ± 0.1	1.0 ± 0.3	5
GluN1/GluN2C	0.4 ± 0.1	0.9 ± 0.3	5
GluN1/GluN2D	0.5 ± 0.3	0.8 ± 0.1	5

desensitization[28] were significantly less sensitive to the compound **19**. The responses induced by 5 μM GABA were inhibited by compound **19**, with IC_{50} not significantly different from that determined for NMDA receptor responses (Figure 4 and Table 3).

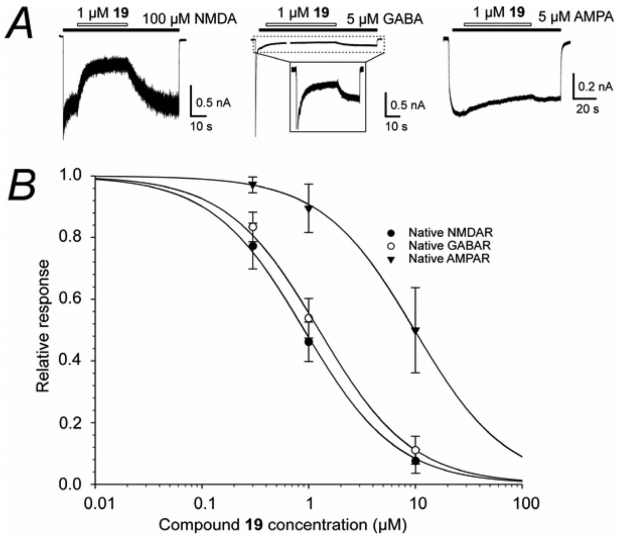


Figure 4. Effect of compound **19** at native AMPA/kainate, NMDA, and GABA receptors. (A) Example of trace obtained from cultured hippocampal neurons. Compound **19** (1 μM) was applied simultaneously with AMPA (5 μM), NMDA (100 μM), and GABA (5 μM) (duration of steroid and agonist application is indicated by filled and open bars, respectively). (B) Concentration–response curves for the compound **19** effect at AMPA, NMDA, and GABA receptors. Data points are averaged values of normalized responses from minimum of five cultured hippocampal neurons. Error bars represent SD. The relative agonist induced responses (I) recorded in the presence of the compound **19** (0.3–10 μM) and determined in individual cells were fit to the following logistic equation: $I = 1/(1 + ([\text{steroid}]/IC_{50})^h)$, where IC_{50} is the concentration of steroid that produces a 50% inhibition of agonist-evoked current, [steroid] is the steroid concentration, and h is the apparent Hill coefficient.

Table 3. Effect of Compound 19 on NMDA, AMPA, and GABA Receptor Responses in Hippocampal Neurons

	IC_{50} ± SD (μM)	h ± SD	n
NMDA R	0.9 ± 0.3	1.1 ± 0.3	6
AMPA R	9.5 ± 2.1	1.2[a]	5
GABA R	1.2 ± 0.2	1.1 ± 0.3	6

[a]Hill coefficient was fixed at 1.2.

The Computational Estimate of Thermodynamic Properties of Sulfated Neuroactive Steroids. In this computational analysis, we have investigated lipophilic qualities of the studied inhibitors in connection with the inhibitory effect. The relevant physicochemical properties of these neuroactive steroids (**3**, **5**, **7**, **12**, **15**, **17**, **19**, **21**, **25**, **30**, **36a**, **36b**, **43**, **48**, and **51**) were calculated by quantum mechanics (QM) computational methods and by physicochemical properties predictor.

The computational results are summarized in the Table 4. The calculated data of the studied compounds correlate well with the experimental ΔG_{exp} data. The correlation between ΔG_{exp} and the values estimated by the accurate QM computational methods (ΔG_{solv}, log P) is higher than between the values obtained by the physicochemical properties predictor (log P, log D), which is in agreement with the theory. The difference in the accuracy of both methods is plotted for log P values in Figure 5, where is $R^2 = 0.92$ for QM computations and $R^2 = 0.79$ for predictor, see below). Compound **12**, the inhibitor with iodine moiety at C-17, is the outlier among the values, which were computed by QM methods and therefore was not included in the correlation. The description of iodine by QM computational methods is nontrivial and less reliable. As the results show, the lipophilic character of this iodine compound is significantly underestimated, its log P is even less than log P of 3α5βS, while is more potent inhibitor.

The high correlation between ΔG_{exp} and ΔG_{solv} (in the case of water/n-octanol phase $R^2 = 0.94$ for neutral systems and $R^2 = 0.92$ for charged systems; in the case of vacuum/water phase $R^2 = 0.71$ for neutral systems and $R^2 = 0.74$ for charged systems) indicate that the (de)solvation free energy plays an important part in an inhibitory effect. The similar results for log P ($R^2 = 0.92$) and log D ($R^2 = 0.78$) show that the inhibition activity of this group of neuroactive steroids closely relates with their lipophilicity. These results are in accordance with expectations and can be used as valid parameters for further structural predictions: comparison of log P values (QM computation) vary from 3.62 to 5.83 for this structural group. However, the inhibitory effect of neurosteroid is multiparameter nature and, therefore, for the purpose of design of new compounds, especially drug candidate, other aspects should considered, e.g., enthalpy, entropy, solubility, permeability data, Lipinski rule of five, etc.

■ CONCLUSIONS

In this study, we were able to show that the pregnane acetyl group can be substituted with a variety of nonpolar substituents while still maintaining biological activity. In turn, this discovery has led to the development of NMDA receptor inhibitors that are even more potent than the endogeneous ligand–pregnanolone sulfate. In addition, we have shown that nonpolar substitution did not lead to NMDA subtype selectivity and we have shown that there is higher potency to inhibit NMDA receptor responses than AMPA responses.

Our computational data also revealed a correlation between the lipophilicity and the IC_{50} values, even throughout the relatively broad degree of structural variations. This supports our theory that lipophilic modification, and thus conveniently log P, could offer some guidance in the design of new neurosteroid inhibitors. The finding that the increase in the steroid potency was correlated with the lipophilicity also highlights the importance of the plasmatic membrane as a route of the steroid access to the receptor.[12,26]

The results of our previous experiments show that steroids have behavioral effects associated with altered brain function (neuroprotective effect)[18] and importantly, do not induce psychotomimetic symptoms, which can be the result of combined effect of the steroid on NMDA, AMPA, and

DOI: 10.1021/acs.jmedchem.5b00570
J. Med. Chem. 2015, 58, 5950–5966

PDF-XChange Editor
KOUPIT plnou verzi!
www.pdfxchange.cz

Table 4. Summary of Computational Values of Physicochemical Properties of Sulfated Neuroactive Steroids[a]

			ΔG_{solv} [kcal/mol] (SMD) transfer:						
			from vacuum to water		from *n*-octanol to water		QM computations	physicochemical properties predictor	
steroids	IC_{50} [μmol/L]	ΔG_{exp} [kcal/mol]	neutral	charged	neutral	charged	log *P*	log *P*	log *D*
3α5βS	29.60	−6.20	−21.43	−75.18	1.78	−5.53	2.93	4.04	1.67
3	0.40	−8.77	−13.49	−68.48	4.46	−3.02	4.94	5.22	2.84
5	0.50	−8.63	−14.06	−68.71	4.23	−3.20	4.77	5.16	2.78
7	0.16	−9.31	−13.04	−67.98	4.87	−2.68	5.26	5.51	3.13
12	0.60	−8.52	−17.86	−71.21	1.83	−5.46	2.49	5.13	2.75
15	1.20	−8.11	−14.00	−68.80	3.53	−3.92	4.07	4.49	2.11
17	1.60	−7.94	−14.59	−69.40	3.52	−3.98	3.88	4.43	2.05
19	0.60	−8.52	−13.56	−68.48	4.00	−3.52	4.46	4.78	2.40
21	0.80	−8.35	−14.56	−69.54	4.10	−3.37	4.65	4.82	2.44
25	7.00	−7.06	−17.41	−71.52	3.06	−4.42	3.70	4.36	1.98
30	1.10	−8.16	−13.97	−68.92	3.96	−3.49	4.46	4.93	2.56
36a	0.90	−8.28	−13.86	−68.85	3.76	−3.77	4.19	4.48	2.10
36b	0.70	−8.43	−13.65	−68.53	3.93	−3.57	4.38	4.48	2.10
43	2.20	−7.75	−14.73	−69.05	3.53	−3.79	4.04	4.43	2.05
45	N/A	N/A	−15.05	−69.73	3.10	−4.25	3.62	4.13	1.75
48	5.40	−7.22	−14.24	−69.45	3.43	−3.95	3.90	4.19	1.81
51	0.09	−9.69	−12.91	−67.69	5.42	−2.13	5.83	5.95	3.58

[a]The negative values of ΔG_{solv} signify the energy gained and the positive values energy required during the transfer from the first phase to the second phase.

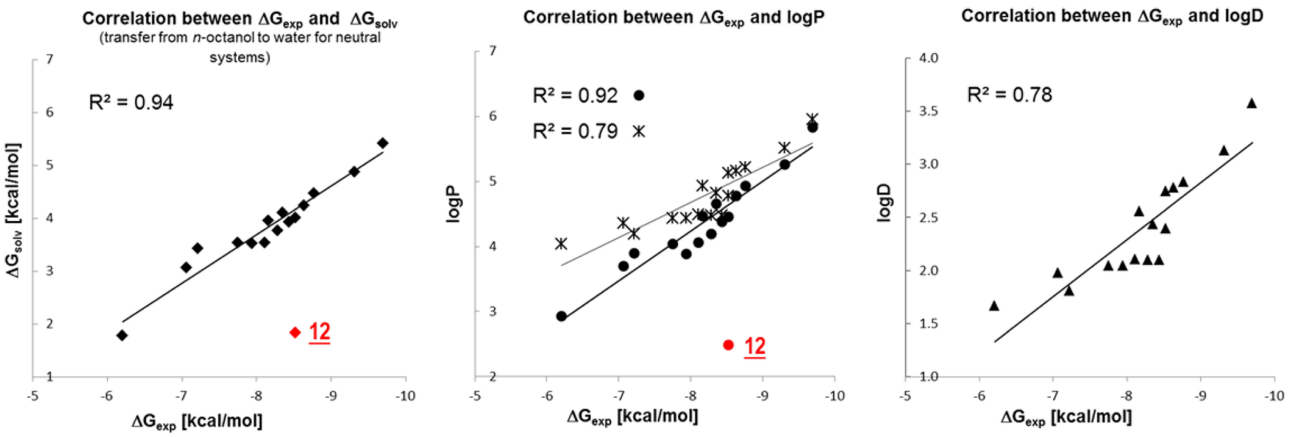


Figure 5. Correlation between the experimental ΔG_{exp} values and ΔG_{solv} (transfer from *n*-octanol to water for neutral systems), log *P* and log *D* values for synthesized neuroactive steroids (**3**, **5**, 7, **12**, **15**, **17**, **19**, **21**, **25**, **30**, **36a**, **36b**, **43**, **48**, and **51**).

GABA receptors. However, the impact of the steroid lipophilicity to cross the blood−brain barrier has to be established.

Furthermore, this structural flexibility offers new prospects for the further modification and optimization of the pharmacological and pharmacokinetic properties of these new neuroactive steroids. On the other hand, this data revealed a new avenue of investigation, steroid lipophilicity, and how it correlates with plasma membrane interaction. For instance, it is the lower IC_{50} value caused by the steroid's high affinity toward the NMDA receptor or by its high concentration near the receptor?[26]

Finally, as the sulfate moiety at position C-3 is susceptible to hydrolysis by sulfatases, the synthesis of a hemiester or carboxylic acid derivative with a nonpolar substituent on the steroidal D-ring may offer a more metabolically stable compound, one which could penetrate into the CNS without succumbing to metabolic degradation.

EXPERIMENTAL SECTION

Chemistry. *General.* Melting points were determined on a micromelting point apparatus Hund/Wetzlar (Germany) and are uncorrected. Optical rotations were measured in chloroform using an Autopol IV (Rudolf Research Analytical, Flanders, USA). $[\alpha]_D$ values are given in deg (10^{-1} deg cm^2 g^{-1}). IR spectra were recorded on a Bruker IFS 55 spectrometer (wavenumbers in cm^{-1}). Proton and carbon NMR spectra were measured on a FT NMR spectrometer Bruker AVANCE-400 (400 MHz, 101 MHz) in $CDCl_3$ with tetramethylsilane as the internal standard; NMR spectra of compounds **35a** and **35b** were measured on Bruker AVANCE-600 (^{1}H at 600.13 MHz and ^{13}C at 150.9 MHz frequency) in $CDCl_3$. Chemical shifts are given in ppm (δ scale). Coupling constants (J) and width of multiplets (W) are given in Hz. High resolution MS spectra were performed with a Q-Tof microspectrometer (Waters). Thin layer chromatography (TLC) was performed on silica gel (ICN Biochemicals). Preparative TLC (prep-TLC) was carried out on 200 mm × 200 mm plates coated with a 0.4 mm thick layer of the same material. For column chromatography, neutral silica gel 60 μm (Merck) was used. Analytical

DOI: 10.1021/acs.jmedchem.5b00570
J. Med. Chem. 2015, 58, 5950−5966

PDF-XChange Editor
KOUPIT plnou verzi!
www.pdfxchange.cz

samples were dried over phosphorus pentoxide at 50 °C/100 Pa. Anhydrous THF was prepared by distillation with benzophenone/Na immediately prior to use. Jones reagent has been prepared from chromium trioxide (67 g, 0.67 mmol) and a solution of sulfuric acid (58 mL of H_2SO_4 in 100 mL of water), and the mixture was diluted to 250 mL with water. The HPLC system consisted of high pressure pump (model 361, Gilson), Rheodyne injection valve . Preparative column (10 mm × 250 mm) with silica gel filling (Biospher PSI 200, 7 μm; Labio) and preparative ELSD detector (Gilson) connected with PC (software Trilution LC, Gilson). The purity of the final compounds was assessed by a combination of NMR and on the basis of analysis LC-HR-MS, and the results were greater than 95%.

General Procedure for Sulfation. A mixture of the hydroxy derivative (0.15 mmol) and sulfur trioxide pyridine complex (0.31 mmol) was dried in vacuo (25 °C, 100 Pa) for 30 min. Then, freshly dried chloroform (5 mL/50 mg) and dry pyridine (1 drop) were added, and the reaction mixture was stirred at room temperature under inert atmosphere. The progress of the reaction was checked by TLC. Then, the reaction mixture was allowed to stand at −5 °C for 2 h and solids were filtered off through a plug of cotton wool in a glass Pasteur pipet. The filtrate was evaporated and dried (25 °C, 100 Pa) for 1 h to afford a mix of sulfate and sulfur trioxide pyridine complex. The crude material was dissolved in a minimal amount of freshly dried chloroform, allowed to stand at −5 °C for 2 h, and the solids were filtered off through a plug of cotton wool in a glass Pasteur pipet. The filtrate was evaporated and dried (25 °C, 100 Pa) for 1 h to afford the corresponding steroidal sulfate.

Computational Section. *Preparation of Structures.* The compounds were obtained by modeling the ligand as taken from the crystal structure (PDB code 3CAV[29]) using PyMOL program[30] and were relaxed by the RI-DFT/B-LYP/SVP method with the Turbomole program.[31] The empirical dispersion correction (D)[32] and COSMO continuum solvation model[33] were applied on the gradient optimization. The most stable local minima of the compounds were obtained by the quenched molecular dynamics simulation method with PM6-D3H4X.[34] The resulting structures were reoptimized by the RI-DFT-D3/B-LYP/TZVPP//COSMO method.[35]

Computational Methods. The solvation free energy (ΔG_{solv}) of the neuroactive steroids was calculated in the SMD continuum solvation model (the transfer from vacuum to water and from *n*-octanol to water) at the HF/6-31G* level with the Gaussian program.[36] The partition coefficients (log *P*) of water/*n*-octanol phase were calculated at the M06-2X/6-31G* level in SMD with the Gaussian program as the difference between the total energies in water and in *n*-octanol. The iodine compound **12** was described by using cc-pVDZ-PP basis set, which is defined for iodine atom. The log *P* and distribution-coefficients (log *D*) of water/*n*-octanol phase were predicted by the MarvinSketch program.[37] The calculated values ΔG_{solv}, log *P*, and log *D* were compared with the experimental free energies (ΔG_{exp}) expressed from the IC_{50} values via the equation $\Delta G_{exp} = RT \ln(IC_{50})$. The linear regression was used for description of the relationship between ΔG_{exp} and the calculated data. The coefficient of determination (R^2) shows how well the calculated data fit the experimental data. The range of R^2 is from 0 to 1, where 0 indicates impossibility and 1 indicates certainty.

Biological Activity. Electrophysiological experiments were performed on human embryonic kidney cells (HEK293) transfected with plasmids encoding GluN1-a/GluN2A-D/GFP genes and cultured hippocampal neurons as described previously.[10,38,39] Glutamate-induced responses were voltage-clamped at a holding potential of −60 mV. Whole-cell voltage clamp recordings were made with a patch-clamp amplifier (Axopatch 200B; Axon Instruments. Inc., Foster City, CA) after a serial resistance (<10 MΩ) and capacitance compensation of 80−90%. For the application of test and control solutions, a microprocessor controlled multibarrel fast-perfusion system was used, with a time constant of solution exchange around cells of ∼10 ms. Agonist-induced responses were low-pass filtered at 2 kHz, digitally sampled at 5 kHz, and analyzed with pClamp software version 9.2 (Molecular Devices). Patch pipettes (3−5 MΩ) pulled from borosilicate glass were filled with Cs^+-based intracellular solution (ICS) containing the following (in mM): 120 gluconic acid, 15 CsCl, 10 BAPTA, 10 HEPES, 3 $MgCl_2$, 1 $CaCl_2$ and 2 ATP-Mg salt (pH-adjusted to 7.2 with CsOH). The extracellular solution (ECS) contained the following (in mM): 160 NaCl, 2.5 KCl, 10 HEPES, 10 glucose, (pH-adjusted to 7.3 with NaOH). NMDA receptor responses were induced by 1 mM glutamate (in recombinant receptors) and 100 μM NMDA (native receptors) and the ECS contained 0.2 mM EDTA, 0.7 mM CaCl2 10 μM glycine plus 10 μM CNQX, 10 μM bicuculline and 0.5 μM TTX for native receptors. AMPA receptors were induced by 5 μM AMPA and the ECS contained 50 μM D-AP5, 10 μM bicuculline, 0.5 μM TTX, and 10 μM cyclothiazide (citaceece Vyklicky J Neurosci). GABA receptor responses were induced by 5 μM GABA and the ECS contained 50 μM D-AP5, 10 μM CNQX, 0.5 μM TTX. Steroid solutions were prepared fresh, as a stock solution of either 5 or 20 mM in dimethyl sulfoxide (DMSO) before each experiment (1% DMSO final concentration). The same concentration of DMSO was added in all extracellular solutions. Experiments were performed at room temperature (21−25 °C).

Light Scattering Analysis. Light scattering (Zetasizer Nano ZS, Malvern Instruments, United Kingdom) was used to characterize particle size of compound **19** in ECS.[26]

Experimental Data for Compounds 2−9, 10a, 11, 12, 14, 15, 17−34, 35b, 36a, 36b, 37−45, 47, 48, 50, and 51. *5β-Pregnan-3α-ol (2).* Compound **2** was prepared according to the literature:[19] mp 150−152 °C (lit.[19] 148−149 °C). ^{1}H NMR (400 MHz, $CDCl_3$): δ 0.54 (3H, s, H-18), 0.87 (3H, t, *J* = 7.3, H-21), 0.93 (1H, s, H-19), 3.63 (1H, m, H-3).

5β-Pregnan-3α-yl 3-Sulfate Pyridinium Salt (3). Compound **3** was prepared according to General Procedure for Sulfation. Starting from compound **2** (60 mg, 0.2 mmol), compound **3** (52 mg, 57%) was obtained as a white solid: mp 182−184 °C; $[\alpha]_D$ +61.5 (*c* 0.26, $CHCl_3$). ^{1}H NMR (400 MHz, $CDCl_3$): δ 0.53 (3H, s, H-18), 0.86 (3H, t, *J* = 7.3, H-21), 0.92 (1H, s, H-19), 4.47 (1H, tt, J_1 = 11.3, J_2 = 4.9, H-3), 8.10−8.31 (2H, m, H-2′ and H-4′, pyridinium), 8.48 (1H, t, *J* = 7.9, H-3′, pyridinium), 8.96 (2H, d, *J* = 7.9, H-1′ and H-5′, pyridinium). ^{13}C NMR (101 MHz, $CDCl_3$): δ 145.7 (C-1′ and C-5′, pyridinium), 142.4 (C-3′, pyridinium), 127.2 (C-2′ and C-4′, pyridinium), 79.8 (C-3), 56.2, 53.1, 42.4, 42.4, 41.1, 38.5, 36.0, 35.5, 34.7, 33.5, 28.4, 27.9, 27.2, 26.7, 24.7, 23.5, 23.2, 20.7, 13.5, 12.7. IR spectrum ($CHCl_3$): 1264, 1173, 970, 947 (OSO_3). MS ESI: *m*/*z* 383.1 (100%, M − pyH). HR-MS (ESI) *m*/*z*: For $C_{21}H_{35}O_4S$ [M − pyH] calcd, 383.2261; found, 383.2258.

20-Methylene-5β-pregnan-3α-ol (4). *n*-Butyllithium (1.6 M in hexanes, 5.8 mL, 9.4 mmol) was added dropwise to a solution of methyltriphenylphosphonium iodide (3.9 g, 9.7 mmol) in anhydrous tetrahydrofuran (35 mL) under inert atmosphere, and the reaction mixture was stirred at room temperature for 1 h. Then, a solution of **1** (1 g, 3.13 mmol) in anhydrous tetrahydrofuran (10 mL) was added. After 48 h of stirring at 80 °C, an aqueous solution of ammonium chloride was added. The product was extracted with chloroform (2 × 70 mL), and combined organic extracts were washed with brine and dried. Solvents were evaporated, and the residue was purified by chromatography on silica gel (10% ethyl acetate in petroleum ether) to afford compound **4** (760 mg, 76%): mp 149−151 °C (acetone/*n*-heptane); $[\alpha]_D$ +16.6 (*c* 0.39, $CHCl_3$). ^{1}H NMR (400 MHz, $CDCl_3$): δ 0.54 (3H, s, H-18), 0.91 (3H, s, H-19), 1.75 (3H, s, H-21), 2.02 (1H, t, *J* = 9.1, H-17), 3.62 (1H, m, H-3), 4.69 (1H, s, H-22a), 4.83 (1H, s, H-22b). ^{13}C NMR (101 MHz, $CDCl_3$): δ 145.8 (C-20), 110.7 (=CH_2), 71.9 (C-3), 57.5 (C-17), 56.4 (C-14), 43.5, 42.3, 40.8, 39.2, 36.6, 36.3, 35.5, 34.8, 30.7, 27.3, 26.5, 25.6, 24.7, 24.3, 23.5, 21.0, 13.0. IR spectrum ($CHCl_3$): 3609, 3447, 1033 (OH); 3085, 1639 (=CH_2); 1376 (CH_3). MS (ESI) *m*/*z*: 339.2 (100%, M + Na). For $C_{22}H_{36}O$ (316.5) calcd: 83.48%, C; 11.46%, H. Found: 83.49%, C; 11.55%, H.

20-Methylene-5β-pregnan-3α-yl 3-Sulfate Pyridinium Salt (5). Compound **5** was prepared according to General Procedure for Sulfation. Starting from compound **4** (50 mg, 0.15 mmol), compound **5** (59 mg, 78%) was obtained as a white solid: mp 170−172 °C; $[\alpha]_D$ +42.0 (*c* 0.17, $CHCl_3$). ^{1}H NMR (400 MHz, $CDCl_3$): δ 0.52 (3H, s, H-18), 0.90 (3H, s, H-19), 1.73 (3H, s, H-21), 4.45 (1H, m, H-3), 4.67 (1H, s, H-22a), 4.82 (1H, s, H-22b), 7.47 (2H, ddd, J_1 = 7.7, J_2 = 4.7,

DOI: 10.1021/acs.jmedchem.5b00570
J. Med. Chem. 2015, 58, 5950−5966

PDF-XChange Editor
KOUPIT plnou verzi!
www.pdfxchange.cz

J_3 = 1.3, H-2′ and H-4′, pyridinium), 7.88 (1H, tt, J_1 = 7.7, J_2 = 1.7, H-3′, pyridinium), 8.70 (2H, d, J = 4.5, H-1′ and H-5′, pyridinium). ^{13}C NMR (101 MHz, $CDCl_3$): δ 147.8 (C-1′ and C-5′, pyridinium), 145.8 (C-20), 138.6 (C-3′, pyridinium), 124.7 (C-2′ and C-4′, pyridinium), 110.7 (=CH_2), 79.6 (C-3), 57.4, 56.4, 43.5, 42.2, 40.6, 39.2, 36.2, 35.4, 34.6, 33.4, 27.8, 27.1, 26.4, 25.6, 24.8, 24.3, 23.4, 20.9, 12.9. IR spectrum ($CHCl_3$): 3140, 3073, 1683, 1490 (pyridinium); 3085, 1639 (=CH_2), 1262, 1172, 1046 (SO_3). MS: ESI m/z 395.2 (100%, M − pyH). HR-MS (ESI) m/z for $C_{22}H_{35}O_4S$ [M − pyH] calcd, 395.2261; found, 395.2259.

*20-Methyl-5β-pregnan-3α-ol (**6**).* Compound **4** (200 mg, 0.63 mmol) was dissolved in ethyl acetate (2 mL) and ethanol (8 mL). To this, Pd/$CaCO_3$ (5%, 40 mg) was added. The reaction mixture was hydrogenated under slight pressure at room temperature for 7 h. Then, the reaction mixture was filtered through a short column of silica gel to remove the catalyst by washing with chloroform (30 mL). Solvents were removed under vacuo. A mixture of products was purified by column chromatography on silica gel (10% ethyl acetate in petroleum ether) to afford 174 mg (86%) of compound **6**: mp 195−195.5 °C (acetone/*n*-heptane); $[\alpha]_D$ +17.0 (c 0.29, $CHCl_3$). ^{1}H NMR (400 MHz, $CDCl_3$): δ 0.63 (3H, s, H-18), 0.83 (3H, d, J = 6.6, H-22a), 0.91 (3H, s, H-19), 0.92 (3H, d, J = 6.5, H-22b), 3.62 (1H, m, H-3). ^{13}C NMR (101 MHz, $CDCl_3$): δ 72.0 (C-3), 58.5 (C-17), 56.6 (C-14), 42.8, 42.3, 40.6, 40.2, 36.6, 36.0, 35.5, 34.7, 31.1, 30.7, 28.6, 27.4, 26.6, 24.4, 23.5, 23.3, 22.6, 20.9, 12.3. IR spectrum ($CHCl_3$): 3606, 3480, 1033 (OH); 1383, 1366 (*i*-propyl); 1377 (CH_3). MS ESI: m/z 341.4 (100%, M + Na). For $C_{22}H_{38}O$ (318.5) calcd: 82.95%, C; 12.02%, H. Found: 82.74%, C; 11.77%, H.

*20-Methyl-5β-pregnan-3α-yl 3-Sulfate Pyridinium Salt (**7**).* Compound 7 was prepared according to General Procedure for Sulfation. Starting from compound **6** (50 mg, 0.15 mmol), compound **7** (69 mg, 93%) was obtained as a white solid: mp 190−194 °C; $[\alpha]_D$ +26.2 (c 0.29, $CHCl_3$). ^{1}H NMR (400 MHz, $CDCl_3$): δ 0.62 (3H, s, H-18), 0.82 (3H, d, J = 6.6, H-22a), 0.90 (3H, s, H-19), 0.91 (3H, d, J = 6.3, H-22b), 4.46 (1H, m, H-3), 8.01 (2H, dd, J_1 = 7.7, J_2 = 6.7, H-2′ and H-4′, pyridinium), 8.48 (1H, tt, J_1 = 7.9, J_2 = 1.4, H-3′, pyridinium), 8.98 (2H, d, J = 5.4, H-1′ and H-5′, pyridinium). ^{13}C NMR (101 MHz, $CDCl_3$): δ 145.8 (C-1′ and C-5′, pyridinium), 142.3 (C-3′, pyridinium), 127.3 (C-2′ and C-4′, pyridinium), 80.0 (C-3), 58.4 (C-17), 56.6 (C-14), 42.8, 42.3, 40.5, 40.2, 35.9, 35.4, 34.6, 33.4, 31.1, 28.6, 27.8, 27.2, 26.5, 24.3, 23.4, 23.3, 22.6, 20.9, 12.2. IR spectrum ($CHCl_3$): 3140, 3100, 3073, 1637 (pyH); 1376 (*i*-propyl), 1263, 1171, 1046 (SO_3). MS: ESI m/z 397.2 (100%, M − pyH). HR-MS (ESI) m/z: For $C_{22}H_{37}O_4S$ [M− pyH] calcd, 397.2418; found, 397.2415.

*3α-Methoxymethoxy-5β-pregnan-20-one (**8**).* *N*,*N*-Diisopropylethylamine (13.7 mL, 78.5 mmol) was added to a solution of compound **1** (10.0 g, 31.4 mmol) in dry dichloromethane (70 mL). The solution was cooled to 0 °C, methoxymethyl bromide (1.4 mL, 17.2 mmol) was added, and the mixture was stirred under inert atmosphere at room temperature. After 30 h, chloroform (140 mL) was added and the organic layer was washed with the aqueous citric acid (5%, 2 × 30 mL), a saturated solution of sodium bicarbonate, and brine, and then dried. Solvents were evaporated to afford compound **8** as brownish oil (11.15 g, 98%), which was crystallized from ethyl acetate/*n*-heptane: mp 72−73 °C (ethyl acetate/*n*-heptane); $[\alpha]_D$ +105.8 (c 0.25, $CHCl_3$). ^{1}H NMR (400 MHz, CDCl3): δ 0.59 (3H, s, H-18), 0.92 (3H, s, H-19), 2.11 (3H, s, H-21), 2.53 (1H, t, J = 9.0, H-17), 3.38 (3H, s, OCH_3), 3.54 (1H, tt, J_1 = 11.2, J_2 = 4.7, H-3), 4.69 (2H, s, OCH_2O). ^{13}C NMR (101 MHz, $CDCl_3$): δ 209.7 (C-20), 94.5 (OCH_2O), 76.7 (C-3), 63.8, 56.7, 55.1 (CH_3O), 44.3, 42.0, 40.3, 39.2, 35.8, 35.3, 34.7, 33.5, 31.5, 27.7, 27.0, 26.3, 24.4, 23.3, 22.8, 20.7, 13.4. IR spectrum ($CHCl_3$): 2940, 2889, 2869 (OCH_2O); 1689 (C=O); 1385, 1373, 1659 (CH_3); 1145, 1103, 1047, 1039 (MOM). MS ESI: m/z 385.4 (100%, M + Na), 747.7 (7%, 2 M + Na). For $C_{23}H_{38}O_3$ calcd: 76.20%, C; 10.56%, H. Found: 76.12%, C; 10.52%, H.

*(20R)-3α-Methoxymethoxy-5β-pregnan-20-ol (**9**).* Ketone **8** (11.15 g, 30.8 mmol) was dissolved in methanol (250 mL), and the solution was cooled to 0 °C. Sodium borohydride (1.78 g, 47.05 mmol) was added slowly while stirring, After 2 h, the reaction mixture was partly evaporated (to $^1/_3$ of volume) and then poured into a solution of citric acid (5%, 100 mL). Product was extracted with ether (3 × 50 mL), combined organic extracts were washed with a saturated solution of sodium bicarbonate (100 mL) and brine (100 mL), and then dried with magnesium sulfate. Evaporation of solvents afforded mixture of stereoisomers, which were separated by column chromatography (10% ethyl acetate in hexanes) to afford compound **9** as colorless oil (9.84 g, 86%) and the minor *S*-isomer as white crystals (619 mg, 7%): $[\alpha]_D$ +17.9 (c 0.19, $CHCl_3$). ^{1}H NMR (400 MHz, $CDCl_3$): δ 0.73 (3H, s, H-18), 0.92 (3H, s, H-19), 1.13 (3H, d, J = 6.1. H-21), 3.37 (3H, s, OCH_3), 3.53 (1 H, tt, J_1 = 11.2, J_2 = 4.5. H-3), 3.72 (1H, dq, J_1 = 9.5, J_2 = 6.0, H-20), 4.62 (2H, s, OCH_2O). ^{13}C NMR (101 MHz, $CDCl_3$): δ 94.5, 76.8, 70.6, 58.6, 56.0, 55.1, 42.6, 42.1, 40.4, 40.3, 35.7, 35.4, 34.7, 33.6, 27.7, 27.2, 26.4, 25.7, 24.5, 23.6, 23.4, 20.7, 12.5. IR spectrum ($CHCl_3$): 3611 (OH); 2942, 2933, 2890, 2869 (OCH_2O); 1450, 1377 (CH_3); 1040 (C−OH). MS ESI: m/z 387.3 (67%, M + Na), 751.6 (100%, 2 M + Na). For $C_{23}H_{40}O_3$ calcd: 75.77%, C; 11.06%, H. Found: 75.77%, C; 11.08%, H.

*17β-Iodo-3α-methoxymethoxy-5β-androstane (**10a**).* Alcohol **9** (9.85 g, 27.0 mmol), iodine (6.90 g, 27.2 mmol), and diacetoxyiodobenzene (9.95 g, 30.9 mmol) were dissolved in dichloromethane (750 mL) in a 500 mL jacketed flask. The reaction mixture was cooled to 15 °C, and the reaction vessel was irradiated by halogen floodlight (500 W) for 3 h. Then it was quenched with an aqueous solution (200 mL) containing sodium thiosulfate (20 g) and sodium bicarbonate (10 g). The colorless organic phase was washed with brine (200 mL), dried with $MgSO_4$, and concentrated in vacuo. The resulting oil was dissolved in a minimum amount of hexanes and crystallized at 5 °C to yield 4.19 g of colorless crystals of (20*R*)-18-iodo-3α-methoxymethoxy-5β-pregnan-20-ol (**10**). The mother liquor was concentrated in vacuo, adsorbed on a column of Florisil (4 × 30 cm), and eluted with 5−15% ethyl acetate in hexanes to afford mixture of 17α and 17β-iodo derivatives **10a** and **10b** (304 mg, 1:1 according to ^{1}H NMR, 2.5%) as white crystalline solid, followed by another portion of **10** (3.49 g, 58% together with crystalline fraction) as an off-white solid.

*Compound **10**.* Melting point 124−125.5 °C (hexanes); $[\alpha]_D$ +9.4 (c 0.23, $CHCl_3$). ^{1}H NMR (400 MHz, $CDCl_3$): δ 0.92 (3H, s, H-19), 1.14 (3H, d, J = 6.2. H-21), 2.25 (1H, d, J = 4.2), 2.39 (1H, dt, J_1 = 13.4, J_2 = 3.0. CH-12β), 3.13 (1H, dd, J_1 = 10.6, J_2 = 1.1, CH-18b), 3.32 (1H, dd, J_1 = 10.6, J_2 = 1.3, CH-18a), 3.37 (3H, s, OCH_3), 3.53 (1H, tt, J_1 = 11.2, J_2 = 4.6, H-3), 4.06 (1H, tt, J_1 = 10.1, J_2 = 6.1, H-20), 4.69 (2H, d, J = 1.1, OCH_2O). ^{13}C NMR (101 MHz, $CDCl_3$): δ 94.6 (OCH_2O), 76.7 (C-3), 68.3 (C-20), 58.8 (C-17), 56.2 (C-14), 55.1 (CH_3O), 44.4, 41.8, 40.8, 40.3, 36.4, 35.3, 34.7, 33.5, 27.6, 27.1, 26.2, 25.4, 24.3, 23.3, 22.2, 20.2, 11.2. IR spectrum ($CHCl_3$): 3600 (OH); 2944, 2932, 2887 (OCH_2O); 1423 (CH_2I); 1376 (CH_3); 1145, 1102 (OCH_2O); 1045 (C−OH). MS ESI: m/z 513.2 (98%, M + Na), 1003.5 (100%, 2 M + Na). HR-MS (ESI) m/z: for $C_{23}H_{39}INaO_3$ [M + Na] calcd, 513.1836; found, 513.1835.

*Compound **10a**.* $[\alpha]_D$ +88.5 (c 0.287, $CHCl_3$). ^{1}H NMR (400 MHz, $CDCl_3$): δ 0.79 (3H, s, H-18), 0.93 (3H, s, H-19), 3.36 (3H, s, OCH_3), 3.48−3.58 (1H, m, H-3), 3.75 (1H, t, J = 9.4, H-17), 4.68 (2H, s, OCH_2O). ^{13}C NMR (101 MHz, $CDCl_3$): δ 94.7, 76.9, 55.3, 50.1, 44.3, 42.3, 42.1, 40.7, 37.4, 37.1, 35.5, 34.9, 34.4, 33.7, 27.8, 27.2, 26.4, 25.5, 23.5, 20.5, 17.1. IR spectrum ($CHCl_3$): 2940, 2869 (CH_2); 1145, 1047, 1036, 1102, 915 (COCOC). MS ESI: m/z 469.3 (80%, M + Na). HR-MS (ESI) m/z: for $C_{21}H_{35}INaO_2$ [M + Na] calcd, 469.1573; found, 469.1573.

*17β-Iodo-5β-androstan-3α-ol (**11**).* Compound **10a** (250 mg, 0.56 mmol) was dissolved in methanol (10 mL), and concentrated HCl (two drops) and triethylamine (one drop) were added to the stirred solution. After 48 h, the reaction mixture was quenched with a saturated solution of sodium bicarbonate (10 mL). Solvents were partially evaporated (to $^1/_2$ of volume), and the product was extracted with ethyl acetate (3 × 10 mL), the combined organic extracts were washed with brine and dried over magnesium sulfate, and the solvents were evaporated to afford compound **11** (190 mg, 84%): 167−169 °C (acetone/*n*-heptane); $[\alpha]_D$ +63.1 (c 0.28, $CHCl_3$). ^{1}H NMR (400 MHz, $CDCl_3$): δ 0.79 (3H, s, H-18), 0.93 (3H, s, H-19), 3.63 (1H, tt, J_1 = 11.0, J_2 = 4.7, H-3), 3.76 (1H, t, J = 9.5, H-17α). ^{13}C NMR (101

DOI: 10.1021/acs.jmedchem.5b00570
J. Med. Chem. 2015, 58, 5950−5966

PDF-XChange Editor
KOUPIT plnou verzi!
www.pdfxchange.cz

MHz, $CDCl_3$): δ 71.8 (C-3), 50.1, 44.2 (C-17), 42.3, 42.1, 40.8, 37.4, 37.1, 36.5, 35.5, 34.8, 34.4, 30.6, 27.1, 26.5, 25.5, 23.4, 20.6, 17.1. IR spectrum ($CHCl_3$): 3609 (OH); 1031 (C−O); 606 (C−I). MS ESI: m/z 425.1 (25%, M + Na). HR-MS (ESI) m/z: for $C_{19}H_{31}$ OINa [M + Na] calcd, 425.1322; found, 425.1306.

*17β-Iodo-5β-androstan-3α-yl 3-Sulfate Pyridinium Salt (**12**).* Compound **12** was prepared according to General Procedure for Sulfation. Starting from compound **11** (255 mg, 0.63 mmol), compound **12** (298 mg, 72%) was obtained as a white solid: mp 118−120 °C; $[\alpha]_D$ +58.5 (c 0.39, $CHCl_3$/MeOH 1.94:0.20). ^{1}H NMR (400 MHz, $CDCl_3$): δ 0.79 (3H, s, H-18), 0.92 (3H, s, H-19), 3.76 (1H, t, J = 9.4, H-17α), 4.39 (1H, tt, J_1 = 11.0, J_2 = 5.0. H-3), 7.32 (2H, ddd, J_1 = 7.6, J_2 = 4.3, J_3 = 1.5. H-2′ and H-4′, pyridinium), 7.72 (1H, tt, J_1 = 7.7, J_2 = 1.8, H-3′, pyridinium), 8.64 (2H, dt, J_1 = 4.6, J_2 = 1.7, H-1′ and H-5′, pyridinium). ^{13}C NMR (101 MHz, $CDCl_3$): δ 149.6 (C-1′ and C-5′, pyridinium), 136.4 (C-3′, pyridinium), 128.6 (C-2′ and C-4′, pyridinium), 78.8, 50.1, 46.4, 44.2, 42.3, 42.1, 40.6, 37.2, 35.5, 34.7, 34.4, 33.4, 27.9, 27.0, 26.4, 25.5, 23.1, 20.5, 17.0. IR spectrum ($CHCl_3$): 3434, 3608 (OH); 1385 (CH_3); 1027, 1034 (C−O). MS (ESI): m/z 481.2 (100%, M − pyH). HR-MS (ESI) m/z: for $C_{19}H_{30}O_4IS$ [M-pyH] calcd, 481.0904; found, 481.0908.

*5β-Androstan-3α-ol (**14**).* Trimethylsilyl chloride (84 mL, 0.65 mol) was added dropwise to a stirred solution of compound **13** (6 g, 0.02 mol) and zinc powder (42 g, 0.38 mol) in dichloromethane and methanol (1:1, 180 mL) at 0 °C. The reaction mixture was stirred at room temperature. After 4 h, heterogeneous zinc pellets were removed by filtration and to the filtrate was added a saturated solution of sodium bicarbonate (to pH 7). To clear the white emulsion, chloroform (3 × 50 mL) and an aqueous solution of hydrochloric acid (5%, 30 mL) was added. The now transparent organic and aqueous layers were separated, and the organic phase was separated, washed with brine, and dried. Solvents were evaporated, and the residue was purified by column chromatography (4% of acetone in petroleum ether) to afford white solids of **14** (4.5 g, 79%): mp 143−144 °C (acetone/n-heptane); $[\alpha]_D$ +10.9 (c 0.27, $CHCl_3$). ^{1}H NMR (400 MHz, $CDCl_3$): δ 0.68 (3H, s, H-18), 0.92 (3H, s, H-19), 3.58−3.67 (1H, m, H-3). ^{13}C NMR (101 MHz, $CDCl_3$): δ 72.0 (C-3), 54.7, 42.2, 41.0, 40.9, 40.6, 39.2, 36.6, 36.3, 35.6, 34.8, 30.7, 27.3, 26.9, 25.7, 23.5, 20.9, 20.7, 17.6. IR spectrum ($CHCl_3$): 3608, 3446 (OH); 2972, 2887, 1377 (CH_3); 2935, 2865, 1450 (CH_2); 1081, 1065, 1034 (CO). For $C_{19}H_{32}O$ (276.2) calcd: 82.55%, C; 11.67%, H. Found: 82.31% C, 11.82% H.

*5β-Androstan-3α-yl 3-Sulfate Pyridinium Salt (**15**).* Compound **15** was prepared according to General Procedure for Sulfation. Starting from compound **14** (200 mg, 0.72 mmol), compound **15** (211 mg, 67%) was obtained as a white solid: mp 180−182 °C (chloroform); $[\alpha]_D$ +16.0 (c 0.28, $CHCl_3$/MeOH, 2:0.1). ^{1}H NMR (400 MHz, $CDCl_3$): δ 0.67 (3H, s, H-18), 0.92 (1H, s. H-19), 4.48 (1H, tt, J_1 = 11.3, J_2 = 4.9, H-3), 7.94−8.04 (2H, m, H-2′ and H-4′, pyridinium), 8.47 (1H, tt, J_1 = 7.9, J_2 = 1.6, H-3′, pyridinium), 8.97 (2H, dt, J_1 = 5.6, J_2 = 1.5, H-1′ and H-5′, pyridinium). ^{13}C NMR (101 MHz, $CDCl_3$/CD_3OD): δ 145.5 (C-1′ and C-5′, pyridinium), 142.3 (C-3′, pyridinium), 127.0 (C-2′ and C-4′, pyridinium), 79.7 (C-3), 54.6, 42.2, 40.9, 40.7, 40.5, 39.1, 36.2, 35.4, 34.6, 33.3, 27.8, 27.1, 26.8, 25.5, 23.3, 20.8, 20.6, 17.5. IR spectrum ($CHCl_3$): 1260, 1178, 1050, 970 (OSO_3). MS (EI): m/z 355.2 (100%, M − pyH). HR-MS (ESI) m/z: for $C_{19}H_{31}O_4S$ [M − pyH] calcd, 355.1949; found, 355.1949.

*17-Methylene-5β-androstan-3α-ol (**16**).* Sodium hydride (50% in parafine oil, 80 mg, 1.70 mmol) was added to a solution of methyltriphenylphosphonium bromide (619 mg, 1.73 mmol) in dry DMSO (4 mL) under inert atmosphere, and the reaction mixture was stirred at room temperature for 1 h. Then, a solution of **13** (100 mg, 0.34 mmol) in dry DMSO (3 mL) was added. After 1.5 h of stirring at 70 °C, an aqueous solution of ammonium chloride was added. The product was extracted with chloroform (2 × 20 mL), and the combined organic extracts were washed with brine and dried. Solvents were evaporated, and the residue was purified by chromatography on pre-TLC plates (40% ether in petroleum ether) to afford compound **16** (90 mg, 90%): mp 147−149 °C (acetone/n-heptane); $[\alpha]_D$ +30.5 (c 0.22, $CHCl_3$). ^{1}H NMR (400 MHz, $CDCl_3$): δ 0.75 (3H, s, H-18), 0.93 (3H, s, H-19), 2.22 (1H, dtt, J_1 = 17.7, J_2 = 8.8, J_3 = 2, H-16a), 2.47 (1H, dddd, J_1 = 16.9, J_2 = 10, J_3 = 4.4, J_4 = 2.2. H-16b), 3.62 (1H, m, H-3), 4.50−4.62 (2H, m, =CH_2). ^{13}C NMR (101 MHz, $CDCl_3$): δ 162.0 (C-17), 100.7 (C-20), 71.9 (C-3), 54.6, 44.3, 42.3, 40.8, 36.5, 36.0, 35.9, 35.5, 34.8, 30.6, 29.6, 27.2, 26.5, 24.3, 23.5, 20.8, 18.6. IR spectrum ($CHCl_3$): 3609, 3451, 1031 (OH); 1653 (C=C). MS (ESI): m/z 311.3 (100%, M + Na). HR-MS (ESI) m/z: for $C_{20}H_{32}ONa$ [M + Na] calcd, 311.2345; found, 311.2344.

*17-Methylene-5β-androstan-3α-yl 3-Sulfate Pyridinium Salt (**17**).* Compound **17** was prepared according to General Procedure for Sulfation. Starting from compound **16** (50 mg, 0.17 mmol), compound **17** (63 mg, 81%) was obtained as a white solid: mp 155−159 °C; $[\alpha]_D$ +41.6 (c 0.25, $CHCl_3$). ^{1}H NMR (400 MHz, $CDCl_3$): δ 0.73 (3H, s, H-18), 0.91 (3H, s, H-19), 2.22 (1H, dt, J_1 = 17.3, J_2 = 8.7, H-16a), 2.47 (1H, m, H-16b), 4.44 (1H, m, H-3), 4.59 (2H, m, =CH_2), 7.51 (2H, ddd, J_1 = 7.7, J_2 = 4.7, J_3 = 1.4, H-2′ and H-4′, pyridinium), 7.93 (1H, tt, J_1 = 7.7, J_2 = 1.7, H-3′, pyridinium), 8.74 (2H, d, J = 4.5, H-1′ and H-5′, pyridinium). ^{13}C NMR (101 MHz, $CDCl_3$): δ 162.0 (C-17), 147.4 (C-1′ and C-5′, pyridinium), 139.2 (C-3′, pyridinium), 124.9 (C-2′ and C-4′, pyridinium), 100.7 (C-20), 79.5 (C-3), 54.6, 44.3, 42.3, 40.8, 36.0, 35.8, 35.4, 34.7, 33.4, 29.5, 27.8, 27.0, 26.4, 24.2, 23.4, 20.8, 18.6. IR spectrum ($CHCl_3$): 3140, 3093, 1490, 826 (pyridinium); 1653 (C=C). MS ESI: m/z 367.1 (100%, M − pyH). HR-MS (ESI) m/z: for $C_{20}H_{32}O_4S$ [M − pyH] calcd, 367.1948; found, 367.1946.

*7β-Methyl-5β-pregn-3α-ol (**18**).* Compound **18** was prepared in the same manner as compound **6**. Starting from compound **16** (100 mg, 0.34 mmol), a mixture of 17α- and 17β-isomers (1:10) was obtained. Further crystallization from acetone/n-heptane compound afforded 17β-methyl derivative **18** (75 mg, 75%): mp 151−153 °C (acetone/n-heptane); $[\alpha]_D$ +18.1 (c 0.21, $CHCl_3$). ^{1}H NMR (400 MHz, $CDCl_3$): δ 0.52 (3H, s, H-18), 0.82 (3H, d, J = 6.8, 17-Me), 0.92 (3H, s, H-19), 3.62 (1H, m, H-3). ^{13}C NMR (101 MHz, $CDCl_3$): δ 72.0 (C-3), 56.0, 45.3, 42.4, 42.3, 41.0, 37.9, 36.7, 36.2, 35.6, 34.9, 30.7, 30.4, 27.4, 26.8, 24.9, 23.5, 20.7, 13.9, 12.1. IR spectrum ($CHCl_3$): 3610, 1034 (OH); 1379 (CH_3). MS (ESI): m/z 313.2 (100%, M + Na). For $C_{20}H_{34}O$ (290.5) calcd: 82.69%, C; 11.80%, H. Found: 82.62%, C; 11.37%, H.

*17β-Methyl-5β-pregn-3α-yl 3-Sulfate Pyridinium Salt (**19**).* Compound **19** was prepared according to General Procedure for Sulfation. Starting from compound **18** (50 mg, 0.17 mmol), compound **19** (66 mg, 85%) was obtained as a white solid: mp 174−175 °C; $[\alpha]_D$ +21.6 (c 0.18, $CHCl_3$). ^{1}H NMR (400 MHz, $CDCl_3$): δ 0.51 (3H, s, H-18), 0.81 (3H, d, J = 6.8, 17-Me). 0.91 (3H, s, H-19), 4.46 (1H, m, H-3), 8.00 (2H, m, H-2′ and H-4′, pyridinium), 8.48 (1H, t, J = 7.8, H-3′, pyridinium), 8.97 (2H, d, J = 5.4, H-1′ and H-5′, pyridinium). ^{13}C NMR (101 MHz, $CDCl_3$): δ 145.8 (C-1′ and C-5′, pyridinium), 142.3 (C-3′, pyridinium), 127.2 (C-2′ and C-4′, pyridinium), 79.9 (C-3), 56.0, 45.2, 42.3, 42.3, 40.9, 37.8, 36.1, 35.5, 34.7, 33.4, 30.3, 27.8, 27.1, 26.7, 24.8, 23.4, 20.6, 13.9, 12.1. IR spectrum ($CHCl_3$): 3140, 3100, 1490, 1028 (pyridinium); 1263, 1172 (SO_3); 1486, 1379 (CH_3). MS ESI: m/z 369.2 (100%, M − pyH). HR-MS (ESI) m/z: For $C_{20}H_{33}O_4S$ [M − pyH] calcd, 369.2105; found, 369.2103.

*(17Z)-5β-Pregn-17(20)-en-3α-ol (**20**).* Compound **20** was prepared according to the literature.[21] ^{1}H NMR (400 MHz, $CDCl_3$): δ 0.85 (3H, s, H-18), 0.93 (3H, s, H-19), 1.64 (3H, dt, J_1 = 7.1, J_2 = 2.0, H-21), 3.62 (1H, bm, H-3), 5.11 (1H, qt. J_1 = 7.1, J_2 = 2.0, H-20). ^{13}C NMR (101 MHz, $CDCl_3$): δ 150.4 (C-20), 113.2 (C-20), 71.8 (C-3), 56.3, 44.4, 42.1, 40.5, 37.4, 36.4, 35.4, 35.3, 34.6, 31.5, 30.5, 27.1, 26.3, 24.4, 23.3, 21.0, 16.8, 13.0.

*(17Z)-5β-Pregn-17(20)-en-3α-yl 3-Sulfate Pyridinium Salt (**21**).* Compound **21** was prepared according to the General Procedure for Sulfation. Starting from compound **20** (100 mg, 0.33 mmol), compound **21** (95 mg, 63%) was obtained as a white solid: mp 171−173 °C (chloroform); $[\alpha]_D$ +35.1 (c 0.21, $CHCl_3$). ^{1}H NMR (400 MHz, $CDCl_3$): δ 0.84 (3H, s, H-18), 0.91 (3H, s, H-19), 1.64 (3H, dt, J_1 = 7.1, J_2 = 2.0, H-21), 4.45 (1H, tt, J_1 = 10.9, J_2 = 4.9, H-3), 5.10 (1H, qt, J_1 = 7.1, J_2 = 2.1, H-20), 8.01 (2H, m, H-2′ and H-4′, pyridinium), 8.47 (1H, tt, J_1 = 7.9, J_2 = 1.6, H-3′, pyridinium), 8.99

DOI: 10.1021/acs.jmedchem.5b00570
J. Med. Chem. 2015, 58, 5950−5966

PDF-XChange Editor
KOUPIT plnou verzi!
www.pdfxchange.cz

(2H, m, H-1′ and H-5′, pyridinium). ^{13}C NMR (101 MHz, $CDCl_3$): δ 150.5 (C-20), 145.8 (C-1′ and C-5′, pyridinium), 142.4 (C-3′, pyridinium), 127.3 (C-2′ and C-4′, pyridinium), 113.3 (C-17), 79.7 (C-3), 56.4, 44.5, 42.2, 40.6, 37.5, 35.4, 35.4, 34.6, 33.4, 31.6, 27.9, 27.1, 26.3, 24.5, 23.4, 21.1, 16.9, 13.2. IR spectrum ($CHCl_3$): 3140, 3099, 3072 (pyridinium); 2943, 2868 (CH_3); 1665 (C═C); 1262, 1253, 1179 (OSO_3). MS (ESI): m/z 381.2 (100%, M + H − pyridine). HR-MS (ESI) m/z: For $C_{21}H_{33}O_4S$ [M + pyH] calcd, 381.2103; found, 381.2103.

*3α-Methoxymethoxy-5β-androstan-17-one (**22**).* The MOM-protecting group was introduced to compound **22** in the same manner as described for compound **8**. Starting from compound **13** (2 g, 6.88 mmol), compound **22** (2.14 g, 93%) was obtained as an oily product by column chromatography (10% ethyl acetate in petroleum ether): $[\alpha]_D$ +98.5 (*c* 0.13, $CHCl_3$). ^{1}H NMR (400 MHz, $CDCl_3$): δ 0.83 (3H, s, H-18), 0.92 (3H, s, H-19), 2.06 (1H, m, H-16a), 2.41 (1H, m, H-16b), 3.35 (3H, s, OCH_3), 3.51 (1H, m, H-3), 4.66 (2H, s, OCH_2O). ^{13}C NMR (101 MHz, $CDCl_3$): δ 221.3 (C-17), 94.7 (OCH_2O), 76.8 (C-3), 55.2 (CH_3O), 51.6, 47.9, 42.2, 40.8, 36.0, 35.5, 35.4, 35.0, 33.6, 31.8, 27.8, 27.0, 25.4, 23.4, 21.9, 20.2, 13.9. IR spectrum ($CHCl_3$): 2939, 2868, 2890 (OCH_2O); 1732 (C═O); 1045 (C−O). MS ESI: m/z 357.2 (100%, M + Na). HR-MS (ESI) m/z: for $C_{21}H_{34}O_3Na$ [M + Na] calcd, 357.2400; found, 357.2398.

*17,17-Difluoro-3α-methoxymethoxy-5β-androstane (**23**).* Bis(2-methoxyethyl)aminosulfur trifluoride (Deoxo-fluor, 50% solution in THF, 5 mL, 11.6 mmol) was added to compound **22** (820 mg, 2.45 mmol) in a glass tube. The tube was filled with argon and sealed, and the reaction mixture was stirred and heated to 80 °C for 48 h. Then, the tube was cooled to 0 °C and opened. The mixture was diluted with ethyl acetate (3 × 40 mL), washed with a saturated solution of potassium bicarbonate and water, and dried over $MgSO_4$. Solvents were evaporated, and the residue was purified by column chromatography (10% ether in petroleum ether) to afford oily product **23** (240 mg, 27%): $[\alpha]_D$ +8.7 (*c* 0.42, $CHCl_3$). ^{1}H NMR (400 MHz, $CDCl_3$): δ 0.85 (3H, d, *J* = 2.0, H-18), 0.93 (3H, s, H-19), 3.37 (3H, s, OCH_3), 3.49−3.57 (1H, m, H-3), 4.68 (2H, s, OCH_2O). ^{13}C NMR (101 MHz, $CDCl_3$): δ 132.7 (C-17), 94.7 (OCH_2O), 76.9 (C-3), 55.3 (OCH_3), 49.6, 45.5, 42.2, 40.4, 35.9, 35.5, 34.9, 33.7, 33.1, 29.2, 27.8, 27.1, 25.7, 23.4, 22.4, 20.0, 13.5. IR spectrum ($CHCl_3$): 2825 (OCH_3); 1317, 1167 (CF_2); 1106 (MOM). MS ESI: m/z 379.1 (100%, M + Na). HR-MS (ESI) m/z: for $C_{21}H_{34}O_2F_2Na$ [M + Na] calcd, 379.2419; found, 379.2422.

*17,17-Difluoro-5β-androstan-3α-ol (**24**).* Starting from compound **23** (150 mg; 0.42 mmol), compound **24** (120 mg, 91%) was obtained by the hydrolysis of the MOM protecting group described for compound **11**, followed by crystallization: mp 130−132 °C (acetone/*n*-heptane); $[\alpha]_D$ +2.7 (*c* 0.29, $CHCl_3$). ^{1}H NMR (400 MHz, CDCl3): δ 0.85 (3H, d, *J* = 2.0, H-18), 0.93 (3H, s, H-19), 3.58−3.68 (1H, m, H-3). ^{13}C NMR (101 MHz, $CDCl_3$): δ 132.7 (C-17), 71.8 (C-3), 49.6, 45.5, 42.2, 40.5, 36.5, 35.9, 35.5, 34.8, 33.1, 30.7, 29.2, 27.0, 25.7, 23.4, 22.4, 20.0, 13.5. IR spectrum ($CHCl_3$): 3609 (OH); 1317, 1168 (CF_2); 1035 (C−OH). MS ESI: m/z: 335.2 (75%, M + Na), 313.2 (5%, M + 1). HR-MS (ESI) m/z: for $C_{19}H_{30}OF_2Na$ [M + Na] calcd, 335.2156; found, 335.2161.

*17.17-Difluoro-5β-androstan-3α-yl 3-Sulfate Pyridinium Salt (**25**).* Compound **25** was prepared according to General Procedure for Sulfation. Starting from compound **24** (86 mg, 0.28 mmol), compound **25** (96 mg, 73%) was obtained as a white solid: mp 185−187 °C; $[\alpha]_D$ +12.5 (*c* 0.28, $CHCl_3$/MeOH, 1.97:0.04). ^{1}H NMR (400 MHz, $CDCl_3$): δ 0.84 (3H, d, *J* = 2.0, H-18), 0.92 (3H, s, H-19), 4.46 (1H, tt, J_1 = 10.8, J_2 = 5.1, H-3), 8.09−7.99 (2H, m, H-2′ and H-4′, pyridinium), 8.44−8.51 (1H, m, H-3′, pyridinium), 7.96−8.02 (2H, m, H-1′ and H-5′, pyridinium). ^{13}C NMR (101 MHz, $CDCl_3$/MeOH): δ 145.8 (C-1′ and C-5′, pyridinium), 142.4 (C-3′, pyridinium), 127.2 (C-2′ and C-4′, pyridinium), 79.5, 58.6, 49.6, 42.2, 40.4, 35.72, 35.4, 34.7, 33.4, 33.0, 29.2, 27.8, 26.8, 25.6, 23.3, 22.4, 20.0, 18.5, 13.4. IR spectrum ($CHCl_3$): 1350, 1121 (CF_2); 1247, 1168, 973, 947 (OSO_3). MS (ESI): m/z 391.2 (100%, M − pyH). HR-MS (ESI) m/z: for $C_{19}H_{29}F_2S$ [M − pyH] calcd, 391.1760; found, 391.1757.

*17β-Spiro-(5β-androstan-17.2′-oxiran)-3α-ol (**26**).* Potassium *tert*-butoxide (267 mg, 2.38 mmol) and trimethylsulfonium iodide (486 mg, 2.38 mmol) were added in one portion to a solution of compound **13** (346 mg, 1.19 mmol) in anhydrous *N*,*N*′-dimethylformamide (6 mL) under inert atmosphere. The reaction mixture was stirred at room temperature overnight. Then, brine was added and the product was extracted with chloroform (3 × 30 mL), combined organic extracts were dried, and solvent was evaporated. The residue was purified by column chromatography (0−15% ethyl acetate in petroleum ether) to afford compound **26** (284 mg, 78%):[40] mp 149−150 °C (ether/petroleum ether), mp 155−158 °C (ether/heptane).[40] ^{1}H NMR (400 MHz, $CDCl_3$): δ 0.85 (3H, s, H-18), 0.92 (3H, s, H-19), 2.60 (1H, d, *J* = 5.1, H-20a), 2.89 (1H, d, *J* = 5.1, H-20b), 3.63 (1H, m, H-3). ^{13}C NMR (101 MHz, $CDCl_3$): δ 71.8 (C-3), 70.7 (C-17), 53.7 (C-20), 53.0 (C-14), 42.2, 40.7, 40.3, 36.5, 36.1, 35.5, 34.8, 34.3, 30.6, 29.2, 27.1, 26.0, 23.7, 23.4, 20.3, 14.4. HR-MS (ESI) m/z: For $C_{20}H_{32}O_2Na$ [M + Na] calcd, 327.2294; found, 327.2293.

*17α-Azidomethyl-3α-17β-dihydroxy-5β-androstane (**27**).* A solution of compound **26** (560 mg, 1.83 mmol), sodium azide (341 mg, 5.68 mmol), and ammonium chloride (341 mg, 6.37 mmol) in ethanol (28 mL) and water (5.6 mL) was heated at 90 °C overnight. Then, water was added, ethanol was evaporated, and the product was extracted with chloroform (2 × 50 mL), combined organic extracts were dried, and solvent was evaporated. The product was purified by column chromatography (30% ether in petroleum ether) to afford compound **27** (500 mg, 78%) as a white foam: $[\alpha]_D$ 0.0 (*c* 0.11, $CHCl_3$). ^{1}H NMR (400 MHz, $CDCl_3$): δ 0.86 (3H, s, H-18), 0.93 (3H, s, H-19), 3.26 (1H, d, *J* = 12, H_a-CH_2N_3), 3.54 (1H, d, *J* = 12, H_b-CH_2N_3), 3.63 (1H, m, H-3). ^{13}C NMR (101 MHz, $CDCl_3$): δ 83.6 (C-17), 71.8 (C-3), 58.5 (CH_2N_3), 51.5, 46.1, 42.1, 40.6, 36.6, 36.5, 35.4, 34.9, 34.8, 32.3, 30.6, 27.1, 26.34, 23.7, 23.4, 20.5, 14.3. IR spectrum ($CHCl_3$): 3613, 1037 (3α-OH); 3562, 1116 (17β-OH); 2106 (azide). MS ESI: m/z 370.2 (100%, M + Na). HR-MS (ESI) m/z: for $C_{20}H_{33}O_2N_3Na$ [M + Na] calcd, 370.2465; found, 370.2464.

*17a-Oxo-D-homo-5β-androstan-3α-ol (**28**).* Sodium iodide (948 mg, 6.3 mmol) was added to a solution of compound **27** (220 mg, 0.63 mmol) in dry acetonitrile (10 mL). Then, trimethylsilyl chloride (0.8 mL, 6.26 mmol) was added dropwise under inert atmosphere. The reaction mixture was stirred at room temperature, and the progress of the reaction was checked by TLC. An aqueous solution of hydrochloride acid (5%, 10 mL) was added, and the product was extracted with chloroform (2 × 40 mL), combined organic extracts were washed with sodium sulfite and brine and dried, and solvent was evaporated. Yellow solids were purified by column chromatography (30% ether in petroleum ether) to afford compound **28** (140 mg, 73%): mp 201−201 °C (ether/petroleum ether); $[\alpha]_D$ −23.6 (*c* 0.12, $CHCl_3$). ^{1}H NMR (400 MHz, $CDCl_3$): δ 0.91 (3H, s, H-18), 1.06 (3H, s, H-19), 2.04 (1H, m, H_a-16), 2.19 (1H, m, H_a −17), 2.61 (1H, td, J_1 = 14.0, J_2 = 6.8, H_b-17), 3.61 (1H, m, H-3). ^{13}C NMR (101 MHz, $CDCl_3$): δ 216.7 (C-17a), 71.8 (C-3), 51.7, 48.5, 41.7, 39.8, 37.3, 36.3, 35.6, 35.0, 35.0, 32.7, 30.7, 27.2, 26.1, 25.9, 23.49, 23.1, 19.8, 17.0. IR spectrum ($CHCl_3$): 3609, 1037 (OH); 1698 (C═O). MS ESI: m/z 327.2 (100%, M + Na), 631.5 (15%, 2 M + Na). For $C_{20}H_{32}O_2$ (304.4) Calcd: 78.90%, C; 10.59%, H. Found: 78.55%, C; 10.49%, H.

*D-Homo-5β-androstan-3α-ol (**29**).* Starting from compound **28** (110 mg, 0.36 mmol), compound **29** (68 mg, 65%) was obtained by the same deoxygenation procedure as compound **14** followed by column chromatography on silica gel (30% of ether in petroleum ether): mp 187−189 °C (acetone/*n*-heptane); $[\alpha]_D$ +17.1 (*c* 0.20, $CHCl_3$). ^{1}H NMR (400 MHz, $CDCl_3$): δ 0.78 (3H, s, H-18), 0.89 (3H, s, H-19), 3.62 (1H, m, H-3). ^{13}C NMR (101 MHz, $CDCl_3$): δ 72.0 (C-3), 51.2, 42.5, 42.4, 42.0, 40.7, 36.5, 36.0, 35.2, 35.0, 33.7, 30.7, 27.4, 27.3, 25.5, 24.2, 23.6, 21.6, 20.3, 17.0. IR spectrum ($CHCl_3$): 3609, 3447, 1031 (OH). MS ESI: m/z 313.3 (100%, M + Na). For $C_{20}H_{34}O$ (290.4) Calcd: 82.69%, C; 11.80%, H. Found: 82.42%, C; 11.71%, H.

*D-Homo-5β-androstan-3α-yl 3-Sulfate Pyridinium Salt (**30**).* Compound **30** was prepared according to General Procedure for Sulfation. Starting from compound **29** (30 mg, 0.10 mmol),

DOI: 10.1021/acs.jmedchem.5b00570
J. Med. Chem. 2015, 58, 5950−5966

PDF-XChange Editor
KOUPIT plnou verzi!
www.pdfxchange.cz

compound **30** (43 mg, 93%) was obtained as a white solid: mp 173−174 °C; $[\alpha]_D$ +20.4 (*c* 0.27, $CHCl_3$). ^1H NMR (400 MHz, $CDCl_3$): δ 0.76 (3H, s, H-18), 0.87 (3H, s, H-19), 4.45 (1H, m, H-3), 8.00 (2H, m, H-2′ and H-4′, pyridinium), 8.48 (1H, t, *J* = 7.8, H-3′, pyridinium), 8.98 (2H, d, *J* = 5.5, H-1′ and H-5′, pyridinium). ^{13}C NMR (101 MHz, $CDCl_3$): δ 145.8 (C-1′and C-5′, pyridinium), 142.3 (C-3′, pyridinium), 127.3 (C-2′ and C-4′, pyridinium), 79.8 (C-3), 51.2, 42.5, 42.4, 42.0, 40.6, 35.9, 35.1, 34.9, 33.7, 33.3, 27.9, 27.3, 27.2, 25.4, 24.2, 23.5, 21.6, 20.4, 17.0. IR ($CHCl_3$): 3139, 3100, 1637, 1490 (pyH); 1263, 1238, 1235, 1043 (SO_3). MS ESI: *m*/*z* 369.3 (100%. M − pyH). HR-MS (ESI) *m*/*z*: for $C_{20}H_{33}O_4S$ [M − pyH] calcd, 369.2105; found, 369.2103.

*3α-Methoxymethoxy-5β-androstan-17β-ol (**31**).* Compound **31** was prepared in the same manner as compound **9**. Starting from compound **22** (600 mg, 1.79 mmol), compound **31** (568 mg, 94%) was obtained as oily product by introduction of the MOM protecting group described for derivative **9**, followed by column chromatography on silica gel (20−30% of ether in petroleum ether): $[\alpha]_D$ +24.6 (*c* 0.39, $CHCl_3$). ^1H NMR (400 MHz, $CDCl_3$): δ 0.71 (3H, s, H-18), 0.91 (3H, s, H-19), 2.05 (1H, m, H-16a), 3.35 (3H, s, OCH_3), 3.52 (1H, m, H-3), 3.62 (1H, t, *J* = 8.6, H-17), 4.67 (2H, s, OCH_2O). ^{13}C NMR (101 MHz, $CDCl_3$): δ 94.6 (OCH_2O), 82.0 (C-17), 76.9 (C-3), 55.2 (OCH_3), 51.2, 43.2, 42.2, 40.7, 37.0, 36.0, 35.5, 34.9, 33.6, 30.7, 27.8, 27.2, 26.1, 23.5 (2 × C), 20.5, 11.2. IR spectrum ($CHCl_3$): 3614 (OH); 1450, 1042 (C−O). MS ESI: *m*/*z* 359.3 (100%, M + Na), 695.7 (15%, 2 M + Na). HR-MS (ESI) *m*/*z*: for $C_{21}H_{36}O_3Na$ [M + Na] calcd, 359.2556; found, 359.2556.

*3α-Methoxymethoxy-5β-androstan-17β-yl 17-Tosylate (**32**).* A solution of compound **31** (548 mg, 1.62 mmol), 4-dimethylaminopyridine (10 mg, 0.08 mmol), and *p*-TsCl (555 mg, 2.9 mmol) in anhydrous pyridine (15 mL) was heated at 45 °C for 35 h. Then, additional portions of 4-dimethylaminopyridine (10 mg, 0.08 mmol), and *p*-TsCl (92 mg, 0.48 mmol) were added and the reaction mixture was heated at 45 °C overnight. Then, it was poured into water; the product was extracted with chloroform (2 × 50 mL), and combined organic extracts were washed with aqueous hydrochloric acid (5%, 2 × 20 mL), sodium bicarbonate and brine and then dried. After solvent evaporation, the oily residue was purified by column chromatography (10% ether in petroleum ether) to give compound **32** (650 mg, 81%) as an oily product: $[\alpha]_D$ +5.5 (*c* 0.29, $CHCl_3$). ^1H NMR (400 MHz, $CDCl_3$): δ 0.75 (3H, s, H-18), 0.87 (3H, s, H-19), 2.43 (3H, s, CH_3, tosyl), 3.34 (3H, s, OCH_3), 3.49 (1H, m, H-3), 4.21 (1H, t, *J* = 8.5, H-17), 4.65 (2H, s, OCH_2O), 7.31 (2H, m, H-3′ and H-5′, tosyl), 7.77 (2H, m, H-2′and H-6′, tosyl). ^{13}C NMR (101 MHz, $CDCl_3$): δ 144.4 (C-1′, tosyl), 134.3 (C-4′, tosyl), 129.7 (C-2′ and C-6′, tosyl), 127.9 (C-3′ and C-5′, tosyl), 94.6 (OCH_2O), 90.1 (C-17), 76.6 (C-3), 55.2 (OCH_3), 50.1, 43.2, 42.1, 40.4, 36.4, 35.6, 35.4, 34.8, 33.6, 27.8, 27.7, 27.0, 25.9, 23.4, 21.7, 20.1, 14.3, 11.8. IR spectrum ($CHCl_3$): 3020 (phenyl); 1600 (C═C); 1357, 1175 (SO_2); 1098 (C−O). MS ESI: *m*/*z* 513.1 (100%, M + Na), 1003.3 (55%. 2 M + Na). HR-MS (ESI) *m*/*z*: for $C_{28}H_{42}O_5NaS$ [M + Na] calcd, 513.2645; found, 513.2645.

*3α-Methoxymethoxy-10,17β-methyl-5β-gon-13(17)-ene (**33**).* Compound **32** (600 mg, 1.22 mmol) was dissolved in anhydrous toluene (30 mL) and heated at 100 °C under inert atmosphere. Then, methyl magnesium bromide (3.0 M in ether, 2 mL, 6.25 mmol) was added to the stirring hot solution under inert atmosphere as a white precipitate appeared. The reaction mixture was heated at 120 °C for 1 h. The flask was cooled, a few pieces of crushed ice were added, and the pH of the solution was adjusted to pH 2 by dropwise addition of 2 N HCl. The toluene layer was separated, and the aqueous layer was extracted with ethyl acetate (2 × 50 mL). The combined extracts were washed with brine and dried and the solvents evaporated. Column chromatography on silica gel (5% ether in petroleum ether) gave compound **33** (247 mg, 63%) as an oily product: $[\alpha]_D$ −2.2 (*c* 0.13, $CHCl_3$). ^1H NMR (400 MHz, $CDCl_3$): δ 0.82 (3H, s, H-19), 1.58 (3H, s, CH_3), 3.37 (3H, s, OCH_3), 3.54 (1H, m, H-3), 4.69 (2H, s, OCH_2O). ^{13}C NMR (101 MHz, $CDCl_3$): δ 136.7 (C-13), 127.7 (C-17), 94.7 (OCH_2O), 76.6 (C-3), 55.2 (OCH_3), 53.9, 45.8, 42.4, 38.9, 37.3, 35.4, 34.9, 33.6, 28.3, 28.1, 27.1, 26.6, 26.1, 25.7, 23.6, 13.5. IR spectrum ($CHCl_3$): 2824, 1145, 1043, 1102 (OCH_2O); 1375 (CH_3). MS ESI: *m*/*z* 341.2 (100%, M + Na), 659.5 (50%, 2 M + Na). HR-MS (ESI) *m*/*z*: for $C_{21}H_{34}O_2Na$ [M + Na] calcd, 341.2451; found, 341.2449.

*3α-Methoxymethoxy-10,17α-dimethyl-5β,13α-gonane and 3α-Methoxymethoxy-10,17β-dimethyl-5β-gonane, a mixture of isomers (**34**).* Compound **33** (119 mg, 0.37 mmol) was dissolved in ethyl acetate (2 mL) and ethanol (6 mL). To this, Pd/C (10%, 30 mg) was added. The reaction mixture was hydrogenated under slight pressure at room temperature for 7 h. Then, the reaction mixture was filtered through a short column of silica gel to remove the catalyst and washing with ethyl acetate (30 mL). Solvents were removed under vacuo. A mixture of products was purified by chromatography on preparative TLC (three plates, 15% ether in petroleum ether) to afford 99 mg (83%) of compound **34** as a mixture of two inseparable products. ^1H NMR (400 MHz, $CDCl_3$): δ 0.76 (3H, d, *J* = 7.2, H-13*β*, 17*β*-Me). 0.86 (6H, s, H-19), 0.92 (3H, d, *J* = 6.5, H-13*α*, 17*α*-Me), 3.36 (6H, s, OCH_3), 3.53 (2H, m, H-3), 4.68 (4H, s, OCH_2O). ^{13}C NMR (101 MHz, $CDCl_3$): δ 94.7 (OCH_2O), 55.2 (OCH_3), 53.4, 53.2, 49.1, 48.4, 43.1, 42.8, 42.4, 42.4, 39.9, 39.8, 39.3, 35.6, 34.9, 34.9, 34.4, 33.7, 32.6, 32.3, 30.0, 29.4, 28.0, 27.9, 27.6, 27.2, 26.9, 26.7, 25.8, 25.5, 23.6, 18.8, 17.8. IR spectrum ($CHCl_3$): 2826, 1145, 1043, 1103 (OCH_2O); 1375 (CH_3). MS ESI: *m*/*z* 343.2 (100%, M + Na). HR-MS (ESI) *m*/*z*: for $C_{21}H_{36}O_2Na$ [M + Na] calcd, 343.2607; found, 343.2608.

*10,17α-Dimethyl-5β,13α-gonan-3α-ol (**35a**) and 10,17β-Dimethyl-5β-gonan-3α-ol (**35b**).* Acyl chloride (0.4 mL, 5.6 mmol) was added dropwise to a solution of stereoisomers **34** (173 mg, 0.53 mmol) in methanol (5 mL) and benzene (1 mL), and the reaction mixture was stirred at room temperature for 7 h. Then, a saturated solution of sodium bicarbonate was added (up to pH 7), the products were extracted with chloroform (2 × 20 mL), combined organic extracts were washed with brine and dried, and solvents were evaporated. The crude products were prepurified by chromatography on preparative TLC plates (three plates, 40% ether in petroleum ether) to afford a mixture of isomers (128 mg, 86%). Isomers were separated by HPLC (5% ethyl acetate in hexanes) to afford compounds **35a** (45 mg, 30%) and **35b** (46 mg, 30%) as pure products:

*Compound **35a**.* Melting point 83−86 °C (ether/petroleum ether); $[\alpha]_D$ −21.9 (*c* 0.11, $CHCl_3$). IR spectrum ($CHCl_3$): 3608, 1031 (OH); 1378, 1367 (CH_3). MS ESI: *m*/*z* 299.2 (45%, M + Na), 553.5 (15%, 2 M + 1). HR-MS (ESI) *m*/*z*: for $C_{19}H_{32}ONa$ [M + Na] calcd, 299.2345; found, 299.2344.

*Compound **35b**.* Melting point 110−113 °C (ether/petroleum ether); $[\alpha]_D$ +9.7 (*c* 0.12, $CHCl_3$). IR spectrum ($CHCl_3$): 3608, 1031 (OH); 1376, 1366 (CH_3). MS ESI: *m*/*z* 299.2 (30%, M + Na), 553.5 (20%, 2 M + 1). HR-MS (ESI) *m*/*z*: for $C_{19}H_{32}ONa$ [M + Na] calcd, 299.2345; found, 299.2340.

*10β,17α-Dimethyl-5β,13α-gonan-3α-yl 3-Sulfate Pyridinium Salt (**36a**).* Compound **36a** was prepared according to General Procedure for Sulfation. Starting from compound **35a** (34 mg, 0.12 mmol), compound **36a** (45 mg, 85%) was obtained as a white solid: mp 152−154 °C; $[\alpha]_D$ −0.5 (*c* 0.19, $CHCl_3$). ^1H NMR (400 MHz, $CDCl_3$): δ 0.75 (3H, d, *J* = 7.2, 17-Me). 0.85 (3H, s, H-19), 4.46 (1H, m, H-3), 7.50 (2H, ddd, J_1 = 7.7. J_2 = 4.6, J_3 = 1.4, H-2′ and H-4′, pyridinium), 7.92 (1H, tt, J_1 = 7.7, J_2 = 1.7, H-3′, pyridinium), 8.73 (2H, d, *J* = 4.5, H-1′ and H-5′, pyridinium). ^{13}C NMR (101 MHz, $CDCl_3$): δ 147.5 (C-1′ and C-5′, pyridinium), 139.1 (C-3′, pyridinium), 124.9 (C-2′ and C-4′, pyridinium), 79.7 (C-3), 49.0, 48.4, 43.0, 42.3, 39.7, 35.5, 34.6, 34.3, 33.3, 32.5, 29.4, 27.9, 27.6, 26.9, 26.8, 25.7, 23.4, 17.8. IR spectrum ($CHCl_3$): 3140, 3073, 1490 (pyridinium); 1263, 1172, 1046 (SO_3); 1475, 1377 (CH_3). MS ESI: *m*/*z* 355.2 (100%, M − pyH). HR-MS (ESI) *m*/*z*: for $C_{19}H_{31}O_4S$ [M − pyH] calcd, 355.1948; found, 355.1947.

*10,17β-Dimethyl-5β-gonan-3α-yl 3-Sulfate Pyridinium Salt (**36b**).* Compound **36b** was prepared according to General Procedure for Sulfation. Starting from compound **35b** (37 mg, 0.13 mmol), compound **36b** (56 mg, 96%) was obtained as a white solid: mp 155−157 °C; $[\alpha]_D$ +26.9 (*c* 0.18, $CHCl_3$). ^1H NMR (400 MHz, $CDCl_3$): δ 0.85 (3H, s, H-19), 0.90 (3H, d, *J* = 7.2, 17-Me), 4.45 (1H, m, H-3), 7.37 (2H, ddd, J_1 = 7.7, J_2 = 4.5, J_3 = 1.4, H-2′ and H-4′, pyridinium),

DOI: 10.1021/acs.jmedchem.5b00570
J. Med. Chem. 2015, 58, 5950−5966

PDF-XChange Editor
KOUPIT plnou verzi!
www.pdfxchange.cz

7.70 (1H, tt, J_1 = 7.7, J_2 = 1.8, H-3′, pyridinium), 8.65 (2H, d, J = 4.3, H-1′ and H-5′, pyridinium). ^{13}C NMR (101 MHz, $CDCl_3$): δ 148.8 (C-1′ and C-5′, pyridinium), 137.4 (C-3′, pyridinium), 124.3 (C-2′ and C-4′, pyridinium), 79.7 (C-3), 53.3, 53.2, 42.7, 42.3, 39.8, 39.3, 35.7, 35.5, 34.6, 33.3, 32.2, 30.0, 27.9, 26.9, 26.6, 26.6, 26.5, 25.4, 23.4, 18.8. IR spectrum ($CHCl_3$): 3140, 3073, 1490 (pyH); 1263, 1172, 1046 (SO_3); 1464, 1374 (CH_3). MS ESI: m/z 355.2 (100%, M − pyH). HR-MS (ESI) m/z: for $C_{19}H_{31}O_4S$ [M − pyH] calcd, 355.1948; found, 355.1946.

*3α-Methoxymethoxy-5β-androstan-17-tosylhydrazone (**37**).* Molecular sieves (40 msh, 2 g) were added to a solution of ketone **22** (1 g, 3 mmol) and tosylhydrazide (1.63 g, 8.5 mmol) in dry methanol (70 mL), and the reaction mixture was refluxed for 72 h under inert atmosphere. The progress of the reaction was monitored by TLC. Then, the sieves were filtered off and the solvent was evaporated in vacuo. The residue was dissolved in toluene (100 mL), the precipitate was filtered off, and the solvent was evaporated. The residue was dissolved in ethyl acetate (2 × 50 mL), washed with a saturated solution of sodium bicarbonate (3 × 25 mL), a saturated solution of sodium chloride, and dried. Solvents were evaporated, and the residue was purified by column chromatography (15% of ethyl acetate in petroleum ether) to afford white solids of **37** (1.05g, 67%): mp 97.4−99.5 °C (benzene); $[\alpha]_D$ +44.2 (c 0.33, $CHCl_3$). ^{1}H NMR (400 MHz, $CDCl_3$): δ 0.82 (3H, s, H-18), 0.92 (3H, s, H-19), 2.43 (3H, s, CH_3, tosyl), 3.36 (3H, s, OCH_3), 3.52 (1H, m, H-3), 4.67 (2H, s, OCH_2O) 7.29 (2H, m, H-2′ and H-4′, tosyl), 7.81 (2H, d, J = 8.3, H-1′ and H-5′, tosyl). ^{13}C NMR (101 MHz, $CDCl_3$): δ 161.0 (C-17), 144.3 (C-1′, tosyl), 129.4 (C-2′, tosyl), 128.6 (C-6′, tosyl), 128.0 (C-3′, tosyl), 125.9 (C-5′, tosyl), 94.6 (OCH_2O), 77.4 (C-3), 55.1 (OCH_3), 53.2, 41.9, 40.5, 35.3, 35.2, 34.8, 33.5, 31.7, 27.6, 26.9, 25.8, 25.3, 23.2, 21.8, 21.6, 20.1, 20.0, 16.6, 13.6. IR spectrum ($CHCl_3$): 2938 (CH_2); 1659 (C═N); 1167 (SO_3); 1045, 1036 (MOM). MS (ESI): m/z 503.2 (10%, M − CH_3). For $C_{28}H_{42}N_2O_5S$ (518.7) Calcd: 64.84%, C; 8.16%, H; 5.40%, N. Found: 65.17%, C; 8.30%, H; 5.18%, N.

*3α-Methoxymethoxy-5β-androst-16-ene (**38**).* Methyllithium (14 mL, 1.6 M in ether, 22.4 mmol) was added at 0 °C to a solution of tosylhydrazone **37** (1 g, 1.93 mmol) in dry tetrahydrofuran (30 mL) under inert atmosphere. Reaction mixture was stirred at 0 °C for 2 h. Then, the excess reagent was quenched with water (50 mL). The product was extracted with ethyl acetate (3 × 25 mL), combined organic extracts were washed with a solution of citric acid (3 × 25 mL), a saturated solution of sodium chloride, and dried, and solvents were evaporated. The residue was purified by column chromatography (1% of acetone in petroleum ether) to afford solids of **38** (606 mg, 98%) that did not crystallize: $[\alpha]_D$ +20.2 (c 0.35, $CHCl_3$). ^{1}H NMR (400 MHz, $CDCl_3$): δ 0.74 (3H, s, H-18), 0.95 (3H, s, H-19), 3.37 (3H, s, OCH_3), 3.53 (1H, tt, J_1 = 11.2, J_2 = 4.7, H-3), 4.69 (2H, s, OCH_2O), 5.67 (1H, ddd, J_1= 5.8, J_2 = 3.0, J_3 = 1.5, H-17), 5.83 (1H, ddd, J_1= 5.8, J_2 = 2.5, J_3 = 1.1, H-16). ^{13}C NMR (101 MHz, $CDCl_3$): δ 144.0 (C-17), 129.4 (C-16), 94.7 (OCH_2O), 77.0 (C-3), 56.3 (C-14), 55.3 (OCH_3), 45.8, 42.4, 41.4, 36.2, 35.5, 35.2, 34.6, 33.8, 32.1, 27.8, 27.3, 26.7, 23.5, 20.8, 17.1. IR spectrum ($CHCl_3$): 3049 (C═C); 2935 (CH_2); 1047, 1036 (MOM). MS (ESI): m/z 341.4 (100%, M + Na). HR-MS (ESI) m/z: for $C_{21}H_{34}O_2Na$ [M + Na] calcd, 341.2451; found, 341.2452.

*3α-Methoxymethoxy-5β-androst-16α-ol (**39**).* A solution of compound **38** (2 g, 6.30 mmol) in tetrahydrofuran (42 mL) was added at 0 °C to a solution of dimer of 9-borabicyclo[3.3.1]nonane (102 mL, 51 mmol) under inert atmosphere. The reaction mixture was stirred at 0 °C for 4 h. Then, water (32.5 mL), an aqueous solution of sodium hydroxide (10%, 32.5 mL), and hydrogen peroxide (30%, 48.5 mL) were added and the mixture was stirred overnight at room temperature. Then, sodium sulfite (3.36 g), acetic acid (98%, 16.4 mL), water (81 mL), and an aqueous solution of citric acid (5%, 82 mL) were added. The product was extracted with ethyl acetate (3 × 80 mL), combined organic extracts were washed with brine (50 mL) and dried, and solvents were evaporated. The residue was purified by column chromatography (1−5% of acetone in petroleum ether) to afford solids of **39** (1.26 g, 60%): mp 98.7−100 °C (acetone/n-heptane); $[\alpha]_D$ +16.6 (c 0.33, $CHCl_3$). ^{1}H NMR (400 MHz, $CDCl_3$): δ 0.69 (3H, s, H-18), 0.91 (3H, s, H-19), 3.37 (3H, s, OCH_3), 3.53 (1H, tt, J_1 = 11.2, J_2 = 4.7, H-3), 4.45 (1H, tdd, J_1= 7.6, J_2 = 6.0, J_3 = 1.6, H-16), 4.69 (2H, s, OCH_2O). ^{13}C NMR (101 MHz, $CDCl_3$): δ 94.7 (OCH_2O), 77.0 (C-3), 72.0 (C-16), 55.3 (OCH_3), 52.3, 52.2, 42.2, 42.1, 40.8, 39.0, 37.4, 35.8, 35.5, 35.0, 33.7, 27.8, 27.3, 26.8, 23.5, 20.5, 18.8. IR spectrum ($CHCl_3$): 3612 (OH); 2941 (CH_2); 1040 (MOM). MS (ESI): m/z 359.3 (100%, M + Na). HR-MS (ESI) m/z: for $C_{21}H_{35}O_3$ [M + H] calcd, 359.2558; found, 359.2558.

*3α-Methoxymethoxy-5β-androst-16-on (**40**).* Dry pyridine (10 mL) and pyridinium chlorochromate (16.7 g, 77.5 mmol) were added to a solution of compound **39** (3.17 g, 9.4 mmol) in freshly dried dichloromethane (150 mL), and the reaction mixture was stirred at room temperature for 2 h. Then, the solids were filtered off through a short column of silica gel (15 g), washing with ethyl acetate. Solvents were evaporated, the residue was dissolved in ethyl acetate (3 × 50 mL), washed with an aqueous solution of citric acid (5%, 2 × 40 mL), brine (50 mL), a saturated solution of sodium bicarbonate (2 × 30 mL), and brine, and then dried, and solvents were evaporated to afford compound **40** (2.59 g, 95%): mp 107.9−108 °C (acetone/n-heptane); $[\alpha]_D$ −134.7 (c 0.35, $CHCl_3$). ^{1}H NMR (400 MHz, $CDCl_3$): δ 0.86 (3H, s, H-18), 0.95 (3H, s, H-19), 3.37 (3H, s, OCH_3), 3.54 (1H, ddd, J_1 = 15.8, J_2 = 11.1, J_3 = 4.7, H-3), 4.69 (2H, s, OCH_2O). ^{13}C NMR (101 MHz, $CDCl_3$): δ 218.9 (C-16), 94.7 (OCH_2O), 77.0 (C-3), 56.1, 55.3 (OCH_3), 51.9, 42.0, 40.6, 39.4, 39.4, 38.5, 35.4, 35.2, 35.1, 33.7, 27.8, 27.1, 26.8, 23.4, 20.5, 18.2. IR spectrum ($CHCl_3$): 2937 (OCH_2O); 1737 (C═O); 1045, 1037 (MOM). MS (ESI): m/z 335.3 (32%, M + H) 273.2 (100%). For $C_{21}H_{34}O_3$ (334.5) Calcd: 75.41%, C; 10.25%, H. Found: 75.66%, C; 10.33%, H.

*16-Oxo-5β-androstan-3α-ol (**41**).* Compound **41** was prepared in the same manner as compound **11**. Starting from compound **40** (3.4 g, 10.2 mmol), compound **41** (3.17 g, 93%) was obtained by crystallization: mp 135.8−136.7 °C (acetone/n-heptane); $[\alpha]_D$ −167.4 (c 0.33, $CHCl_3$). ^{1}H NMR (400 MHz, $CDCl_3$): δ 0.86 (3H, s, H-18), 0.96 (3H, s, H-19), 3.65 (1H, tt, J_1 = 10.8, J_2 = 4.7, H-3). ^{13}C NMR (101 MHz, $CDCl_3$): δ 218.8 (C═O), 71.8 (C-3), 56.1, 51.9, 42.0, 40.7, 39.4, 39.4, 38.5, 36.5, 35.4, 35.2, 34.9, 30.6, 27.0, 26.9, 23.4, 20.5, 18.2. IR spectrum ($CHCl_3$): 3609, 1032 (OH); 2936 (CH_2); 1736 (C═O). MS (ESI): m/z 290.2 (100%, M). HR-MS (ESI) m/z: for $C_{19}H_{30}O_2Na$ [M + Na] calcd, 313.2138; found, 313.2137.

*16-Methylen-5β-androstan-3α-ol (**42**).* Compound **42** was prepared in the same manner as compound **16**. Starting from compound **41** (800 mg, 2.67 mmol), compound **42** (756 mg, 95%) was obtained by chromatography on preparative TLC plates (1−5% acetone in petroleum ether): mp 165.3−165.6 °C (acetone/n-heptane); $[\alpha]_D$ −69.8 (c 0.35, $CHCl_3$). ^{1}H NMR (400 MHz, $CDCl_3$): δ 0.72 (3H, s, H-18), 0.93 (3H, s, H-19), 2.33 (1H, ddt, J_1 = 16.1, J_2 = 7.5, J_3 = 1.6, H-16a) . 3.63 (1H, tt, J_1 = 11.1, J_2 = 4.7, H-3), 4.88 (2H, ddt, J_1 = 4.4, J_2 = 3.0, J_2 = 1.6, ═CH_2). ^{13}C NMR (101 MHz, $CDCl_3$): δ 151.3 (═CH_2), 107.0 (C-16), 71.9 (C-3), 54.3, 49.6, 42.2, 40.8, 40.7, 38.7, 36.6, 35.9, 35.5, 34.9, 33.5, 30.7, 27.2, 26.8, 23.5, 20.9, 17.7. IR spectrum ($CHCl_3$): 3609 (OH); 3015, 1658 (═CH_2); 2934 (CH_2). MS (ESI): m/z 311.3 (100%, M + Na). HR-MS (ESI) m/z: for $C_{20}H_{32}ONa$ [M + Na] calcd, 311.2345; found, 311.2344.

*16-Methylen-5β-androstan-3α-yl 3-Sulfate Pyridinium Salt (**43**).* Compound **43** was prepared according to General Procedure for Sulfation. Starting from compound **42** (83 mg, 0.29 mmol), compound **43** (66 mg, 56%) was obtained as a white solid: mp 180−182 °C (chloroform); $[\alpha]_D$ −41.9 (c 0.35, $CHCl_3$). ^{1}H NMR (400 MHz, $CDCl_3$): δ 0.70 (3H, s, H-18), 0.91 (3H, s, H-19), 2.30 (1H, dd, J_1 = 16.0, J_2 = 7.7, H-16a), 4.45 (1H, tt, J_1 = 11.2, J_2 = 4.9, H-3), 4.87 (2H, m, ═CH_2), 8.02 (2H, m, H-2′ and H-4′, pyridinium), 8.48 (1H, t, J = 8.6, H-3′, pyridinium), 8.99 (2H, d, J = 5.2, H-1′ and H-5′, pyridinium). ^{13}C NMR (101 MHz, $CDCl_3$): δ 151.3 (═CH_2), 145.8 (C-1′ and C-5′, pyridinium), 142.3 (C-3′, pyridinium), 127.3 (C-2′ and C-4′, pyridinium), 107.0 (C-16), 79.5 (C-3), 56.1, 51.9, 42.0, 40.6, 39.4, 39.3, 38.5, 35.4, 35.2, 34.8, 33.4, 27.8, 26.8, 26.8, 23.6, 20.4, 18.0. IR spectrum ($CHCl_3$): 1736 (C═O); 1656 (C═C); 1460 (═CH, pyridine); 1263, 1171, 969, 947 (OSO_3). MS (ESI): m/z 367.2 (100%, M − pyH). HR-MS (ESI) m/z: for $C_{20}H_{31}O_4S$ [M − pyH] calcd, 367.1946; found, 367.1945.

DOI: 10.1021/acs.jmedchem.5b00570
J. Med. Chem. 2015, 58, 5950−5966

PDF-XChange Editor KOUPIT plnou verzi! www.pdfxchange.cz

*5β-Androst-16-ene-3α-ol (**44**).* Starting from compound **38** (1.76 g, 5.53 mmol), compound **44** (0.95 g, 63%) was obtained by hydrolysis of the MOM protecting group in the same manner as described for compound **11** followed by crystallization: mp 150−151 °C (ethyl acetate/*n*-heptane); $[\alpha]_D$ +17.6 (*c* 0.44, $CHCl_3$). ^{1}H NMR (400 MHz, $CDCl_3$): δ 0.74 (3H, s, H-18), 0.96 (3H, s, H-19), 3.63 (1H, m, H-3), 5.69 (1H, ddd, J_1 = 5.6, J_2 = 2.9, J_3 = 1.4, H-17), 5.84 (1H, m, H-16). ^{13}C NMR (101 MHz, $CDCl_3$): δ 143.9 (C-16), 129.2 (C-15), 71.8 (C-3), 56.1, 45.6, 42.20, 41.3, 36.5, 36.1, 35.3, 34.9, 34.5, 32.0, 30.5, 27.1, 26.6, 23.3, 20.7, 17.0. IR spectrum ($CHCl_3$): 3609 (OH); 3046, 1588, 834 (=CH); 2934, 2865 (CH_3). For $C_{19}H_{30}O$ (274.4) Calcd: 83.15%, C; 11.02%, H. Found: 83.12%, C; 11.28%, H.

*5β-Androst-16-ene-3α-yl 3-Sulfate Pyridinium Salt (**45**).* Compound **45** was prepared according to General Procedure for Sulfation. Starting from compound **44** (17 mg, 0.06 mmol), compound **45** (14 mg, 52%) was obtained as a white solid: mp 163−165 °C (benzene); $[\alpha]_D$ +18.7 (*c* 0.17, $CHCl_3$). ^{1}H NMR (400 MHz, $CDCl_3$): δ 0.73 (3H, s, H-18), 0.94 (3H, s, H-19), 4.45 (1H, tt, J_1 = 10.9, J_2 = 4.9, H-3), 5.67 (1H, ddd, J_1 = 5.9, J_2 = 2.3, J_3 = 1.0, H-17), 5.81 (1H, ddd, J_1 = 5.8, J_2 = 2.9, J_3 = 1.3, H-16), 8.0 (2H, t, *J* = 7.0, H-2′ and H-4′, pyridinium), 8.47 (1H, m, H-3′, pyridinium), 8.98 (2H, d, *J* = 5.7, H-1′ and H-5′, pyridinium). ^{13}C NMR (101 MHz, $CDCl_3$): δ 144.0 (C-16), 145.8 (C-1′ and C-5′, pyridinium), 142.4 (C-3′, pyridinium), 129.4 (C-17), 127.3 (C-2′ and C-4′, pyridinium), 79.7 (C-3), 56.3, 45.1, 42.3, 41.3, 36.2, 35.4, 34.9, 34.6, 33.5, 32.1, 27.8, 27.1, 26.7, 23.4, 20.8, 18.0, 17.1. IR spectrum ($CHCl_3$): 3140, 3100, 3072 (pyridinium); 2971, 2937 (CH_3); 1604 (C=C); 1260, 1249, 1237 (OSO_3). MS (ESI): *m*/*z* 353.2 (100%, M − pyH). HR-MS (ESI) *m*/*z*: for $C_{19}H_{29}O_4S$ [M − pyH] calcd, 353.1789; found, 353.1789.

*3α-Hydroxy-5β-estrane (**47**).* Compound **47** was prepared in the same manner as compound **14**. Starting from compound **46** (90 mg, 0.33 mmol), compound **47** (82 mg, 96%) was obtained by the deoxygenation procedure described for derivative **14**, followed by column chromatography on silica gel (20% of ether in petroleum ether): mp 131−132 °C (chloroform); $[\alpha]_D$ +19.3 (*c* 0.23, $CHCl_3$). ^{1}H NMR (400 MHz, $CDCl_3$): δ 0.70 (3H, s, H-18), 1.93 (1H, ddt, J_1 = 8.3, J_2 = 5.9, J_3 = 2.8), 3.63 (1H, tt, J_1 = 10.4, J_2 = 4.8, H-3). ^{13}C NMR (101 MHz, $CDCl_3$): δ 72.0 (C-3), 53.7, 42.4, 41.1, 40.8, 40.2, 39.1, 38.8, 36.6, 35.8, 31.7, 29.9, 26.8, 26.2, 25.9, 25.5, 20.6, 17.7. IR spectrum ($CHCl_3$): 3609, 3457, 1034 (OH); 2925, 2871 (CH_3). MS (EI): *m*/*z* 285.2 (100%, M + Na). For $C_{18}H_{30}O$ (262.4) Calcd: 82.38%, C; 11.52%, H. Found: 82.11%, C; 11.37%, H.

*5β-Estran-3α-yl 3-Sulfate Pyridinium Salt (**48**).* Compound **48** was prepared according to General Procedure for Sulfation. Starting from compound **47** (75 mg, 0.29 mmol), compound **48** (40 mg, 33%) was obtained as a white solid: mp 192−194 °C (chloroform); $[\alpha]_D$ +19.0 (*c* 0.22, $CHCl_3$). ^{1}H NMR (400 MHz, $CDCl_3$): δ 0.66 (3H, s, H-18), 4.29−4.55 (1H, m, H-3), 7.98−8.06 (2H, m, H-2′ and H-4′, pyridinium), 8.48 (1H, tt, J_1 = 7.9, J_2 = 1.6, H-3′, pyridinium), 8.97−9.03 (2H, m, H-1′ and H-5′, pyridinium). ^{13}C NMR (101 MHz, $CDCl_3$): δ 145.9 (C-1′ and C-5′, pyridinium), 142.4 (C-3′, pyridinium), 127.3 (C-2′ and C-4′, pyridinium), 79.7 (C-3), 53.7, 42.3, 41.1, 40.7, 40.0, 39.0, 38.7, 35.9, 33.6, 31.6, 27.0, 26.7, 26.2, 25.8, 25.4, 20.6, 17.6. IR spectrum ($CHCl_3$): 950 (COS); 1045, 1264 (SO_3); 2919 (CH_3). MS (EI): *m*/*z* 341.2 (100%, M − pyH). HR-MS (EI) *m*/*z*: for $C_{18}H_{29}O_4S$ [M − pyH] calcd, 341.1792; found, 341.1791.

*24-Nor-5β-cholan-3α-ol (**50**).* Silver nitrate was added (350 mg, 2.1 mmol) to a solution of lithocholic acid **49** (200 mg, 0.53 mmol) in dimethyl sulfoxide (15 mL), and the reaction mixture was heated at 80 ° C for 20 h. Then, the solids were removed by filtration. The filtrate was poured into water (20 mL), the product extracted with ethyl acetate (3 × 20 mL), combined organic extracts were washed with a solution of hydrochloric acid (5%, 20 mL), sodium bicarbonate, and brine, and then dried. Solvents were evaporated, and the residue was purified by column chromatography (3−10% acetone in petroleum ether). Recrystallization from ether afforded 63 mg (36%) of compound **50**:[24] mp 159−161 °C (ether); $[\alpha]_D$ +31.7 (*c* 0.12, $CHCl_3$). ^{1}H NMR (400 MHz, $CDCl_3$): δ 0.64 (3H, s, H-18), 0.82 (3H, t, *J* = 7.4, H-23), 0.89 (3H, d, *J* = 6.5, H-21), 0.92 (3H, s, H-19), 3.62 (1H, m, H-3). ^{13}C NMR (101 MHz, $CDCl_3$): δ 72.0 (C-3), 56.6, 55.9, 42.7, 42.2, 40.6, 40.3, 37.1, 36.6, 36.0, 35.5, 34.7, 30.7, 28.4, 28.3, 27.3, 26.6, 24.4, 23.5, 20.9, 18.1, 12.1, 10.5.

*24-Nor-5β-cholan-3α-yl 3-Sulfate Pyridinium Salt (**51**).* Compound **51** was prepared according to General Procedure for Sulfation. Starting from compound **50** (26 mg, 0.16 mmol), compound **51** (34 mg, 83%) was obtained as a white solid: mp 186−188 °C; $[\alpha]_D$ +13.8 (*c* 0.11, $CHCl_3$). ^{1}H NMR (400 MHz, $CDCl_3$): δ 0.62 (3H, s, H-18), 0.81 (3H, t, *J* = 7.4, H-23), 0.88 (3H, d, *J* = 6.5, H-21), 0.90 (3H, s, H-19), 4.46 (1H, m, H-3), 7.79 (2H, m, H-2′ and H-4′, pyridinium), 8.19 (1H, t, *J* = 7.7, H-3′, pyridinium), 8.84 (2H, d, *J* = 4.9, H-1′ and H-5′, pyridinium). ^{13}C NMR (101 MHz, $CDCl_3$): δ 145.0 (C-1′ and C-5′, pyridinium), 142.3 (C-3′, pyridinium), 126.0 (C-2′ and C-4′, pyridinium), 79.8 (C-3), 56.7, 55.9, 42.8, 42.3, 40.5, 40.3, 37.1, 35.9, 35.4, 34.6, 33.5, 28.4, 28.3, 27.9, 27.2, 26.5, 24.4, 23.4, 20.9, 18.1, 12.1, 10.5. IR spectrum ($CHCl_3$): 3140, 3073, 1490 (pyridinium); 1263, 1170, 1043 (SO_3). MS ESI: *m*/*z* 411.4 (100%, M − pyH). For $C_{28}H_{45}NO_4S$ (491.7) Calcd: 68.39%, C; 9.22%, H; 2.85%, N. Found: 68.65%, C; 9.36%, H; 2.70%, N.

■ ASSOCIATED CONTENT

Ⓢ Supporting Information

^{13}C and ^{1}H NMR data (in $CDCl_3$) of compounds **35a** and **35b**, dependency of the particle size of compound **19** on concentration (PDF), and molecular strings file for target compounds (CSV). The Supporting Information is available free of charge on the ACS Publications website at DOI: 10.1021/acs.jmedchem.5b00570.

■ AUTHOR INFORMATION

Corresponding Author

*Phone: +420-220-183-273. Fax: +420-220-183-578. E-mail: kudova@uochb.cas.cz. Address: Eva Kudova, Department of Neuroprotectives. Institute of Organic Chemistry and Biochemistry, Academy of Sciences of the Czech Republic, v.v.i., Flemingovo nam 2, Prague 6−Dejvice, 16610, Czech Republic.

Author Contributions

‖The computational analysis was done by M.N.

Notes

The authors declare no competing financial interest.

■ ACKNOWLEDGMENTS

This work was supported by grant TE01020028 Center for Development of Original Drugs from the Technology Agency of the Czech Republic, grant 303/12/1464 from the Grant Agency of the Czech Republic, research project of the RVO 67985823, RVO 61388963, and BIOCEV (CZ.1.05/1.1.00/02.0109), Biotechnology and Biomedicine Centre of the Academy of Sciences and Charles University in Vestec, project supported from European Regional Development Fund. We thank M. Sedlackova and D. Hybsova for their excellent technical assistance and Dr. Kacer for light scattering analysis. We thank Dr. Laurel McGrane for language corrections.

■ ABBREVIATIONS USED

NMDA, *N*-methyl-D-aspartate; TLC, thin layer chromatography

■ REFERENCES

(1) Citri, A.; Malenka, R. C. Synaptic plasticity: multiple forms, functions, and mechanisms. *Neuropsychopharmacology* **2008**, *33*, 18−41.

(2) Doble, A. The role of excitotoxicity in neurodegenerative disease: implications for therapy. *Pharmacol. Ther.* **1999**, *81*, 163−221.

DOI: 10.1021/acs.jmedchem.5b00570
J. Med. Chem. 2015, 58, 5950−5966

PDF-XChange Editor
KOUPIT plnou verzi!
www.pdfxchange.cz

(3) Mota, S. I.; Ferreira, I. L.; Rego, A. C. Dysfunctional synapse in Alzheimer's disease − A focus on NMDA receptors. *Neuropharmacology* **2014**, *76* (Pt A), 16−26.
(4) Rotaru, D. C.; Yoshino, H.; Lewis, D. A.; Ermentrout, G. B.; Gonzalez-Burgos, G. Glutamate receptor subtypes mediating synaptic activation of prefrontal cortex neurons: relevance for schizophrenia. *J. Neurosci.* **2011**, *31*, 142−156.
(5) Zhou, X.; Ding, Q.; Chen, Z.; Yun, H.; Wang, H. Involvement of the GluN2A and GluN2B subunits in synaptic and extrasynaptic N-methyl-D-aspartate receptor function and neuronal excitotoxicity. *J. Biol. Chem.* **2013**, *288*, 24151−24159.
(6) Baulieu, E. E. Neurosteroids: A novel function of the brain. *Psychoneuroendocrinology* **1998**, *23*, 963−987.
(7) Korinek, M.; Kapras, V.; Vyklicky, V.; Adamusova, E.; Borovska, J.; Vales, K.; Stuchlik, A.; Horak, M.; Chodounska, H.; Vyklicky, L., Jr. Neurosteroid modulation of N-methyl-D-aspartate receptors: Molecular mechanism and behavioral effects. *Steroids* **2011**, *76*, 1409−1418.
(8) Vallee, M.; Mayo, W.; Darnaudery, M.; Corpechot, C.; Young, J.; Koehl, M.; Le Moal, M.; Baulieu, E. E.; Robel, P.; Simon, H. Neurosteroids: deficient cognitive performance in aged rats depends on low pregnenolone sulfate levels in the hippocampus. *Proc. Natl. Acad. Sci. U. S. A.* **1997**, *94*, 14865−14870.
(9) Reddy, D. S. Neurosteroids: endogenous role in the human brain and therapeutic potentials. *Prog. Brain Res.* **2010**, *186*, 113−137.
(10) Petrovic, M.; Sedlacek, M.; Horak, M.; Chodounska, H.; Vyklicky, L., Jr. 20-oxo-5beta-pregnan-3alpha-yl sulfate is a use-dependent NMDA receptor inhibitor. *J. Neurosci.* **2005**, *25*, 8439−8450.
(11) Park-Chung, M.; Wu, F. S.; Farb, D. H. 3alpha-Hydroxy-5beta-pregnan-20-one sulfate: a negative modulator of the NMDA-induced current in cultured neurons. *Mol. Pharmacol.* **1994**, *46*, 146−150.
(12) Borovska, J.; Vyklicky, V.; Stastna, E.; Kapras, V.; Slavikova, B.; Horak, M.; Chodounska, H.; Vyklicky, L., Jr. Access of inhibitory neurosteroids to the NMDA receptor. *Br. J. Pharmacol.* **2012**, *166*, 1069−1083.
(13) Weaver, C. E.; Land, M. B.; Purdy, R. H.; Richards, K. G.; Gibbs, T. T.; Farb, D. H. Geometry and charge determine pharmacological effects of steroids on N-methyl-D-aspartate receptor-induced Ca^{2+} accumulation and cell death. *J. Pharmacol. Exp. Ther.* **2000**, *293*, 747−754.
(14) Park-Chung, M.; Wu, F. S.; Purdy, R. H.; Malayev, A. A.; Gibbs, T. T.; Farb, D. H. Distinct sites for inverse modulation of N-methyl-D-aspartate receptors by sulfated steroids. *Mol. Pharmacol.* **1997**, *52*, 1113−1123.
(15) Stastna, E.; Chodounska, H.; Pouzar, V.; Kapras, V.; Borovska, J.; Cais, O.; Vyklicky, L., Jr. Synthesis of C3. C5, and C7 pregnane derivatives and their effect on NMDA receptor responses in cultured rat hippocampal neurons. *Steroids* **2009**, *74*, 256−263.
(16) Weaver, C. E., Jr.; Marek, P.; Park-Chung, M.; Tam, S. W.; Farb, D. H. Neuroprotective activity of a new class of steroidal inhibitors of the N-methyl-D-aspartate receptor. *Proc. Natl. Acad. Sci. U. S. A.* **1997**, *94*, 10450−10454.
(17) Lapchak, P. A. The neuroactive steroid 3-alpha-ol-5-beta-pregnan-20-one hemisuccinate. a selective NMDA receptor antagonist improves behavioral performance following spinal cord ischemia. *Brain Res.* **2004**, *997*, 152−158.
(18) Rambousek, L.; Bubenikova-Valesova, V.; Kacer, P.; Syslova, K.; Kenney, J.; Holubova, K.; Najmanova, V.; Zach, P.; Svoboda, J.; Stuchlik, A.; Chodounska, H.; Kapras, V.; Adamusova, E.; Borovska, J.; Vyklicky, L.; Vales, K. Cellular and behavioural effects of a new steroidal inhibitor of the N-methyl-d-aspartate receptor 3alpha5beta-pregnanolone glutamate. *Neuropharmacology* **2011**, *61*, 61−68.
(19) Huang-Minlon. Reduction of steroids ketones and other carbonyl compounds by modified Wollf-Kishner method. *J. Am. Chem. Soc.* **1949**, *71*, 3301−3303.
(20) Xu, S.; Toyama, T.; Nakamura, J.; Arimoto, H. One-pot reductive cleavage of exo-olefin to methylene with a mild ozonolysis-Clemmensen sequence. *Tetrahedron Lett.* **2010**, *51*, 4534−4537.
(21) Yoshizawa, I.; Itoh, S.; Nagata, K.; Kawahara, N. Mechanism of the D-homoannulation of pregnanediol disulfate in refluxing 3N hydrochloric acid. *Chem. Pharm. Bull.* **1983**, *31*, 3819−3828.
(22) Möller, G.; Deluca, D.; Gege, C. H.; Rosinus, A.; Kowalik, D.; Peters, O.; Droescher, P.; Elger, W.; Adamski, J.; Hillisch, A. Structure-based design, synthesis and in vitro characterization of potent 17β-hydroxysteroid dehydrogenase type 1 inhibitors based on 2-substitutions of estrone and D-homo-estrone. *Bioorg. Med. Chem. Lett.* **2009**, *19*, 6740−6744.
(23) Stastna, E.; Rath, N. P.; Covey, D. F. The use of symmetry in enantioselective synthesis: Four pairs of chrysene enantiomers prepared from 19-nortestosterone. *Org. Biomol. Chem.* **2011**, *9*, 4685−4694.
(24) Upasani R. B.; Fick D. B.; Hogenkamp D. J.; Lan N. C. Neuroactive steroids of the androstane and pregnane series. U.S. Patent US5925630(A), July 20, 1999.
(25) (a) Schiesser, C. H.; Skidmore, M. A.; White, J. M. Stannanes from cholic acid as enantioselective free-radical reducing agents. *Aust. J. Chem.* **2001**, *54*, 199−204. 25. (b) Faucher, F.; Cantin, L.; Luu-The, V.; Labrie, F.; Breton, R. The crystal structure of human Delta 4 3-ketosteroid 5beta-reductase defines the functional role of the residues of the catalytic tetrad in the steroid double bond reduction mechanism. *Biochemistry* **2008**, *47*, 8261−8270.
(26) Vyklicky, V.; Krausova, B.; Cerny, J.; Balik, A.; Zapotocky, M.; Novotny, M.; Lichnerova, K.; Smejkalova, T.; Kaniakova, M.; Korinek, M.; Petrovic, M.; Kacer, P.; Horak, M.; Chodounska, H.; Vyklicky, L. Block of NMDA receptor channels by endogenous neurosteroids: implications for the agonist induced conformational states of the channel vestibule. *Sci. Rep.* **2015**, *5*, 10935.
(27) Flint, A. C.; Maisch, U. S.; Weishaupt, J. H.; Kriegstein, A. R.; Monyer, H. NR2A subunit expression shortens NMDA receptor synaptic currents in developing neocortex. *J. Neurosci.* **1997**, *17*, 2469−2476.
(28) Patneau, D. K.; Vyklicky, L., Jr.; Mayer, M. L. Hippocampal neurons exhibit cyclothiazide-sensitive rapidly desensitizing responses to kainate. *J. Neurosci.* **1993**, *13*, 3496−3509.
(29) Faucher, F.; Cantin, L.; Luu-The, V.; Labrie, F.; Breton, R. The crystal structure of human Delta4−3-ketosteroid 5beta-reductase defines the functional role of the residues of the catalytic tetrad in the steroid double bond reduction mechanism. *Biochemistry* **2008**, *47*, 8261−8270.
(30) *The PyMOL Molecular Graphics System*, version 1.5.0.4; Schrödinger, LLC, 2002.
(31) Ahlrichs, R.; Bar, M.; Haser, M.; Horn, H.; Kolmel, C. Electronic structure calculations on workstation computers: The program system Turbomole. *Chem. Phys. Lett.* **1989**, *162*, 165−169.
(32) Jurecka, P.; Cerny, J.; Hobza, P.; Salahub, D. Density functional theory augmented with an empirical dispersion term. Interaction energies and geometries of 80 noncovalent complexes compared with ab initio quantum mechanics calculations. *J. Comput. Chem.* **2007**, *28*, 555−569.
(33) Klamt, A.; Schüürmann, G. COSMO: A new approach to dielectric screening in solvents with explicit expressions for the screening energy and its gradient. *J. Chem. Soc., Perkin Trans. 2* **1993**, *5*, 799−805.
(34) (a) Rezac, J.; Fanfrlik, J.; Salahub, D.; Hobza, P. Semiempirical quantum chemical PM6 method augmented by dispersion and H-bonding correction terms reliably describes various types of noncovalent complexes. *J. Chem. Theory Comput.* **2009**, *5*, 1749−1760. (b) Rezac, J.; Hobza, P. Advanced corrections of hydrogen bonding and dispersion for semiempirical quantum mechanical methods. *J. Chem. Theory Comput.* **2012**, *8*, 141−151.
(35) Grimme, S.; Antony, J.; Ehrlich, S.; Krieg, H. A consistent and accurate *ab initio* parametrization of density functional dispersion correction (DFT-D) for the 94 elements H-Pu. *J. Chem. Phys.* **2010**, *132*, 154104−154119.
(36) Frisch, M. J.; Trucks, G. W.; Schlegel, H. B.; Scuseria, G. E.; Robb, M. A.; Cheeseman, J. R.; Scalmani, G.; Barone, V.; Mennucci, B.; Petersson, G. A.; Nakatsuji, H.; Caricato, M.; Li, X.; Hratchian, H.

DOI: 10.1021/acs.jmedchem.5b00570
J. Med. Chem. 2015, 58, 5950−5966

PDF-XChange Editor
KOUPIT plnou verzi!
www.pdfxchange.cz

P.; Izmaylov, A. F.; Bloino, J.; Zheng, G.; Sonnenberg, J. L.; Hada, M.; Ehara, M.; Toyota, K.; Fukuda, R.; Hasegawa, J.; Ishida, M.; Nakajima, T.; Honda, Y.; Kitao, O.; Nakai, H.; Vreven, T.; Montgomery Jr. J. A.; Peralta, J. E.; Ogliaro, F.; Bearpark, M.; Heyd, J. J.; Brothers, E.; Kudin, K. N.; Staroverov, V. N.; Kobayashi, R.; Normand, J.; Raghavachari, K.; Rendell, A.; Burant, J. C.; Iyengar, S. S.; Tomasi, J.; Cossi, M.; Rega, N.; Millam, N. J.; Klene, M.; Knox, J. E.; Cross, J. B.; Bakken, V.; Adamo, C.; Jaramillo, J.; Gomperts, R.; Stratmann, R. E.; Yazyev, O.; Austin, A. J.; Cammi, R.; Pomelli, C.; Ochterski, J. W.; Martin, R. L.; Morokuma, K.; Zakrzewski, V. G.; Voth, G. A.; Salvador, P.; Dannenberg, J. J.; Dapprich, S.; Daniels, A. D.; Farkas, Ö.; Foresman, J. B.; Ortiz, J. V.; Cioslowski, J.; Fox, D. J. *Gaussian 09*; Gaussian Inc.: Wallingford CT, 2009.

(37) Marvin was used for drawing, displaying and characterizing chemical structures, substructures and reactions . *Marvin* 15.1.19; ChemAxon: Budapest, 2015; http://www.chemaxon.com.

(38) Cais, O.; Sedlacek, M.; Horak, M.; Dittert, I.; Vyklicky, L., Jr. Temperature dependence of NR1/NR2B NMDA receptor channels. *Neuroscience* **2008**, *151*, 428−438.

(39) Korinek, K.; Sedlacek, M.; Cais, O.; Dittert, I.; Vyklicky, L. Temperature dependence of N-methyl-D-aspartate receptor excitatory postsynaptic currents. *Neuroscience* **2010**, *165* (3), 736−748.

(40) Anderson, A.; Boyd, A. C.; Clark, J. K.; Fielding, L.; Gemmell, D. K.; Hamilton, N. M.; Maidment, M. S.; May, V.; McGuire, R.; McPhail, P.; Sansbury, F. H.; Sundaram, H.; Taylor, R. Conformationally constrained anaesthetic steroids that modulate GABAA receptors. *J. Med. Chem.* **2000**, *43*, 4118−4125.

DOI: 10.1021/acs.jmedchem.5b00570
J. Med. Chem. 2015, 58, 5950−5966

PDF-XChange Editor
KOUPIT plnou verzi!
www.pdfxchange.cz

Journal of Medicinal Chemistry

Article

pubs.acs.org/jmc

Neurosteroid-like Inhibitors of *N*-Methyl-D-aspartate Receptor: Substituted 2-Sulfates and 2-Hemisuccinates of Perhydrophenanthrene

Barbora Slavikova,[†] Hana Chodounska,[†] Michaela Nekardova,[†,§,∥] Vojtech Vyklicky,[‡] Marek Ladislav,[‡] Pavla Hubalkova,[‡] Barbora Krausova,[‡] Ladislav Vyklicky,[‡] and Eva Kudova*[,†]

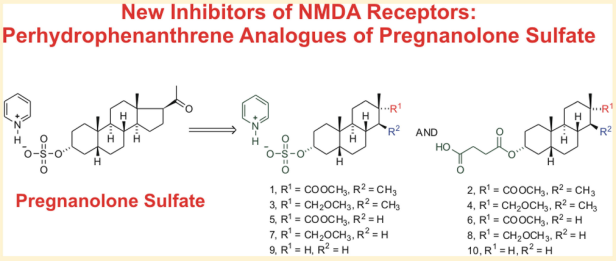
[†]Institute of Organic Chemistry and Biochemistry, Academy of Sciences of the Czech Republic, v.v.i., Flemingovo nam. 2, Dejvice, Prague 6, 16610, Czech Republic

[‡]Institute of Physiology CAS, Videnska 1083, 142 20 Prague 4, Czech Republic

[§]Faculty of Mathematics and Physics, Charles University in Prague, Ke Karlovu 3, Prague 2, 121 16, Czech Republic

Supporting Information

ABSTRACT: *N*-Methyl-D-aspartate receptors (NMDARs) display a critical role in various diseases of the central nervous system. The activity of NMDARs can be modulated by neurosteroids. Herein, we report a structure−activity relationship study for perhydrophenanthrene analogues possessing a framework that mimics the steroidal ring system. This study comprises the design, synthesis, and assessment of the biological activity of a library of perhydrophenanthrene 2-sulfates and 2-hemisuccinates (**1**−**10**). Their ability to modulate NMDAR-induced currents was tested on recombinant GluN1/GluN2B receptors. Our results demonstrate that such structural optimization leads to compounds that are inhibitors of NMDARs. Notably, compound **9** (IC_{50} = 15.6 μM) was assessed as a more potent inhibitor of NMDAR-induced currents than the known endogenous neurosteroid, pregnanolone sulfate (IC_{50} = 24.6 μM).



INTRODUCTION

N-Methyl-D-aspartate receptors (NMDARs) are glutamate-gated, calcium-permeable ion channels involved in excitatory synaptic transmission and synaptic plasticity.[1] The design of new NMDAR modulators could lead to the development of pharmaceutically attractive, druglike compounds, as a broad variety central nervous system diseases (neurodegeneration, ischemia, traumatic brain injury, etc.)[2−4] have been associated with glutamate induced excitotoxicity under pathological conditions, a specific form of neuronal cell death caused by overactivation of NMDARs.

Neurosteroids have both positive and negative effects on NMDARs, and such modulatory effects play a role in many physiological processes. Our previous studies of neurosteroid effect on NMDAR modulation demonstrated that these molecules do have neuroprotective effect in animal models of various indications.[5−7] In addition, we have shown that particular structural modifications afford neurosteroids that have a higher preference for tonically activated NMDARs than for NMDARs activated during synaptic transmission.[8] Finally, we have identified the molecular basis of the use-dependent and voltage-independent inhibitory effect of neurosteroids on NMDAR responses.[9] The site of action is located at the extracellular vestibule of the receptor's ion channel pore and is accessible after receptor activation.

As a part of our continuing interest in the structure−activity relationship (SAR) study of neurosteroid modulators of NMDARs, we recently reported[10] a new, nonpolar structural modification at positions C-17 and C-20 of the steroidal skeleton D-ring (methyl, ethyl, 17-methylene, 20-ethylene, etc.). Compounds with such modifications were shown to be potent modulators of NMDAR-induced currents (e.g., 5β-androstane-3α-yl 3-sulfate, Figure 1b, IC_{50} = 1.2 μM). Moreover, these compounds were established as more potent inhibitors of NMDAR-induced currents than the known, endogenous NMDAR inhibitor, pregnanolone sulfate[11] (20-oxo-5β-pregnan-3α-yl sulfate, IC_{50} = 24.6 μM; Figure 1).

In order to extend our previous study[10] that demonstrated the expandable role of C-17 acetyl moiety, we wanted to evaluate the critical role of the steroidal D-ring (Figure 1). Therefore, we have synthesized a series of fully saturated phenanthrenes (Figure 2) that have not been previously reported. The two major steroidal structural features necessary for maintaining inhibitory biological activity on NMDARs are retention of the 5β-stereochemistry and axial 3α-configuration.[11] In addition, the stereochemistry at steroidal positions C-8 and C-9 was maintained. As such, these new perhydrophenanthrene analogues (**1**−**10**) closely mimic steroidal ABC ring arrangement.

The inhibitory effect of neurosteroids on NMDARs is also associated with the presence of a positively or negatively charged

Received: January 16, 2016
Published: April 11, 2016

ACS Publications © 2016 American Chemical Society

DOI: 10.1021/acs.jmedchem.6b00079
J. Med. Chem. 2016, 59, 4724−4739

PDF-XChange Editor
KOUPIT plnou verzi!
www.pdfxchange.cz

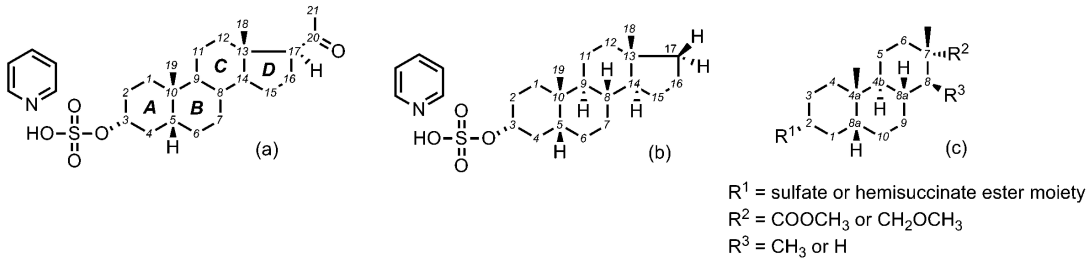


Figure 1. Structures of (a) pregnanolone sulfate, (b) 5β-androstane-3α-yl 3-sulfate, and (c) perhydrophenanthrene 2-sulfate or 2-hemisuccinate with their ring numbering system.

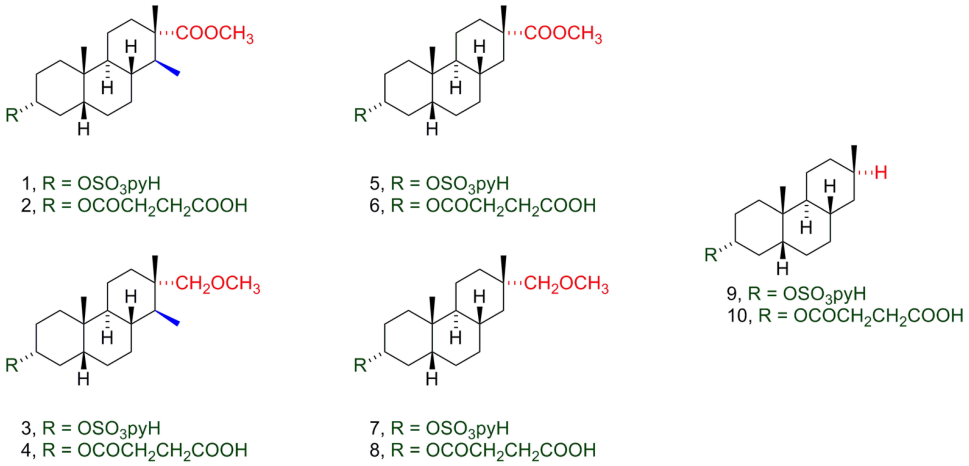
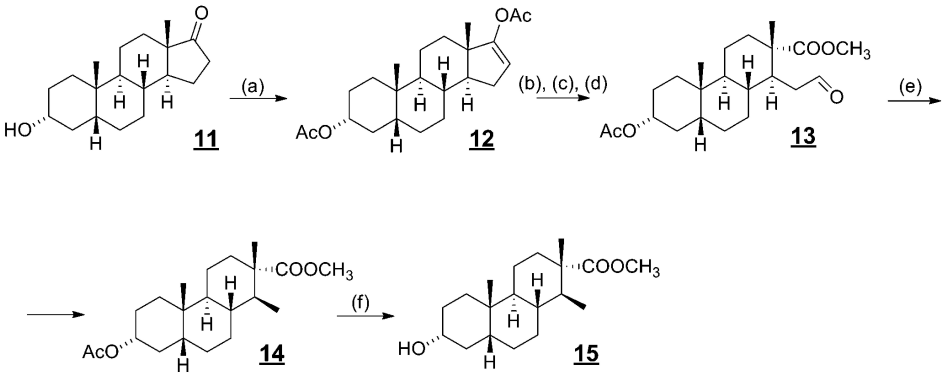


Figure 2. Overview of 2-sulfates (**1**, **3**, **5**, **7**, **9**) and 2-hemisuccinates (**2**, **4**, **6**, **8**, **10**) of perhydrophenanthrenes.

Scheme 1. Synthesis of Compounds 11−15[a]



[a]Reagents and conditions: (a) $CH_3CO_2C(CH_3)=CH_2$, H_2SO_4; (b) O_3, CH_3COOH, DCM, −70 °C; (c) Me_2S, CH_3COOH, H_2O, rt; (d) CH_2N_2, Et_2O; (e) $[(C_6H_5)_3P]_3RhCl$, PhCN, 160 °C; (f) KOH, MeOH, H_2O.

substituent at the C-3 position.[11,12] Hence, the sulfate moiety was selected as the primary choice. With the intention to evaluate these new perhydrophenanthrene analogues as druglike candidates, we drew inspiration from the published data for pregnanolone C-3 hemisuccinate ester, a compound with neuroprotective activity both in vitro and in vivo models of neurodegeneration.[13,14] Thus, the hemisuccinate moiety was chosen to extend this SAR study.

The skeleton modifications were achieved by two types of degradation reactions of the steroidal D-ring: (i) enol-acetate formation at steroidal C-17 followed by ozonolysis (Scheme 1) and (ii) degradation of the steroidal D-ring via a perhydrophenathreneindoxyl derivative (Scheme 5).[15] These particular approaches allowed us to maintain/degrade the methyl substituent at position C-8 of the perhydrophenanthrene skeleton (compounds **1**−**4** vs compounds **5**−**10**) and moreover led to intermediates that allowed us to prepare compounds with differing oxidative states at C-7 (methyl esters **1**, **2**, **5**, **6** and methyl ethers **3**, **4**, **7**, **8**). These methyl ester and methyl ether moieties were anticipated to affect the biological activity. Finally, we combined the previously described approaches, degrading both substituents at C-7 and C-8 to prepare the unsubstituted, steroidal ABC ring-mimics **9** and **10**.

The biological activity of these new perhydrophenanthrene derivatives on NMDARs was evaluated on human embryonic kidney 293 (HEK293) cells transfected with plasmids encoding

DOI: 10.1021/acs.jmedchem.6b00079
J. Med. Chem. 2016, 59, 4724−4739

PDF-XChange Editor
KOUPIT plnou verzi!
www.pdfxchange.cz

GluN1-1a/GluN2B/GFP genes. In addition, we have evaluated the action of compound **9** on recombinant GluN1/GluN2A-D, native NMDA, AMPA/kainate, and GABA receptors (GABARs) expressed in hippocampal neurons.

RESULTS AND DISCUSSION

Chemistry. The transformation of the steroidal skeleton into the perhydrophenanthrene was achieved by a series of degradation reactions (Scheme 1). First, the 17-keto group of the starting material (commercially available), 3α-hydroxy-5β-androstan-17-one (**11**), was converted to the enol acetate **12** while protecting the 3α-hydroxy group as an acetate ester (72%).[16] Second, the steroidal D-ring was opened by ozonolysis, followed by treatment with dimethyl sulfide in acetic acid, affording compound **13** in 88% yield. Finally, the Wilkinson decarbonylation led to compound **14** (69%), which was then hydrolyzed with potassium hydroxide in methanol into 7-hydroxy derivative **15** (94%).

Treatment of compound **15** with sulfur trioxide pyridine complex in $CHCl_3$ afforded 2-sulfate derivative **1** (35% yield, Scheme 2). 2-Hemisuccinate ester **2** (51%) was prepared by the reaction of compound **15** with succinic anhydride in the presence of DMAP and pyridine.

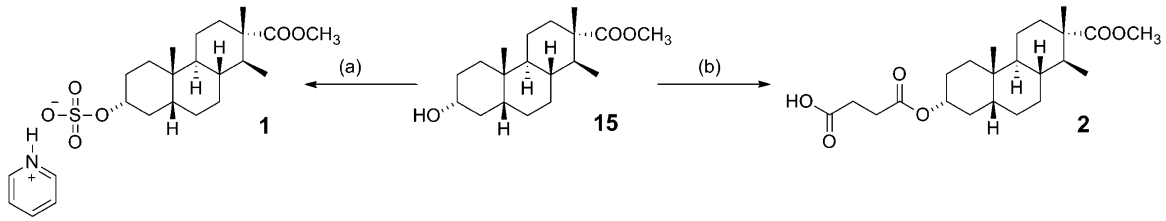
The methyl ester moiety of compound **14** (Scheme 3) was reduced by reflux with lithium aluminum hydride. Simultaneously, the acetate ester moiety was reduced to the hydroxyl group, affording compound **16** (73%). Then, the 2-hydroxy group of compound **16** was selectively oxidized to the ketone by sodium hypochlorite in acetic acid (**17**, 71%). The 2-oxo group was protected as a cyclic ketal (**18**, 85%), and the 7-hydroxymethyl moiety was converted into the methyl ether using NaH/methyl iodide. To avoid potential instability issues, the cyclic ketal moiety was directly deprotected, affording compound **20** (83%, 2 steps). Finally, sodium borohydride reduction in methanol at 0 °C gave 2-hydroxy derivative **21** in 80% yield.

Treatment of compound **21** with sulfur trioxide pyridine complex in $CHCl_3$ afforded 2-sulfate derivative **3** (33% yield). 2-Hemisuccinate ester **4** (83%) was prepared by the reaction of compound **21** with succinic anhydride in the presence of DMAP and pyridine (Scheme 4).

For the synthesis of compound **26** (Scheme 5), we used a previously reported methodology[15] utilizing the treatment of the steroidal 17-oxo group with *o*-nitrobenzaldehyde in a methanolic solution of potassium hydroxide. Starting from 3β-hydroxy-5β-androstan-17-one (commercially available, **22**), we have prepared steroidal indoxyl **23** (84%). Then, the 2-carboxylic moiety was protected as the methyl ester by ethereal diazomethane solution, giving compound **24** in 98% yield, and subsequently the 7-hydroxy group was protected as acetate ester (**25**, 89%). The synthetic strategy used to prepare compound **15** was also utilized to prepare compound **30** (Scheme 5). Thus, ozonolysis of compound **25** followed by treatment with dimethyl sulfide in acetic acid gave compound **26** in 80% yield. Then, Wilkinson decarbonylation led to compound **27** (71%) and the acetate protecting group was hydrolyzed with potassium hydroxide in methanol, affording 7-hydroxy derivative **28** (83%). The proper stereochemistry of the 7-hydroxy group was achieved by Jones oxidation (**29**, 84%) and selective reduction using lithium tri-*tert*-butoxyaluminum hydride, giving compound **30** in 71% yield.

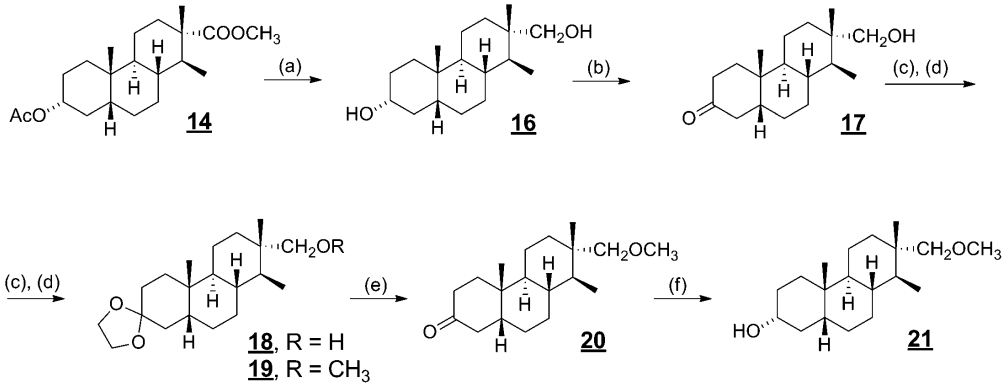
Treatment of compound **30** with sulfur trioxide pyridine complex in $CHCl_3$ afforded 2-sulfate derivative **5** (47% yield). 2-Hemisuccinate ester **6** (52%) was prepared by the reaction of compound **30** with succinic anhydride in the presence of DMAP and pyridine (Scheme 5).

Scheme 2. Synthesis of Compounds 1 and 2[a]



[a]Reagents and conditions: (a) py·SO_3 complex, $CHCl_3$, pyridine, rt; (b) succinic anhydride, DMAP, pyridine, 120 °C.

Scheme 3. Synthesis of compounds 14−21[a]

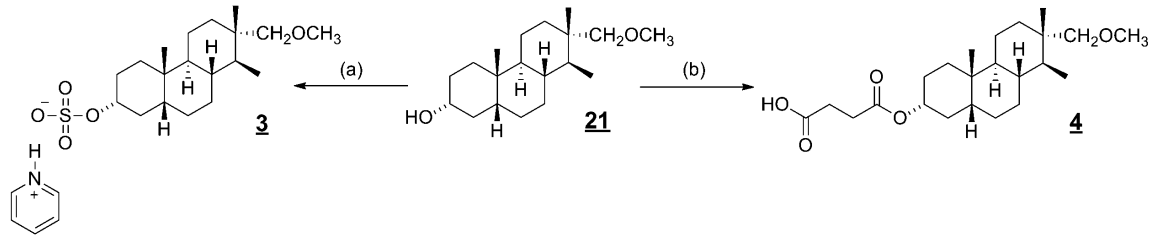


[a]Reagents and conditions: (a) (a) $LiAlH_4$, THF, reflux; (b) NaOCl, CH_3COOH, *i*-PrOH, rt; (c) $CH(OC_2H_5)_3$, ethylene glycol, TsOH·H_2O, benzene; (d) MeI, NaH, THF, 90 °C; (e) HCl, H_2O, acetone; (f) $NaBH_4$, MeOH, 0 °C.

DOI: 10.1021/acs.jmedchem.6b00079
J. Med. Chem. 2016, 59, 4724−4739

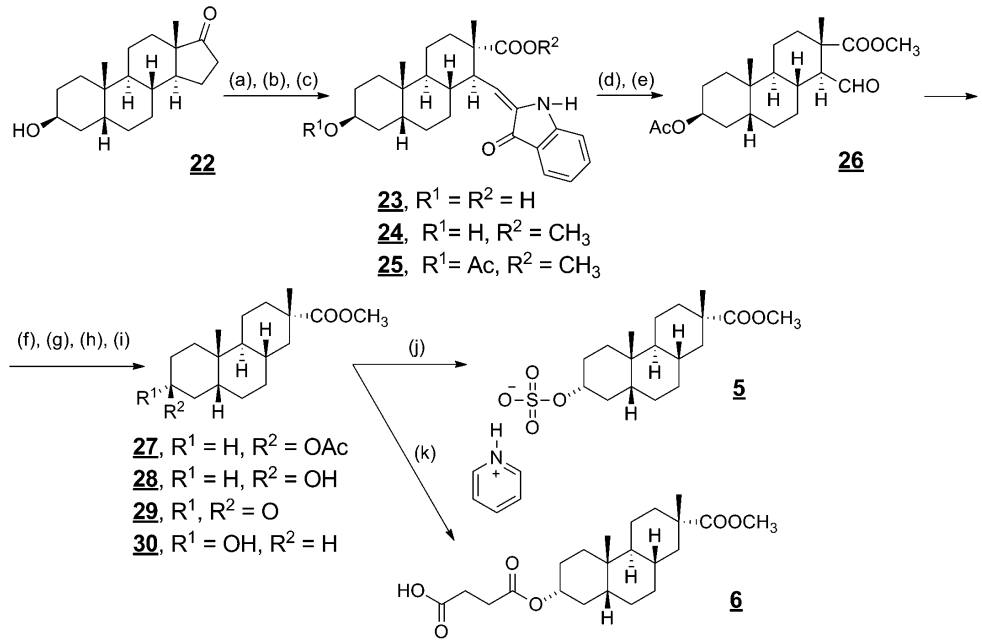
PDF-XChange Editor
KOUPIT plnou verzi!
www.pdfxchange.cz

Scheme 4. Synthesis of Compounds 3 and 4[a]



[a]Reagents and conditions: (a) py·SO_3 complex, $CHCl_3$, pyridine, rt; (b) succinic anhydride, DMAP, pyridine, 120 °C.

Scheme 5. Synthesis of Compounds 5 and 6[a]



[a]Reagents and conditions: (a) *o*-nitrobenzaldehyde, KOH, MeOH, rt; (b) CH_2N_2, ether, 0 °C; (c) Ac_2O, DMAP, pyridine, rt; (d) O_3, AcOH, DCM, −70 °C; (e) Me_2S, AcOH, rt; (f) $[(C_6H_5)_3P]_3RhCl$, PhCN, 160 °C; (g) KOH, MeOH, H_2O; (h) Jones, acetone, rt; (i) $Li(O^tBu)_3AlH$, THF, −40 °C; (j) py·SO_3 complex, $CHCl_3$, pyridine, rt; (k) succinic anhydride, DMAP, pyridine, 120 °C.

The synthetic sequence used for the synthesis of compounds **14**−**21** was also used for the synthesis of compound **36** (Scheme 6): Compound **27** was treated with lithium aluminum hydride under reflux to afford compound **31** (92%). Then, the hydroxy group of compound **31** was selectively oxidized into the ketone by sodium hypochlorite in acetic acid (**32**, 60%), followed by cyclic ketal formation (**18**, 82%). The 7-hydroxymethyl moiety was converted into the methyl ether using NaH/methyl iodide (**34**, 92%), and the cyclic ketal moiety was deprotected by an aqueous solution of hydrochloric acid in acetone, affording compound **35** in (96%). Finally, sodium borohydride reduction in methanol at 0 °C gave 2-hydroxy derivative **36** in 70% yield. Treatment of compound **36** with sulfur trioxide pyridine complex in $CHCl_3$ afforded 2-sulfate derivative **7** (68% yield). 2-Hemisuccinate ester **8** (50%) was prepared by the reaction of compound **36** with succinic anhydride in the presence of DMAP and pyridine (Scheme 6).

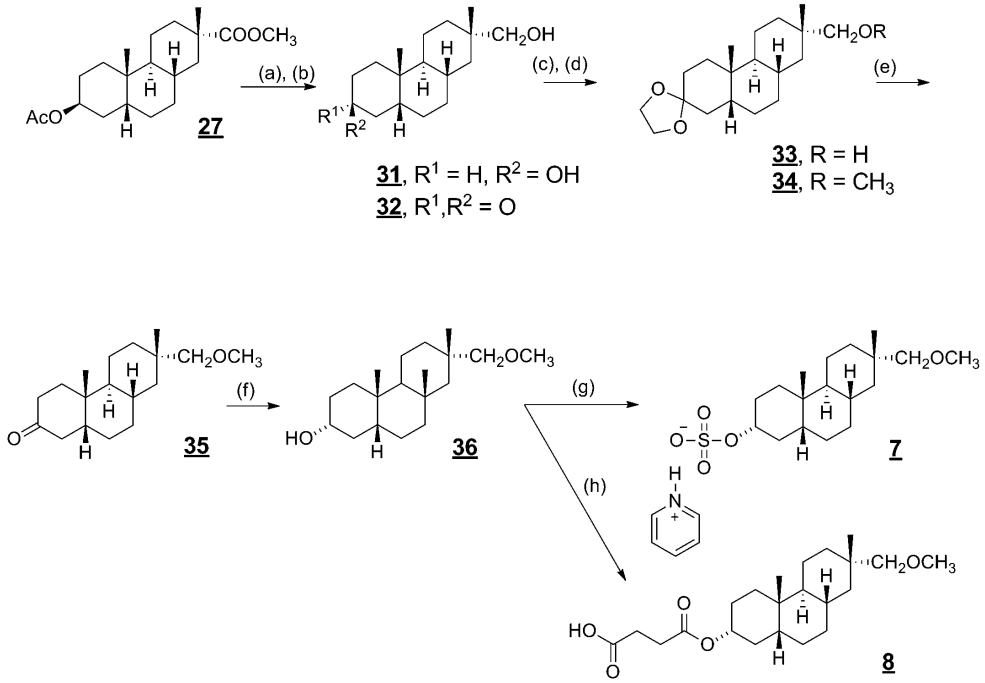
Decarbonylation of the substituent at position C-2 to give compound **39a** (Scheme 7) was achieved via a 4-step reaction, utilizing Wilkinson decarbonylation. Both hydroxyl groups of compound **31** were oxidized by pyridinium chlorochromate using sodium acetate as a buffer, affording compound **37** in 89% yield. Wilkinson decarbonylation of compound **37** gave an inseparable mixture **38** of the desired 2-ketone and two isomeric olefins. Therefore, the crude mixture was next reduced by lithium tri-*tert*-butoxyaluminum hydride and then treated with sodium acetate buffered peracetic acid affording a mixture of epoxides **39b** and **39c** and desired compound **39a**, which was easily isolated by column chromatography (36%, 3 steps). Note that the Wilkinson decarbonylation proceeds in a stereospecific manner and stereochemistry of the β-methyl group at C-2 and C-7 of compounds **37** and **39** is retained without any epimerization. Such stereospecific decarbonylation using Wilkinson's catalyst has been already described in the literature.[17,18]

Analogously, we attempted to afford decarbonylation of compound **16** bearing 7-aldehyde moiety at position C-7. All attempts to proceed with Wilkinson decarbonylation (increased temperature, extended period of reaction time) failed, and only starting material was recovered. We assume that this was caused by steric hindrance of the C-7 and C-8 methyl groups. For the synthesis of C-8 methyl analogue of compound **39a**, the recently published methodology of total synthesis of steroidal skeleton[19] could be used.

DOI: 10.1021/acs.jmedchem.6b00079
J. Med. Chem. 2016, 59, 4724−4739

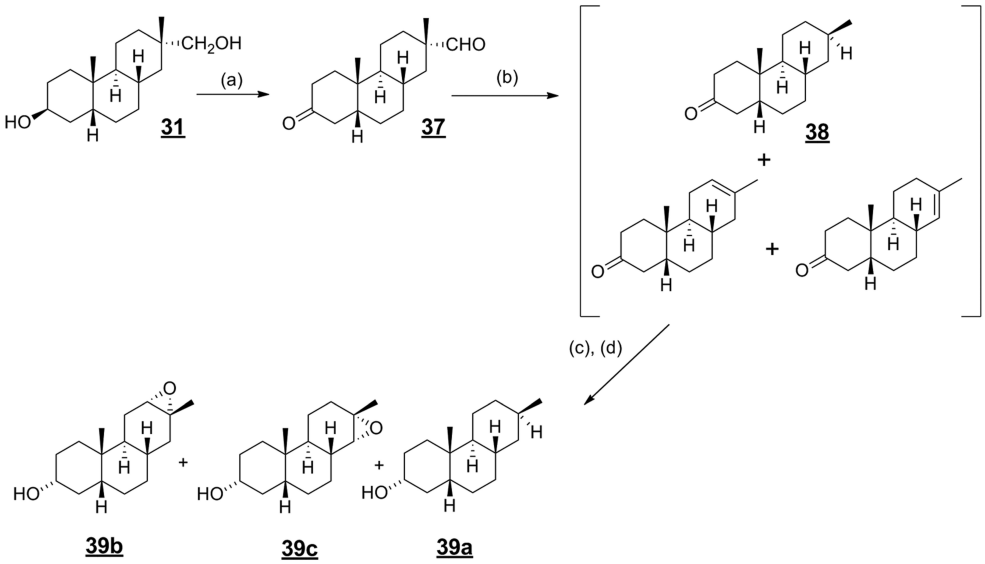
PDF-XChange Editor
KOUPIT plnou verzi!
www.pdfxchange.cz

Scheme 6. Synthesis of Compounds 7 and 8[a]



[a]Reagents and conditions: (a) $LiAlH_4$, THF, reflux; (b) NaOCl, CH_3COOH, *i*-PrOH, rt; (c) $CH(OC_2H_5)_3$, ethylene glycol, $TsOH{\cdot}H_2O$, benzene; (d) MeI, NaH, THF, 90 °C; (e) HCl, H_2O, acetone; (f) $NaBH_4$, EtOH, 0 °C; (g) py·SO_3 complex, $CHCl_3$, pyridine, rt; (h) succinic anhydride, DMAP, pyridine, 120 °C.

Scheme 7. Synthesis of Compound 39a[a]



[a]Reagents and conditions: (a) CH_3COONa, PCC, DCM, rt; (b) $[(C_6H_5)_3P]_3RhCl$, PhCN, 160 °C; (c) $Li(O^tBu)_3AlH$, THF, −40 °C; (d) CH_3COONa, H_2O, CH_3COOOH, DCM, rt.

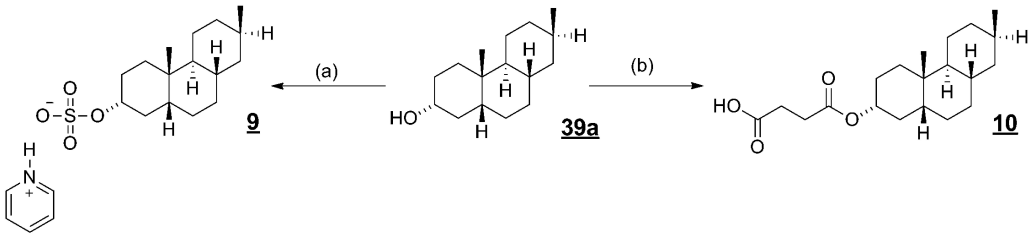
Finally, compound **39a** was treated with sulfur trioxide pyridine complex in $CHCl_3$, affording 2-sulfate derivative **9** (36% yield). 2-Hemisuccinate ester **10** (43%) was prepared by the reaction of compound **39a** with succinic anhydride in the presence of DMAP and pyridine (Scheme 8).

Biological Activity. To investigate the activity of pregnanolone sulfate and its analogues on NMDARs, cDNA encoding for the rat GluN1-1a and GluN2A-D subunits was co-transfected into HEK293 cells. Cells expressing GluN1-1a/GluN2B receptors were used to select the promising candidate for further detailed receptor selectivity analysis. As the amphipathic character of compounds **1**−**10** is similar to our previously published D-modified steroids,[10] we have used an identical approach for the assessment of the obtained data and calculation of the IC_{50}

DOI: 10.1021/acs.jmedchem.6b00079
J. Med. Chem. 2016, 59, 4724−4739

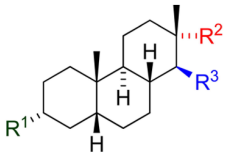
PDF-XChange Editor
KOUPIT plnou verzi!
www.pdfxchange.cz

Scheme 8. Synthesis of Compounds 9 and 10[a]



[a]Reagents and conditions: (a) py·SO_3 complex, $CHCl_3$, pyridine, rt; (b) succinic anhydride, DMAP, pyridine, 120 °C.

Table 1. Effect of Compounds 1−10 (Figure 2) on Current Responses of GluN1/GluN2B Receptors in HEK293 Cells to Glutamate



compd	R^1	R^2	R^3	IC_{50} (μM) (h = 1.2), (n)	concn (μM)
pregnanolone sulfate (Figure 1a)[a]	OSO_3pyH	$CH(COCH_3)(CH_2)_2$ ($R^2 = R^3$)	$CH(COCH_3)(CH_2)_2$ ($R^2 = R^3$)	24.6 ± 5.3 (n = 5)	100
5β-androstane-3α-yl sulfate (Figure 1b)[b]	OSO_3pyH	$CH_2CH_2CH_2$ ($R^2 = R^3$)	$CH_2CH_2CH_2$ ($R^2 = R^3$)	1.2 ± 0.2 (n = 11)	3
1	OSO_3pyH	$COOCH_3$	CH_3	74.6 ± 20.3 (n = 5)	50
2	$OCO(CH_2)_2COOH$	$COOCH_3$	CH_3	63.4 ± 5.5 (n = 3)	10
3	OSO_3pyH	CH_2OCH_3	CH_3	33.0 ± 6.3 (n = 5)	50
4	$OCO(CH_2)_2COOH$	CH_2OCH_3	CH_3	29.2 ± 0.7 (n = 3)	10
5	OSO_3pyH	$COOCH_3$	H	224.0 ± 28.0 (n = 4)	50
6	$OCO(CH_2)_2COOH$	$COOCH_3$	H	87.6 ± 47.0 (n = 4)	10
7	OSO_3pyH	CH_2OCH_3	H	77.0 ± 10.0 (n = 6)	50
8	$OCO(CH_2)_2COOH$	CH_2OCH_3	H	33.3 ± 10.9 (n = 7)	10
9	OSO_3pyH	H	H	15.6 ± 3.0 (n = 4)	10
10	$OCO(CH_2)_2COOH$	H	H	23.2 ± 6.4 (n = 5)	10

[a]See refs 12 and 20. [b]See ref 10.

values. In brief, the IC_{50} for the newly synthesized perhydrophenanthrene analogues was determined from a single dose of the compound using the following formula:

$$IC_{50} = [\text{compound}] \sqrt[h]{\frac{1 - I_I}{I_I}}$$

where I_I is the relative degree of inhibition, [compound] is the perhydrophenanthrene analogue concentration used, and h stands for the Hill coefficient (fixed at 1.2). The IC_{50} value was determined for a minimum of two perhydrophenanthrene analogue doses, differing 3-fold in the concentration range. If the difference in the IC_{50} values was <10%, then the mean IC_{50} was calculated from the concentration most proximal to that inducing 50% inhibition. If the difference in the IC_{50} values determined for two doses was >10%, then the dose−response analysis was determined at lower concentrations to reach the formal criterion. In accordance with previous results, IC_{50} calculations were made assuming 100% inhibition at saturating concentration.[12,20] Table 1 summarizes the IC_{50} determined for perhydrophenanthrene analogues.

Ability of Perhydrophenanthrene Derivatives (1−10) To Modulate NMDAR Currents. Comparison of the IC_{50} values of simplified compounds **9** and **10** (IC_{50} = 15.6 ± 3.0 and 23.2 ± 6.4 μM, respectively), which bear only the ABC-ring motif of steroidal skeleton, to that of pregnanolone sulfate (Figure 1a, IC_{50} = 24.6 ± 5.3 μM) clearly indicates that this simplified framework is sufficient for maintaining inhibitory activity. However, the IC_{50} value of 5β-androstane-3α-yl sulfate (Figure 1b, IC_{50} = 1.2 ± 0.2 μM),[10] with an unsubstituted five-membered D-ring, gave a ∼10-fold decrease in IC_{50} value relative to perhydrophenanthrene 2-sulfate (Figure 1c, i.e. compound **9**). Therefore, we can conclude that while complete degradation of the D-ring is an "allowed" modification, doing so may lead to a decrease in lipophilicity of the skeleton, which may affect the IC_{50} value in an undesirable manner.

Effect of the Methyl Ester vs Methyl Ether Moiety of Compounds 1−10 on Modulation of NMDARs. The obtained data (Table 1, Figure 2) show that compounds with a methyl ester moiety at position C-8 have comparatively higher IC_{50} values than their methyl ether analogues: **1** vs **3** (IC_{50} of 74.6 ± 20.3 and 33.0 ± 6.3 μM) and **2** vs **4** (IC_{50} of 63.4 ± 5.5 and 29.2 ± 0.7 μM), with methyl ethers **3** and **4** both showing a favorable ∼2.2-fold decrease in the IC_{50} value. Accordingly, the comparison of **5** vs **7** (IC_{50} of 224.0 ± 28.0 and 77.0 ± 10.0 μM) and **6** vs **8** (IC_{50} of 87.6 ± 47.0 and 33.3 ± 10.9 μM) also shows a ∼2.9-fold and ∼2.6-fold decrease in the IC_{50} value, favoring methyl ether **7** and **8**, respectively.

Effect of the Sulfate vs Hemisuccinate Moiety of Compounds 1−10 on Modulation of NMDARs. In order to compare the effects of the sulfate and hemisuccinate moiety on the IC_{50} value, the compounds were divided into two groups.

DOI: 10.1021/acs.jmedchem.6b00079
J. Med. Chem. 2016, 59, 4724−4739

PDF-XChange Editor
KOUPIT plnou verzi!
www.pdfxchange.cz

Those bearing the sulfate moiety, **1**, **3**, **5**, 7, and **9**, and those bearing the hemisuccinate moiety, **2**, **4**, **6**, **8**, and **10** (Figure 2). Interestingly, while the comparison of sulfated vs hemisuccinate compounds with an oxygen substituent at position C-7 found all hemiester compounds to have lower IC_{50} values (**1** vs **2**, **3** vs **4**, **5** vs **6**, and 7 vs **8**), the opposite trend was seen for unsubstituted compounds **9** and **10** (IC_{50} of 15.6 ± 3.0 and 23.2 ± 6.4 μM), wherein the sulfated analogue has a ~50% lower IC_{50} value.

We have concluded that the structural degradation of the D-ring (methyl ester vs methyl ether) has provided new structural motifs that could be useful modifiers for various C-2 substituted analogues with miscellaneous hemiester moieties while maintaining the inhibitory activity. However, it is worth mentioning that the particular modulatory action of such derivatives may be further significantly affected by other aspects such as solubility, permeability, Lipinski rule of five, etc.

Effect of Compound 9 on Native and Recombinant NMDA Ionotropic Receptors. As compound **9** (Figure 2) was evaluated as the most potent modulator of a focused library of perhydrophenanthrene analogues (**1**−**10**), it was chosen for further biological evaluation. To investigate the subunit selectivity of compound **9** on the NMDARs, cDNAs encoding for the GluN1 and GluN2A-D subunits were co-transfected into HEK293 cells. Comparing the IC_{50} values of compound **9** at GluN1/GluN2A-D receptors revealed a significant difference between the IC_{50} value for GluN2B and those of the remaining GluN2A,C,D subunit containing receptors (ANOVA; $P \leq 0.007$). Notably, the comparison did not show any significant differences between the IC_{50} values for any combination of GluN2A,C,D. This indicates that the action of the perhydrophenanthrene analogue is weakly subunit dependent, as the GluN2B subunit is less sensitive to the perhydrophenanthrene analogue than other GluN2A,C,D subunit containing receptors (Figure 3 and Table 2). Similarly, no significant differences were found between native NMDARs expressed in cultured hippocampal neurons and recombinant GluN1/GluN2A-B receptors likely to be expressed in these cells.[21] In contrast to NMDAR response induced by 100 μM NMDA, the response of the α-amino-3-hydroxy-5-methyl-4-isoxazolepropionic acid receptor (AMPAR) induced by 100 μM AMPA, recorded in the presence of 10 μM cyclothiazide to block the receptor desensitization,[22] was significantly less sensitive to compound **9**. We have shown in our previous study[10] that the IC_{50} values of highly potent neurosteroid 17β-methyl-5β-androstan-3α-yl 3-sulfate are not significantly different for NMDAR and GABAR currents. On the contrary, the responses induced by 5 μM GABA were inhibited by compound **9** with IC_{50} values significantly different from that determined for NMDAR responses (Figure 4 and Table 3). This indicates that the steroidal D-ring plays a significant role for NMDAR/GABAR selectivity and gives a perspective for a further design of receptor selective neurosteroid based drugs. Despite this dual target effect, we have shown that neurosteroid derivatives with inhibitory effects on both NMDAR and GABAR show neuroprotective effects without psychomimetic symptoms.[5−8] We hypothesize that the inhibition of GABAR may help to minimize the undesired psychomimetic side effects; however the exact role of the inhibitory action on GABAR is unclear.

Computational Estimate of Thermodynamic Properties of Compounds 1−10. In the computational study, we have investigated the lipophilic qualities of the studied inhibitors in the context of their inhibitory effect, since the lipophilicity belongs to the basic characteristics of the neurosteroids, which influences their interactions with NMDAR.[10] The relevant physicochemical properties[23] of compounds **1**−**10** were estimated by quantum mechanics computational methods and

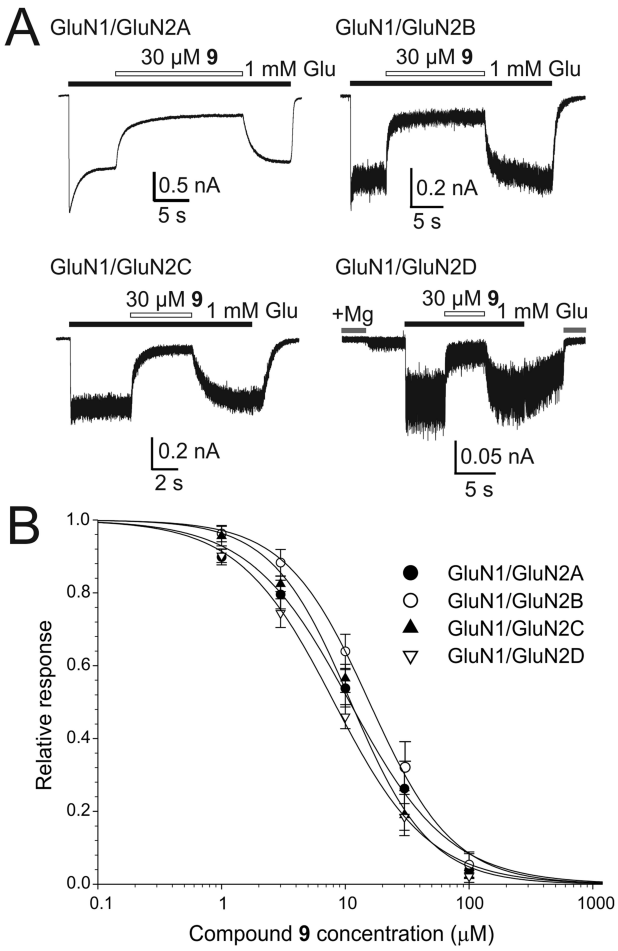


Figure 3. Effect of compound **9** on GluN1/GluN2A-D receptors. (A) Example of trace obtained from HEK293 cells transfected with cDNAs encoding GluN1/GluN2A (GluN2A), GluN1/GluN2B (GluN2B), GluN1/GluN2C (GluN2C), and GluN1/GluN2D (GluN2D) receptors. Compound **9** (30 μM) was applied simultaneously with 1 mM glutamate (duration of glutamate and perhydrophenanthrene analogue application is indicated by filled and open bars, respectively). The gray bar indicates application of ECS containing 1 mM Mg^{2+}. (B) Concentration−response curves for the effect of compound **9** at GluN1/GluN2A-D receptors. Data points are averaged values of normalized responses from minimum four HEK293 cells. Error bars represent SD. The relative glutamate induced responses (I) recorded in the presence of the perhydrophenanthrene analogue (1−100 μM) and determined in individual cells were fit to the following logistic equation: $I = 1/(1 + ([\text{perhydrophenanthrene analogue}]/IC_{50})^h)$, where IC_{50} is the concentration of compound **9** that produces a 50% inhibition of agonist-evoked current, [perhydrophenanthrene analogue] is the compound **9** concentration, and h is the apparent Hill coefficient.

Table 2. Effect of Compound 9 on Responses Induced in GluN1/GluN2A-D Receptors in HEK293 Cells to Glutamate

	IC_{50} ± SD (μM)	h ± SD	n
GluN1/GluN2A	10.9 ± 0.9	1.1 ± 0.1	6
GluN1/GluN2B	15.6 ± 0.8	1.3 ± 0.1	5
GluN1/GluN2C	11.1 ± 0.8	1.4 ± 0.1	4
GluN1/GluN2D	8.1 ± 0.5	1.1 ± 0.1	4

DOI: 10.1021/acs.jmedchem.6b00079
J. Med. Chem. 2016, 59, 4724−4739

PDF-XChange Editor
KOUPIT plnou verzi!
www.pdfxchange.cz

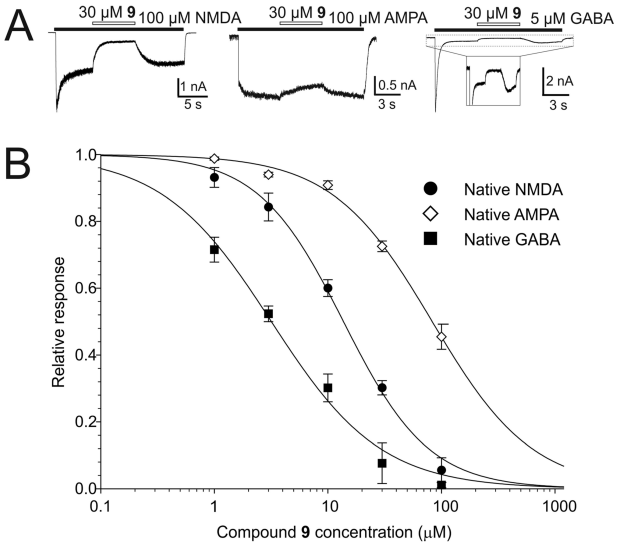


Figure 4. Effect of compound **9** on native AMPA/kainate, NMDA, and GABA receptors. (A) Example of trace obtained from cultured hippocampal neurons. Compound **9** (30 μM) was applied simultaneously with AMPA (100 μM), NMDA (100 μM), and GABA (5 μM) (duration of agonist and perhydrophenanthrene analogue application is indicated by filled and open bars, respectively). (B) Concentration–response curves for the compound **9** effect at AMPA, NMDA, and GABA receptors. Data points are averaged values of normalized responses from minimum of five cultured hippocampal neurons. Error bars represent SD. The relative agonist induced responses (I) recorded in the presence of the compound **9** (1–100 μM) and determined in individual cells were fit to the following logistic equation: $I = 1/(1 + ([\text{perhydrophenanthrene analogue}]/IC_{50})^h)$, where IC_{50} is the concentration of perhydrophenanthrene analogue that produces a 50% inhibition of agonist-evoked current, [perhydrophenanthrene analogue] is the perhydrophenanthrene analogue concentration, and h is the apparent Hill coefficient.

Table 3. Effect of Compound 9 on NMDA, AMPA, and GABA Receptor Responses in Hippocampal Neurons[a]

	$IC_{50} \pm$ SD (μM)	$h \pm$ SD	n
NMDAR	13.7 ± 0.9	1.2 ± 0.1	5
AMPAR	83.0 ± 5.2	1.0 ± 0.1	6
GABAR	3.1 ± 0.3	0.9 ± 0.1	6

[a]Hill coefficient was fixed at 1.2.

by physicochemical properties predictor. The computational results are summarized in Table 4.

The interactions of neurosteroid/neurosteroid-like compounds with NMDAR constitute the complicated process. First, the micelles occurring in the extracellular liquid fuse with the membrane; thereafter the single-molecules leave the membrane and finally enter the channel vestibule, which is the hydrophobic site of action.[9] The solvation free energy (ΔG_{solv}) estimates the behavior of the single-molecules in water and in n-octanol which represents the membrane environment. The negative values of ΔG_{solv} signify the free energy gained, and the positive values signify free energy required during the transfer from the first phase to the second phase occurs. The $\Delta G_{solv}^{octanol/water}$ values indicate that the charged molecules prefer water while the neutral ones n-octanol. These results suggest that the transfer between n-octanol and water is possible and it can be accompanied by the transition between the neutral and the ionized state.

The lipophilic character of compounds **1**–**10** was estimated by the log P and log D coefficients. The log P is defined as the logarithm of the ratio of neutral solute concentrations in n-octanol and water. On the other hand, the log D is the logarithm of the ratio of the sum of the concentrations of the neutral and the ionized form of the solute in each of the two phases and thus is depending on pH. As compounds **1**–**10** can be both ionized and neutral, the description of the lipophilicity by the log D is more appropriate.[24] The correlation between the calculated data and the experimental ΔG_{exp} data shows the two different groups of the compounds that evince the similar behavior only for ΔG_{solv} during the transfer from n-octanol to water (for the details, see the R^2 values in Table 4 and graphs in Supporting Information). The correlation for the sulfated analogues (**1**, **3**, **5**, **7**, **9**; R^2 = 0.80/0.77 (neutral/charged form) for $\Delta G_{solv}^{octanol/water}$; R^2 = 0.81/0.71 for log P/log D) is a little lower than for the hemisuccinate analogues (**2**, **4**, **6**, **8**, **10**; R^2 = 0.97/0.96 (neutral/charged form) for $\Delta G_{solv}^{octanol/water}$; R^2 = 0.93/0.28 for log P/log D). The correlation between log D values of the hemisuccinates and the ΔG_{exp} values has not found. This indicates that the real ratio of the neutral and ionized form of the solute of the hemisuccinates is different from calculated which is most likely caused by the different character of their functional hemisuccinate group in the aqueous and n-octanol environment (e.g., pK_a) as compared with sulfate moiety. The hemisuccinate analogues with slightly better inhibitory effect than the sulfated ones (except for the compound **10**) also evince the log D values lower and log P values higher than the sulfates. The sulfate and hemisuccinate analogues bearing ether of ester moiety on the skeleton have a similar inhibitory effect except for the significantly different values of the compound **5** (sulfate) and compound **10** (hemisuccinate). We hypothesize such phenomenon can be explained by conformation/deformation energy of the molecule during its motion inside NMDAR to the site of the action.[9] The hemisuccinate derivative is considerably more flexible, as it has more rotational C–C bonds and therefore more conformers. On the other hand, the sulfate moiety is rather rigid. The deformation energy is expressed as the difference of the single point energies between the global minimum (extended form) and the local minimum (compact conformer) in aqueous phase. The deformation energy is 5.08 kcal/mol for compound **5** and 13.47 kcal/mol for compound **6**. The results suggest that compound **6** inclines to compose the compact form through the intramolecular interaction of the aliphatic chain with the carbon skeleton and the ester moiety (Figure 5A). Although this intramolecular interaction has an adverse energy effect, it facilitates the passage of the molecule to the site of the inhibitory action.[9] On the contrary, the conformation of the compound **5** remains nearly extended (Figure 5B). Therefore, the conformers can have different ΔG_{solv} as well. The methyl ether of methyl ester substituents can also contribute to the conformation change of the particular molecule; e.g., compound **4** tends to form the compact conformer, probably just as all hemisuccinate analogues, but the methyl group at C-8 fastens the ether moiety at C-7. Therefore, the conformer is less clenched (Figure 5C) and the deformation energy is 11.82 kcal/mol.

A comparison of pregnanolone sulfate (IC_{50} = 24.6 μM, log P = 2.93, and log D = 1.67)[10] with compounds **9** (IC_{50} = 15.6 μM, log P = 3.11, and log D = 1.55) and **10** (IC_{50} = 23.2 μM, log P = 5.10, and log D = 1.04) shows better inhibitory effect of both compounds with log D vales lower and log P values higher than pregnanolone sulfate. Also, 5β-androstan-3α-yl sulfate (IC_{50} = 1.2 μM, log P = 4.07, and log D = 2.11)[10] evinces

DOI: 10.1021/acs.jmedchem.6b00079
J. Med. Chem. 2016, 59, 4724–4739

PDF-XChange Editor
KOUPIT plnou verzi!
www.pdfxchange.cz

Table 4. Summary of the Computational Values of the Physicochemical Properties of Neuroactive Steroids[a]

compd	IC_{50} [μmol/L]	ΔG_{exp} [kcal/mol]	ΔG_{solv} [kcal/mol], transfer from vacuum to water: neutral	vacuum to water: charged	*n*-octanol to water: neutral	*n*-octanol to water: charged	log *P*	log *D*
1	74.6	−5.7	−20.70	−75.89	0.98	−6.58	2.10	1.47
2	63.4	−5.8	−23.96	−84.84	2.35	−6.03	4.08	0.97
3	33.0	−6.1	−16.21	−71.51	2.46	−5.02	3.07	1.49
4	29.2	−6.2	−19.55	−80.19	3.89	−4.40	5.25	0.99
5	224.0	−5.0	−20.77	−75.69	0.68	−6.84	1.71	1.18
6	87.6	−6.1	−23.99	−84.64	2.13	−6.26	3.92	0.68
7	77.0	−5.6	−17.18	−72.67	1.94	−5.55	2.74	1.21
8	33.3	−6.1	−20.58	−81.33	3.34	−5.02	4.98	0.70
9	15.6	−6.6	−14.15	−69.60	2.61	−4.95	3.11	1.55
10	23.2	−6.3	−17.46	−78.33	4.03	−4.33	5.10	1.04
correlation for sulfate derivatives (**1**, **3**, **5**, **7**, **9**)			0.78	0.78	0.80	0.77	0.81	0.71
correlation for hemiester derivatives (**2**, **4**, **6**, **8**, **10**)			0.93	0.93	0.97	0.96	0.93	0.28
correlation for compounds **1**−**10**			0.36	0.05	0.63	0.77	0.36	0.03

[a]The negative values of ΔG_{solv} signify the free energy gained and the positive values signify free energy required during the transfer from the first phase to the second phase. The correlation between ΔG_{exp} and ΔG_{solv}, log *P*, and log *D* is expressed as coefficient of determination (R^2).

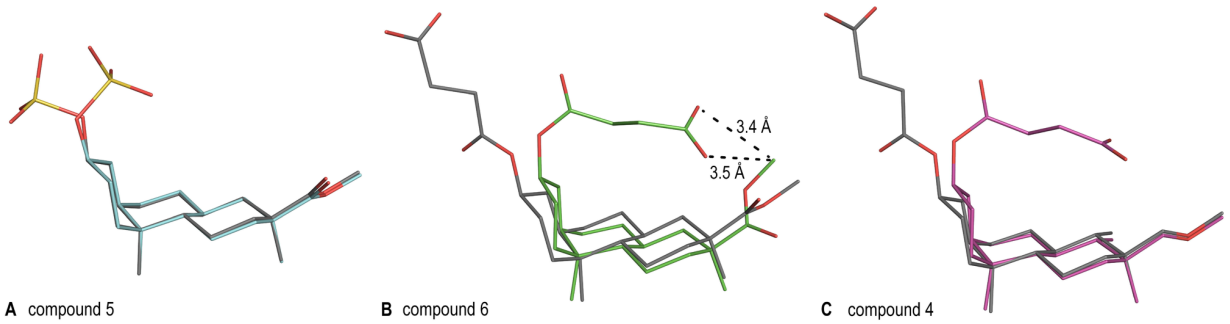


Figure 5. Conformers of compounds **4**−**6**. (A) Global (gray) and local minimum (blue) of compound **5**. (B) Global (gray) and local minimum (green) of compound **6**. (C) Global (gray) and local minimum (magenta) of compound **4**.

significantly better inhibitory activity than compounds **9** and **10**, while its log *D* value is significantly higher than in the cases of compounds **9** and **10** and it has lower log *P* value than compound **10**. Compound **9** (sulfate) shows the best inhibitory activity from series of compounds **1**−**10**, and it has the highest log *D* among the studied compounds and the highest log *P* among the sulfated analogues (Table 4). Compound **10** (hemisuccinate), which is the second best studied inhibitor, has the highest log *D* among the hemisuccinate analogues but lower log D value than the sulfated analogues; its log *P* is the second best among all compounds (Table 4). Our results denote the importance of the lipophilicity and the solvation free energy for the action of the steroids at the NMDAR, which is in an agreement with our previous results for sulfated steroids modified on the D-ring.[10] The results also indicate that the decrease of the lipophilicity related to the structural modification need not lead to the decrease of the inhibitory activity. In addition, the results point out the weighty effect of the conformation change of the steroids. Therefrom, we conclude that the results more likely suggest a different character of the inhibitory action of both inhibitory groups.

■ CONCLUSIONS

In this study, we have examined new compounds (**1**−**10**), with fully saturated phenanthrene skeletons that mimic the steroidal ABC ring system in order to evaluate their ability to modulate NMDAR-induced current. We have shown that the steroidal D-ring can be fully or partially degraded with a variety of polar substituents while maintaining inhibitory activity. We have also shown that the potency of these new inhibitors is comparable with the endogenous ligand, pregnanolone sulfate. In addition, we have shown that the degradation of the steroidal D-ring did not lead to NMDAR subtype selectivity and that there is a higher potency to inhibit NMDAR responses than AMPAR responses. Moreover, the IC_{50} values determined for GABAR responses were different from that determined for NMDAR responses for compound **9** that was evaluated as the most potent modulator of a focused library of perhydrophenanthrene analogues. This indicates that the steroidal D-ring plays a significant role for NMDAR/GABAR selectivity and gives a perspective for a further design of receptor selective neurosteroid-like based drugs. This new structural motif offers new prospects for the further modification and optimization of the pharmacological and pharmacokinetic properties of these neuroactive compounds. Finally, the computational analysis has defined the structure−function relationship of the steroid-like compounds in connection with their lipophilicity, solvation free energy, and conformation change which have a significant effect on the their inhibition of NMDAR responses.

■ EXPERIMENTAL SECTION

Chemistry. General. Melting points were determined on a micro-melting point apparatus Hund/Wetzlar (Germany) and are uncorrected.

DOI: 10.1021/acs.jmedchem.6b00079
J. Med. Chem. 2016, 59, 4724−4739

PDF-XChange Editor
KOUPIT plnou verzi!
www.pdfxchange.cz

Optical rotations were measured in chloroform using an Autopol IV (Rudolf Research Analytical, Flanders, USA). $[\alpha]_D$ values are given in deg (10^{-1} deg cm^2 g^{-1}). IR spectra were recorded on a Bruker IFS 55 spectrometer (wavenumbers in cm^{-1}). Proton and carbon NMR spectra were measured on a FT NMR spectrometer Bruker AVANCE-400 (400 MHz, 101 MHz) in $CDCl_3$ with tetramethylsilane as the internal standard. Chemical shifts are given in ppm (δ scale). Coupling constants (J) and width of multiplets (W) are given in Hz. High resolution MS spectra were performed with a Q-Tof microspectrometer (Waters). Thin layer chromatography (TLC) was performed on silica gel (ICN Biochemicals). Preparative TLC (prep-TLC) was carried out on 200 mm × 200 mm plates coated with a 0.4 mm thick layer of the same material. For column chromatography neutral silica gel 60 μm (Merck) was used. Analytical samples were dried over phosphorus pentoxide at 50 °C/100 Pa. Anhydrous THF was prepared by distillation with benzophenone/Na immediately prior to use. Jones reagent has been prepared from chromium trioxide (67 g, 0.67 mmol) and a solution of sulfuric acid (58 mL of H_2SO_4 in 100 mL of water), and the mixture was diluted to 250 mL with water. The purity of the final compounds was assessed by a combination of NMR and on the basis of analysis LC−HR-MS, and the results were greater than 95%.

Computational Section. Preparation of Structures. The compounds were obtained by modeling the inhibitor as taken from the crystal structure (PDB code 3CAV[25]) using PyMOL program[26] and were relaxed by the RI-DFT/B-LYP/SVP method with the Turbomole program.[27] The empirical dispersion correction (D)[28] and COSMO continuum solvation model[29] were applied on the gradient optimization. The most stable local minima of the compounds were obtained by the quenched molecular dynamics simulation method with PM6-D3H4X.[30] The resulting geometries were minimized by the RI-DFT-D/B-LYP/SVP//COSMO method, and their single-point energies were calculated at the RI-DFT-D3/B-LYP/TZVPP//COSMO level.[31]

Computational Methods. The solvation free energy (ΔG_{solv}) of the perhydrophenanthrene analogues was calculated in the SMD continuum solvation model (the transfer from vacuum to water and from n-octanol to water)[32] at the HF/6-31G* level with the Gaussian program.[33] In this method, the single-point energies were computed at the identical molecular geometry both for the transfer from vacuum to water and from n-octanol to water. The partition coefficient (log P) was estimated on the basis of the change of the molecular conformation related to the transfer between n-octanol and water. The compounds were optimized at the M06-2X/6-31G* level in the SMD in the aqueous and n-octanol environments with the Gaussian program and log P was expressed as the difference between the total energies in water and in n-octanol[34] because this energy includes the internal energy of the molecule. The distribution coefficients (log D) of water/n-octanol phase were predicted at pH = 7.4, which is the physiological pH of blood serum, by the MarvinSketch program.[35] The estimated values of ΔG_{solv}, log P, and log D were compared with the experimental free energies (ΔG_{exp}) expressed from the IC_{50} values via the equation $\Delta G_{exp} = RT \ln(IC_{50})$. The linear regression was used for the description of the relationship between ΔG_{exp} and ΔG_{solv}, log P, and log D. The coefficient of determination (R^2), which is the square of the Pearson correlation coefficient between experimental and predicted data values, expresses how well the regression line approximates the real data points. It acquires values 0−1, where 0 means impossibility and 1 means a certainty.

Biological Activity. Electrophysiological experiments were performed on HEK293 cells transfected with plasmids encoding GluN1-1a/GluN2A-D/GFP genes and cultured hippocampal neurons as described previously.[17,36,37] Agonist-induced responses were voltage-clamped at a holding potential of −60 mV. Whole-cell voltage-clamp recordings were made with a patch-clamp amplifier (Axopatch 200B; Axon Instruments. Inc., Foster City, CA) after a serial resistance (<10 MΩ) and capacitance compensation of 80−90%. For the application of test and control solutions, a microprocessor controlled multibarrel fast-perfusion system was used, with a time constant of solution exchange around cells of ∼10 ms. Agonist-induced responses were low-pass-filtered at 2 kHz, digitally sampled at 5 kHz, and analyzed with pClamp software, version 9.2 (Molecular Devices). Patch pipettes (3−5 MΩ) pulled from borosilicate glass were filled with Cs^+-based intracellular solution (ICS) containing the following (in mM): 120 gluconic acid, 15 CsCl, 10 BAPTA, 10 HEPES, 3 $MgCl_2$, 1 $CaCl_2$, and 2 ATP-Mg salt (pH-adjusted to 7.2 with CsOH). The extracellular solution (ECS) contained the following (in mM): 160 NaCl, 2.5 KCl, 10 HEPES, 10 glucose, 0.2 EDTA, 0.7 $CaCl_2$ (pH-adjusted to 7.3 with NaOH). NMDAR responses were induced by 1 mM glutamate (in recombinant receptors) and 100 μM NMDA (native receptors). The ECS used for native receptors had the same composition as the ECS used for recombinant receptors. For native NMDAR recordings ECS contained additionally 10 μM CNQX, 10 μM bicuculline, and 0.5 μM TTX. AMPA receptors currents were induced by 100 μM AMPA and the ECS contained additionally 50 μM D-AP5, 10 μM bicuculline, 0.5 μM TTX, and 10 μM cyclothiazide. GABA receptor responses were induced by 5 μM GABA, and the ECS contained additionally 50 μM D-AP5, 10 μM CNQX, and 0.5 μM TTX. Steroid/perhydrophenanthrene analogue solutions were prepared fresh as a stock solution of either 5 or 20 mM in dimethyl sulfoxide (DMSO) before each experiment (1% DMSO final concentration). The same concentration of DMSO was added in all extracellular solutions. Experiments were performed at room temperature (21−25 °C).

Experimental Data for Compounds 1−39a. General Procedure I: Sulfonation. A mixture of the hydroxy derivative (0.15 mmol) and sulfur trioxide pyridine complex (0.31 mmol) was dried in vacuo (25 °C, 100 Pa) for 30 min. Then, freshly dried chloroform (5 mL/50 mg) and dry pyridine (1 drop) were added and the reaction mixture was stirred at room temperature under inert atmosphere. The progress of the reaction was checked by TLC. Then, the reaction mixture was allowed to stand at −5 °C for 2 h, and the solid was filtered off through a plug of cotton wool in a glass Pasteur pipet. The filtrate was evaporated and dried (25 °C, 100 Pa) for 1 h to afford a mix of sulfate and sulfur trioxide pyridine complex. The crude material was dissolved in a minimal amount of freshly dried chloroform, allowed to stand at −5 °C for 2 h, and the solid was filtered off through a plug of cotton wool in a glass Pasteur pipet. The filtrate was evaporated and dried (25 °C, 100 Pa) for 1 h to afford the corresponding sulfate.

General Procedure II: Synthesis of Hemisuccinate Ester. A mixture of hydroxy derivative (100 mg, 0.32 mmol) and succinic anhydride (7 equiv) was dried overnight at 50 °C. Dry pyridine (4 mL/100 mg of starting material) and 4-(dimethylamino)pyridine (2.4 equiv) were added. The mixture was heated at 120 °C for 4 h. Then, it was poured into water and extracted with chloroform. Combined organic extracts were washed with brine and dried.

General Procedure III: Wilkinson's Decarbonylation. A mixture of carbonyl derivative (3.65 mmol) and tris(triphenylphosphine)-rhodium(I) chloride (1.1 equiv) in benzonitrile (25 mL/1.3 g of starting material) was heated under inert atmosphere at 160 °C for 20 h. The reaction mixture was cooled to room temperature and filtered to remove yellow solid. The filtrate was evaporated under reduced pressure. In addition, the yellow solid was washed with dichloromethane, and the washings were added to the first solid residue. The resulting mixture was filtered again to remove additional yellow solid which formed subsequently. The filtrate was again evaporated under reduced pressure.

General Procedure IV: Hydrolysis with Potassium Hydroxide. A solution of acetoxy derivative in methanol (5 mL/100 mg of starting material) was stirred overnight at room temperature with a solution of potassium hydroxide (4 equiv) in minimum amount of water. The reaction mixture was poured into water, the product was extracted with ethyl acetate, and combined organic extracts were washed with 5% aqueous solution of HCl, saturated aqueous solution of sodium bicarbonate, dried over Na_2SO_4, and evaporated under reduced pressure.

General Procedure V: LAH Reduction. A mixture of methyl ester derivative and $LiAlH_4$ (3 equiv) in THF (30 mL/1 g of starting material) was refluxed under atmosphere for 2 h. The excess of reagent was carefully quenched with aqueous solution of sodium sulfate, and inorganic material was filtered off, washing with ethyl acetate. The filtrate was washed with 5% aqueous solution of HCl, water, saturated aqueous solution of sodium bicarbonate, dried over Na_2SO_4, and evaporated.

General Procedure VI: Sodium Hypochlorite Oxidation. An aqueous solution of sodium hypochlorite (4.5%, 7.7 mL) was added into a solution of alcohol (2.09 mmol) in acetic acid (18 mL). After stirring at

DOI: 10.1021/acs.jmedchem.6b00079
J. Med. Chem. 2016, 59, 4724−4739

PDF-XChange Editor
KOUPIT plnou verzi!
www.pdfxchange.cz

rt for 1 h, isopropanol (11 mL) was added and the mixture was stirred for another 30 min. Then, it was diluted with water and extracted with dichloromethane. The combined organic extracts were washed with brine, dried over Na_2SO_4 and the solvents evaporated.

General Procedure VII: Cyclic Ketal Formation. Ketone (550 mg, 1.98 mmol), triethyl orthoformate (7 equiv), and ethylene glycol (19 equiv) were dissolved in benzene (10 mL/550 mg of starting material), and TsOH·H_2O (0.1 equiv) was added with stirring at rt. The reaction mixture was allowed to stand at 50 °C for 17 h, then cooled to rt, diluted with brine, and extracted with ethyl acetate. The combined organic extracts were washed with brine, dried over $MgSO_4$ and the solvents evaporated.

General Procedure VIII: Williamson Ether Synthesis. Cyclic ketal was dissolved in dry THF (30 mL/430 mg of starting material), and sodium hydride (60% dispersion in mineral oil, 10 equiv) was added. The mixture was stirred in an argon atmosphere at 90 °C for 1 h, then methyl iodide (8.5 equiv) was added and the mixture was stirred in an argon atmosphere at 90 °C for 5 h. After cooling, the product was extracted with ethyl acetate, combined organic extracts were washed with brine, dried over $MgSO_4$, and the solvents were evaporated under reduced pressure.

General Procedure IX: Sodium Borohydride Reduction. Ketone was dissolved in methanol (20 mL/400 mg of starting material), cooled to 0 °C (bath temperature), and sodium borohydride (1.1 equiv) was added. The mixture was stirred for 1 h at 0 °C, then warmed slowly to room temperature. The reaction was quenched with 5% aqueous HCl, the organic layer separated, and the aqueous fraction was extracted with ethyl acetate. The combined extracts were washed with saturated aqueous solution of sodium bicarbonate, dried with $MgSO_4$, and evaporated.

(2*R*,4a*S*,4b*S*,7*S*,8*S*,8a*S*,10a*R*)-7-(Methoxycarbonyl)-4a,7,8-trimethyltetradecahydrophenanthren-2-ylpyridinium Sulfate (1). Compound **1** was prepared according to general procedure I (sulfonation). Starting from compound **15** (104 mg, 0.34 mmol), compound **1** (55 mg, 35%) was obtained as a white solid: mp 168−169 °C (chloroform); $[\alpha]_D^{20}$ +10.9 (*c* 0.403, $CHCl_3$). ^{1}H NMR (400 MHz, CD_3OD): δ 0.71 (3H, d, *J* = 6.6, H_8-Me), 0.88 (3H, s, H_{4a}-18), 1.05 (3H, s, H_7-Me), 3.67 (3H, s, OCH_3), 4.47 (1H, tt, J_1 = 10.9, J_2 = 5.0, H-2), 8.02 (2H, m, H-2′ and H-4′, pyridinium), 8.49 (1H, t, *J* = 7.8, H-3′, pyridinium), 8.96−9.02 (2H, m, H-1′ and H-5′, pyridinium). ^{13}C NMR (101 MHz, CD_3OD): δ 179.30, 145.89 (C-1′, C-5′), 142.41, 127.33(C-2′, C-4′), 79.53, 51.85, 47.75, 42.37, 41.77, 39.62, 37.72, 37.09, 35.10, 34.73, 33.27, 27.91, 27.07, 25.55, 23.32, 20.06, 15.36, 14.64. IR spectrum ($CHCl_3$): 3140, 3100, 1490 (pyH); 1264, 1183, 1175, 1044, 954 (SO_3); 1720 (C═O); 1245, 1192 (C−O). MS: ESI *m*/*z* 387.2 (100%, M − pyH). HR-MS (ESI) *m*/*z*: for $C_{19}H_{31}O_6S$ [M − pyH] calcd, 387.18468; found, 387.18443.

4-(((2*R*,4a*S*,4b*S*,7*S*,8*S*,8a*S*,10a*R*)-7-(Methoxycarbonyl)-4a,7,8-trimethyltetradecahydrophenanthren-2-yl)oxy)-4-oxobutanoic Acid (2). Compound **2** was prepared according to general procedure II (synthesis of hemisuccinate ester). Starting from compound **15** (100 mg, 0.32 mmol), compound **2** (68 mg, 51%) was obtained as a white solid by column chromatography (10% acetone in petroleum ether): mp 145−147 °C (acetone/*n*-heptane); $[\alpha]_D^{20}$ +21.5 (*c* 0.21, $CHCl_3$). ^{1}H NMR (400 MHz, CD_3OD): δ 0.73 (3H, d, J, 6.7, H_8-Me), 0.90 (3H, s, H_{4a}-Me), 1.06 (3H, s, H_7-Me), 2.72−2.55 (4H, m, $OCCH_2CH_2CO$), 3.67 (3H, s, OCH_3), 4.70−4.81 (1H, m, H-2). ^{13}C NMR (101 MHz, CD_3OD): δ 179.30, 171.91, 74.93, 51.88, 47.77, 42.33, 41.58, 39.67, 37.74, 37.03, 34.87, 34.83, 32.11, 29.83, 29.47, 29.03, 27.06, 26.70, 25.51, 23.34, 20.09, 15.34, 14.63. IR spectrum ($CHCl_3$): 1724, 1718 (C═O); 1243, 1166 (COC); 3020, 1361 (CH_3); 2950 (CH_2). MS: ESI *m*/*z* 431.2 (100%, M + Na). HR-MS (ESI) *m*/*z*: for $C_{23}H_{36}O_6Na$ [M + Na] calcd, 431.2404; found, 431.2403.

(2*R*,4a*S*,4b*S*,7*S*,8*S*,8a*S*,10a*R*)-7-(Methoxymethyl)-4a,7,8-trimethyltetradecahydrophenanthren-2-ylpyridinium Sulfate (3). Compound **3** was prepared according general procedure I (sulfonation). Starting from compound **21** (78 mg, 0.26 mmol), compound **3** (40 mg, 33%) was obtained as a white solid: mp 159−161 °C (chloroform); $[\alpha]_D^{20}$ +4.0 (*c* 0.30, $CHCl_3$ + MeOH, 1.849:0.341). ^{1}H NMR (400 MHz, $CDCl_3$): δ 0.68 (3H, s, H_{4a}-Me), 0.75 (3H, d, *J* = 6.1, H_8-Me), 0.86 (3H, s, H_7-Me), 3.06 (2H, dd, J_1 = 112.6, J_2 = 9.1, CH_2O), 3.31 (3H, s, OCH_3), 4.46 (1H, tt, J_1 = 10.9, J_2 = 4.9, H-2), 8.01 (2H, m, H-2′ and H-4′, pyridinium), 8.49 (1H, t, *J* = 8.6, H-3′, pyridinium), 8.92−9.05 (2H, m, H-1′ and H-5′, pyridinium). ^{13}C NMR (101 MHz, $CDCl_3$): δ 145.84 (C-1′, C-5′), 142.41 (C-3′), 127.30 (C-2′, C-4′), 82.13, 79.89, 59.43, 41.84, 41.00, 39.82, 38.04, 37.70, 36.50, 35.10, 34.84, 33.25, 27.91, 27.31, 26.01, 23.43, 20.50, 15.95, 12.66. IR spectrum ($CHCl_3$): 2976, 2933 (CH_2OCH_3); 1263, 1255, 1183, 1044, 954 (SO_3). MS: ESI *m*/*z* 373.2 (100%, M − pyH). HR-MS (ESI) *m*/*z*: for $C_{19}H_{33}O_5S$ [M − pyH] calcd, 373.20542; found, 301.20542.

4-(((2*R*,4a*S*,4b*S*,7*S*,8*S*,8a*S*,10a*R*)-7-(Methoxymethyl)-4a,7,8-trimethyltetradecahydrophenanthren-2-yl)oxy)-4-oxobutanoic Acid (4). Compound **4** was prepared according to general procedure II (synthesis of hemisuccinate ester). Starting from compound **21** (70 mg, 0.24 mmol), compound **4** (78 mg, 83%) was obtained as a white solid by column chromatography (20% acetone in petroleum ether): mp 126−128 °C (acetone/*n*-heptane); $[\alpha]_D^{20}$ +6.5 (*c* 0.27, $CHCl_3$). ^{1}H NMR (400 MHz, $CDCl_3$): δ 0.68 (3H, s, H_{4a}-Me), 0.77 (3H, d, *J* = 6.1, H_8-Me), 0.88 (3H, s, H_7-Me), 2.51−2.76 (4H, m, $OCCH_2CH_2CO$), 3.08 (2H, dd, J_1 = 126.8, J_2 = 9.0, CH_2O), 3.33 (3H, s, OCH_3), 4.75 (1H, tt, J_1 = 11.3, J_2 = 4.8, H-2). ^{13}C NMR (101 MHz, $CDCl_3$) δ 177.20, 171.85, 81.97, 75.13, 59.44, 41.63, 40.80, 39.85, 38.03, 37.71, 36.45, 34.97, 34.85, 32.06, 29.45, 29.05, 27.29, 26.67, 25.97, 23.45, 20.55, 16.00, 12.63. IR spectrum ($CHCl_3$): 2935 (CH_2OCH_3); 1717 (C═O, COOH); 1100 (COC). MS: ESI *m*/*z* 393.3 (100%, M − 1). HR-MS (ESI) *m*/*z*: for $C_{23}H_{37}O_5$ [M − 1] calcd, 393.26465; found, 393.26433. For $C_{23}H_{38}O_5$ (394.3) calcd: 70.02%, C; 9.71% H. Found: 69.76%, C; 9.68%, H.

(2*R*,4a*S*,4b*S*,7*S*,8a*S*,10a*R*)-7-(Methoxycarbonyl)-4a,7-dimethyltetradecahydrophenanthren-2-yl Sulfate Pyridinium Salt (5). Compound **5** was prepared according general procedure I (sulfonation). Starting from compound **30** (100 mg, 0.34 mmol), compound **5** (72 mg, 47%) was obtained as a white solid: mp 115−118 °C (acetone/*n*-heptane); $[\alpha]_D^{20}$ +24.1 (*c* 0.23, $CHCl_3$). ^{1}H NMR (400 MHz, $CDCl_3$): δ 0.89 (3H, s, H_{4a}-Me), 1.17 (3H, s, H_7-Me), 3.65 (3H, s, OCH_3), 4.45 (1H, tt, J_1 = 11.0, J_2 = 5.0, H-2), 8.01 (2H, m, H-2′ and H-4′, pyridinium), 8.48 (1H, tt, J_1 = 7.9, J_2 = 1.5, H-3′, pyridinium), 8.99 (2H, dd, J_1 = 6.5, J_2 = 1.4, H-1′ and H-5′, pyridinium). ^{13}C NMR (101 MHz, $CDCl_3$): δ 179.39, 145.90 (C-1′, C-5′), 142.46 (C-3′), 127.33 (C-2′, C-4′), 79.55, 64.51, 51.87, 42.40, 42.33, 39.91, 34.83, 34.55, 34.48, 33.38, 31.84, 29.02, 28.01, 27.05, 23.38, 20.57, 20.29. IR spectrum ($CHCl_3$): 3140, 3099, 1490 (pyH); 1254, 1049, 957 (SO_3); 1435, 1380 (methyl); 1720 (C═O); 1245, 1192, 1013 (C−O). MS: ESI *m*/*z* 373.2 (100%, M − pyH). HR-MS (ESI) *m*/*z*: for $C_{18}H_{29}O_6S$ [M − pyH] calcd, 373.1690; found, 373.1688.

4-(((2*R*,4a*S*,4b*S*,7*S*,8a*S*,10a*R*)-7-(Methoxycarbonyl)-4a,7-dimethyltetradecahydrophenanthren-2-yl)oxy)-4-oxobutanoic Acid (6). Compound **6** was prepared according general procedure II (synthesis of hemisuccinate ester). Starting from compound **30** (60 mg, 0.20 mmol), compound **6** (42 mg, 52%) was obtained as a white solid by column chromatography (15% acetone in petroleum ether): mp 110−111 °C (acetone/*n*-heptane); $[\alpha]_D^{20}$ +23.3 (*c* 0.29, $CHCl_3$). ^{1}H NMR (400 MHz, $CDCl_3$): δ 0.91 (3H, s, H_{4a}-Me), 1.19 (3H, s, H_7-Me), 2.72−2.56 (4H, m, H-2′ and H-4′, succinate), 3.66 (3H, s, OCH_3), 4.755 (1H, tt, J_1 = 11.3, J_2 = 4.7, H-2). ^{13}C NMR (101 MHz, $CDCl_3$): δ 179.37, 176.38, 171.86, 75.02, 51.91, 42.42, 42.39, 42.15, 39.97, 34.70, 34.58, 34.48, 32.24, 31.89, 29.46, 29.02, 28.92, 27.06, 26.83, 23.42, 20.58, 20.36. IR spectrum ($CHCl_3$): 1718 (C═O); 2937 (OCH_3); 1242, 1126, 1102 (C−O). MS: ESI *m*/*z* 393.3 (100%, M − 1), 394.3 (25%, M). HR-MS (ESI) *m*/*z*: for $C_{22}H_{33}O_6$ [M − 1] calcd, 393.2283; found, 393.2283.

(2*R*,4a*S*,4b*S*,7*S*,8a*S*,10a*R*)-7-(Methoxymethyl)-4a,7-dimethyltetradecahydrophenanthren-2-ylpyridinium Sulfate (7). Compound 7 was prepared according general procedure I (sulfonation). Starting from compound **36** (98 mg, 0.35 mmol), compound 7 (105 mg, 68%) was obtained as a white solid: mp 132−134 °C (acetone/*n*-heptane); $[\alpha]_D^{20}$ +22.0 (*c* 0.26, $CHCl_3$). ^{1}H NMR (400 MHz, $CDCl_3$): δ 0.87 (3H, s, H_{4a}-Me), 0.88 (3H, s, H_7-Me), 2.99 (2H, s, CH_2O), 3.32 (3H, s, OCH_3), 4.46 (1H, tt, J_1 = 11.1, J_2 = 4.8, H-2), 8.00 (2H, m, H-2′ and H-4′, pyridinium), 8.47 (1H, tt, J_1 = 7.9, J_2 = 1.7, H-3′,

DOI: 10.1021/acs.jmedchem.6b00079
J. Med. Chem. 2016, 59, 4724−4739

PDF-XChange Editor
KOUPIT plnou verzi!
www.pdfxchange.cz

pyridinium), 8.92−9.06 (2H, m, H-1′ and H-5′, pyridinium). ^{13}C NMR (101 MHz, $CDCl_3$): δ 145.78 (C-1′, C-5′), 142.52 (C-3′), 127.27 (C-2′, C-4′), 85.23, 79.75, 59.53, 43.20, 42.47, 40.43, 35.22, 34.94, 34.91, 34.63, 33.39, 32.01, 29.34, 28.01, 27.17, 23.47, 20.79, 20.51. IR spectrum ($CHCl_3$): 3140, 3099, 1490, 1024 (pyH); 1262, 1254, 1173, 1047 (SO_3); 1388, 1381 (methyl); 1109, 1101 (COC). MS: ESI *m/z* 359.3 (100%, M − pyH). HR-MS (ESI) *m/z*: for $C_{18}H_{31}O_5S$ [M − pyH] calcd, 359.1898; found, 359.1895.

4-(((2*R*,4a*S*,4b*S*,7*S*,8a*S*,10a*R*)-7-(Methoxymethyl)-4a,7-dimethyltetradecahydrophenanthren-2-yl)oxy)-4-oxobutanoic Acid (8). Compound **8** was prepared according general procedure II (synthesis of hemisuccinate ester). Starting from compound **36** (60 mg, 0.21 mmol), compound **8** (41 mg, 50%) was obtained as a white solid by column chromatography (10% acetone in petroleum ether): mp 107−109 °C (acetone/*n*-heptane); $[\alpha]_D^{20}$ +38.8 (*c* 0.26, $CHCl_3$). ^{1}H NMR (400 MHz, $CDCl_3$): δ 0.88 (3H, s, H_{4a}-Me), 0.90 (3H, s, H_7-Me), 2.53−2.72 (4H, m, $OCCH_2CH_2CO$), 3.01 (2H, s, CH_2OH), 3.34 (3H, s, OCH_3), 4.69−4.81 (1H, m, H-2). ^{13}C NMR (101 MHz, $CDCl_3$): δ 177.12, 171.83, 85.10, 75.17, 59.55, 43.06, 42.26, 40.44, 35.24, 34.78 (2x), 34.68, 32.24, 32.04, 29.45, 29.33, 29.04, 27.17, 26.81, 23.50, 20.85, 20.55. IR spectrum ($CHCl_3$): 1726, 1717 (C═O); 1385 (methyl); 1169, 1101 (COC). MS: ESI *m/z* 403.2 (100%, M + Na). HR-MS (ESI) *m/z*: for $C_{22}H_{36}O_5Na$ [M + Na] calcd, 403.2455; found, 403.2455.

(2*R*,4a*S*,4b*S*,7*R*,8a*S*,10a*R*)-4a,7-Dimethyltetradecahydrophenanthren-2-ylpyridinium Sulfate (9). Compound **9** was prepared according general procedure I (sulfonation). Starting from compound **39a** (108 mg, 0.46 mmol), compound **9** (66 mg, 36%) was obtained as a white solid: mp 147−149 °C (chloroform); $[\alpha]_D^{20}$ +25.3 (*c* 0.25, $CHCl_3$). ^{1}H NMR (400 MHz, $CDCl_3$): δ 0.88 (3H, s, H_7-Me), 0.92 (3H, d, *J* = 7.2, H_{4a}-Me), 4.46 (1H, tt, J_1 = 11.3, J_2 = 4.8, H-2), 8.00 (2H, m, H-2′ and H-4′, pyridinium), 8.47 (1H, t, *J* = 8.6, H-3′, pyridinium), 8.95−9.01 (2H, m, H-1′ and H-5′, pyridinium). ^{13}C NMR (101 MHz, $CDCl_3$): δ 145.78 (C-1′, C-5′), 142.51 (C-3′), 127.26 (C-2′, C-4′), 79.87, 42.52, 41.06, 40.74, 34.81, 34.70, 33.45, 32.72, 30.89, 29.40, 28.05, 27.81, 27.20, 23.54, 19.33, 18.30. IR spectrum ($CHCl_3$): 3140, 3099, 1490, 826 (pyH); 1263, 1255, 1173, 1047, 953 (SO_3); 1380 (methyl). MS: ESI *m/z* 315.3 (100%, M − pyH). HR-MS (ESI) *m/z*: for $C_{16}H_{27}O_4S$ [M − pyH] calcd, 315.1636; found, 315.1634.

4-(((2*R*,4a*S*,4b*S*,7*R*,8a*S*,10a*R*)-4a,7-Dimethyltetradecahydrophenanthren-2-yl)oxy)-4-oxobutanoic Acid (10). Compound **10** was prepared according general procedure II (synthesis of hemisuccinate ester). Starting from compound **39a** (65 mg, 0.27 mmol), compound **10** (40 mg, 43%) was obtained as a white solid by column chromatography (10% acetone in petroleum ether): mp 119−121 °C (acetone/*n*-heptane); $[\alpha]_D^{20}$ +43.9 (*c* 0.27, $CHCl_3$). ^{1}H NMR (400 MHz, $CDCl_3$): δ 0.90 (3H, s, H_7-Me), 0.94 (3H, d, *J* = 7.2, H_{4a}-Me), 2.74−2.54 (4H, m, H-2′ and H-4′), 4.75 (1H, tt, J_1 = 11.4, J_2 = 4.7, H-2). ^{13}C NMR (101 MHz, $CDCl_3$): δ 171.26, 171.83, 75.29, 42.32, 40.99, 40.78, 34.84, 34.53, 32.67, 32.33, 30.92, 29.45, 29.40, 29.06, 27.80, 27.20, 26.89, 23.58, 19.36, 18.31. IR spectrum ($CHCl_3$): 1727, 1716 (C═O); 1280 (C−O, dimer); 1232, 1176 (COC). MS: ESI *m/z* 335.4 (100%, M − H), 336.4 (22%, M). HR-MS (ESI) *m/z*: for $C_{20}H_{31}O_4$ [M − H] calcd, 335.2228; found, 335.2228.

(3*R*,5*R*,8*R*,9*S*,10*S*,13*S*,14*S*)-10,13-Dimethyl-2,3,4,5,6,7,8,9,10,11,12,13,14,15-tetradecahydro-1*H*-cyclopenta[*a*]phenanthrene-3,17-diyl Diacetate (12). A solution of 3α-hydroxy-5β-androstan-17-one **11** (18 g, 62 mmol), isopropenyl acetate (110 mL), and 2% H_2SO_4 in isopropenyl acetate (6.5 mL) was boiled for 2 h with slow fractionation of 30 mL. Further isopropenyl acetate (110 mL) and 2% H_2SO_4 in isopropenyl acetate (6.5 mL) were added. Again, the reaction mixture was boiled for 2 h with slow fractionation of 110 mL. Then, the solution was allowed to attain room temperature and poured into a mixture of petroleum ether (780 mL) and benzene (780 mL). The mixture was filtered over the column of aluminum oxide, washing with petroleum ether/benzene (1:1), and solvents were evaporated. The product was purified by column chromatography (2% ethyl acetate in petroleum ether/benzene (1:1)), affording compound **12** (16.7 g, 72%): ^{1}H NMR (400 MHz, CD_3OD): δ 0.87 (3H, s, H-18), 0.95 (3H, s, H-19), 2.03 (3H, s, OAc), 2.15 (3H, s, OAc), 4.65−4.78 (1H, m, H-3), 5.45 (1H, s, H-16).

(1*S*,2*S*,4a*S*,4b*S*,7*R*,8a*R*,10a*R*)-Methyl 7-Acetoxy-2,4b-dimethyl-1-(2-oxoethyl)tetradecahydrophenanthrene-2-carboxylate (13). A stirred solution of enol acetate **12** (5.0 g, 13.35 mmol) in dichloromethane and glacial acetic acid (13 mL) at −70 °C was ozonized until the blue color persisted. Dimethyl sulfide (2 mL, 27.37 mmol) in small portions, glacial acetic acid (130 mL), and water (28 mL) were added, and the solution was stirred for 18 h at room temperature. The product was extracted with dichloromethane (3 × 40 mL), the combined organic extracts were washed with water, dried over $MgSO_4$, and the solvents were evaporated. The residue was dissolved in ether, cooled to 0 °C, and esterified with ethereal solution of diazomethane. Chromatography on a column of silica gel (10% ethyl acetate in petroleum ether) gave 4.45 g (88%) of compound **13**: mp 151−153 °C (acetone/*n*-heptane); $[\alpha]_D^{20}$ −9.6 (*c* 0.24, CH_3OH). ^{1}H NMR (400 MHz, CD_3OD): δ 0.89 (3H, s, H_2-Me), 1.11 (3H, s, H_{4b}-Me), 2.02 (3H, s, OAc), 3.65 (3H, s, OCH_3), 4.66−4.76 (1H, m, H-7), 9.67 (1H, s, CHO). ^{13}C NMR (101 MHz, CD_3OD): δ 201.97, 178.37, 170.76, 74.08, 52.12, 47.59, 46.71, 41.69, 41.46, 39.83, 37.80, 36.78, 34.88, 34.77, 32.10, 26.96, 26.72, 26.31, 23.33, 21.55, 19.83, 15.56. IR spectrum ($CHCl_3$): 1721 (C═O); 2828 (CHO); 1385, 1364, 1435 (CH_3); 1253 (COO). MS: ESI *m/z* 401.3 (100%, M + Na). HR-MS (ESI) *m/z*: for $C_{22}H_{34}O_5Na$ [M + Na] calcd, 401.2299; found, 401.2297.

(1*S*,2*S*,4a*S*,4b*S*,7*R*,8a*R*,10a*S*)-Methyl-7-acetoxy-1,2,4b-trimethyltetradecahydrophenanthrene 2-Carboxylate (14). Compound **14** was prepared according to general procedure III (Wilkinson's decarbonylation). Starting from compound **13** (1.33 g, 3.65 mmol), compound **14** (1.33 g, 69%) was obtained by column chromatography (3% acetone in petroleum ether): mp 55−57 °C (aqueous ethanol); $[\alpha]_D^{20}$ 19.3 (*c* 0.31, CH_3OH). ^{1}H NMR (400 MHz, CD_3OD): δ 0.72 (3H, d, *J* = 6.7, H_1-Me), 0.89 (3H, s, H_2-Me), 1.06 (3H, s, H_{4b}-Me), 2.03 (3H, s, OAc), 3.66 (3H, s, OCH_3), 4.66−4.76 (1H, m, H-7). ^{13}C NMR (101 MHz, CD_3OD): δ 179.21, 170.77, 74.35, 51.85, 47.76, 42.36, 41.56, 39.66, 37.74, 37.05, 34.86 (2xC), 32.19, 27.07, 26.75, 25.52, 23.36, 21.58, 20.09, 15.34, 14.64. IR spectrum ($CHCl_3$): 1721 (C═O); 1467, 1386, 1024 (acetate); 1364, 1160 ($COOCH_3$). MS: ESI *m/z* 373.2 (100%, M + Na). HR-MS (ESI) *m/z*: for $C_{21}H_{34}O_4Na$ [M + Na] calcd, 373.2349; found, 373.2348.

(1*S*,2*S*,4a*S*,4b*S*,7*R*,8a*R*,10a*S*)-Methyl 7-Hydroxy-1,2,4b-trimethyltetradecahydrophenanthrene-2-carboxylate (15). Compound **15** was prepared according to general procedure IV (hydrolysis with potassium hydroxide). Starting from compound **14** (100 mg, 0.29 mmol), compound **15** (83 mg, 94%) was obtained: mp 144−146 °C (ethyl acetate/*n*-heptane); $[\alpha]_D^{20}$ +6.2 (*c* 0.33, $CHCl_3$). ^{1}H NMR (400 MHz, CD_3OD): δ 0.73 (3H, d, *J* = 6.7, H_1-Me), 0.89 (3H, s, H_2-Me), 1.06 (3H, s, H_{4b}-Me), 3.67 (3H, s, OCH_3), 3.58−3.68 (1H, m, H-7). ^{13}C NMR (101 MHz, CD_3OD): δ 179.26, 71.92, 51.87, 47.78, 42.32, 41.78, 39.69, 37.81, 37.06, 36.43, 35.18, 34.86, 30.73, 27.25, 25.62, 23.41, 20.10, 15.38, 14.66. IR spectrum ($CHCl_3$): 3020, 2942 (CH_3); 1720 (C═O); 3609, 1054, 1033 (OH); 1243 (COC). MS: ESI *m/z* 331.3 (100%, M + Na). HR-MS (ESI) *m/z*: for $C_{19}H_{32}O_3Na$ [M + Na] calcd, 331.2244; found, 331.2243.

(2*R*,4a*S*,4b*S*,7*S*,8*S*,8a*S*,10a*R*)-7-(Hydroxymethyl)-4a,7,8-trimethyltetradecahydrophenanthren-2-ol (16). Compound **16** was prepared according to general procedure V (LAH reduction). Starting from compound **14** (1.00 g, 2.86 mmol), compound **16** (585 mg g, 73%) was obtained: mp 141−143.5 °C (acetone/*n*-heptane); $[\alpha]_D^{20}$ −3.4 (*c* 0.33, $CHCl_3$). ^{1}H NMR (400 MHz, CD_3OD): δ 0.69 (3H, s, H_7-Me), 0.78 (3H, d, *J* = 6.3, H_8-Me), 0.89 (3H, s, H_{4a}-19), 2.03 (3H, s, OAc), 3.35 (2H, dd, J_1 = 92.2, J_2 = 10.9), 3.56−3.66 (1H, m, H-2). ^{13}C NMR (100 MHz, CD_3OD): δ 72.01, 71.74, 41.80, 40.57, 39.96, 38.21, 38.15, 36.46, 35.80, 35.17, 34.98, 30.79, 27.46, 26.13, 23.53, 20.49, 15.69, 12.61. IR ($CHCl_3$): 3628, 3616 (OH); 1035 (C-OH); 1380 (CH_3); 2935, 2866 (CH_2). MS: ESI *m/z*: 303.3 (100%, M + Na). HR-MS (ESI) *m/z*: for $C_{18}H_{32}O_2Na$ [M + Na] calcd; 303.2295, found, 303.2295.

(4a*S*,4b*S*,7*S*,8*S*,8a*S*,10a*R*)-7-(Hydroxymethyl)-4a,7,8-trimethyldodecahydrophenanthren-2(3*H*)-one (17). Compound **17** was prepared according to general procedure VI (sodium hypochlorite

DOI: 10.1021/acs.jmedchem.6b00079
J. Med. Chem. 2016, 59, 4724−4739

PDF-XChange Editor
KOUPIT plnou verzi!
www.pdfxchange.cz

oxidation). Starting from compound **16** (585 mg, 2.09 mmol), compound **17** (412 mg, 71%) was obtained by column chromatography (4−10% acetone in petroleum ether) as an oily product: $[\alpha]_D^{20}$ −2.7 (*c* 0.29, $CHCl_3$). ^1H NMR (400 MHz, $CDCl_3$): δ 0.73 (3H, s, H_{4a}-Me), 0.82 (3H, d, J = 6.3, H_8-Me), 0.99 (3H, s, H_7-Me), 3.38 (2H, dd, J_1 = 101.4, J_2 = 10.9, CH_2OH). ^{13}C NMR (101 MHz, $CDCl_3$): δ 213.44, 71.47, 44.04, 42.38, 40.44, 40.22, 38.18, 37.87, 37.40, 36.89, 35.68, 35.34, 26.93, 25.51, 22.83, 20.80, 15.72, 12.56. IR spectrum ($CHCl_3$): 3630 (OH); 1032 (CCO); 1708 (C═O); 1383 (methyl); 2935, 2860 (CH_2). MS: ESI *m*/*z* 301.2 (100%, M + Na). HR-MS (ESI) *m*/*z*: for $C_{18}H_{30}O_2Na$ [M + Na] calcd, 301.21380; found, 301.21388.

((4a′*S*,4b′*S*,7′*S*,8′*S*,8a′*S*,10a′*R*)-4a′,7′,8′-Trimethyldodecahydro-1′*H*-spiro[[1,3]dioxolane-2,2′-phenanthren]-7′-yl)methanol (18). Compound **18** was prepared according to general procedure VII (cyclic ketal formation). Starting from compound **17** (550 mg, 1.98 mmol), compound **18** (542 mg, 85%) was obtained by column chromatography (10% ethyl acetate in petroleum ether with 1% of triethyl amine) as an oily product: $[\alpha]_D^{20}$ −2.7 (*c* 0.26, $CHCl_3$). ^1H NMR (400 MHz, $CDCl_3$): δ 0.70 (3H, s, H_{4a}-Me), 0.78 (3H, d, J = 6.3, H_8-Me), 0.92 (3H, s, H_7-Me), 3.35 (2H, dd, J_1 = 89, J_2 = 10.9, CH_2OH), 3.93 (4H, OCH_2CH_2O). ^{13}C NMR (101 MHz, $CDCl_3$): δ 110.20, 71.76, 64.37, 64.22, 40.60, 40.59, 39.28, 38.15, 38.00, 35.78, 35.66, 34.99, 34.00, 30.32, 27.02, 25.90, 23.27, 20.69, 15.69, 12.58. IR spectrum ($CHCl_3$): 3630 (OH); 1030 (COH); 2976, 2881, 1381 (methyl); 2928, 1471 (CH_2); 1471, 1094, 947 (OCH_2CH_2O). MS: CI *m*/*z* 321.2 (52%, M − H), 323.2 (54%, M + H). HR-MS (CI) *m*/*z*: for $C_{20}H_{33}O_3$ [M − H] calcd, 321.2433; found, 321.2430.

(4a*S*,4b*S*,7*S*,8*S*,8a*S*,10a*R*)-7-(Methoxymethyl)-4a,7,8-trimethyldodecahydrophenanthren-2(3*H*)-one (20). Compound **19** was prepared according to general procedure VIII (Williamson ether synthesis). Starting from compound **18** (430 mg, 1.33 mmol), compound **19** was prepared (400 mg). Then, the crude residue was dissolved in acetone (10 mL), and 5% aq HCl (150 μL) was added to the stirred solution. After 1 h of stirring at room temperature, the reaction mixture was quenched with saturated aqueous solution of sodium bicarbonate (10 mL) and the product was extracted with ethyl acetate. The combined organic fraction was washed with brine, dried over Na_2SO_4, and the solvents were evaporated affording compound **20** (322 mg, 83%, 2 steps) as an oily product: $[\alpha]_D^{20}$ −3.5 (*c* 0.37, $CHCl_3$/MeOH, 2.034:0.139). ^1H NMR (400 MHz, $CDCl_3$): δ 0.72 (3H, s, H_{4a}-Me), 0.80 (3H, d, J = 6.3, H_8-Me), 0.98 (3H, s, H_7-Me), 3.09 (2H, dd, J_1 = 129.6, J_2 = 9.1, CH_2O), 3.32 (3H, OCH_3). ^{13}C NMR (101 MHz, $CDCl_3$): δ 213.49, 81.78, 59.45, 44.12, 42.39, 40.75, 40.11, 37.76, 37.40, 36.94, 36.34, 35.32, 29.85, 26.94, 25.44, 22.80, 20.85, 15.99, 12.59. IR spectrum ($CHCl_3$): 1101 (COC); 1707 (C═O); 1382 (methyl); 2928 (CH_2). MS: CI *m*/*z* 293.2 (72%, M + H). HR-MS (CI) *m*/*z*: for $C_{19}H_{33}O_2$ [M + H] calcd, 293.2481; found, 293.2477.

(2*R*,4a*S*,4b*S*,7*S*,8*S*,8a*S*,10a*R*)-7-(Methoxymethyl)-4a,7,8-trimethyltetradecahydrophenanthren-2-ol (21). Compound **21** was prepared according to general procedure IX (sodium borohydride reduction). Starting from compound **20** (400 mg, 1.37 mmol), compound **21** (323 mg, 80%) was obtained by column chromatography (7% acetone in petroleum ether): mp 106−108 °C (acetone/*n*-heptane); $[\alpha]_D^{20}$ −9.2 (*c* 0.37, $CHCl_3$). ^1H NMR (400 MHz, $CDCl_3$): δ 0.69 (3H, s, H_{4a}-Me), 0.77 (3H, d, J = 6.4, H_8-Me), 0.88 (3H, s, H_7-Me), 3.07 (2H, dd, J_1 = 114.3, J_2 = 9.1, H-17), 3.32 (3H, OCH_3), 3.57−3.66 (1H, m, H-2). ^{13}C NMR (101 MHz, $CDCl_3$): δ 82.11, 72.04, 59.45, 41.85, 40.93, 39.88, 38.11, 37.71, 36.48, 36.46, 35.20, 34.96, 30.78, 27.48, 26.06, 23.52, 20.54, 15.96, 12.68. IR spectrum ($CHCl_3$): 3609 (OH); 2977 (CH_3); 1100 (COC). MS: ESI *m*/*z* 317.2 (100%, M + Na). HR-MS (ESI) *m*/*z*: for $C_{19}H_{34}O_2Na$ [M + Na] calcd, 317.24510; found, 317.24510.

(1*R*,2*S*,4a*S*,4b*S*,7*S*,8a*R*,10a*R*)-7-Hydroxy-2,4b-dimethyl-1-((*E*)-(3-oxoindolin-2-ylidene)methyl)tetradecahydrophenanthrene-2-carboxylic Acid (23). Solution of *o*-nitrobenzaldehyde (2.75 g) in methanol (25 mL) was added to a solution of 3β-hydroxy-5β-androstan-17-one (**22**) (5.0 g, 17.22 mmol) in 125 mL of 4% methanolic solution of potassium hydroxide. The reaction mixture was allowed to stand at room temperature for 18 h, and then a solution of potassium hydroxide (0.5 g) in methanol (1 mL) and solution of *o*-nitrobenzaldehyde (275 mg) in methanol (2.5 mL) were added. After 20 h the reaction mixture was concentrated ($^1/_3$ of the volume) and acidified with dilute hydrochloric acid (to pH ≈ 1). The resulting yellow precipitate was collected by filtration, washed with water, and dried affording compound **23** (6.1 g, 84%): mp 242−245 °C (methanol/water); $[\alpha]_D^{20}$ −182.2 (*c* 0.29, CH_3OH). ^1H NMR (400 MHz, CD_3OD): δ 0.98 (3H, s, H_{4b}-Me), 1.24 (3H, s, H_2-Me), 2.86 (1H, dd, J_1 = 11.4, J_2 = 10.0, H-1), 4.02−4.07 (1H, m, H-7), 5.81 (1H, d, J = 11.6, CH═C(CO−)NH), 6.79 (1H, t, J = 7.7), 6.93 (1H, d, J = 8.2), 7.41(1H, t, J = 7.7), 7.52 (1H, d, J = 7.7). ^{13}C NMR (101 MHz, CD_3OD): δ 187.72, 181.39, 155.99, 140.14, 137.88, 125.48, 121.86, 119.96, 117.67, 112.83, 67.68, 48.85, 48.09, 39.98, 38.12, 37.64, 37.60, 36.53, 34.23, 30.63, 28.55, 27.74, 27.64, 24.26, 21.01, 16.09. IR spectrum (KBr): 3445, 3343 (OH + NH); 1003 (C−OH); 2613 (OH, dimer); 1708 (C═O, dimer); 1693 (C═O, indolone); 1639 (C═C); 1613, 1486, 1468, 1448 (ring, indolone); 2976, 1383 (methyl). MS: ESI *m*/*z*: 446.3 (100%, M + Na), 424.3 (45%, M + H). HR-MS (ESI) *m*/*z*: for $C_{26}H_{33}O_4NNa$ [M + Na] calcd, 446.2302; found, 446.2301.

(1*R*,2*S*,4a*S*,4b*S*,7*S*,8a*R*,10a*R*)-Methyl 7-Hydroxy-2,4b-dimethyl-1-((*E*)-(3-oxoindolin-2-ylidene)methyl)tetradecahydrophenanthrene-2-carboxylate (24). A freshly prepared ethereal diazomethane was added to a suspension of acid **23** (5 g, 11.80 mmol) in ether while stirring at 0 °C. The progress of the reaction was checked by TLC. Then, the excess of diazomethane was evaporated affording compound **24** (5.1 g, 98%): mp 143−145 °C (methanol); $[\alpha]_D^{20}$ −208.1 (*c* 0.26, $CHCl_3$). ^1H NMR (400 MHz, $CDCl_3$): δ 0.97 (3H, s, H_{4b}-Me), 1.24 (3H, s, H_2-Me), 2.72 (1H, t, J = 10.7, H-1), 3.56 (1H, s, OCH_3), 4.12−4.14 (1H, m, H-7), 5.77 (1H, d, J = 11.1, CH═C(CO−)NH), 6.87 (1H, t, J = 7.7), 6.93 (1H, d, J = 8.2), 7.42 (1H, t, J = 7.7), 7.66 (1H, d, J = 7.7). ^{13}C NMR (101 MHz, $CDCl_3$): δ 185.93, 179.78, 154.04, 138.80, 136.25, 125.06, 122.45, 119.89, 116.52, 112.22, 67.03, 52.44 (OCH_3), 47.65, 47.54, 38.67, 37.81, 36.59, 36.33, 35.60, 33.58, 29.64, 28.00, 26.94, 26.51, 23.85, 19.91, 16.00. IR spectrum ($CHCl_3$): 3616 (OH); 1003 (COH); 1716 (C═O); 1249, 1032 (C−O); 1701 (C═O, indolone); 1644 (C═C); 1615, 1485, 1470, 1448 (ring, indolone); 2979, 1435, 1384 (methyl). MS: ESI *m*/*z* 460.4 (100%, M + Na), 438.4 (52%, M + H). HR-MS (ESI) *m*/*z*: for $C_{27}H_{36}O_4N$ [M + H] calcd, 438.2639; found, 438.2639.

(1*R*,2*S*,4a*S*,4b*S*,7*S*,8a*R*,10a*R*)-Methyl 7-Acetoxy-2,4b-dimethyl-1-((*E*)-(3-oxoindolin-2-ylidene)methyl)tetradecahydrophenanthrene-2-carboxylate (25). Acetic anhydride (46 mL) was added dropwise to a solution of methyl ester **24** (7.2 g, 16.45 mmol) and 4-(dimethylamino)pyridine (200 mg, 1.64 mmol) in pyridine (50 mL) at 0 °C while stirring. The reaction mixture was allowed to attain room temperature. After 2 h, excess of reagent was quenched with small portion of water (5 mL). The mixture was poured into 5% aqueous solution of HCl (150 mL) and extracted with ethyl acetate (3 × 50 mL). The combined organic extracts were washed with water, saturated aqueous solution of sodium bicarbonate and brine, dried over $MgSO_4$, and the solvents were evaporated affording compound **25** (7.0 g, 89%): mp 217−219 °C (methanol); $[\alpha]_D^{20}$ −221.1 (*c* 0.27, $CHCl_3$). ^1H NMR (400 MHz, $CDCl_3$): δ 0.98 (3H, s, H_{4b}-Me), 1.24 (3H, s, H_2-Me), 2.04 (3H, s, OAc), 2.73 (1H, t, J = 10.7, H-1), 3.56 (3H, s, OCH_3), 5.05−5.11 (1H, m, H-7), 5.76 (1H, d, J = 11.2, CH═C(CO−)NH), 6.87 (1H, t, J = 7.7), 6.93 (1H, d, J = 8.2), 7.42 (1H, t, J = 7.7), 7.65 (1H, d, J = 7.7). ^{13}C NMR (101 MHz, $CDCl_3$): δ 185.92, 179.66, 170.81, 154.04, 138.83, 136.28, 125.04, 122.43, 119.90, 116.31, 112.23, 70.55, 52.44, 47.61, 38.82, 47.46, 37.74, 37.14, 36.60, 35.35, 30.63, 30.46, 26.82, 26.36, 25.18, 23.80, 21.62, 19.90, 16.00. IR spectrum ($CHCl_3$): 1727 (C═O, OAc); 1261 (C−O, OAc); 1367 (CH_3, OAc); 1717 (C═O, COOMe); 1249, 1025 (C−O, COOMe); 1435 (CH_3, COOMe); 1702 (C═O, indolone); 1645 (C═C); 1615, 1485, 1470, 1448 (ring, indolone); 2979, 1385, 1379 (methyl). MS: ESI *m*/*z* 502.4 (100%, M + Na), 480.4 (30%, M + H). HR-MS (ESI) *m*/*z*: for $C_{29}H_{38}O_5$ [M + H] calcd, 480.2745; found, 480.2746.

(1*S*,2*S*,4a*S*,4b*S*,7*S*,8a*R*,10a*R*)-Methyl 7-Acetoxy-1-formyl-2,4b-dimethyltetradecahydrophenanthrene-2-carboxylate (26). A solution of **25** (7.0 g, 14.60 mmol) in dichloromethane (120 mL) and glacial acetic acid (15 mL) was ozonized at −70 °C until the blue color persisted. Then, dimethyl sulfide (3.4 mL) was added in

DOI: 10.1021/acs.jmedchem.6b00079
J. Med. Chem. 2016, 59, 4724−4739

PDF-XChange Editor
KOUPIT plnou verzi!
www.pdfxchange.cz

small portions and the reaction mixture was stirred at room temperature for 1 h. Solvents were evaporated, the product was extracted with chloroform (3 × 60 mL), combined organic extracts were washed with water, dried over $MgSO_4$, and solvents were evaporated. The residue was purified by column chromatography on silica gel (6% acetone in petroleum ether), affording compound **26** (4.27 g, 80%). The structure of the compound was confirmed by NMR spectra, and then it was directly used into the next step: ^{1}H NMR (400 MHz, $CDCl_3$): δ 0.99 (3H, s, H_{4b}-Me), 1.24 (3H, s, H_2-Me), 2.04 (3H, s, OAc), 2.62 (1H, dd, J_1 = 11.2, J_2 = 3.0, H-14), 3.69 (3H, s, OCH_3), 5.05−5.11 (1H, m, H-7), 9.72 (1H, d, J = 3.0, CHO). ^{13}C NMR (101 MHz, $CDCl_3$): δ 204.77, 177.45, 170.75, 70.45, 60.18, 52.32, 38.45, 45.24, 36.97, 36.85, 35.27, 32.41, 30.58, 30.51, 26.33, 26.26, 25.10, 23.71, 21.61, 19.73, 16.89.

(2*S*,4a*S*,4b*S*,7*S*,8a*R*,10a*S*)-Methyl 7-Acetoxy-2,4b-dimethyltetradecahydrophenanthrene-2-carboxylate (27). Compound **27** was prepared according to general procedure III (Wilkinson's decarbonylation). Starting from compound **26** (2 g, 5.49 mmol), compound **27** (1.31 g, 71%) was obtained by column chromatography (3% acetone in petroleum ether) as an oily product: $[\alpha]_D^{20}$ +14.6 (c 0.31, $CHCl_3$). ^{1}H NMR (400 MHz, $CDCl_3$): δ 0.95 (3H, s, H_{4b}-Me), 1.19 (3H, s, H_2-Me), 2.05 (3H, s, OAc), 3.66 (3H, s, OCH_3), 5.03−5.1 (1H, m, H-7). ^{13}C NMR (101 MHz, $CDCl_3$): δ 179.37, 170.84, 70.79, 51.89, 42.43, 39.41, 37.56, 34.97, 34.49, 31.73, 30.65, 30.32, 28.82, 26.53, 25.21, 23.93, 21.65, 20.57, 20.51. IR spectrum ($CHCl_3$): 1722 (C═O); 2975, 2941, 1491, 1378 (methyl); 1262, 1243, 1025 (C-O). MS: ESI m/z 359.2 (100%, M + Na). HR-MS (ESI) m/z: for $C_{20}H_{32}O_4Na$ [M + Na] calcd, 359.2193; found, 359.2191.

(2*S*,4a*S*,4b*S*,7*S*,8a*R*,10a*S*)-Methyl 7-Hydroxy-2,4b-dimethyltetradecahydrophenanthrene-2-carboxylate (28). Compound **28** was prepared according general procedure IV (hydrolysis with potassium hydroxide). Starting from compound **27** (1.7 g, 5.1 mmol), compound **28** (1.24 g, 83%) was obtained as an oily product: $[\alpha]_D^{20}$ +13.5 (c 0.47, $CHCl_3$). ^{1}H NMR (400 MHz, $CDCl_3$): δ 0.94 (3H, s, H_{4b}-Me), 1.19 (3H, s, H_2-Me), 3.66 (3H, s, OCH_3), 4.07−4.15 (1H, m, H-7). ^{13}C NMR (101 MHz, $CDCl_3$): δ 179.45, 67.19, 51.87, 42.49, 39.26, 36.76, 35.22, 34.53, 33.54, 31.71, 29.50, 28.96, 28.06, 26.68, 23.97, 20.57, 20.51. IR spectrum ($CHCl_3$): 1719 (C═O); 1381 (methyl); 1245, 1033 (C-O). MS: ESI m/z 317.2 (100%, M + Na). HR-MS (ESI) m/z: for $C_{18}H_{30}O_3Na$ [M + Na] calcd, 317.2087; found, 317.2087.

(2*S*,4a*S*,4b*S*,8a*R*,10a*S*)-Methyl 2,4b-Dimethyl-7-oxotetradecahydrophenanthrene-2-carboxylate (29). Jones reagent was added to a solution of compound **28** (300 mg, 1.02 mmol) in acetone (5 mL). After stirring for 10 min at room temperature, the excess of reagent was decomposed with methanol (2 mL). Then, the reaction mixture was diluted with saturated aqueous solution of sodium bicarbonate and extracted with ethyl acetate (3 × 15 mL). Combined organic extracts were again washed with saturated aqueous solution of sodium bicarbonate, water, dried over Na_2SO_4, and evaporated affording compound **29** (250 mg, 84%): $[\alpha]_D^{20}$ +22.9 (c 0.38, $CHCl_3$). ^{1}H NMR (400 MHz, $CDCl_3$): δ 1.00 (3H, s, H_{4b}-Me), 1.22 (3H, s, H_7-Me), 3.66 (3H, s, OCH_3). ^{13}C NMR (101 MHz, $CDCl_3$): δ 213.04, 179.09, 51.93, 44.51, 42.38, 42.24, 40.24, 37.38, 36.61, 35.02, 34.38, 31.58, 29.83, 28.38, 26.66, 22.75, 20.60, 20.55. IR spectrum ($CHCl_3$): 1720, 1711 (C═O); 2980, 2934, 1465, 1435, 1383 (methyl); 1244, 1124 (C−O). MS: ESI m/z 315.2 (100%, M + Na). HR-MS (ESI) m/z: for $C_{18}H_{28}O_3Na$ [M + Na] calcd, 315.1931; found, 315.1929.

(2*S*,4a*S*,4b*S*,7*R*,8a*R*,10a*S*)-Methyl 7-Hydroxy-2,4b-dimethyltetradecahydrophenanthrene-2-carboxylate (30). A solution of compound **29** (100 mg, 0.34 mmol) in THF (10 mL) was cooled to −40 °C, and then lithium tri-*tert*-butoxyaluminum hydride (104 mg, 0.41 mmol) was added portionwise while stirring. After 2 h, the reaction mixture was allowed to attain room temperature and then quenched with 5% aqueous solution of HCl (20 mL). The product was extracted with $CHCl_3$ (3 × 15 mL), washed with saturated aqueous solution of sodium bicarbonate, brine, and dried over Na_2SO_4. Evaporation of solvents followed by chromatography (6% acetone in petroleum ether) gave compound **30** (71 mg, 71%) as an oily product: $[\alpha]_D^{20}$ +21.6 (c 0.19, $CHCl_3$). ^{1}H NMR (400 MHz, $CDCl_3$): δ 0.90 (3H, s, H_{4b}-Me), 1.18 (3H, s, H_2-Me), 3.66 (3H, s, OCH_3), 3.58−3.65 (1H, m, H-7). ^{13}C NMR (101 MHz, $CDCl_3$): δ 179.37, 71.94, 51.88, 42.41, 42.39, 42.33, 39.98, 36.52, 34.91, 34.66, 34.48, 31.91, 30.82, 29.10, 27.22, 23.46, 20.59, 20.33. IR spectrum ($CHCl_3$): 3608 (OH); 192, 1126, 1036, 1022 (C−O); 1720 (C═O); 2976, 2936, 1435, 1389 (methyl); 2936, 2865 (CH_2). MS: ESI m/z 317.2 (100%, M + Na). HR-MS (ESI) m/z: for $C_{18}H_{30}O_3Na$ [M + Na] calcd, 317.2087; found, 317.2088.

(2*S*,4a*S*,4b*S*,7*S*,8a*S*,10a*R*)-7-(Hydroxymethyl)-4a,7-dimethyltetradecahydrophenanthren-2-ol (31). Compound **31** was prepared according to general procedure V (LAH reduction). Starting from compound **27** (1.25 g, 3.71 mmol), compound **31** (905 mg g, 92%) was obtained: mp 139−140 °C (ethyl acetate/*n*-heptane); $[\alpha]_D^{20}$ +13.1 (c 0.29, $CHCl_3$). ^{1}H NMR (400 MHz, $CDCl_3$): δ 0.89 (3H, s, H_{4a}-Me), 0.95 (3H, s, H_7-Me), 3.24−3.30 (2H, m, CH_2OH), 4.08−4.14 (1H, m, H-2). ^{13}C NMR (101 MHz, $CDCl_3$): δ 74.89, 67.29, 42.71, 39.88, 39.08, 35.85, 35.34, 34.37, 33.59, 31.92, 29.62, 29.34, 28.10, 26.79, 24.09, 20.74, 20.32. IR spectrum ($CHCl_3$): 3630, 3618 (OH); 2936, 2863 (CH_2); 1031, 998 (C−OH). MS: ESI m/z 289.2 (100%, M + Na). HR-MS (CI) m/z: for $C_{17}H_{29}O_2$ [M − H] calcd, 265.2168; found, 265.2170.

(4a*S*,4b*S*,7*S*,8a*S*,10a*R*)-7-(Hydroxymethyl)-4a,7-dimethyldodecahydrophenanthren-2(3*H*)-one (32). Compound **32** was prepared according to general procedure VI (sodium hypochlorite oxidation). Starting from compound **31** (80 mg, 0.30 mmol), compound **32** (48 mg, 60%) was obtained by column chromatography (4−10% acetone in petroleum ether) as an oily product: $[\alpha]_D^{20}$ +26.1 (c 0.38, $CHCl_3$). ^{1}H NMR (400 MHz, $CDCl_3$): δ 0.92 (3H, s, H_{4a}-Me), 1.01 (3H, s, H_7-Me), 3.24−3.34 (2H, m, CH_2OH). ^{13}C NMR (101 MHz, $CDCl_3$): δ 213.36, 74.67, 44.65, 42.48, 42.47, 40.85, 37.42, 36.74, 35.86, 35.14, 34.24, 31.79, 28.77, 26.76, 22.85, 20.84, 20.28. IR spectrum ($CHCl_3$): 3630 (OH); 1034 (CCO); 1705 (C═O); 1383 (methyl); 2931, 2867 (CH_2). MS: ESI m/z 287.2 (100%, M + Na). HR-MS (ESI) m/z: for $C_{17}H_{28}O_2Na$ [M + Na] calcd, 287.1982; found, 287.1981.

((4a′*S*,4b′*S*,7′*S*,8a′*S*,10a′*R*)-4a′,7′-Dimethyldodecahydro-1′*H*-spiro[[1,3]dioxolane-2,2′-phenanthren]-7′-yl)methanol (33). Compound **33** was prepared according to general procedure VII (cyclic ketal formation). Starting from compound **32** (350 mg, 1.32 mmol), compound **33** (336 mg, 82%) was obtained by column chromatography (10% ethyl acetate in petroleum ether with 1% of triethyl amine) as an oily product: $[\alpha]_D^{20}$ +19.5 (c 0.11, $CHCl_3$). ^{1}H NMR (400 MHz, $CDCl_3$): δ 0.89 (3H, s, $H_{4a'}$-Me), 0.93 (3H, s, $H_{7'}$-Me), 3.26 (2H, s, CH_2OH), 3.93 (4H, s, OCH_2CH_2O). ^{13}C NMR (101 MHz, $CDCl_3$): δ 110.20, 74.94, 64.39, 64.22, 42.70, 41.22, 39.96, 35.82, 35.75, 34.77, 34.39, 33.86, 31.90, 30.37, 29.23, 26.86, 23.30, 20.74, 20.27. IR spectrum ($CHCl_3$): 3630, 3475 (OH); 1183, 1093, 1068, 947 (COCOC); 1382, 1364 (methyl); 1034 (CCO). MS: ESI m/z 331.3 (100%, M + Na). HR-MS (ESI) m/z: for $C_{19}H_{32}O_3Na$ [M + Na] calcd, 331.2244; found, 331.2246.

(4a′*S*,4b′*S*,7′*S*,8a′*S*,10a′*R*)-7′-(Methoxymethyl)-4a′,7′-dimethyldodecahydro-1′*H*-spiro[[1,3]dioxolane-2,2′-phenanthrene] (34). Compound **34** was prepared according to general procedure VIII (Williamson ether synthesis). Starting from compound **33** (250 mg, 0.81 mmol), compound **34** (240 mg, 92%) was prepared as an oily material: $[\alpha]_D^{20}$ +15.9 (c 0.41, $CHCl_3$). ^{1}H NMR (400 MHz, $CDCl_3$): δ 0.89 (3H, s, $H_{4a'}$-Me), 0.92 (3H, s, $H_{7'}$-Me), 2.99 (2H, s, CH_2O), 3.33 (3H, s, OCH_3), 3.93 (4H, m, OCH_2CH_2O). ^{13}C NMR (101 MHz, $CDCl_3$): δ 110.24, 85.24, 64.37, 64.21, 59.54, 43.20, 41.25, 39.85, 35.75, 35.23, 34.91, 34.76, 33.87, 31.87, 30.36, 29.19, 26.89, 23.30, 20.81, 20.73. IR spectrum ($CHCl_3$): 1186, 1094, 1068, 947 (COCOC); 2832, 1438, 1387, 1381, 1366 (methyl); 1102 (COC); 2928, 1449 (CH_2). MS: ESI m/z 345.3 (55%, M + Na). HR-MS (ESI) m/z: for $C_{20}H_{35}O_3$ [M + H] calcd, 323.2581; found, 323.2580.

(4a*S*,4b*S*,7*S*,8a*S*,10a*R*)-7-(Methoxymethyl)-4a,7-dimethyldodecahydrophenanthren-2(3*H*)-one (35). Cyclic ketal **34** (145 mg, 0.45 mmol) was dissolved in acetone (2.5 mL), and 5% aqueous solution of HCl (50 μL) was added to the stirred solution. After 1 h of stirring at room temperature, the reaction mixture was quenched with saturated aqueous solution of sodium bicarbonate (10 mL), and the product was extracted with ethyl acetate (3 × 5 mL). Combined organic fraction was washed with brine, dried over Na_2SO_4, and the solvents were evaporated affording compound **35** (120 mg, 96%) as an oily product: $[\alpha]_D^{20}$ + 24.8 (c 0.42, $CHCl_3$). ^{1}H NMR (400 MHz, $CDCl_3$): δ 0.91 (3H, s, H_{4a}-Me),

DOI: 10.1021/acs.jmedchem.6b00079
J. Med. Chem. 2016, 59, 4724−4739

PDF-XChange Editor
KOUPIT plnou verzi!
www.pdfxchange.cz

1.00 (3H, s, H_7-Me), 3.02 (2H, s, CH_2OH), 3.34 (3H, s, OCH_3). ^{13}C NMR (101 MHz, $CDCl_3$): δ 213.45, 84.91, 59.55, 46.05, 42.93, 42.49, 40.71, 37.43, 36.77, 35.27, 35.13, 34.70, 31.77, 28.72, 26.79, 22.85, 20.85, 20.83. IR spectrum ($CHCl_3$): 1706 (C═O); 1102 (COC); 1383 (methyl); 2931, 2866 (CH_2). MS: ESI m/z 301.3 (100%, M + Na), 279.3 (20%, M + H). HR-MS (ESI) m/z: for $C_{18}H_{30}O_2Na$ [M + Na] calcd, 301.2138; found, 301.2138.

(2*R*,4a*S*,4b*S*,7*S*,8a*S*,10a*R*)-7-(Methoxymethyl)-4a,7-dimethyltetradecahydrophenanthren-2-ol (36). Compound **36** was prepared according to general procedure IX (sodium borohydride reduction). Starting from compound **35** (40 mg, 0.14 mmol), compound **36** (28 mg, 70%) was obtained by column chromatography (10% acetone in petroleum ether) as an oily product: $[\alpha]_D^{20}$ +19.7 (*c* 0.44, $CHCl_3$). ^1H NMR (400 MHz, $CDCl_3$): δ 0.88 (3H, s, H_{4a}-Me), 0.89 (3H, s, H_7-Me), 3.00 (2H, s, CH_2OH), 3.33 (3H, s, OCH_3), 3.58−3.67 (1H, m, H-2). ^{13}C NMR (101 MHz, $CDCl_3$): δ 85.22, 72.05, 59.55, 43.15, 42.44, 40.48, 36.53, 35.21, 35.00, 34.88, 34.73, 32.06, 30.82, 29.40, 27.32, 23.54, 20.79, 20.52. IR spectrum ($CHCl_3$): 3609, 3451 (OH); 1036 (C-OH); 2956, 2865, 1388, 1380 (methyl); 1102 (COC). MS: ESI m/z 303.4 (100%, M + Na). HR-MS (ESI) m/z: for $C_{18}H_{32}O_2Na$ [M + Na] calcd, 303.2295; found, 303.2295.

(2*S*,4a*S*,4b*S*,8a*R*,10a*S*)-2,4b-Dimethyl-7-oxotetradecahydrophenanthrene-2-carbaldehyde (37). Anhydrous sodium acetate (158 mg, 1.93 mmol) and pyridinium chlorochromate (826 mg, 3.86 mmol) were added to a solution of the **31** (320 mg, 1.20 mmol) in dichloromethane (20 mL). After stirring for 2 h at room temperature under inert atmosphere, the reaction mixture was diluted with ethyl acetate (60 mL), filtered through a column of alumina (12 g) and the product was eluted with ethyl acetate (3 × 10 mL). Collected filtrate was evaporated yielding 280 mg (89%) of aldehyde **37** which was used in the next reaction step without further purification: ^1H NMR (400 MHz, $CDCl_3$): δ 1.02 (3H, s, H_{4a}-Me), 1.12 (3H, s, H_7-Me), 9.41 (1H, s, CHO). ^{13}C NMR (101 MHz, $CDCl_3$) δ 212.89, 206.05, 44.45, 42.37, 40.38, 39.05, 37.35, 36.57, 35.11, 31.29, 31.17, 29.85, 28.45, 26.60, 22.81, 20.02, 17.58.

(2*R*,4a*S*,4b*S*,7*R*,8a*S*,10a*R*)-4a,7-Dimethyltetradecahydrophenanthren-2-ol (39a). Compound **39a** was prepared according general procedure III (Wilkinson's decarbonylation). Starting from compound **37** (280 mg, 1.07 mmol), inseparable mixture **38** of saturated derivative and two olefins (210 mg, 91.1:4.3:4.6 according to ^1H NMR) were obtained. The mixture was dissolved in THF (18 mL) and cooled to −40 °C. Then, lithium tri-*tert*-butoxyaluminum hydride (210 mg, 0.83 mmol) was added portionwise. After 2 h, the reaction mixture was allowed to attain room temperature and the reaction was quenched with 5% aqueous solution of HCl (20 mL). The products were extracted with $CHCl_3$ (3 × 15 mL), washed with saturated aqueous solution of sodium bicarbonate, brine, and dried over Na_2SO_4. Evaporation of the solvents afforded a mixture of hydroxy derivatives. The crude residue was dissolved in dichloromethane (15 mL), and a mixture of sodium acetate (66 mg, 0.81 mmol), water (0.6 mL), and peracetic acid (9% solution, 2.4 mL) was added. After stirring for 2 h at room temperature, sodium sulfite (5 mL) was added. The products were extracted with $CHCl_3$ (3 × 15 mL), combined organic extracts were washed with water, dried over $MgSO_4$, and solvents were evaporated. Purification by column chromatography (5% acetone in petroleum ether) afforded white waxy solid **39a** (90 mg, 36%, 3 steps): $[\alpha]_D^{20}$ +24.0 (*c* 0.30, $CHCl_3$). ^1H NMR (400 MHz, $CDCl_3$): δ 0.79 (3H, s, H_7-Me), 0.84 (3H, d, J = 7.3, H_{4a}-18), 3.53 (1H, tt, J_1 = 11.1, J_2 = 4.7, H-2). ^{13}C NMR (101 MHz, $CDCl_3$): δ 72.11, 42.49, 41.02, 40.80, 36.58, 34.86, 34.81, 32.70, 30.95, 30.87, 29.48, 27.81, 27.37, 23.62, 19.35, 18.31. IR spectrum ($CHCl_3$): 3608 (OH); 2958, 2866 (methyl); 1038, 1029 (C-OH). MS: CI m/z 236.2 (8%, M), 235.2 (15%, M − H). HR-MS (CI) m/z: for $C_{16}H_{27}O$ [M − H] calcd, 235.2062; found, 235.2070.

■ ASSOCIATED CONTENT

Supporting Information

The Supporting Information is available free of charge on the ACS Publications website at DOI: 10.1021/acs.jmedchem.6b00079.

Correlation between the experimental ΔG_{exp} values and ΔG_{solv} (transfer from *n*-octanol to water for neutral systems) and log *P* and log *D* values for compounds **1**−**10** (PDF)

Molecular formula strings (CSV)

■ AUTHOR INFORMATION

Corresponding Author

*Phone: +420-220-183-273. Fax: +420-220-183-578. E-mail: kudova@uochb.cas.cz.

Author Contributions

‖The computational analysis was done by M.N.

Notes

The authors declare no competing financial interest.

■ ACKNOWLEDGMENTS

This work was supported by Grant TE01020028 Center for Development of Original Drugs from the Technology Agency of the Czech Republic, Grant 303/12/1464 from the Grant Agency of the Czech Republic, Research Project of the RVO 67985823, RVO 61388963, and LQ1604 NPU II provided by MEYS and CZ.1.05/1.1.00/02.0109 BIOCEV provided by ERDF and MEYS. The Czech Science Foundation [Grant P208/12/G016] supported the computational study by M.N. We thank M. Sedlackova and D. Hybsova for their excellent technical assistance. The authors thank Dr. Laurel McGrane for language corrections.

■ ABBREVIATIONS USED

NMDA, *N*-methyl-D-aspartate; TLC, thin layer chromatography

■ REFERENCES

(1) Citri, A.; Malenka, R. C. Synaptic plasticity: multiple forms, functions, and mechanisms. *Neuropsychopharmacology* **2008**, *33*, 18−41.

(2) Hynd, M. R.; Scott, H. L.; Dodd, P. R. Glutamate-mediated excitotoxicity and neurodegeneration in Alzheimer's disease. *Neurochem. Int.* **2004**, *45*, 583−595.

(3) Dong, X.; Wang, Y.; Qin, Z. Molecular mechanism of excitotoxicity and their relevance to pathogenesis of neurodegenerative disease. *Acta Pharmacol. Sin.* **2009**, *30*, 379−387.

(4) Lai, T. W.; Zhang, S.; Wang, Y. T. Excitotoxicity and stroke: Identifyion novel targets for neuroprotection. *Prog. Neurobiol.* **2014**, *115*, 157−188.

(5) Rambousek, L.; Bubenikova-Valesova, V.; Kacer, P.; Syslova, K.; Kenney, J.; Holubova, K.; Najmanova, V.; Zach, P.; Svoboda, J.; Stuchlik, A.; Chodounska, H.; Kapras, V.; Adamusova, E.; Borovska, J.; Vyklicky, L.; Vales, K. Cellular and behavioural effects of a new steroidal inhibitor of the N-methyl-D-aspartate receptor 3α5β-pregnanolone glutamate. *Neuropharmacology* **2011**, *61*, 61−68.

(6) Kleteckova, L.; Tsenov, G.; Kubova, H.; Stuchlik, A.; Vales, K. Neuroprotective Effect of the 3α5β-pregnanolone glutamate treatment in the model of focal cerebral ischemia in immature rats. *Neurosci. Lett.* **2014**, *564*, 11−15.

(7) Holubova, K.; Nekovarova, T.; Pistovcakova, J.; Sulcova, A.; Stuchlik, A.; Vales, K. Pregnanolone glutamate, a novel use-dependent NMDA receptor inhibitor, exerts antidepressant-like properties in animal models. *Front. Behav. Neurosci.* **2014**, *8*, 130.

(8) Vyklicky, V.; Smejkalova, T.; Krausova, B.; Balik, A.; Korinek, M.; Borovska, J.; Horak, M.; Chvojkova, M.; Kleteckova, L.; Vales, K.; Cerny, J.; Nekardova, M.; Chodounska, H.; Kudova, E.; Vyklicky, L. Preferential inhibition of tonically over phasically activated NMDA receptors by pregnane derivatives. *J. Neurosci.* **2016**, *36*, 2161−2175.

(9) Vyklicky, V.; Krausova, B.; Cerny, J.; Balik, A.; Zapotocky, M.; Novotny, M.; Lichnerova, K.; Smejkalova, T.; Kaniakova, M.; Korinek, M.; Petrovic, M.; Kacer, P.; Horak, M.; Chodounska, H.; Vyklicky, L.

DOI: 10.1021/acs.jmedchem.6b00079
J. Med. Chem. 2016, 59, 4724−4739

PDF-XChange Editor
KOUPIT plnou verzi!
www.pdfxchange.cz

Block of NMDA receptor channels by endogeneous neurosteroids: implications for the agonist induced conformational states of the channel vestibule. *Sci. Rep.* **2015**, *5*, 10935.
(10) Kudova, E.; Chodounska, H.; Slavikova, B.; Budesinsky, M.; Nekardova, M.; Vyklicky, V.; Krausova, B.; Svehla, P.; Vyklicky, L. A new class of potent N-methyl-D-aspartate receptor inhibitors: Sulfated neuroactive steroids with lipophilic D-ring modifications. *J. Med. Chem.* **2015**, *58*, 5950−5966.
(11) Weaver, C. E.; Land, M. B.; Purdy, R. H.; Richards, K. G.; Gibbs, T. T.; Farb, D. H. Geometry and charge determine pharmacological effects of steroids on N-methyl-D-aspartate receptor-induced Ca^{2+} accumulation and cell death. *J. Pharmacol. Exp. Ther.* **2000**, *293*, 747−754.
(12) Borovska, J.; Vyklicky, V.; Stastna, E.; Kapras, V.; Slavikova, B.; Horak, M.; Chodounska, H.; Vyklicky, L., Jr. Access of inhibitory neurosteroids to the NMDA receptor. *Br. J. Pharmacol.* **2012**, *166*, 1069−1083.
(13) Weaver, C. E., Jr.; Marek, P.; Park-Chung, M.; Tam, S. W.; Farb, D. H. Neuroprotective activity of a new class of steroidal inhibitors of the N-methyl-D-aspartate receptor. *Proc. Natl. Acad. Sci. U. S. A.* **1997**, *94*, 10450−10454.
(14) Lapchak, P. A. The neuroactive steroid 3-alpha-ol-5-beta-pregnan-20-one hemisuccinate. A selective NMDA receptor antagonist improves behavioral performance following spinal cord ischemia. *Brain Res.* **2004**, *997*, 152−158.
(15) Hassner, A.; Haddadin, M. J.; Catsoulacos, P. Steroidal indoxyl, indoles, and quinolines. *J. Org. Chem.* **1966**, *31*, 1363−1369.
(16) Hewett, C. L. 16-Heterocyclic amino steroids. U.S. Patent 3,026,318, March 20, 1962.
(17) Zhang, H.; Padwa, A. Application of a stereospecific $RhCl(PPh_3)_3$ decarbonylation reaction for the total synthesis of 7-(±)-deoxypancratistatin. *Tetrahedron Lett.* **2006**, *47*, 3905−3908.
(18) Hu, Y.; Zorumski, C. F.; Covey, D. F. Neurosteroid analogues: Structure-activity studies of benz[e]indene modulators of $GABA_A$ receptor function. 1. The effect of 6-methyl substitution on the electrophysiological activity of 7-substituted benz[e]indene-3-carbonitriles. *J. Med. Chem.* **1993**, *36*, 3956−3967.
(19) Kapras, V. Synthesis and Properties of Neuroactive Steroids. Ph.D. Dissertation Charles University, Prague, Czech Republic, 2016.
(20) Petrovic, M.; Sedlacek, M.; Horak, M.; Chodounska, H.; Vyklicky, L., Jr. 20-oxo-5beta-pregnan-3alpha-yl sulfate is a use-dependent NMDA receptor inhibitor. *J. Neurosci.* **2005**, *25*, 8439−8450.
(21) Flint, A. C.; Maisch, U. S.; Weishaupt, J. H.; Kriegstein, A. R.; Monyer, H. NR2A Subunit expression shortens NMDA receptor synaptic currents in developing neocortex. *J. Neurosci.* **1997**, *17*, 2469−2476.
(22) Patneau, D. K.; Vyklicky, L., Jr.; Mayer, M. L. Hippocampal neurons exhibit cyclothiazide-sensitive rapidly desensitizing responses to kainate. *J. Neurosci.* **1993**, *13*, 3496−3509.
(23) Faassen, F.; Kelder, J.; Lenders, J.; Onderwater, R.; Vromans, H. Physicochemical properties and transport of steroids across Caco-2 cells. *Pharm. Res.* **2003**, *20*, 177−186.
(24) Kah, M.; Brown, C. D. LogD: Lipophilicity for ionisable compounds. *Chemosphere* **2008**, *72*, 1401−1408.
(25) Faucher, F.; Cantin, L.; Luu-The, V.; Labrie, F.; Breton, R. The crystal structure of human Delta4-3-ketosteroid 5beta-reductase defines the functional role of the residues of the catalytic tetrad in the steroid double bond reduction mechanism. *Biochemistry* **2008**, *47*, 8261−8270.
(26) *The PyMOL Molecular Graphics System*, version 1.5.0.4; Schrödinger, LLC.
(27) Ahlrichs, R.; Bar, M.; Haser, M.; Horn, H.; Kolmel, C. Electronic structure calculations on workstation computers: The program system Turbomole. *Chem. Phys. Lett.* **1989**, *162*, 165−169.
(28) Jurecka, P.; Cerny, J.; Hobza, P.; Salahub, D. Density functional theory augmented with an empirical dispersion term. Interaction energies and geometries of 80 noncovalent complexes compared with ab initio quantum mechanics calculations. *J. Comput. Chem.* **2007**, *28*, 555−569.
(29) Klamt, A.; Schüürmann, G. COSMO: A new approach to dielectric screening in solvents with explicit expressions for the screening energy and its gradient. *J. Chem. Soc., Perkin Trans. 2* **1993**, *5*, 799−805.
(30) (a) Rezac, J.; Fanfrlik, J.; Salahub, D.; Hobza, P. Semiempirical quantum chemical PM6 method augmented by dispersion and H-bonding correction terms reliably describes various types of noncovalent complexes. *J. Chem. Theory Comput.* **2009**, *5*, 1749−1760. (b) Rezac, J.; Hobza, P. Advanced corrections of hydrogen bonding and dispersion for semiempirical quantum mechanical methods. *J. Chem. Theory Comput.* **2012**, *8*, 141−151.
(31) Grimme, S.; Antony, J.; Ehrlich, S.; Krieg, H. A Consistent and accurate *ab initio* parametrization of pensity functional dispersion correction (DFT-D) for the 94 elements H-Pu. *J. Chem. Phys.* **2010**, *132*, 154104−154119.
(32) Marenich, A. V.; Cramer, C. J.; Truhlar, D. G. Universal solvation model based on solute electron density and on a continuum model of the solvent defined by the bulk dielectric constant and atomic surface tensions. *J. Phys. Chem. B* **2009**, *113*, 6378−6396.
(33) Frisch, M. J.; Trucks, G. W.; Schlegel, H. B.; Scuseria, G. E.; Robb, M. A.; Cheeseman, J. R.; Scalmani, G.; Barone, V.; Mennucci, B.; Petersson, G. A.; Nakatsuji, H.; Caricato, M.; Li, X.; Hratchian, H. P.; Izmaylov, A. F.; Bloino, J.; Zheng, G.; Sonnenberg, J. L.; Hada, M.; Ehara, M.; Toyota, K.; Fukuda, R.; Hasegawa, J.; Ishida, M.; Nakajima, T.; Honda, Y.; Kitao, O.; Nakai, H.; Vreven, T.; Montgomery, J. A., Jr.; Peralta, J. E.; Ogliaro, F.; Bearpark, M.; Heyd, J. J.; Brothers, E.; Kudin, K. N.; Staroverov, V. N.; Kobayashi, R.; Normand, J.; Raghavachari, K.; Rendell, A.; Burant, J. C.; Iyengar, S. S.; Tomasi, J.; Cossi, M.; Rega, N.; Millam, N. J.; Klene, M.; Knox, J. E.; Cross, J. B.; Bakken, V.; Adamo, C.; Jaramillo, J.; Gomperts, R.; Stratmann, R. E.; Yazyev, O.; Austin, A. J.; Cammi, R.; Pomelli, C.; Ochterski, J. W.; Martin, R. L.; Morokuma, K.; Zakrzewski, V. G.; Voth, G. A.; Salvador, P.; Dannenberg, J. J.; Dapprich, S.; Daniels, A. D.; Farkas, Ö.; Foresman, J. B.; Ortiz, J. V.; Cioslowski, J.; Fox, D. J. *Gaussian 09*; Gaussian Inc., Wallingford, CT, 2009.
(34) Kolar, M.; Fanfrlik, J.; Lepsik, M.; Forti, F.; Luque, F. J.; Hobza, P. Assessing the accuracy and performance of implicit solvent models for drug molecules: conformational ensemble approaches. *J. Phys. Chem. B* **2013**, *117*, 5950−5962.
(35) Marvin was used for drawing, displaying, and characterizing chemical structures, substructures, and reactions. *Marvin*, version 15.1.19; ChemAxon, 2015 (http://www.chemaxon.com).
(36) Cais, O.; Sedlacek, M.; Horak, M.; Dittert, I.; Vyklicky, L., Jr. Temperature dependence of NR1/NR2B NMDA receptor channels. *Neuroscience* **2008**, *151*, 428−438.
(37) Korinek, K.; Sedlacek, M.; Cais, O.; Dittert, I.; Vyklicky, L. Temperature dependence of N-methyl-D-aspartate receptor excitatory postsynaptic currents. *Neuroscience* **2010**, *165*, 736−748.

DOI: 10.1021/acs.jmedchem.6b00079
J. Med. Chem. 2016, 59, 4724−4739

PDF-XChange Editor
KOUPIT plnou verzi!
www.pdfxchange.cz

Steroids 117 (2017) 52–61

Contents lists available at ScienceDirect

Steroids

journal homepage: www.elsevier.com/locate/steroids

Physicochemical and biological properties of novel amide-based steroidal inhibitors of NMDA receptors

Santosh Kumar Adla [a], Barbora Slavikova [a], Marketa Smidkova [a], Eva Tloustova [a], Martin Svoboda [a], Vojtech Vyklicky [b], Barbora Krausova [b], Pavla Hubalkova [b,d], Michaela Nekardova [a,c], Kristina Holubova [b], Karel Vales [b], Milos Budesinsky [a], Ladislav Vyklicky [b], Hana Chodounska [a], Eva Kudova [a,*]

[a] Institute of Organic Chemistry and Biochemistry, Academy of Sciences of the Czech Republic, v.v.i., Flemingovo nam. 2, Prague 6 – Dejvice, 166 10, Czech Republic
[b] Institute of Physiology of the Czech Academy of Sciences, Videnska 1083, 142 20 Prague 4, Czech Republic
[c] Faculty of Mathematics and Physics, Charles University in Prague, Ke Karlovu 3, Prague 2, 121 16, Czech Republic
[d] Charles University in Prague, Third Faculty of Medicine, Ruska 87, Prague 10, 100 00, Czech Republic

ARTICLE INFO

Article history:
Received 25 April 2016
Received in revised form 4 August 2016
Accepted 8 August 2016
Available online 17 August 2016

Keywords:
Neurosteroid
NMDA receptor
Structure-activity relationship
Amide
Blood-brain-barrier permeability
Caco-2 assay

ABSTRACT

Herein, we report a new class of amide-based inhibitors (**1**–**4**) of *N*-methyl-D-aspartate receptors (NMDARs) that were prepared as analogues of pregnanolone sulfate (PAS) and pregnanolone glutamate (PAG) – the steroidal neuroprotective NMDAR inhibitors. A series of experiments were conducted to evaluate their physicochemical and biological properties: (i) the inhibitory effect of compounds **3** and **4** on NMDARs was significantly improved (IC_{50} = 1.0 and 1.4 μM, respectively) as compared with endogenous inhibitor – pregnanolone sulfate (IC_{50} = 24.6 μM) and pregnanolone glutamate (IC_{50} = 51.7 μM); (ii) physicochemical properties (logP and logD) were calculated; (iii) Caco-2 assay revealed that the permeability properties of compounds **2** and **4** are comparable with pregnanolone glutamate; (iv) compounds **1**–**4** have minimal or no adverse hepatic effect; (v) compounds **1**–**4** cross blood-brain-barrier.

© 2016 Elsevier Inc. All rights reserved.

1. Introduction

N-Methyl-D-aspartate receptors (NMDARs) are glutamate-gated ionotropic receptors that are involved in excitatory neurotransmission and plasticity [1]. However, the abnormal activation of NMDARs is thought to mediate neuronal death [2,3]. The NMDAR overactivation by elevated extracellular concentrations of glutamate under pathological conditions leads to excitotoxic cell death. Excitotoxicity is thought to be a major mechanism contributing to ischemia, traumatic brain injury, or Alzheimer's disease [2,4–6]. As such, inhibition of the NMDARs is extensively pursued as neuroprotective strategy for the development of new compounds that are able to affect such pathological process. The activity of NMDARs can be influenced by various modulators, including neurosteroids. 20-Oxo-5β-pregnan-3α-yl sulfate (PAS, Fig. 1) is an endogenous neurosteroid that is able to inhibit NMDAR-mediated currents (IC_{50} = 24.6 μM). However, unlike simple receptor-ligand interaction in an aqueous solution, PAS binding and inhibition of NMDARs requires plasma membrane as a compartment where the steroid accumulates to reach its binding site on NMDARs [7]. In our ongoing interest in neurosteroids, we have identified the site of action of PAS which is located at the extracellular vestibule of the receptor's ion channel pore and is accessible after receptor activation and/or receptor desensitization [8]. Moreover, the PAS has been shown to be neuroprotective [9].

To elucidate the modulatory effect of neurosteroids on NMDARs, numerous structural analogues of PAS were prepared and assessed – a series of sulfates, hemiesters, permethylated amines, and carboxylic acids [7,10–12]. The results demonstrate that C-3 substituent must bear charge to maintain the biological activity and that the 5β-stereochemistry has to be retained [7,12].

While searching for new drug-like candidates, we drew inspiration from the published data for pregnanolone C-3 hemisuccinate ester, a compound with neuroprotective activity both *in vitro* and *in vivo* models of neurodegeneration [9,13] and therefore, pregnanolone glutamate (PAG, Fig. 1) was established as drug-lead candidate for further development and screening. We have assessed the neuroprotective effect of PAG in several biological models *in vivo*: (i) PAG does not induce psychotomimetic symptoms (such as hyperlocomotion and sensorimotor gating deficit) and reduced an excitotoxic damage of brain tissue and subsequent behavioural impairment in rats [14]; (ii) PAG significantly ameliorated neuronal damage in the dentate gyrus and subiculum and improved

* Corresponding author at: Department of Steroidal Inhibitors, Institute of Organic Chemistry and Biochemistry, Academy of Sciences of the Czech Republic, v.v.i., Flemingovo nam. 2, Prague 6 –Dejvice, 16610, Czech Republic.
E-mail address: kudova@uochb.cas.cz (E. Kudova).

http://dx.doi.org/10.1016/j.steroids.2016.08.010
0039-128X/© 2016 Elsevier Inc. All rights reserved.

PDF-XChange Editor
KOUPIT plnou verzi!
www.pdfxchange.cz

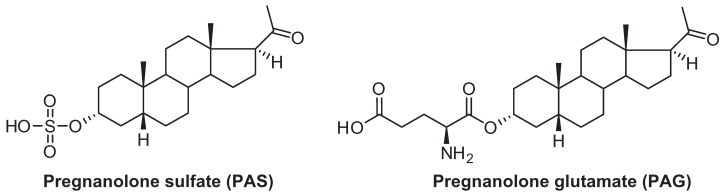


Fig. 1. Structures of pregnanolone sulfate (PAS) and pregnanolone glutamate (PAG).

behavioural performance in active allothetic place avoidance tasks (AAPA, also known as the carousel maze) after bilateral NMDA-induced lesions to the hippocampi [14]; (iii) PAG displayed anxiolytic-like and antidepressant-like properties in elevated plus maze and forced swimming models [15]; (iv) PAG displayed neuroprotective effect in model of focal cerebral ischemia induced by endothelin-1 in immature rats [16].

Hence, we conclude that glutamate moiety at C-3 is a structural modification that lead to potent modulator of NMDARs and such molecule has neuroprotective properties. However, the expected susceptibility of hemiester moiety to hydrolysis at C-3 emerged us to design a new class of compounds bearing negatively charged C-3 substituent *via* amide moiety [17] (Fig. 2). This isosteric replacement of the ester oxygen with a nitrogen atom was supposed to improve solubility, enhance permeability and reduce metabolic liability of new analogues while retaining the structural features necessary for the inhibitory effect. On account of our previous SAR study on non-polar modification of the steroidal D-ring, which lead to potent inhibitors of NMDARs [18], the structural motif of non-substituted D-ring in combination with amide-based C-3 substituent of various length (**1**–**4**) was exploited for the development of new NMDAR inhibitors.

As the physicochemical properties and consequently their biological properties of a drug-like candidate compounds are of crucial importance and should be a part of the early stage drug discovery process, we have incorporated the evaluation of the permeability experiments into our SAR screening cascade as well as the *in vivo* test of blood-brain-barrier permeability (Fig. 3).

As such, the structure-activity relationship of compounds **1**–**4** (the ability to inhibit the NMDAR-mediated currents) was evaluated on human embryonic kidney 293 cells (HEK293 cells) transfected with plasmids encoding GluN1-1a/GluN2B/GFP genes. Then, the logP and logD values were calculated to evaluate the lipophilicity of compounds **1**–**4**. The obtained data were correlated with the *in vivo* Caco-2 assay (permeability assay). The toxicity of compounds **1**–**4** was evaluated using 72 h XTT assay on HepG2 cells. Finally, compounds **1**–**4** were tested for their ability to cross blood-brain-barrier in spontaneous locomotor activity test in mice after 100 mg/kg dose administration.

2. Experimental

2.1. General experimental procedures

Melting points were determined on a micromelting point apparatus Hund/Wetzlar (Germany) and are uncorrected. Optical rotations were measured in chloroform using an Autopol IV (Rudolf Research Analytical, Flanders, USA). The $[\alpha]_D$ values are given in deg (10^{-1} deg cm^2 g^{-1}). IR spectra were recorded on a Bruker IFS 55 spectrometer (wavenumbers in cm^{-1}). Proton and carbon NMR spectra were measured on a FT NMR spectrometer Bruker AVANCE-400 (400 MHz, 101 MHz) in $CDCl_3$ with tetramethylsilane as the internal standard. Chemical shifts are given in ppm (δ scale). Coupling constants (J) are given in Hz. The NMR spectra for compounds **8**–**11** were measured on Bruker AVANCE III HD 500 instrument (^{1}H at 500 MHz and ^{13}C at 125.7 MHz) or Bruker AVANCE III HD 600 instrument (^{1}H at 600 MHz and ^{13}C at 150.9 MHz) equipped with 5 mm cryoprobes in $CDCl_3$ or d_6DMSO. Spectra in $CDCl_3$ were referenced to TMS (^{1}H) or solvent peak (^{13}C, using $\delta_C(CDCl_3) = 77.0$ ppm). Spectra in DMSO were referenced to solvent peak (using δ_H(DMSO) = 2.50 ppm; δ_C(DMSO) = 39.7 ppm). Complete structural assignment of proton and carbon signals was done using 2D-H,H-COSY, 2D-H,C-HSQC and 2D-H,C-HMBS spectra. High resolution MS spectra were performed with a Q-Tof microspectrometer (Waters). Thin layer chromatography (TLC) was performed on silica gel (ICN Biochemicals). Preparative TLC (prep-TLC) was carried out on 200 mm × 200 mm plates coated with a 0.4 mm thick layer of the same material. For column chromatography neutral silica gel 60 μm (Merck) was used. Analytical samples were dried over phosphorus pentoxide at 50 °C/100 Pa.

2.2. Synthesis

2.2.1. Synthesis of compounds *1* and *2*

PAS, PAG and compounds **1**, **2** were prepared according to the literature [7,17].

2.2.2. Synthesis of compounds *3* and *4*

*2.2.2.1. 5β-Androstan-3α-yl 1H-isoindole-1,3(2H)-dione (**6**).* Triphenylphosphine (328 mg, 1.25 mmol) and phtalimide (184 mg, 1.25 mmol) were added to a solution of compound **5** (288 mg, 1.04 mmol) in tetrahydrofuran (5 mL) at 0 °C under inert atmosphere. The reaction mixture was stirred at 0 °C for 1 h. Then, diisopropylazodicarboxylate (DIAD, 246 μL, 1.25 mmol) was added at 0 °C and the reaction mixture was allowed to stir at 0 °C to room temperature over 19 h. Afterwards, water (10 mL) was added to the reaction mixture and tetrahydrofuran was evaporated. The aqueous phase was extracted with chloroform (4 × 30 mL). The combined organic extracts were washed with water (1 × 30 mL), dried over sodium sulfate and concentrated *in vacuo*. The residue was purified by column chromatography on silica gel (10–20% ethyl acetate in petroleum ether) to afford compound **6** (366 mg,

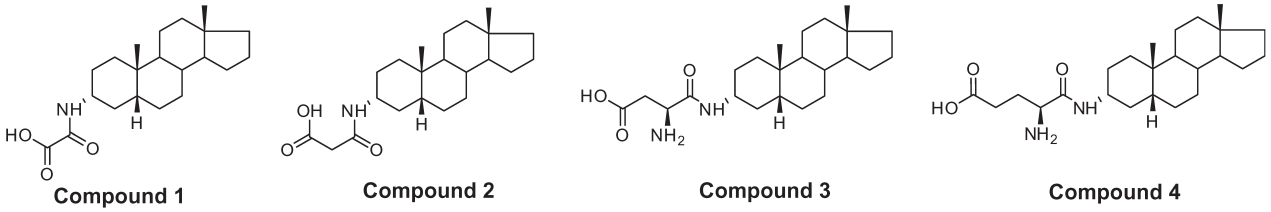


Fig. 2. Structures of new inhibitors of NMDA receptor.

PDF-XChange Editor
KOUPIT plnou verzi!
www.pdfxchange.cz

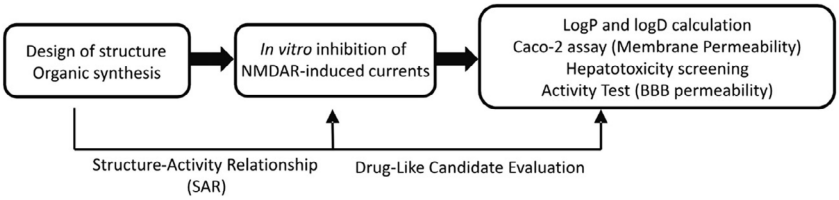


Fig. 3. Drug-like candidate screening cascade.

87%) as a brown amorphous solid. $[\alpha]_D^{20}$ +20.5 (*c* 0.29, $CHCl_3$). IR ($CHCl_3$, cm^{-1}) 2933 (CH_2), 1706 (C=O), 1374 (CH_3). ^1H NMR (400 MHz, $CDCl_3$): δ 0.70 (3H, s, H-18), 0.98 (3H, s, H-19), 1.02–1.36 (11H, m), 1.40–1.51 (5H, m), 1.56–1.75 (5H, m), 1.85–1.95 (2H, m), 2.32–2.42 (1H, m), 2.75 (1H, q, *J* = 12.8 Hz), 4.19 (1H, tt, *J* = 12.5, 4.4 Hz, H-3), 7.69 (2H, dd, *J* = 5.4, 3.0 Hz, phtalimide), 7.81 (2H, dd, *J* = 5.4, 3.0 Hz, phtalimide). ^{13}C NMR (101 MHz, $CDCl_3$): δ 168.51, 133.75, 132.11, 122.93, 122.90, 54.40, 51.34, 43.14, 40.95, 40.78, 40.45, 38.97, 36.77, 36.18, 34.78, 29.84, 27.15, 26.77, 25.55, 24.29, 23.50, 20.91, 20.62, 17.60. ESI-MS *m/z* 406.3 (100%, M+H). HR-ESI MS *m/z* 406.2745 [M+H], $C_{27}H_{36}O_2N$ requires 406.2746.

*2.2.2.2. 3α-Amino-5β-androstane hydrochloride (**7**).* Hydrazine monohydrate (18 mL, 215.27 mmol) was added to a solution of compound **6** (856 mg, 2.11 mmol) in methanol (30 mL) at room temperature. The reaction mixture was refluxed for 4 h under argon atmosphere. After cooling to room temperature, the reaction mixture was diluted with sodium hydroxide (6 N, 40 mL) and extracted with dichloromethane (4 × 50 mL). The combined organic extracts were dried over sodium sulfate and concentrated *in vacuo*. The residue was dissolved in minimum amount of ethyl acetate (2 mL) and poured into aqueous solution of hydrochloric acid (5%, 50 mL). The product was extracted into chloroform (5 × 50 mL). Combined organic extracts were dried over sodium sulfate, solvents evaporated, and the residue was recrystallized from chloroform/heptane to obtain pure title compound **7** (471 mg, 72%) as a white amorphous solid. $[\alpha]_D^{20}$ +9.0 (*c* 0.27, $CHCl_3$). IR ($CHCl_3$, cm^{-1}) 3439 (br, NH), 3104 (br, NH_3^+), 2973 (CH_3), 2931 (CH_2), 2866 (CH_3), 1450 (CH_3). ^1H NMR (400 MHz, $CDCl_3$): δ 0.66 (3H, s, H-18), 0.94 (3H, s, H-19), 0.96–1.49 (9H, m), 1.51–1.76 (6H, m), 1.80–1.94 (3H, m), 2.01 (1H, q, *J* = 12.6 Hz), 3.17 (1H, tt, *J* = 12.3, 3.1 Hz), 8.31 (3H, br, s, NH_3^+). ^{13}C NMR (101 MHz, $CDCl_3$): δ 54.19, 52.11, 42.41, 41.02, 40.73, 40.48, 38.88, 36.35, 35.41, 34.87, 31.75, 26.98, 26.86, 26.30, 25.68, 23.58, 21.01, 20.70, 17.65. ESI-MS *m/z* 276.3 (120%, M–Cl), 275.3 (85%, M). HR-ESI MS *m/z* 276.2677 [M–Cl], $C_{19}H_{34}N$ requires 276.2686, 275.2615 [M], $C_{19}H_{33}N$ requires 275.2613.

*2.2.2.3. Benzyl (3S)-3-((tert-butoxycarbonyl)amino)-4-((5β-androstan-3α-yl)-amino)-4-oxobutanoate (**8**).* A solution of compound **7** (200 mg, 0.64 mmol), Boc-Asp(OBzl)-OH (229 mg, 0.71 mmol), and DIPEA (168 μL, 0.96 mmol) in benzene (30 mL) was partially evaporated (1/3 of volume). Then, DMAP (4 mg, 0.03 mmol) and dicyclohexylcarbodiimide (375 mg, 1.80 mmol) were added. The reaction mixture was stirred at room temperature for 18 h. The reaction mixture was poured into aqueous solution of sodium bicarbonate (40 mL) and the product was extracted with ethyl acetate (4 × 50 mL). The combined organic extracts were washed with water (1 × 50 mL), dried over sodium sulfate, and concentrated *in vacuo*. The residue was purified by column chromatography in silica gel (20–30% ether in petroleum ether) to afford compound **8** (373 mg, 100%) as a white amorphous solid. Compound **8** was characterized as a mixture of rotamers (5:1) according to NMR spectroscopy. IR ($CHCl_3$, cm^{-1}) 2935 (CH_2). 1716 (C=O), 1669 (amide), 1496 (amide), 1163 (^{t}Bu). Ratio of rotamers in $CDCl_3$: 6:1. Major rotamer: ^1H NMR (600 MHz, $CDCl_3$): δ 0.67 (3H, s, H-18), 0.91 (3H, s, H-19), 0.95 (1H, m, H-14), 1.00 and 1.78 (2H, H-1), 1.05 and 1.42 (2H, H-7), 1.13 and 1.62 (2H, H-15), 1.13 and 1.71 (2H, H-12), 1.14 and 1.42 (2H, H-17), 1.14 and 1.55 (2H, H-2), 1.20 and 1.83 (2H, H-6), 1.23 and 1.38 (2H, H-11), 1.31 (1H, H-8), 1.33 (1H, H-9), 1.41 (1H, m, H-5), 1.44 (9H, s, $((CH_3)_3C$-O), 1.44 and 1.58 (2H, H-4), 1.58-1.62 (2H, H-16), 2.69 (1H, dd, *J* = 17.0, 6.6 Hz) and 2.99 (1H, dd, *J* = 17.0, 4.5 Hz, CO-CH_2-CHNH), 3.69 (1H, m, H-3), 4.44 (1H, m, CH_2-CHNH), 5.09 and 5.14 (2H, 2xd, *J* = 12.2 Hz, O-CH_2-Ph), 5.66 (1H, br d, *J* = 8.0 Hz, O-CO-NH-CH), 6.29 (1H, br d, *J* = 8.0 Hz, CO-NH-CH), 7.30–7.35 (5H, m, C_6H_5). ^{13}C NMR (150.9 MHz, $CDCl_3$): δ 171.78 ($COOCH_2Ph$), 169.53 (CHCONH), 155.57 (CO, carbamate), 135.36 (*i*-Ph), 128.54 (2C, *o*-Ph), 128.32 (*p*-Ph), 128.17 (2C, *m*-Ph), 80.38 $(CH_3)_3C$-O), 66.74 (OCH_2Ph), 54.56 (C-14), 50.66 (CH_3-CHNH), 49.63 (C-3), 42.35 (C-5), 40.89 (C-13), 40.76 (C-9), 40.46 (C-17), 39.00 (C-12), 36.20 (CO-CH_2-CHNH), 36.12 (C-8), 35.89 (C-1), 34.66 (C-10), 33.40 (C-4), 28.26 ($(CH_3)_3$C-O), 27.57 (C-2), 26.95 (C-6), 26.74 (C-7), 25.48 (C-15), 23.52 (C-19), 20.77 (C-11), 20.54 (C-16), 17.44 (C-18). Minor rotamer (only observed separate signals of substituent at C-3 of minor isomer are given): ^1H NMR (600 MHz, $CDCl_3$): 1.40 (9H, s, $(CH_3)_3$C-O), 2.67 (1H, dd, *J* = 17.0, 6.6 Hz) and 2.81 (1H, dd, *J* = 17.0, 4.5 Hz, CO-CH_2-CHNH), 3.65 (1H, m, H-3), 4.81 (1H, m, CH_2-CHNH), 5.28 (1H, br d, *J* = 8.0 Hz, O-CO-NH-CH), 7.30 (1H, br d, *J* = 8.0 Hz, CO-NH-CH). ^{13}C NMR (150.9 MHz, $CDCl_3$): δ 170.29 ($COOCH_2Ph$), 153.02 (CO, carbamate), 135.28 (*i*-Ph), 80.48 $(CH_3)_3$C-O), 66.91 (OCH_2Ph), 37.29 (CO-CH_2-CHNH), 28.22 ($(CH_3)_3$C-O). ESI-MS *m/z* 603.3 (100%, M+Na), 581.4 (65%, M+H). HR ESI MS *m/z* 603.3767 [M+Na], $C_{35}H_{52}O_5N_2Na$ requires 603.3768, 581.3950 [M+H], $C_{35}H_{53}O_5N_2$ requires 581.3949.

*2.2.2.4. Benzyl (4S)-4-((tert-butoxycarbonyl)amino)-5-((5β-androstan-3α-yl)-amino)-5-oxopentanoate (**9**).* Compound **9** was prepared in the same manner as compound **8**. Starting from compound **7** (200 mg, 0.64 mmol) and using Boc-Glu(OBzl)-OH (239 mg, 0.71 mmol), compound **9** (378 mg, 99%) was obtained as a white amorphous solid. Compound **9** was characterized as a mixture of rotamers (5:1) according to NMR spectroscopy. IR ($CHCl_3$, cm^{-1}) 2935 (CH_2). 1726 (C=O), 1708 (carbamate), 1671 (amide), 1497 (amide), 1166 (^{t}Bu). Ratio of rotamers in $CDCl_3$: 5:1. Major rotamer: ^1H NMR (600 MHz, $CDCl_3$): δ 0.67 (3H, s, H-18), 0.92 (3H, s, H-19), 0.95 (1H, m, H-14), 1.03 and 1.79 (2H, H-1), 1.05 and 1.43 (2H, H-7), 1.13 and 1.72 (2H, H-12), 1.14 and 1.42 (2H, H-17), 1.14 and 1.62 (2H, H-15), 1.17 and 1.61 (2H, H-2), 1.21 and 1.84 (2H, H-6), 1.24 and 1.38 (2H, H-11), 1.32 (1H, m, H-8), 1.33 (1H, m, H-9), 1.425 (1H, m, H-5), 1.43 (9H, s, $(CH_3)_3$C-O), 1.48 and 1.58 (2H, H-4), 1.60 (2H, m, H-16), 1.90 and 2.10 (2H, NHCH(CH_2)CO), 2.42 and 2.52 (2H, NHCH(CH_2CH_2)CO), 3.72 (1H, br, H-3), 4.07 (1H, br, NHCHCO), 5.11 (1H. d, *J* = 12.3 Hz) and 5.14 (1H. d, *J* = 12.3 Hz, O-CH_2-Ph), 5.21 (1H, br, Boc-NH), 5.91 (1H, bd, *J* = 8.0 Hz, NH), 7.32–7.36 (5H, m, C_6H_5).

PDF-XChange Editor
KOUPIT plnou verzi!
www.pdfxchange.cz

^{13}C NMR (150.9 MHz, $CDCl_3$): δ 173.13 ($COOCH_2Ph$), 170.35 (CHCONH), 162.00 (*HO*, carbamate), 135.72 (*i*-Ph), 128.59 (2x, *o*-Ph), 128.31 (*p*-Ph), 128.23 (2x, *m*-Ph), 80.01 $(CH_3)_3CO$), 66.55 (OCH_2Ph), 54.63 (C-14), 53.72 (NHC*H*CO), 49.58 (C-3), 42.38 (C-5), 40.94 (C-13), 40.82 (C-9), 40.50 (C-17), 39.05 (C-12), 36.17 (C-8), 35.90 (C-1), 34.71 (C-10), 33.49 (C-4), 30.46 ($CHCH_2CH_2COO$), 28.30 (3C, $(CH_3)_3CO$-), 28.16 ($CHCH_2CH_2COO$), 27.79 (C-2), 27.00 (C-6), 26.78 (C-7), 25.52 (C-15), 23.54 (C-19), 20.82 (C-11), 20.58 (C-16), 17.48 (C-18). Minor rotamer (only observed separate signals of substituent at C-3 of minor isomer are given): ^{1}H NMR (600 MHz, $CDCl_3$): δ 1.41 (9H, s, $(CH_3)_3$C-O), 3.66 (1H, br, H-3), 4.42 (1H, br, NHC*H*CO), 5.09 (1H. d, *J* = 12.3 Hz) and 5.12 (1H. d, *J* = 12.3 Hz, O-CH_2-Ph). ^{13}C NMR (150.9 MHz, $CDCl_3$): δ 135.78 (*i*-Ph), 128.53 (2x, *o*-Ph), 128.31 (*p*-Ph), 128.25 (2x, *m*-Ph), 66.53 (OCH_2Ph), 52.53 (NHC*H*CO), 50.13 (C-3), 28.25 (3C, $(CH_3)_3$C-O). ESI-MS *m*/*z* 1211 (40%, 2M+Na), 617 (100%, M+Na). HR ESIMS *m*/*z* 617.3926 [M+Na], $C_{36}H_{54}O_5N_2Na$ requires 617.3925.

*2.2.2.5. (3S)-3-((Tert-butoxycarbonyl)amino)-4-((5β-androstan-3α-yl)-amino)-4-oxobutanoic acid (**10**).* Compound **8** (221 mg, 0.38 mmol) was dissolved in methanol (30 mL). Then, Pd/C (10%, 40 mg) was added. The reaction mixture was hydrogenated under slight hydrogen overpressure at room temperature for 7 h at room temperature. The catalyst was filtered over a pad of cotton/celite and the solvent was evaporated. The residue was purified by preparative TLC (ethyl acetate/petroleum ether/acetic acid, 2:1:0.1) to afford compound **10** (121 mg, 65%) as an oily product. $[\alpha]_D^{20}$ +19.3 (*c* 0.19, $CHCl_3$). IR ($CHCl_3$, cm^{-1}) 3507 (OH), 3421 (NH), 2934 (CH_2). 1710 (C=O), 1668 (amide), 1522 (amide), 1496 (amide), 1163 (^{t}Bu). ^{1}H NMR (500 MHz, T = 45 °C , $CDCl_3$): δ 0.62 (3H, s, H-18), 0.87 (3H, s, H-19), 0.90 (1H, m, H-14), 0.97 and 1.75 (2H, H-1), 1.00 and 1.37 (2H, H-7), 1.08 and 1.56 (2H, H-15), 1.08 and 1.66 (2H, H-12), 1.09 and 1.36 (2H, H-17), 1.14 and 1.58 (2H, H-2), 1.16 and 1.79 (2H, H-6), 1.19 and 1.34 (2H, H-11), 1.27 (1H, m, H-8), 1.29 (1H, m, H-9), 1.37 (1H, m, H-5), 1.39 (9H, s, $(CH_3)_3$C-O), 1.42 and 1.56 (2H, H-4), 1.52-1.58 (2H, m, H-16), 2.64 (1H, dd, *J* = 16.6 Hz) and 2.82 (1H, dd, *J* = 16.6 Hz, CHCH_2-COOH), 3.64 (1H, br, H-3), 4.35 (1H, m, NHC*H*CO), 5.66 (1H, d, *J* = 5.4 Hz, O-CONHCH), 6.44 (1H, br, C-CONHCH). ^{13}C NMR (125.7 MHz, T = 45 °C , $CDCl_3$): δ 174.33 (*C*OOH), 170.41 (CHCONH), 155.90 (*C*O, carbamate), 80.78 $(CH_3)_3$C-O), 54.74 (C-14), 51.02 (NHCHC(=O)NH), 50.02 (C-3), 42.53 (C-5), 41.00 (C-13), 40.97 (C-9), 40.59 (C-17), 39.14 (C-12), 36.60 ($CHCH_2COOH$), 36.30 (C-8), 36.02 (C-1), 34.81 (C-10), 33.46 (C-4), 28.35 (3C, $(CH_3)_3$C-O), 27.67 (C-2), 27.10 (C-6), 26.86 (C-7), 25.58 (C-15), 23.57 (C-19), 20.92 (C-11), 20.64 (C-16), 17.54 (C-18). ESI-MS *m*/*z* 1003.5 (15%, 2M+Na), 513.2 (100%, M+Na). HR ESI MS *m*/*z* 513.3299 [M+Na], $C_{28}H_{46}O_5N_2Na$ requires 513.3299, 491.3479 [M+H], $C_{28}H_{47}O_5N_2$ requires 491.3480.

*2.2.2.6. (4S)-4-((Tert-butoxycarbonyl)amino)-5-((3α5β-androstanyl)-amino)-5-oxopentanoic acid (**11**).* Compound **11** was prepared in the same manner as compound **10**. Starting from compound **9** (360 mg, 0.61 mmol), compound **11** (300 mg, 98%) was obtained as an amorphous solid. $[\alpha]_D^{20}$ +20.0 (*c* 0.28, $CHCl_3$). IR ($CHCl_3$, cm^{-1}) 3519 (OH), 2934 (CH_2). 1712 (C=O), 1663 (amide), 1504 (amide), 1497 (amide), 1163 (^{t}Bu). ^{1}H NMR (600 MHz, DMSO): δ 0.67 (3H, s, H-18), 0.91 (3H, s, H-19), 0.95 (1H, m, H-14), 0.96 and 1.74 (2H, H-1), 1.08 and 1.41 (2H, H-7), 1.12 and 1.70 (2H, H-12), 1.13 and 1.40 (2H, H-17), 1.13 and 1.62 (2H, H-15), 1.20 and 1.38 (2H, H-11), 1.20 and 1.81 (2H, H-6), 1.25 and 1.42 (2H, H-2), 1.29 and 1.70 (2H, H-4), 1.30 (1H, m, H-8), 1.36 (1H, m, H-5), 1.365 (9H, s, $(CH_3)_3$C-O), 1.41 (1H, m, H-9), 1.56 and 1.61 (2H, H-16), 1.68 (2H, m, CHCH_2CH$_2$COOH), 1.98 (2H, m, CHCH$_2$CH_2-COOH), 3.76 (1H, br, H-3), 4.17 (1H, br, NHC*H*CO), 7.28 (1H, br, Boc-NH), 7.80 (1H, br d, *J* = 7.2 Hz, NH). ^{13}C NMR (150.9 MHz, DMSO): δ 176.79 (COOH), 171.37 (CHCONH), 155.43 (*C*O, carbamate), 77.94 $(CH_3)_3$C-O), 54.98 (C-3), 54.45 (C-14), 53.72 (NHCHC(=O)NH), 42.16 (C-5), 40.78 (C-13), 40.38 (C-9), 40.30 (C-17), 38.81 (C-12), 35.91 (C-8), 35.03 (C-1), 34.57 (C-10), 34.12 ($CHCH_2$-CH_2COOH), 33.08 (C-4), 28.95 ($CHCH_2CH_2COOH$), 28.44 (3C, $(CH_3)_3$C-O), 27.36 (C-2), 26.94 (C-6), 26.73 (C-7), 25.33 (C-15), 23.54 (C-19), 20.60 (C-11), 20.41 (C-16), 17.52 (C-18). ESI-MS *m*/*z* 1007.6 (20%, 2M+H), 503 (90%, M). HR ESI MS *m*/*z* 503.3488 [M], $C_{29}H_{47}O_5N_2$ requires 503.3491.

*2.2.2.7. (3S)-3-(Amino)-4-((5β-androstan-3α-yl)-amino)-4-oxobutanoic acid (**3**).* Trifluoroacetic acid (2 mL) was added dropwise to compound **10** (85 mg, 0.17 mmol) in dichloromethane (5 mL). The reaction was stirred for 1 h at room temperature. Then, solvent was evaporated and the excess of trifluoroacetic acid was flushed out with a stream of nitrogen. The resultant brownish oil dissolved in pyridine/methanol (4.5:0.5 mL) and was added dropwise to ice cold water (50 mL). The aqueous solution was kept at 5 °C for 24 h. The precipitate was filtered off and dried in high vacuum to give the desired title compound **3** (61 mg, 91%) as a brown amorphous solid. $[\alpha]_D^{20}$ +26.1 (*c* 0.18, $CHCl_3$). IR ($CHCl_3$, cm^{-1}) 3416 (br, NH), 3223 (br, NH), 3400-3000 (br, COOH), 2934 (CH_2). 1666 (amide), 1526 (amide). ^{1}H NMR (400 MHz, $CDCl_3$ (10% MeOD)): δ 0.52 (3H, s, H-18), 0.67–1.34 (19H, m), 0.78 (3H, s, H-19), 1.36–1.78 (9H, m), 2.40–2.70 (2H, br, m), 3.18 (1H, br), 3.45–3.56 (1H, br), 3.80–3.95 (1H, br). ^{13}C NMR (101 MHz, $CDCl_3$, (10% MeOD)): δ 173.69, 167.19, 76.84, 54.50, 49.92, 42.32, 40.74, 40.68, 40.29, 38.87, 36.02, 35.72, 34.56, 32.71, 29.49, 26.99, 26.91, 26.65, 25.34, 24.74, 23.33, 20.65, 20.33, 17.19. ESI-MS *m*/*z* 413.2 (30%, M+Na), 391.3 (M+H). HR ESI MS *m*/*z* 413.2773 [M+Na], $C_{23}H_{39}O_3N_2Na$ requires 413.2775, 391.2954 [M+H], $C_{23}H_{39}O_3N_2$ requires 391.2955.

*2.2.2.8. (4S)-4-(Amino)-5-((5β-androstan-3α-yl)-amino)-5-oxopentanoic acid (**4**).* Compound **4** was prepared in the same manner as compound **3**. Starting from compound **11** (481 mg, 0.95 mmol), compound **4** (352 mg, 92%) was obtained as a brown amorphous solids. $[\alpha]_D^{20}$ +29.9 (*c* 0.30, $CHCl_3$). IR ($CHCl_3$, cm^{-1}) 3420 (br, NH), 3236 (br, NH), 3400-3000 (br, COOH), 2934 (CH_2). 1761 (COOH), 1700 (C=O), 1671 (amide). ^{1}H NMR (400 MHz, $CDCl_3$ (10% MeOD)): δ 0.55 (3H, s, H-18), 0.76–1.33 (18H, m), 0.82 (3H, s, H-19), 1.47–1.90 (11H, m), 2.25-2.35 (2H, m, CH(CH$_2$CH_2COOH)CO), 3.32 (1H, br, H-3), 3.50–3.60 (1H, br), 3.61–3.70 (1H, br, NH$_2$C*H*CONH). ^{13}C NMR (101 MHz, $CDCl_3$ (10% MeOD)): δ 177.78, 168.29, 54.58, 52.90, 49.87, 42.34, 40.80, 40.75, 40.35, 38.94, 36.06, 35.76, 34.62, 32.77, 32.42, 27.68, 27.23, 26.95, 26.71, 25.39, 23.40, 20.70, 20.39, 17.27. ESI-MS *m*/*z* 809.6 (20%, 2M+H), 427.3 (15%, M+Na), 405.3 (M+H). HR ESI MS *m*/*z* 427.2927 [M+Na], $C_{24}H_{40}O_3N_2Na$ requires 427.2931, 405.3109 [M+H], $C_{24}H_{41}O_3N_2$ requires 405.3112.

2.3. Modulation of NMDARs in vitro

Electrophysiological experiments were performed on HEK293 cells transfected with plasmids encoding GluN1-1a/GluN2B/GFP genes as described previously [19]. Glutamate-induced responses were voltage-clamped at a holding potential of −60 mV. Whole-cell voltage-clamp recordings were made with a patch-clamp amplifier (Axopatch 200B; Axon Instruments. Inc., Foster City, CA) after a serial resistance (<10 MΩ) and capacitance compensation of 80–90%. For the application of test and control solutions, a microprocessor controlled multibarrel fast-perfusion system was used, with a time constant of solution exchange around cells of ~10 ms. Agonist-induced responses were low-pass filtered at 2 kHz, digitally sampled at 5 kHz, and analyzed with pClamp software version 9.2 (Molecular Devices). Patch pipettes (3–5 MΩ)

PDF-XChange Editor
KOUPIT plnou verzi!
www.pdfxchange.cz

pulled from borosilicate glass were filled with Cs^+-based intracellular solution (ICS) containing the following (in mM): 120 gluconic acid, 15 CsCl, 10 BAPTA, 10 HEPES, 3 $MgCl_2$, 1 $CaCl_2$ and 2 ATP-Mg salt (pH-adjusted to 7.2 with CsOH). The extracellular solution (ECS) contained the following (in mM): 160 NaCl, 2.5 KCl, 10 HEPES, 10 glucose, 0.7 $CaCl_2$, 0.2 EDTA, 0.01 glycine (pH-adjusted to 7.3 with NaOH). NMDAR responses were induced by 1 mM glutamate. Steroid solutions were prepared fresh, as a stock solution of 5 mM in dimethyl sulfoxide (DMSO) before each experiment (1% DMSO final concentration). The same concentration of DMSO was added in all extracellular solutions. Experiments were performed at room temperature (21–25 °C).

2.4. The computational estimate of lipophilicity of compounds **1–4**

2.4.1. Preparation of structures

The structures of the steroids were obtained by the modeling of the inhibitor taken from the crystal structure (3CAV PDB code) [20] using PyMOL program (version 1.5.0.4.) [21] and were optimized by the RI-DFT/B-LYP/SVP method with Turbomole program (version 6.1) [22]. The empirical dispersion correction (D) [23] and COSMO continuum solvation model [24] were employed on the gradient optimization. The most stable local minima of the compounds were generated by the quenched molecular dynamics simulation (the simulation was run 30 ns; the constant temperature was 400 K) with PM6-D3H4X [25,26]. The resulting geometries were re-optimized by the RI-DFT-D/B-LYP/SVP/COSMO method and their single-point energies were calculated at the RI-DFT-D3/B-LYP/TZVPP//COSMO level.

2.4.2. Computations

The partition coefficient (logP) was calculated on the basis of the change of the geometry (conformation) related to the transfer between *n*-octanol and water. The compounds were optimized at the M06-2X/6-31G* level in the SMD continuum solvation model [27] in the aqueous and *n*-octanol environments with the Gaussian program (version 09) [28] and logP was expressed as the difference between the total energies in water and in *n*-octanol [29], since this energy includes the internal energy of the molecule. The distribution-coefficient (logD) [30] of the water/*n*-octanol phase was predicted at pH = 7.4 (the physiological pH of blood serum) by the MarvinSketch program [31].

2.5. Caco-2 permeability assay

The transport of the tested compounds across the Caco-2 monolayers was studied using the BD BioCoat HTS Caco-2 assay system (BD Biosciences, Bedford, MA) according to the manufacturer's instructions. Caco-2 cell line (Homo sapiens, adult 72 year male) was purchased from LGS Strandards (Teddington, UK). The cells were seeded into the wells of the transwell insert at a concentration of 2×10^5 cells per insert in the seeding basal medium. The cells were left to attach for 48 h, and after that the medium was changed to the enterocyte differentiation medium in which the cells were cultured for next 48 h. Immediately before the transport experiments, the monolayers were washed twice by transport medium (HBSS containing 10 mM HEPES and 25 mM glucose [pH 7.4]) and incubated for 30 min in a CO_2 incubator at 37 °C. The integrity of cell monolayers was assessed by monitoring the transepithelial electrical resistance (TEER) using a Millicell ERS apparatus (Millipore, Bedford, MA) and paracellular flux marker, [^{14}C]mannitol (0.15 μCi/insert). Intact cell monolayers displaying a TEER of >250 Ω cm^2 were used in experiments. The transport was initiated by the addition of 1 mL of the transport medium to the acceptor (basolateral) side and 300 μL of the transport medium containing 25 or 100 μM compounds to the apical side. After 3 h incubation, fluids were collected from the donor and acceptor compartment and lyophilized.

2.6. Mass spectrometry analysis

Mass spectrometry experiment was accomplished using MS system LCQ FLEET ion trap which was equipped with Accela autosampler and HPLC Accela pumps (Thermo Scientific). Reverse phase HPLC column C4, 250 × 2 mm, 5 μm, 300A (Phenomenex) was used for separation and the chromatographic conditions were as follows: column temperature 25 °C, flow rate 400 μL/min, 20 μL injection loop. The mobile phase consisted of water (solvent A) and acetonitrile (solvent B). The 29 min step gradient was applied. Salts were washing out for 11 min by 5% solvent B, then targeted molecules were eluted for 11 min by 95% solvent B and the last 7 min were used for re-equilibration of the column using again 5% solvent B. The 4 μL/min of 1 M ammonium formate was added to the stream post column using external pump Dionex 3000 to achieve better ionization conditions. The MS data was collected in mass range from 250 to 1000 Da in negative ESI mode. Divert valve was used to direct post-column flow to waste for the first 10 min to protect MS detector from salt contamination. The instrument was tuned for each molecule to obtain the best measurement conditions.

Standard for calibration curve preparation were diluted in 80% acetonitrile and stock solution was prepared in concentration 1 mg/mL. Four solutions in concentration 15, 10, 5 and 1 μg/mL were prepared by adding appropriate amount of the stock solution into transport buffer (HBSS containing 10 mM HEPES [pH 7.4]) to final volume 1 mL. Apical samples were filled up by the same buffer to final volume 1 mL. Into both apical and basolateral samples 10 μL of acetonitrile were added and samples were sonicated for 15 min. After this procedure, standard solvents and samples were loaded into autosampler and 20 μL each sample were injected onto column. Each sample was measured 3 times and a blank was applied after this block. Collected data were processed in Qual Browser program version 2.0.7. Chromatogram for given mass with 0.5 Da window was extracted (XIC), smoothened and area under the curve was calculated. Sequentially results from repetition were averaged and five point's calibration curve 'area-to-concentration' was obtained. Calculated averaged area for samples was used to determine concentration using equation from the calibration curve.

2.7. Blood-brain-barrier permeability – spontaneous locomotor activity test

2.7.1. Animals

Naive adult male Balb/c mice (39, breeding colony of Institute of Physiology Academy of Science of the Czech Republic, Prague, Czech Republic), 15 weeks old and weighing 25–35 g, were used for the experiments. The animals were housed in groups of five in the plastic cages (external dimensions in mm: 365 × 205 × 140; floor area 528 cm^2; height 14 cm; Zoonlab GmbH, Germany). The mice had *ad libitum* access to the laboratory chow and water, except during behavioral experiments, and they were kept in a regulated environment (22 °C, 50% humidity) under a 12 h light/dark cycle (lights on at 06:00 a.m.). The animals were habituated to the experimental room. Experiments were approved by the Animal Care and Use Committee of the Institute of Physiology of the Academy of Sciences of the Czech Republic and by The Central Committee of the Academy of Sciences of the Czech Republic (number approval 095/2010). The Institute of Physiology possesses NIH Statement of Compliance with Standards for Human Care and Use of Laboratory Animals No. A5820-01 valid till 1/31/2014. Animal care and experimental procedures are

PDF-XChange Editor
KOUPIT plnou verzi!
www.pdfxchange.cz

conducted in accordance with the guidelines of the European Community Council directives 86/609/EEC.

2.7.2. Spontaneous locomotor activity test

Compounds PAS, PAG, **1**–**4**, and 1% Tween 80, respectively, used as vehicle, were injected *i.p.* at doses of 100 mg/kg at a volume of 10 mL/kg. The animals were placed individually into the center of circular open-field arena (82 cm in diameter), located in a soundproof room. The locomotor activity in the open field was assessed by placing the animal in the arena immediately after *i.p.* application and their movement was recorded using a video tracking system (iTrack, USA). The locomotor activity, expressed as a total distance traveled in 10 min intervals was analyzed.

2.8. Hepatotoxicity Screening

2.8.1. HepG2 cell culture

HepG2 cells (ATCC®, UK) were grown in RPMI Eaglés MEM medium, supplemented with 10% (v/v) fetal calf serum, 200 μg/mL of streptomycin, 200 U/mL of penicillin G and 4 mM glutamine. They were cultured under a humidified atmosphere containing 5% CO_2 at 37 °C.

2.8.2. Cytotoxicity evaluation

The cytotoxicity of the tested compounds was assessed with use of XTT cell proliferation kit II (Roche Diagnostics GmbH, Mannheim, Germany) according to the manufacturer's instructions. Briefly HepG2 cells were seeded in a 96-well plate at a density of 13,500 cells per well. After 24 h, the tested neurosteroids were added to the culture media and incubated for 72 h before the XTT dye was added. The absorbance at 495 nm was recorded after 1 h incubation with the dye. IC_{50} values were determined by GraphPad Prism version 5.00 for Windows (GraphPad Software, La Jolla, CA, USA).

2.8.3. Detection of reactive oxygen species (ROS)

The effect of neurosteroids on oxidative stress was determined using general oxidative stress indicator CM-H_2DCFDA (ThermoFisher Scientific, Waltham, MA, USA) according to the manufacturer's instructions. Briefly HepG2 cells were seeded in a 96-well plate at a density of 13,500 cells per well. After 24 h, the tested neurosteroids were added to the culture media and incubated for 72 h. Subsequently, cells were washed with HBSS, treated with 100 μL of 1 μM CM-H_2DCF-DA solution in HBSS and incubated for 1 h in the dark at 37 °C. Finally, cells were washed three times with HBSS and the fluorescence was measured using 495 nm excitation and 527 nm emission in *fluorescence* microplate reader (Cytation 3, Winooski, VT, *USA*). IC_{50} values were determined by GraphPad Prism version 5.00 for Windows (GraphPad Software, La Jolla, CA, USA).

3. Results and discussion

3.1. Chemistry

Compounds **1** and **2** were prepared according to literature [17], by treatment of commercially available 3α-hydroxy-5β-androstane with oxalyl chloride and Meldrum's acid, respectively. Synthesis of compounds **3** and **4** is summarized in Scheme 1. Commercially available 3β-hydroxy-5β-androstane (**5**) was treated with phtalimide and triphenylphosphine affording compound **6** with inverse configuration at C-3 in 87% yield. Deprotection of amino group was achieved by reflux of compound **6** with hydrazine hydrate that gave 3α-amino derivative **7** in 65% yield. Coupling of compound **7** with protected L-glutamic and L-aspartic acids, respectively gave compounds **8** and **9** in 99% yield. Deprotection of benzyl ether protecting group was achieved by hydrogenation catalyzed by palladium on carbon (compound **10**, 65% yield and **11**, 98% yield). Then, treatment of Boc-protected glutamates **10** and **11** with trifluoroacetic acid gave desired products **3** and **4** in 91% and 92% yield, respectively. The structures of compounds **9**, **10**, and **11** were determined or confirmed by 1D- and 2D-NMR experiments. Structural assignment of proton and carbon signals was achieved combining 1D-^{1}H and 1D-^{13}C-APT (attached proton test) spectra with homonuclear 2D-H,H-COSY, 2D-H,H-ROESY and heteronuclear 2D-H,C-HSQC and 2D-H,C-HMBC spectra.

*3.2. Effect of PAS, PAG and compounds **1**–**4** on modulation of NMDARs*

The activities of PAS, PAG and compounds **1**–**4** on NMDARs were estimated using HEK293 cells co-transfected with cDNA encoding for the ratGluN1-1a and GluN2B subunits. The IC_{50} for the newly synthesized steroids was determined from a single dose of the steroid using the following formula:

$$IC_{50} = [compound] \times \sqrt[h]{\frac{1 - I_I}{I_I}},$$

where I_I is the relative degree of inhibition, [compound] is the steroid concentration used, and *h* stands for the Hill coefficient (fixed at 1.2). The results are summarized in Table 1.

Even though the PAG has been experimentally established as compound with excellent neuroprotective properties, the comparison of the IC_{50} values of PAS (IC_{50} = 24.6 ± 5.3 μM) with PAG (IC_{50} = 51.7 ± 8.6 μM) shows ~2-fold increase in IC_{50} values. However, comparison of the IC_{50} values of PAS (IC_{50} = 24.6 ± 5.3 μM) with compounds **1** and **2** gave ~1.1 and 1.5-fold decrease in IC_{50} values. Moreover, the IC_{50} values of compounds **3** and **4** gave ~24 and 17.5-fold decrease in IC_{50} values, respectively, with respect to amide-based analogues **1** and **2**. These results clearly indicate that the replacement of ester moiety as a linker to steroid skeleton with amide moiety has a positive effect on the ability of neurosteroid to inhibit NMDAR-mediated currents. Therefrom, we conclude that the amino moiety on the C-3 linker is crucial for significantly improved ability of compounds **3** and **4** to inhibit the NMDAR-mediated currents.

3.3. Computational estimate of lipophilicity

The lipophilic character of compounds **1**–**4** was estimated by the logP and logD coefficients. The logP is defined as the logarithm of the ratio of neutral solute concentrations in *n*-octanol and water. On the other hand, the logD is the logarithm of the ratio of the sum of the concentrations of the neutral and the ionized form of the solute in each of the two phases and thus is depending on pH. As compounds **1**–**4** can be both ionized and neutral, the description of the lipophilicity by the logD is more appropriate [30]. The results are summarized in Table 3 and discussed in correlation with Caco-2 permeability data in the following section.

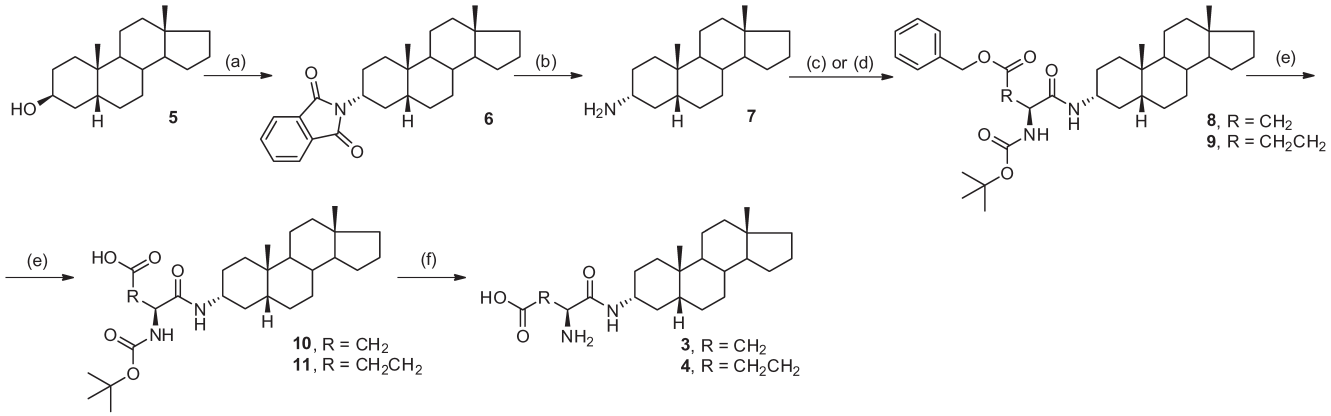
3.4. Caco-2 permeability assay

The permeability of PAS, PAG, and compounds **1**–**4** was evaluated using the Caco-2 cell monolayer as a model of the intestinal mucosa. The apparent permeability coefficient (P_{app}, cm/s) was calculated using the following equation:

$$P_{app} = (C_{baso} * 3.3)/(T * A * C_0)$$

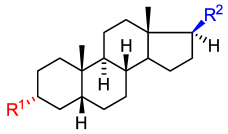
where C_{baso} = concentration of PAS or PAG or compounds **1**–**4** in basolateral chamber (μM), T = incubation time, A = surface area filter insert (0.31 cm^2), and C_0 = initial concentration (μM).

PDF-XChange Editor
KOUPIT plnou verzi!
www.pdfxchange.cz



Scheme 1. Synthesis of compound **3** and **4**: (a) phtalimide, PPh_3, THF, 0 °C to rt, 19 h; (b) NH_2NH_2, MeOH, reflux, 4 h; (c) DIPEA, Boc-Asp(OBzl)-OH, benzene, DMAP, DCC, rt, 5 h; (d) DIPEA, Boc-Glu(OBzl)-OH, benzene, DMAP, DCC, rt, 18 h; (e) Pd/C, H_2, MeOH, rt, 7 h; (f) TFA, CH_2Cl_2, rt, 16 h.

Table 1
Effect of PAS, PAG, and compounds **1–4** on current responses of GluN1/GluN2B receptors in HEK293 cells to glutamate.



Compound	R^1	R^2	IC_{50} (μM) (h = 1.2), (*n*)	Steroid conc. (μM)
PAS (Pregnanolone Sulfate)[a]	OSO_3pyH	(C=O) CH_3)	24.6 ± 5.3 (*n* = 5)	100
PAG (Pregnanolone Glutamate)[a]	HOOC-$(CH_2)_2$CH (NH_2)-COO	(CO) CH_3)	51.7 ± 8.6 (*n* = 5)	200
1	HOOC-CONH	H	21.7 ± 4.8 (*n* = 7)	10
2	HOOC-CH_2-CONH	H	15.4 ± 3.5 (n = 6)	10
3	HOOC-CH_2CH (NH_2)-CONH	H	1.0 ± 0.2 (*n* = 6)	3
4	HOOC-$(CH_2)_2$CH (NH_2)-CONH	H	1.4 ± 0.2 (*n* = 6)	3

[a]See the Ref. [7].

Table 2
Permeability limit values according to literature.

Apparent permeability in Caco-2 cells		
Low permeability limit values	High permeability limit values	Reference
$\leqslant 1 \times 10^{-7}$ cm/s	$\geqslant 1 \times 10^{-6}$ cm/s	[33]
$>1 \times 10^{-5}$ cm/s	$>7 \times 10^{-5}$ cm/s	[34]
	$>3 \times 10^{-5}$ cm/s	[35]

Permeability limit values were proposed by several authors using Caco-2 cells (Table 2) [32].

The lipophilicity is often an important factor affecting biological and physicochemical properties (e.g. solubility, absorption, plasma protein binding, etc.) of steroidal compounds [36]. Moreover, the obtained data from the permeability assay can be influenced by solubility of particular compound and their possible adhering to plastic or accumulation in the cell due to metabolism. Therefore, we have collected the aliquots from both apical and basolateral chambers to calculate the recovery coefficient (% recovery) the following equation:

$$\%\ \text{recovery} = 100 \times (C_d + C_a)/C_0$$

where C_d and C_a represent total concentrations of compound in donor and acceptor compartment, respectively, at the end of experiment. C_0 is the donor compartment concentration at time zero.

As PAG and compounds **1–4** bear carboxylic moiety in their structure, we have considered the possibility of passive, pH-dependent mechanism of transport in the experimental setting. Such mechanism has been already described for several anionic compounds (e.g. atorvastatin, pravastatin, fexofenadine, etc.) [37] of lipophilic character that is comparable to our tested compounds. In addition, it is assumed that the steroidal molecules are predominantly transported passively with emphasis on their absorption affecting the membrane fluidity [38]. Moreover, the active or efflux transport were not described as the prevailing form of transport. Therefore, concentration-dependency and pH-gradient in apical and basolateral chambers (pH 5.5/7.4 vs. pH 7.4/7.4) [39] were tested using PAG as representative for compounds **1–4**. The results are summarized in Table 3. The Caco-2 study revealed that the PAS is permeable with P_{app} coefficients under *iso*-pH 7.4 (100 μM) of 0.94×10^{-6} cm/s with recovery coefficient of 92%. Comparison with P_{app} coefficient of PAG under *iso*-pH 7.4 (100 μM) showed significant improvement of permeability to P_{app} coefficient of ~9.4-folds higher (8.8×10^{-6} cm/s) with respect to PAS and therefore, PAG was established as highly permeable compared to PAS. Such result does not reflect more lipophilic character of PAG (logD = 1.21) as compared to PAS (logD = 1.67) and rather indicate the significance of the C-3 glutamate moiety affecting the physicochemical properties. We hypothesize that improved permeability of PAG might be provoked by bulkier glutamate moiety that would be more water-exposed on the water-membrane interface in addition to larger conformational freedom of the glutamate group of PAG than that of sulfate in PAS. Almost a 30-folds decrease of P_{app} coefficient was measured for PAG under *iso*-pH 7.4 at decreased concentration of 25 μM ($P_{app} = 0.31 \times 10^{-6}$ cm/s, recovery coefficient = 64.2%).

In order to enhance generally weak permeability of organic carboxylic acids and to mimic acidic microclimate of small intestine, the pH was adjusted to 5.5 on the apical side. Moreover, the pH gradient should ameliorate the function of efflux transporters present in the Caco-2 cell lines [39,40]. This approach afforded P_{app} coefficients $P_{app} = 4.4 \times 10^{-6}$ cm/s at 100 μM and $P_{app} = 0.22 \times 10^{-6}$ cm/s at 25 μM, respectively) while the recovery coefficients decreased significantly (16% at 100 μM and 31.3% at 25 μM, respectively). We conclude that the physiological *iso*-pH 7.4

PDF-XChange Editor
KOUPIT plnou verzi!
www.pdfxchange.cz

Table 3
Permeability data from Caco-2 permeability assay and computational estimate of lipophilicity for PAS, PAG, and compounds **1**–**4**.

Steroid	Conc. of steroid applied to apical side	Api pH/Baso pH	Permeability × 10^{-6} (cm/s)	Recovery (%)	LogP	LogD
PAS	100	7.4/7.4	0.94 ± 0.082	92.0 ± 3.2	2.93	1.67
PAG	100	7.4/7.4	8.82 ± 0.885	47.7 ± 4.3	3.09	1.21
PAG	25	7.4/7.4	0.31 ± 0.044	64.2 ± 7.5		
PAG	100	5.5/7.4	4.40 ± 0.001	16.0 ± 4.8		
PAG	25	5.5/7.4	0.22 ± 0.043	31.3 ± 1.5		
1	100	7.4/7.4	1.70 ± 0.480	15.0 ± 2.8	5.41	0.67
1	25		N/A[a]	N/A[a]		
2	100	7.4/7.4	5.41 ± 0.136	11.0 ± 0.9	5.10	0.96
2	25		0.22 ± 0.060	28.2 ± 5.4		
3	100	7.4/7.4	0.24 ± 0.112	48.7 ±	4.24	0.86
3	25		N/A[a]	N/A[a]		
4	100	7.4/7.4	0.58 ± 0.049	51.6 ± 4.5	3.86	1.14
4	25		5.85 ± 2.4	25.1 ± 3.6		

[a] Compound **1** and **3**, respectively nor their metabolites were not detected in the basolateral chamber samples.

gradient afford significantly higher permeability additionally to notably higher recovery coefficients.

For screening of compounds **1**–**4**, the conditions of *iso*-pH 7.4 at concentration 100 μM and 25 μM were used. The P_{app} coefficients of compounds **2** at 100 μM concentration and compound **4** at 25 μM concentration rather resemble the results of PAG. The reasons for the significant divergence of the P_{app} value for compound **2** and **4** remains conjectural; the correlation of the logD values does not reflect neither the P_{app} value, nor the recovery coefficient (%). We conclude that the absolute value of P_{app} coefficient for particular compound will be affected by combination of several factors, including physicochemical properties of the molecule – e.g. solubility, conformational change during the transfer of the molecule into the site of action, solvation free energy (ΔG_{solv}) that estimates the behavior of the single-molecules in water and in *n*-octanol and therefore represents the membrane environment, etc. To confirm this hypothesis, the extended screening of physicochemical properties of these compounds and their analogues bearing C-3 linker of various length is currently ongoing.

3.5. Blood-brain-barrier permeability – spontaneous locomotor activity test

Mice were administered with vehicle or compounds **1**–**4** at the dose of 100 mg/kg immediately prior to behavioral testing in open field. The saline was applied in order to compare its effect to Tween 80. Intact mice received no treatment. Note that Tween 80 application decreased locomotion during the first 10-min interval when compared to intact. No significant difference between saline and Tween 80 was demonstrated when total distance walked during 50-min experiment was analyzed. The application of PAS, PAG, and compounds **1**–**4** (Fig. 4) resulted in reduced locomotion observable during the first 10-min interval of 50-min test with the exception of compound **3**, which has less pronounced effect. Surprisingly, the sedative effect of compound **3** was delayed 20 min and significantly reduced locomotion was not detected during first 10 min when compared to Tween 80. Note that the hypolocomotion or even sedation induced by administration of compounds **2** and **4** do correlate with the permeability data obtained by Caco-2 assay; the strongest sedative effect was observed for compounds **2** and **4** that have significantly higher P_{app} coefficient than compounds **1** and **3** (Table 3). Conversely, compound **3** has significantly lower P_{app} coefficient than compounds **2** and **4** which reflects less pronounced sedative effect as compared with compounds **1**, **2**, and **4**. Intact mice significantly differed from all drug-treated groups ($p < 0.0001$). Vehicle treated mice (saline or Tween 80) significantly differed from all neurosteroid derivative treated mice ($p < 0.0001$) with the two exceptions. Difference in

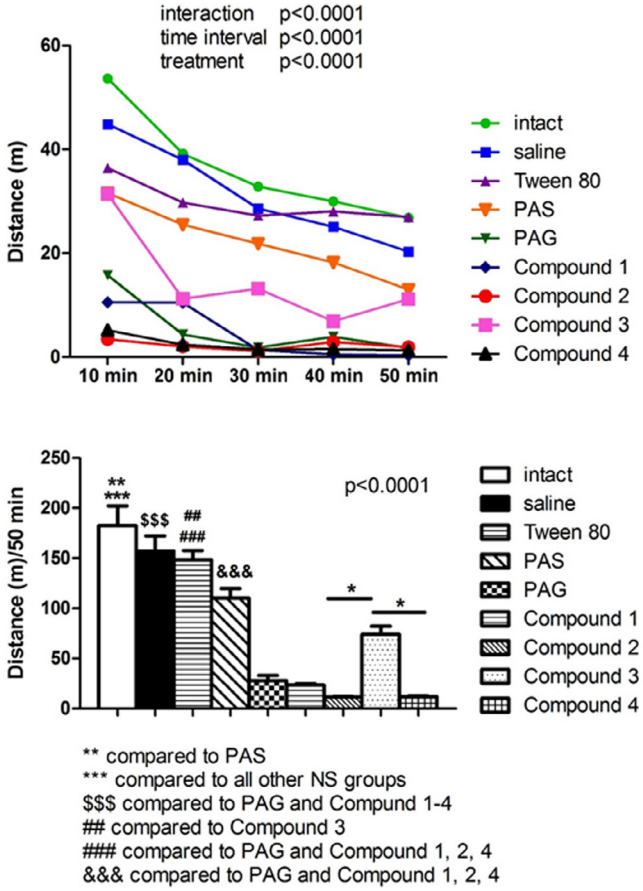


Fig. 4. Spontaneous locomotor activity test of PAS, PAG, and compounds **1**–**4**.

total distance travelled between both vehicles and Compound **3** was less prominent ($p < 0.001$) and PAS did not significantly differed from either vehicle. There was no significant difference between intact animals and either saline or Tween 80 treated mice. To conclude, all new amide-based inhibitors of NMDARs (**1**–**4**) displayed ability to induce hypolocomotion/sedation which indicate their ability to cross blood-brain-barrier.

3.6. Hepatotoxicity screening

The early detection of drug-induced hepatotoxicity is essential limiting factor for rejection of candidate compounds during the later stages of drug development. Therefore, the HepG2 cells has

PDF-XChange Editor
KOUPIT plnou verzi!
www.pdfxchange.cz

Table 4
The cytotoxicity and ROS induced by neurosteroids in HepG2 cells.

Compound	Cytotoxicity IC_{50} (μM)[a]	ROS induction IC_{50} (μM)[b]
Pregnanolone sulfate (PAS)	>200	>200
Pregnanolone glutamate (PAG)	62 ± 9	80 ± 11
1	42 ± 7	52 ± 6
2	148 ± 14	165 ± 18
3	>200	>200
4	65 ± 5	71 ± 9
Amiodarone	4.9 ± 0.2	6.0 ± 0.1
Nimesulide	2.2 ± 0.3	3.5 ± 0.5

[a] IC_{50} values indicate the concentration causing 50% decrease in cells viability using XTT cytotoxicity test (calculated using the non-linear regression method by GraphPad Prism).
[b] IC_{50} values indicate the concentration causing 50% increase of ROS detected using CM-H_2DCFDA (calculated using the non-linear regression method by GraphPad Prism).

been established as a hepatotoxicity screening model of new prospective drugs during "in *vitro*" testing phase [41,42]. As such, we have assessed potential hepatotoxicity of compounds PAS, PAG, and **1**–**4** using 72 h XTT assay on HepG2 cells (Table 4). Further, the involvement of reactive oxygen species (ROS) in the steroid-toxicity was evaluated.

Compounds PAS, **2**, and **3** did not show observable adverse effect on HepG2 cells nor ROS induction up to concentration of ~ 200 μM. Conversely, compounds PAG, **1** and **4** showed week and comparable cytotoxic effect on HepG2 cell line with IC_{50} = 62 μM, IC_{50} = 42 μM, and IC_{50} = 65 μM, respectively (Table 4). In parallel, the reactive oxygen species induction was observed (Table 4). We hypothesize that the cytotoxic effect of compounds PAG and **4** can be associated with the glutamate moiety, as glutamate has been reported to induce lipid peroxidation, decrease reduced glutathione and increase activities of catalase and superoxide dismutase in the liver of animals [43]. The hemioxalate moiety (structural feature of compound **1**) has been connected with lipid peroxidation [44]. However, in normal liver cells the toxic effect can be weaker or even none. Most cancer cells, in fact, are under oxidative stress associated with increased metabolic activity and production of ROS. These biochemical characteristics make the cancer cells vulnerable to damage by additional oxidative stress [45]. Shortening of chain from glutamate to aspartate as in case of compound **3**, and extension of chain from oxalate to malonate (compound **2**) did lead to loss of cytotoxicity without decrease of inhibitory activity.

Finally, we have compared the cytotoxic effect of PAS, PAG, and **1**–**4** to amiodarone and nimesulide (IC_{50} = 4.9 μM, and IC_{50} = 2.2 - μM, respectively). Amiodarone has been used as antiarrhythmic drug. Despite the fact that the chronic use of amiodarone is associated with varying degrees of hepatotoxicity [46], amiodarone was approved by the Food and Drug Administration for the treatment of arrhythmias [47]. Nimesulide is anti-inflammatory drug with analgesic and antipyretic properties. Even though, it is available in many countries worldwide, it is not marketed in United States due to its hepatotoxicity [48,49]. According to these results, we conclude that compounds **1**–**4** showed minimal or no adverse hepatic effect.

4. Conclusions

We have identified new class of NMDARs inhibitors bearing new amide-based structural motif affording proportionate biological properties in several aspects with respect to endogenous pregnanolone sulfate and its synthetic analogue pregnanolone glutamate. First, the ability of these compounds (**1**–**4**) to inhibit the NMDAR-mediated currents was significantly improved specifically in case of compounds **3** and **4** with respect to PAS and PAG. Second, the evaluation of permeability profile of compounds **1**–**4** using Caco-2 assay showed commensurate properties while taking into consideration the modified lipophilicity. Third, we have demonstrated the ability of compounds **1**–**4** to cross blood-brain-barrier using spontaneous locomotor activity test *in vivo*. Finally, we have demonstrated that compounds **1**–**4** have minimal or no adverse hepatic effect. As such, we conclude that these amide-based inhibitors of NMDARs represent a promising tool in development of potential steroidal therapeutics for the treatment of various neurological diseases. Therefore, further investigation of biological properties of compounds **1**–**4** is currently ongoing. These studies do include e.g. locomotor activity in the open-field test in dose 0.1–10 mg/kg, in parallel with their effect on reflexes, behavior and possible signs of side effects as well as animal models revealing neuroprotective properties of compounds **1**–**4** as it has been already done for PAG [12,14,16].

Acknowledgement

This work was supported by grant TE01020028 Center for Development of Original Drugs from the Technology Agency of the Czech Republic, Grant 303/12/1464 from the Grant Agency of the Czech Republic, research project of the RVO 67985823, the National Programme sustainability Ministry of Education (NPU I - LO1302), and by Ministry of Health of the Czech Republic, Grant NV15-29370A. The Czech Science Foundation (grant P208/12/G016) supported the computational study by M.N.

Appendix A. Supplementary data

Supplementary data associated with this article can be found, in the online version, at http://dx.doi.org/10.1016/j.steroids.2016.08.010.

References

[1] S.F. Traynelis, L.P. Wollmuth, C.J. McBain, F.S. Menniti, K.M. Vance, K.K. Ogden, K.B. Hansen, H. Yuan, S.J. Myers, R. Dingledine, D. Sibley, Glutamate receptor ion channels: structure, regulation, and function, Pharmacol. Rev. 62 (2010) 405–496.
[2] S.I. Mota, I.L. Ferreira, A.C. Rego, Dysfunctional synapse in Alzheimer's disease – a focus on NMDA receptors, Neuropharmacology 76 Pt A (2014) 16–26.
[3] M. Sheng, B.L. Sabatini, T.C. Südhof, Synapses and Alzheimer's disease, Cold Spring Harbor Perspect. Biol. 4 (5) (2012) a005777.
[4] A. Doble, The role of excitotoxicity in neurodegenerative disease: implications for therapy, Pharmacol. Ther. 81 (1999) 163–221.
[5] D.C. Rotaru, H. Yoshino, D.A. Lewis, G.B. Ermentrout, G. Gonzalez-Burgos, Glutamate receptor subtypes mediating synaptic activation of prefrontal cortex neurons: relevance for schizophrenia, J. Neurosci. 31 (2011) 142–156.
[6] X. Zhou, Q. Ding, Z. Chen, H. Yun, H. Wang, Involvement of the GluN2A and GluN2B subunits in synaptic and extrasynaptic N-methyl-D-aspartate receptor function and neuronal excitotoxicity, J. Biol. Chem. 288 (2013) 24151–24159.
[7] J. Borovska, V. Vyklicky, E. Stastna, V. Kapras, B. Slavikova, M. Horak, H. Chodounska, L. Vyklicky, Access of inhibitory neurosteroids to the NMDA receptor, Br. J. Pharmacol. 166 (2012) 1069–1083.
[8] V. Vyklicky, B. Krausova, J. Cerny, A. Balik, M. Zapotocky, M. Novotny, K. Lichnerova, T. Smejkalova, M. Kaniakova, M. Korinek, M. Petrovic, P. Kacer, M. Horak, H. Chodounska, L. Vyklicky, Block of NMDA receptor channels by endogenous neurosteroids: implications for the agonist induced conformational states of the channel vestibule, Sci. Rep. 5 (2015) 10935.
[9] C.E. Weaver, P. Marek, M. Park-Chung, S.W. Tam, D.H. Farb, Neuroprotective activity of a new class of steroidal inhibitors of the N-methyl-D-aspartate receptor, Proc. Natl. Acad. Sci. USA 94 (1997) 10450–10454.
[10] E. Stastna, H. Chodounska, V. Pouzar, V. Kapras, J. Borovska, O. Cais, L. Vyklicky, Synthesis of C3, C5 and C7 pregnane derivatives and their effect on NMDA receptor responses in cultured rat hippocampal neurons, Steroids 74 (2009) 256–263.
[11] E. Stastna, H. Chodounska, V. Pouzar, J. Borovska, L. Vyklicky, Synthesis of Pregnane 3-carboxylic acids via Pd-catalyzed alkoxycarbonylation and their effect on NMDA receptor activity, Collect. Czech. Chem. Commun. 76 (2011) 1141–1161.

PDF-XChange Editor
KOUPIT plnou verzi!
www.pdfxchange.cz

[12] V. Vyklicky, T. Smejkalova, B. Krausova, A. Balik, M. Korinek, J. Borovska, M. Horak, M. Chvojkova, L. Kleteckova, K. Vales, J. Cerny, M. Nekardova, H. Chodounska, E. Kudova, L. Vyklicky, Preferential inhibition of tonically over phasically activated NMDA receptors by pregnane derivatives, J. Neurosci. 36 (2016) 2161–2175.
[13] P.A. Lapchak, The neuroactive steroid 3-alpha-ol-5-beta-pregnan-20-one hemisuccinate. A selective NMDA receptor antagonist improves behavioral performance following spinal cord ischemia, Brain Res. 997 (2004) 152–158.
[14] L. Rambousek, V. Bubenikova-Valesova, P. Kacer, K. Syslova, J. Kenney, K. Holubova, V. Najmanova, P. Zach, J. Svoboda, A. Stuchlik, H. Chodounska, V. Kapras, E. Adamusova, J. Borovska, L. Vyklicky, K. Vales, Cellular and behavioural effects of a new steroidal inhibitor of the N-methyl-D-aspartate receptor 3α5β-pregnanolone glutamate, Neuropharmacology 61 (2011) 61–68.
[15] K. Holubova, T. Nekovarova, J. Pistovcakova, A. Sulcova, A. Stuchlik, K. Vales, Pregnanolone glutamate, a novel use-dependent NMDA receptor inhibitor, exerts antidepressant-like properties in animal models, Front. Behav. Neurosci. 8 (2014) 130.
[16] L. Kleteckova, G. Tsenov, H. Kubova, A. Stuchlik, K. Vales, Neuroprotective effect of the 3α5β-pregnanolone glutamate treatment in the model of focal cerebral ischemia in immature rats, Neurosci. Lett. 564 (2014) 11–15.
[17] E. Kudova, H. Chodounska, V. Kapras, L. Vyklicky, K. Vales, U. Jahn, Amphiphilic compounds with neuroprotective properties, Eur. P. Appl. (2016). WO2016029888 A1.
[18] E. Kudova, H. Chodounska, B. Slavikova, M. Budesinsky, M. Nekardova, V. Vyklicky, B. Krausova, P. Svehla, L. Vyklicky, A new class of potent N-methyl-D-aspartate receptor inhibitors: Sulfated neuroactive steroids with lipophilic D-ring modifications, J. Med. Chem. 58 (2015) 5950–5966.
[19] M. Petrovic, M. Sedlacek, M. Horak, H. Chodounska, L. Vyklicky, 20-oxo-5beta-pregnan-3alpha-yl sulfate is a use-dependent NMDA receptor inhibitor, J. Neurosci. 25 (2005) 8439–8450.
[20] F. Faucher, L. Cantin, V. Luu-The, F. Labrie, R. Breton, The crystal structure of human Δ4-3-ketosteroid 5β-reductase defines the functional role of the residues of the catalytic tetrad in the steroid double bond reduction mechanism, Biochemistry 47 (2008) 8261–8270.
[21] W.L. DeLano, The PyMOL molecular graphics system, 2002.
[22] R. Ahlrichs, M. Bär, M. Häser, H. Horn, C. Kölmel, Electronic structure calculations on workstation computers: the program system turbomole, Chem. Phys. Lett. 162 (1989) 165–169.
[23] P. Jurečka, J. Černý, P. Hobza, D.R. Salahub, Density functional theory augmented with an empirical dispersion term. Interaction energies and geometries of 80 noncovalent complexes compared with ab initio quantum mechanics calculations, J. Comput. Chem. 28 (2007) 555–569.
[24] A. Klamt, G. Schüürmann, COSMO: a new approach to dielectric screening in solvents with explicit expressions for the screening energy and its gradient, J. Chem. Soc. Perkin Trans. 2 (1993) 799–805.
[25] J. Řezáč, J. Fanfrlík, D. Salahub, P. Hobza, Semiempirical quantum chemical PM6 method augmented by dispersion and H-bonding correction terms reliably describes various types of noncovalent complexes, J. Chem. Theory Comput. 5 (2009) 1749–1760.
[26] J. Řezáč, P. Hobza, Advanced corrections of hydrogen bonding and dispersion for semiempirical quantum mechanical methods, J. Chem. Theory Comput. 8 (2011) 141–151.
[27] A.V. Marenich, C.J. Cramer, D.G. Truhlar, Universal solvation model based on solute electron density and on a continuum model of the solvent defined by the bulk dielectric constant and atomic surface tensions, J. Phys. Chem. B 113 (2009) 6378–6396.
[28] M. Frisch, G. Trucks, H.B. Schlegel, G. Scuseria, M. Robb, J. Cheeseman, G. Scalmani, V. Barone, B. Mennucci, G. Petersson, Gaussian 09, Revision A. 02, Gaussian, Inc., Wallingford, CT, 200, 2009.
[29] M. Kolář, J. Fanfrlík, M. Lepšík, F. Forti, F.J. Luque, P. Hobza, Assessing the accuracy and performance of implicit solvent models for drug molecules: conformational ensemble approaches, J. Phys. Chem. B 117 (2013) 5950–5962.
[30] M. Kah, C.D. Brown, LogD: lipophilicity for ionisable compounds, Chemosphere 72 (2008) 1401–1408.
[31] M. ChemAxon, ChemAxon, in Ltd, 2015.
[32] J.H. Lin, A.Y. Lu, Role of pharmacokinetics and metabolism in drug discovery and development, Pharmacol. Rev. 49 (1997) 403–449.
[33] P. Artursson, J. Karlsson, Correlation between oral drug absorption in humans and apparent drug permeability coefficients in human intestinal epithelial (Caco-2) cells, Biochem. Biophys. Res. Commun. 175 (1991) 880–885.
[34] W. Rubas, N. Jezyk, G.M. Grass, Comparison of the permeability characteristics of a human colonic epithelial (Caco-2) cell line to colon of rabbit, monkey, and dog intestine and human drug absorption, Pharm. Res. 10 (1993) 113–118.
[35] B.H. Stewart, O.H. Chan, R.H. Lu, E.L. Reyner, H.L. Schmid, H.W. Hamilton, B.A. Steinbaugh, M.D. Taylor, Comparison of intestinal permeabilities determined in multiple in vitro and in situ models: relationship to absorption in humans, Pharm. Res. 12 (1995) 693–699.
[36] F. Faassen, J. Kelder, J. Lenders, R. Onderwater, H. Vromans, Physicochemical properties and transport of steroids across Caco-2 Cells, Pharm. Res. 20 (2003) 177–186.
[37] M. Koljonen, K. Rousu, J. Cierny, A.M. Kaukonen, J. Hirvonen, Transport evaluation of salicylic acid and structurally related compounds across Caco-2 cell monolayers and artificial PAMPA membranes, Eur. J. Pharm. Biopharm. 70 (2008) 531–538.
[38] H.R. Lamche, P.T. Silberstein, A.C. Knabe, D.D. Thomas, H.S. Jacob, D.E. Hammerschmidt, Steroids decrease granulocyte membrane fluidity, while phorbol ester increases membrane fluidity. Studies using electron paramagnetic resonance, Inflammation 14 (1990) 61–70.
[39] S. Neuhoff, A.L. Ungell, I. Zamora, P. Artursson, PH-Dependent passive and active transport of acidic drugs across Caco-2 cell monolayers, Eur. J. Pharm. Sci. 25 (2005) 211–220.
[40] L. Laitinen, H. Kangas, A.M. Kaukonen, K. Hakala, T. Kotiaho, R. Kostiainen, J. Hirvonen, N-in-one permeability studies of heterogeneous sets of compounds across Caco-2 cell monolayers, Pharm. Res. 20 (2003) 187–197.
[41] H.H.J. Gerets, E. Hanon, M. Cornet, S. Dhalluin, O. Depelchin, M. Canning, F.A. Atienzar, Selection of cytotoxicity markers for the screening of new chemical entities in a pharmaceutical context: a preliminary study using a multiplexing approach, Toxicol. In Vitro 23 (2009) 319–332.
[42] W.F.P.M. Van den Hof, M.L.J. Coonen, M. van Herwijnen, K. Brauers, W.K.W.H. Wodzig, J.H.M. van Delft, J.C.S. Kleinjans, Classification of hepatotoxicants using HepG2 cells: a proof of principle study, Chem. Res. Toxicol. 27 (2013) 433–442.
[43] O.O. Onyema, E.O. Farombi, G.O. Emerole, A.I. Ukoha, G.O. Onyeze, Effect of vitamin E on monosodium glutamate induced hepatotoxicity and oxidative stress in rats, Indian J. Biochem. Biophys. 43 (2006) 20–24.
[44] R. Selvam, T. Bijikurien, Induction of lipid peroxidation by oxalate in experimental rat urolithiasis, J. Biol. Sci. 121 (1987) 267–373.
[45] P. Huang, L. Feng, E.A. Oldham, M.J. Keating, W. Plunkett, Superoxide dismutase as a target for the selective killing of cancer cells, Nature 407 (2000) 390–395.
[46] W. Mattar, B. Juliar, I. Gradus-Pizlo, P.Y. Kwo, Amiodarone hepatotoxicity in the context of the metabolic syndrome and right-sided heart failure, J. Gastrointestinal Liver Dis. 18 (2009) 419–423.
[47] Drug Approval Package: Cordarone Amiodarone Hydrochloride Tablets, FDA Application No. 018972. U.S. Food and Drug Administration.
[48] U.A. Boelsterli, H.K. Ho, S. Zhou, K.Y. Leow, Bioactivation and hepatotoxicity of nitroaromatic drugs, Curr. Drug Metab. 7 (2006) 715–727.
[49] R. Tripathi, P. Tripathi, S.S. Pancholi, C.N. Patel, The genotoxic and cytotoxic effect of nimesulide in the mouse bone marrow, Drug Chem. Toxicol. 7 (2014) 255–260.

PDF-XChange Editor
KOUPIT plnou verzi!
www.pdfxchange.cz

frontiers in Molecular Neuroscience

ORIGINAL RESEARCH
published: 06 April 2018
doi: 10.3389/fnmol.2018.00110

Check for updates

Surface Expression, Function, and Pharmacology of Disease-Associated Mutations in the Membrane Domain of the Human GluN2B Subunit

*Vojtech Vyklicky[1†], Barbora Krausova[1†], Jiri Cerny[1], Marek Ladislav[1,2], Tereza Smejkalova[1], Bohdan Kysilov[1], Miloslav Korinek[1], Sarka Danacikova[1,2], Martin Horak[1], Hana Chodounska[3], Eva Kudova[3] and Ladislav Vyklicky[1]**

[1] Department of Cellular Neurophysiology, Institute of Physiology of the Czech Academy of Sciences (CAS), Prague, Czechia, [2] Department of Physiology, Faculty of Science, Charles University, Prague, Czechia, [3] Institute of Organic Chemistry and Biochemistry, Czech Academy of Sciences (CAS), Prague, Czechia

N-methyl-D-aspartate receptors (NMDARs), glutamate-gated ion channels, mediate signaling at the majority of excitatory synapses in the nervous system. Recent sequencing data for neurological and psychiatric patients have indicated numerous mutations in genes encoding for NMDAR subunits. Here, we present surface expression, functional, and pharmacological analysis of 11 *de novo* missense mutations of the human hGluN2B subunit (P553L; V558I; W607C; N615I; V618G; S628F; E657G; G820E; G820A; M824R; L825V) located in the pre-M1, M1, M2, M3, and M4 membrane regions. These variants were identified in patients with intellectual disability, developmental delay, epileptic symptomatology, and autism spectrum disorder. Immunofluorescence microscopy indicated that the ratio of surface-to-total NMDAR expression was reduced for hGluN1/hGluN2B(S628F) receptors and increased for for hGluN1/hGluN2B(G820E) receptors. Electrophysiological recordings revealed that agonist potency was altered in hGluN1/hGluN2B(W607C; N615I; and E657G) receptors and desensitization was increased in hGluN1/hGluN2B(V558I) receptors. The probability of channel opening of hGluN1/hGluN2B (V558I; W607C; V618G; and L825V) receptors was diminished ∼10-fold when compared to non-mutated receptors. Finally, the sensitivity of mutant receptors to positive allosteric modulators of the steroid origin showed that glutamate responses induced in hGluN1/hGluN2B(V558I; W607C; V618G; and G820A) receptors were potentiated by 59–96% and 406-685% when recorded in the presence of 20-oxo-pregn-5-en-3β-yl sulfate (PE-S) and androst-5-en-3β-yl hemisuccinate (AND-hSuc), respectively. Surprisingly hGluN1/hGluN2B(L825V) receptors were strongly potentiated, by 197 and 1647%, respectively, by PE-S and AND-hSuc. Synaptic-like responses induced by brief glutamate application were also potentiated and the deactivation decelerated. Further, we have used homology modeling based on the available crystal structures of GluN1/GluN2B NMDA receptor followed by molecular dynamics simulations to try to relate the functional consequences of mutations to structural changes. Overall, these data suggest that *de novo* missense mutations of the hGluN2B subunit located

OPEN ACCESS

Edited by:
Argentina Lario Lago, University of California, San Francisco, United States

Reviewed by:
Angelo Keramidas, The University of Queensland, Australia
Bodo Laube, Technische Universität Darmstadt, Germany

***Correspondence:**
Ladislav Vyklicky
ladislav.vyklicky@fgu.cas.cz

[†]Co-first authors.

Received: *15 December 2017*
Accepted: *20 March 2018*
Published: *06 April 2018*

Citation:
Vyklicky V, Krausova B, Cerny J, Ladislav M, Smejkalova T, Kysilov B, Korinek M, Danacikova S, Horak M, Chodounska H, Kudova E and Vyklicky L (2018) Surface Expression, Function, and Pharmacology of Disease-Associated Mutations in the Membrane Domain of the Human GluN2B Subunit. Front. Mol. Neurosci. 11:110. doi: 10.3389/fnmol.2018.00110

PDF-XChange Editor
KOUPIT plnou verzi!
www.pdfxchange.cz

in membrane domains lead to multiple defects that manifest by the NMDAR loss of function that can be rectified by steroids. Our results provide an opportunity for the development of new therapeutic neurosteroid-based ligands to treat diseases associated with hypofunction of the glutamatergic system.

Keywords: NMDA receptor, GluN2B, *de novo* missense mutations, neuropsychiatric disorder, neurosteroids

INTRODUCTION

The N-methyl-D-aspartate receptor (NMDAR) is a heteromeric ligand-gated ion channel permeable to Ca^{2+} that is expressed in neurons and glia. Virtually all brain and spinal cord circuits rely on excitation evoked by transient activation of NMDARs by glutamate, giving rise to NMDAR excitatory postsynaptic currents (EPSCs) to regulate physiological functions. In addition, NMDAR signaling is implicated in various forms of synaptic plasticity (Dingledine et al., 1999; Lynch, 2004; Traynelis et al., 2010; Huganir and Nicoll, 2013).

NMDAR is composed of two obligatory subunits (GluN1) and two variable ones, which can include either GluN2(A-D) or GluN3(A-B) (Traynelis et al., 2010). The GluN1 subunit is expressed throughout the central nervous system, whereas the four subtypes of GluN2(A-D) subunits have differential temporal and spatial expression patterns (Akazawa et al., 1994; Monyer et al., 1994). Expression of the GluN2B subunit (encoded by *GRIN2B* gene) dominates during rapid cortical synaptogenesis in late embryogenesis and early postnatal development, and its expression level starts to decline after birth in most brain regions (Hall et al., 2007). Several lines of evidence indicate that GluN2B subunit plays an important role in brain development, circuit formation, differentiation, and synaptic plasticity (Cohen and Greenberg, 2008). The importance of this subunit is stressed by the neonatal lethality of *GRIN2B* knock-out mice (Kutsuwada et al., 1996).

NMDAR dysfunction is implicated in a variety of nervous system disorders. Early studies indicated that glutamate triggers excitotoxicity (Olney, 1969). This form of neuronal death is dependent on calcium influx through NMDARs (Choi, 1987) and is implicated in neurological disorders such as neurodegenerative diseases, stroke, epilepsy, and traumatic brain injury (Parsons and Raymond, 2014).

Recent advances in high-throughput DNA sequencing have allowed examination of the prevalence of mutations in genes encoding NMDAR subunits among afflicted individuals. While the gene encoding for the GluN2B subunit is the most frequently *de novo* mutated *GRIN* gene in psychiatric and neurodevelopmental disorders, *de novo* mutations of *GRIN1* and *GRIN2A* genes encoding for GluN1 and GluN2A are less frequent and, interestingly, in *GRIN2C*, *GRIN3A*, and *GRIN3B*, only rare truncating mutations affecting both healthy individuals and patients suffering from neurodevelopmental disorders have been reported (Tarabeux et al., 2011; Soto et al., 2014).

GRIN2B variants—*de novo* nonsynonymous mutations, missense, nonsense, frame shift, or splice site mutations—were identified in individuals from patient cohorts with defined neurodevelopmental and psychiatric disorders such as intellectual disability, developmental delay, autism spectrum disorder, epileptic encephalopathy, schizophrenia, and to a lesser extent, attention deficit hyperactivity disorder, cerebral visual impairment, and Alzheimer's disease, as has been recently reviewed (Soto et al., 2014; Burnashev and Szepetowski, 2015; Hu et al., 2016). *GRIN2B* variants were found in the amino-terminal domain (ATD), ligand-binding domain (LBD), transmembrane domain (TMD), and carboxyl-terminal domain (CTD); rare *de novo* mutations in the ATD and CTD, but not the LBD and TMD domains, are present in the exomes of a large control population sample (Lek et al., 2016). This implies that mutations in the LBD and TMD domains may significantly alter the NMDAR channel properties. Indeed, in line with this hypothesis are results of functional examination of disease-causing mutations in the LBD (Adams et al., 2014; Lemke et al., 2014; Swanger et al., 2016). In the case of the TMD, the connections between genetic variation and consequences for the NMDAR channel function and/or trafficking are much less understood.

In this study, our goal was to elucidate the consequences of NMDAR mutations found in individuals diagnosed with neurodevelopmental disorders, in regard to the receptor-channel function and surface expression. We investigated 11 disease-associated variants in the *GRIN2B* gene located in the TMD region of the GluN2B subunit which are found as heterozygous *de novo* missense mutations. We found that some diheteromeric variants of the NMDAR have markedly decreased probability of channel opening and altered receptor surface expression. In addition, the effects of two structurally different neurosteroids, 20-oxo-pregn-5-en-3β-yl sulfate (PE-S; pregnenolone sulfate) and androst-5-en-3β-yl hemisuccinate (AND-hSuc), were tested as a pharmacological tool to correct the impaired function of mutated NMDARs.

METHODS

Transfection and Maintenance of Cells

Human embryonic kidney (HEK293T) cells (American Type Culture Collection, ATTC No. CRL1573, Rockville, MD, USA) were cultured in Opti-MEM I (Invitrogen, Carlsbad, CA, USA) with 5% fetal bovine serum (FBS; PAN Biotech, Aidenbach, Germany) at 37°C in 5% CO_2. One day before transfection, cells were plated in 24-well plates at a density of 2×10^5 cells per well. The next day, the cells were transfected with expression vectors containing human wild-type (WT) NMDAR subunits hGluN1-1a (GenBank accession no. NP_015566) and hGluN2B (GenBank accession no. NP_000825) (both genes were generous gifts from Prof. S. Traynelis, Emory University School of Medicine, Atlanta, GA) (Hedegaard et al., 2012) and green

PDF-XChange Editor
KOUPIT plnou verzi!
www.pdfxchange.cz

fluorescent protein (GFP; pQBI 25, Takara, Tokyo, Japan) genes. Briefly, equal amounts (0.2 μg) of cDNAs encoding for hGluN1, hGluN2B and GFP were mixed with 0.6 μL of MATra-A Reagent (IBA, Göttingen, Germany) and added to confluent HEK293T cells cultured in 24-well plates. After trypsinization, the cells were resuspended in Opti-MEM I containing 1% FBS supplemented with 20 mM $MgCl_2$, 3 mM kynurenic acid, 1 mM D,L-2-amino-5-phosphonovaleric acid and 1 μM ketamine, and plated on 30 mm collagen and poly-L-lysine-coated glass coverslips. Transfected cells were revealed by GFP epifluorescence.

Site-directed mutagenesis of the gene encoding for hGluN2B subunit was performed using the QuikChange II XL Site-Directed Mutagenesis Kit (Agilent Technologies, Santa Clara, CA, USA) in accordance with the instructions of the manufacturer using manually designed primers purchased from Sigma-Aldrich. DpnI-treated product of PCR reaction was transformed into ultracompetent XL10-Gold *E.coli* cells, positive clones were selected, and DNA plasmids were isolated using High-Speed Plasmid Mini Kit (Geneaid, New Taipei City, Taiwan) according to the manufacturer instructions. All mutations were verified by DNA sequencing (GenSeq, Benesov u Prahy, Czech Republic and/or Eurofins Genomics, Germany). Amino acids are numbered according to the full-length protein, including the signal peptide, with the initiating methionine as number 1.

Transport

Heterologous Cell Culture

African Green Monkey kidney fibroblast (COS-7) cells were grown in Minimum Essential Medium with Earle's salts (Thermo Fischer Scientific) with 10% FBS (v/v), as described previously (Kaniakova et al., 2012).

Expression Vectors

The human version of the cDNAs encoding for the full-length GluN1-1a subunit tagged with yellow fluorescent protein (YFP-hGluN1) was generated by the QuikChange II XL site-directed mutagenesis kit according to the manufacturer's instructions, and the construct was verified by DNA sequencing.

Immunofluorescence Microscopy

COS-7 or HEK293T cells were transfected in 12-well plates with a total of 1.8 μg of cDNAs (in case of co-transfection, equal amounts of cDNAs containing YFP-hGluN1 and hGluN2B subunits were used) and 4 μl Lipofectamine™ 2000 (Thermo Fischer Scientific), as described previously (Kaniakova et al., 2012). COS-7 cells were preferred for microscopy because they attach well to glass coverslips while extensive washing procedures are being performed. HEK293T cells that attach to glass less firmly were used to confirm differences in the surface expression observed on COS-7 cells. After 24–36 h, the cells were washed in PBS, and then incubated on ice for 10 min in blocking solution containing PBS and 10% normal goat serum (v/v). After this blocking step, the cells were labeled with primary rabbit anti-GFP (Merck Millipore; Burlington, MA, USA; 1:1,000) and secondary goat anti-rabbit Alexa Fluor® 555 (Thermo Fischer Scientific; 1:1,000) antibodies. Antibodies were diluted in the blocking solution and the cells were incubated with each antibody for 30 min. The cells were then washed twice in PBS, fixed in 4% paraformaldehyde in PBS (w/v) for 20 min, and mounted using ProLong Antifade reagent (Thermo Fischer Scientific). Images were taken on an Olympus Cell^R fluorescence microscope, and the intensity of the surface and total fluorescence signals was analyzed using ImageJ software, as described previously (Lichnerova et al., 2014).

Quantitative Assay of Surface and Total Expression

COS-7 cells were prepared as described in the Immunofluorescence Microscopy section. After 38–40 h, COS-7 cells were washed with PBS, fixed for 15 min in 4% paraformaldehyde (w/v) in PBS and incubated for 1 h in PBS containing 0.2% bovine serum albumin (BSA; w/v) without (surface expression) or with (total expression) 0.1% Triton X-100 (TX-100; v/v). Cells were incubated in a primary rabbit anti-GFP antibody (Millipore, Billerica, MA; 1:500 for surface expression and 1:1,000 for total expression) diluted in PBS with 0.2% BSA for 1 h. After being washed in PBS, cells were incubated with a secondary antibody (horseradish peroxidase-conjugated donkey anti-rabbit IgG; GE Healthcare, UK; 1:1,000) for 1 h and washed in PBS. Next, 400 μl of ortho-phenylenediamine (OPD; final concentration 0.4 mg/ml) dissolved in phosphate-citrate buffer containing sodium phosphate (Sigma, St. Louis, MO) was added to cells for 30 min (surface expression) or 15 min (total expression). The color reaction was terminated with 100 μl of 3 M HCl and the optical density was determined at 492 nm using a Personal Densitometer SI (GE Healthcare, Pittsburgh, PA). The average background signal measured from cells transfected with empty vector was subtracted from data obtained from cells transfected with NMDA receptor subunits.

Electrophysiological Recording

Whole-Cell Recordings

Experiments were performed 18–36 h after the end of transfection on cultured HEK293T cells transfected with vectors containing hGluN1/hGluN2B/GFP. Whole-cell voltage clamp current recordings were performed at room temperature (21–25°C) at a holding potential of −60 mV using a patch-clamp amplifier (Axopatch 200B; Molecular Devices, Sunnyvale, CA, USA) after a capacitance and series resistance (<10 MΩ) compensation of 80–90%. Data were collected (low-pass filtered at 2 kHz and sampled at 10 kHz) and analyzed using pClamp 10 (Molecular Devices).

Patch pipettes (3–5 MΩ) were filled with an intracellular solution (ICS) containing (in mM): 120 gluconic acid, 15 CsCl, 10 BAPTA, 10 HEPES, 3 $MgCl_2$, 1 $CaCl_2$, and 2 ATP-Mg salt (pH-adjusted to 7.2 with CsOH) and extracellular solution (ECS) contained the following (in mM): 160 NaCl, 2.5 KCl, 10 HEPES, 10 glucose, 0.2 EDTA, and 0.7 $CaCl_2$ (pH-adjusted to 7.3 with NaOH). Glycine (30 μM), an NMDAR co-agonist, was present in the control and test solutions. All steroid solutions were made from freshly prepared 20 mM 20-oxo-pregn-5-en-3β-yl sulfate (PE-S; pregnenolone sulfate), and 5 mM androst-5-en-3β-yl hemisuccinate (AND-hSuc) (Krausova et al., 2018) stock in dimethyl sulfoxide (DMSO). The final dilution to ECS was made

PDF-XChange Editor
KOUPIT plnou verzi!
www.pdfxchange.cz

at 50°C and followed by 1 min sonication (SONOREX DIGITEC DT 100/H, BADELIN electronic, Berlin, Germany). The same concentration of DMSO was added to all extracellular solutions. Drug applications were made with a microprocessor-controlled multibarrel fast-perfusion system. Changes in the glutamate-induced current in HEK293T cells transfected with hGluN1 and hGluN2B subunits were used to estimate the rate of solution exchange around the cell. Standard ECS was switched to the ECS diluted by water (50%) during glutamate application. The osmolarity was adjusted by sucrose to match the standard ECS. Glutamate (1 mM), glycine (10 μM) and pH was maintained constant in both solutions. The solution exchange rate was estimated to be $\tau = 12.0 \pm 0.9$ ms ($n = 6$) for the dish attached cells and $\tau \sim 200$ μs for open tip pipette (Vyklicky et al., 2016).

Single-Channel Recordings

Outside-out patches were pulled from transfected HEK293T cells, and single-channel recordings were performed at a holding potential of −60 mV (−74 mV after liquid junction potential correction) using an Axopatch 200 A amplifier (filtered at 10 kHz with a 4-pole Bessel filter, and sampled at 25 kHz). ECS and ICS were the same as solutions used for the whole-cell recording. Thick-wall borosilicate patch pipettes were pulled, coated with Sylgard 184 (Dow Corning), and fire-polished achieving resistances between 5 and 10 MΩ. Analysis of single-channel currents was performed using pClamp 10. Recordings were filtered at 2 kHz with an 8-pole Bessel filter. Opening and closing transitions were detected using a 50% threshold criterion. Openings briefer than 446 μs (2.5 × filter rise time) were excluded from the analysis (Colquhoun and Sakmann, 1985).

Data Analysis

Agonist Dose-Response Analysis

Normalized amplitudes *(I)* were fit to the following logistic equation:

$$I = 1/(1 + (\mathrm{EC}_{50}[agonist])^{h}), \quad (1)$$

where EC_{50} is the concentration of agonist that produces a half-maximal response, [*agonist*] is the glutamate or glycine concentration, and h is the apparent Hill coefficient. Dose-response for glutamate was determined from responses made in the presence of 30 μM glycine and dose-response for glycine was determined from responses made in the continuous presence of 1 mM glutamate.

Open Probability

The channel open probability (P_o) was assessed from the kinetics of the MK-801 (1 μM) inhibition of responses to 1 mM glutamate that was fitted to the kinetic model using Gepasi software (version 3.21; Mendes, 1993, 1997; Mendes and Kell, 1998). The glutamate binding steps were not considered because, in the presence of 1 mM glutamate, NMDAR exists with high probability (>99.6% as predicted from calculations using rate constants determined earlier; Cais et al., 2008) only in doubly liganded states with the channel closed (R) or open (O), and/or in a desensitized state (D).

$$D \underset{k_d}{\overset{k_r}{\rightleftharpoons}} R \underset{k_c}{\overset{k_o}{\rightleftharpoons}} O \underset{k_u}{\overset{k_b}{\rightleftharpoons}} B$$

B stands for MK-801 blocked state. The fitting procedure consisted of two steps (Turecek et al., 2004). In the first step, the response induced by 1 mM glutamate in HEK293T cells transfected with the WT or mutated hGluN1/hGluN2B receptors was analyzed for the peak (I_P) and steady state response (I_{SS}), and onset of desensitization was determined by the single exponential function (τ_d). Desensitization (D) and the kinetic constants describing the onset of desensitization (k_d) and resensitization (k_r) were determined from Equations 2–4:

$$D = 1 - (I_{SS}/I_P) \quad (2)$$

$$k_d = D/\tau_d \quad (3)$$

$$k_r = (1 - D)/\tau_d \quad (4)$$

In the second step, k_d and k_r were fixed at values obtained from the first step, and the close rate (k_c) at an arbitrary value of 200 s^{-1}. The NMDAR response recorded in the presence of 1 mM glutamate, and 1 μM MK-801 was fitted to the model while the opening rate (k_o) was set as a free parameter. MK-801 blocking rate (k_b) was set to 25 μM^{-1} s^{-1} (Huettner and Bean, 1988; Jahr, 1992; Rosenmund et al., 1995). The binding of MK-801 was virtually irreversible over the time course of the experiment for the WT and the mutated receptors, with the exception of hGluN1/hGluN2B(N615I) (Supplementary Figure S1). In the case of hGluN1/hGluN2B(N615I) receptors, the onset of MK-801 inhibition was fitted to the model where the MK-801 unblocking rate (k_u) was set as a free parameter. Microscopic open probability (P_o) was calculated as:

$$P_o = 100 \times k_o/(k_o + k_c) \quad (5)$$

Voltage Dependence of the Mg^{2+} Effect

The *I–V* relation of the Mg^{2+} inhibitory effect was fitted to the Boltzmann function equation of the form:

$$I(V) = ag_0(V - V_{\mathrm{rev}})/(a + [\mathrm{Mg}^{2+}]e^{-bV}) \quad (6)$$

in which g_0 is the estimated conductance of the NMDAR whole-cell response in the absence of extracellular Mg^{2+}, V_{rev} is the reversal potential of NMDA-induced current, and a, b are parameters with the following interpretation:

$$a = K_{\mathrm{d}}e^{bV} \quad (7)$$

where K_{d} represents the apparent dissociation constant for Mg^{2+} binding to the NMDAR at a given membrane potential (V) and

$$b = 2\delta F/(RT) \quad (8)$$

where δ indicates the apparent electrical distance of the Mg^{2+} binding site from the outside of the membrane and F, R, and T have their standard thermodynamic meanings (Abdrachmanova et al., 2002). Unless otherwise noted, recordings were performed at a holding potential of −60 mV (values of the holding potential were corrected for the liquid junction potential, 14 mV).

PDF-XChange Editor
KOUPIT plnou verzi!
www.pdfxchange.cz

Analysis of the Steroid Effect

The relative degree of steroid-induced potentiation determined for different steroid doses in individual HEK293T cells was fit to the following logistic equation:

$$I = I_{\max}/(1+(EC_{50}/[steroid])^{h}) \quad (9)$$

where I_{max} is the maximal value of potentiation, EC_{50} is the concentration of the steroid that produces half-maximal potentiation of glutamate induced current, [*steroid*] is the steroid concentration and h is the apparent Hill coefficient.

Molecular Modeling

Homology Modeling

We have used our recently refined all-atom homology model of rat NMDAR based on available crystal structures as templates (PDB IDs-4tll, 4tlm, and 4pe5) (Karakas and Furukawa, 2014; Lee et al., 2014). The receptor in these crystal structures contains various sequence modifications (deletions, substitutions, and introduction of disulfide bridges) in order to stabilize the interaction between amino-terminal domains as well as in the TMD region. The homologous sequences were aligned using MUSCLE and visually inspected within Unipro UGENE program. The all-atom model, including the residues missing in the template structures, was prepared using the automodel function of the MODELLER 9v14 suite of programs (Sali and Blundell, 1993; Webb and Sali, 2014), including symmetry restraints for the Cα atoms of corresponding pairs of subunits. We have further created a WT receptor model with MODELLER, using the rat NMDAR model as a template. This NMDAR model quite likely reflects liganded receptor with the channel in the closed state prior to opening.

Modeling the Effect of Rare Mutations

Amino acid substitutions within the TMD were introduced using MODELLER. The WT model and each of 11 mutated NMDAR models were subjected to a 10 ns molecular dynamics (MD) simulation. The parameters of implicit solvation/lipid membrane model (EEF1/IMM1) (Lazaridis, 2003) simulations were assigned using the web-based graphical user interface CHARMM-GUI (Jo et al., 2008), and the Langevin MD simulation with 2 fs time step was performed using the CHARMM (Brooks et al., 2009) MD package version c41b1.

Visualization of Structures

Graphical representation and analysis of residues surrounding selected regions were performed using PyMOL version 1.8.3.

Statistical Analysis

All data are expressed as mean ± SEM. Group differences were analyzed using a one-way ANOVA followed by multiple comparison procedures, and Student's *t*-test or Mann-Whitney Rank Sum Test was used for comparison between experimental groups using the statistical software package SigmaStat 3.5 (Systat Software Inc., San Jose, CA, USA).

RESULTS

Rare Variants in the TMD Reduce Surface NMDAR Expression

Recently, we elucidated the effects of different NMDAR mutations in an effort to identify sites of action for inhibitory steroids (Vyklicky et al., 2015). A secondary result of these experiments was the finding that mutations in the TMD and adjacent regions often dysregulated the NMDAR function. We therefore screened available databases (https://www.ncbi.nlm.nih.gov/clinvar/) and selected 11 *de novo* mutations (P553L; V558I; W607C; N615I; V618G; S628F; E657G; G820E; G820A; M824R; L825V) located in the pre-M1, M1, M2, M3, and M4 membrane regions of the hGluN2B subunit (**Figure 1**, **Table 1**).

There is no or incomplete information available about the effects of these missense mutations on NMDAR function. We therefore evaluated the amplitude of glutamate-induced responses, relative cell-surface expression, agonist potency, receptor desensitization, relative P_o, and pharmacological properties of each of these variants as an initial step in understanding the potential role NMDAR channelopathy may play in the pathophysiology of neurological diseases. HEK293T cells transfected with WT receptors responded to glutamate (1 mM; applied in the continuous presence of 30 μM glycine) with peak currents of 66 pA/pF. Receptors with mutated hGluN2B subunit either did not respond to glutamate application (currents <5 pA) (P553L; S628F; G820E; M824R) or responded with significantly reduced amplitudes (W607C; N615I; V618G; E657G; G820A). The amplitude of responses was not significantly different for hGluN1/hGluN2B(V558I) and hGluN1/hGluN2B(L825V) receptors (Supplementary Figure S2). The differences in the peak amplitude normalized with respect to the cell capacitance must be interpreted cautiously since this is influenced by factors that we cannot fully control. We have hypothesized that reduced protein levels and/or altered receptor function may underlie reduced responses to 1 mM glutamate in HEK293T cells expressing mutated NMDARs.

Next, we used immunofluorescence microscopy to determine the surface and total protein levels of the mutated NMDARs. First, we generated a gene encoding for YFP-hGluN1 (see Methods). In the second step, COS-7 cells were transfected with genes encoding for YFP-hGluN1 and WT or mutated hGluN2B subunits. Quantitative analysis of images indicated that the ratio of surface-to-total NMDAR expression was significantly reduced for YFP-hGluN1/hGluN2B(W607C) receptors compared to WT receptors (**Figures 2A,B**), and the surface expression of YFP-hGluN1/hGluN2B(S628F) receptors (**Figure 2C**) was quite likely completely lost since the ratio of the surface-to-total receptor levels was the same as that determined for COS-7 cells transfected with YFP-hGluN1 subunit only (Horak et al., 2008; Kaniakova et al., 2012). In addition, the microscopy assay in cells expressing YFP-hGluN1/hGluN2B(G820E) receptors indicated increased surface expression compared to the WT receptors (**Figure 2D**). **Figure 2E** shows relative surface expression of the WT and mutated hGluN2B subunits. YFP-hGluN1 is not surface expressed unless it is co-expressed with the hGluN2B subunit (Okabe et al., 1999; Standley et al.,

PDF-XChange Editor
KOUPIT plnou verzi!
www.pdfxchange.cz

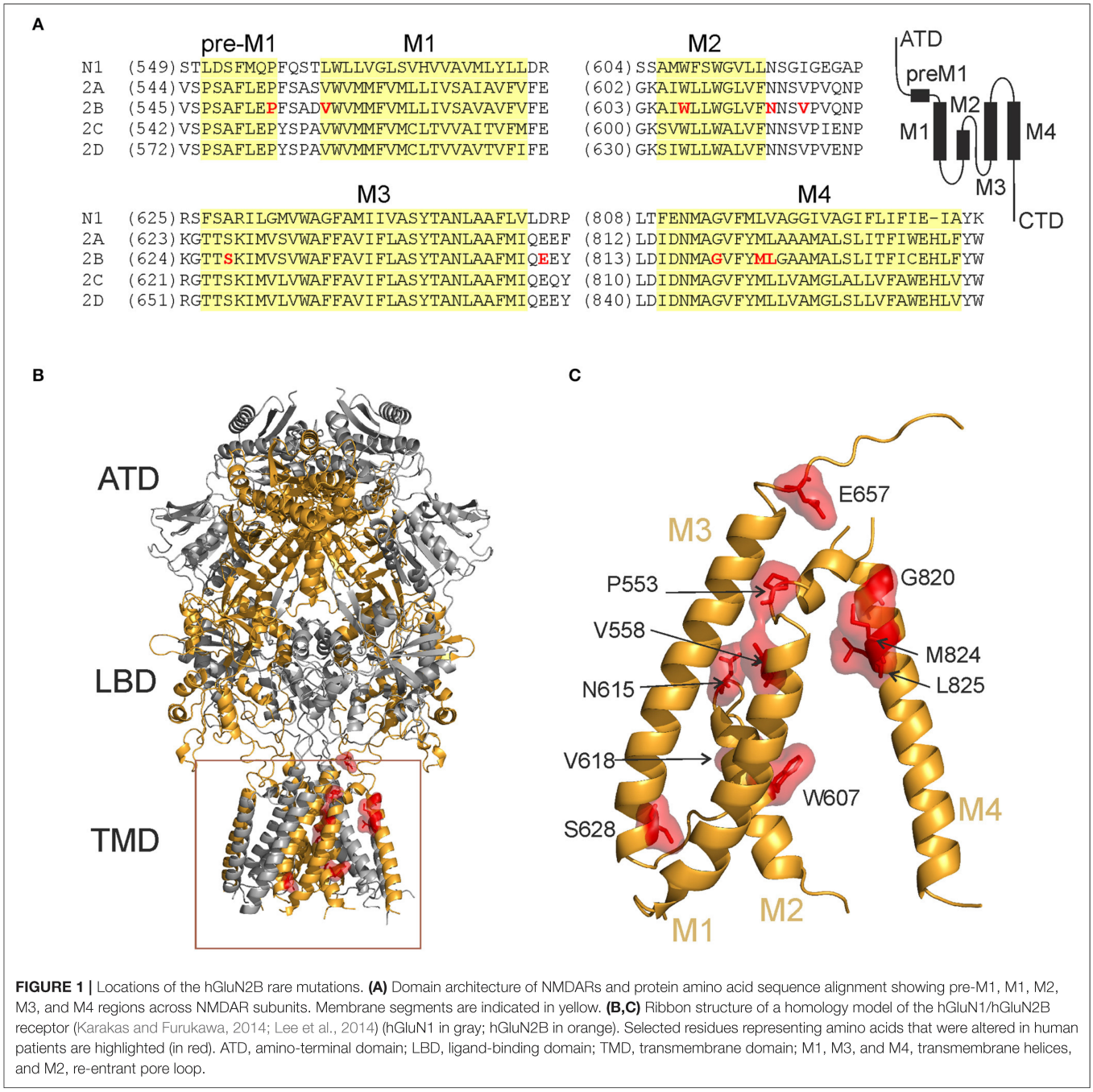


FIGURE 1 | Locations of the hGluN2B rare mutations. **(A)** Domain architecture of NMDARs and protein amino acid sequence alignment showing pre-M1, M1, M2, M3, and M4 regions across NMDAR subunits. Membrane segments are indicated in yellow. **(B,C)** Ribbon structure of a homology model of the hGluN1/hGluN2B receptor (Karakas and Furukawa, 2014; Lee et al., 2014) (hGluN1 in gray; hGluN2B in orange). Selected residues representing amino acids that were altered in human patients are highlighted (in red). ATD, amino-terminal domain; LBD, ligand-binding domain; TMD, transmembrane domain; M1, M3, and M4, transmembrane helices, and M2, re-entrant pore loop.

2000). In addition, surface-to-total expression of the WT and YFP-hGluN1/hGluN2B(W607C; S628F; and G820E) receptors was assessed using immunofluorescence microscopy on HEK293T cells and a quantitative expression assay in COS-7 cells (see Methods). The data obtained using these methods confirmed a significant decrease in the surface expression of YFP-hGluN1/hGluN2B(S628F) receptors compared to the WT and increase in the surface expression of YFP-hGluN1/hGluN2B(G820E) receptors, however, differences in the surface expression of YFP-hGluN1/hGluN2B(W607C) receptors were significant only for data gained by immunofluorescence microscopy on HEK293T cells (Supplementary Figure S3).

Thus, it is possible to explain the insensitivity of hGluN1/hGluN2B(S628F)-transfected cells to glutamate by virtually no surface expression of the receptors. In contrast, insensitivity or reduced sensitivity of cells transfected with hGluN1 and hGluN2B(P553L; W607C; N615I; V618G; E657G; G820E; G820A; or M824R) subunits contrasts with normal or increased surface expression and indicates impaired receptor function.

PDF-XChange Editor
KOUPIT plnou verzi!
www.pdfxchange.cz

TABLE 1 | Selected *de novo GRIN2B* variants and their phenotypic characteristics.

GluN2B mut.	Genotype	Phenotype	Age of onset	Source
P553L	c.1658C>T	ID, hypotonia	Early postnatal	de Ligt et al., 2012
V558I	c.1672G>A	ID	-	Hamdan et al., 2014; Lelieveld et al., 2016
W607C	c.1821G>T	ID, DD, dysmorphic features	-	Yavarna et al., 2015
N615I	c.1844A>T	WS, ID	7 weeks	Lemke et al., 2014
V618G	c.1853T>G	ID, WS, Epi-encephalopathy	4 months	Lemke et al., 2014
S628F	c.1883C>T	ID, DD, Epi-encephalopathy	-	Platzer et al., 2017
E657G	c.1970A>G	ID, DD	-	Platzer et al., 2017
G820E	c.2459G>A	ID, microcephaly	Early postnatal	Hamdan et al., 2014
G820A	c.2459G>C	ID, DD, DMD, ES, GVL, ASD	-	Platzer et al., 2017
M824R	c.2471T>G	ID, DD, microcephaly, Rett-like picture, Epi activity on EEG	2 months	Zhu et al., 2015
L825V	c.2473T>G	ASD	-	Awadalla et al., 2010; Swanger et al., 2016

ID, intellectual disability; DD, developmental delay; WS, West Syndrome; DMD, Dyskinetic Movement Disorder; ES, epileptic spasms; GVL, generalized cerebral volume loss; ASD, Autism Spectrum Disorder; Epi, epilepsy and/or seizures, infantile spasms.

Mutations Related to Human Neurological Diseases Decrease Agonist Potency

Seven mutations in the TMD responded to 1 mM glutamate and 30 μM glycine with currents that allowed reliable dose-response analysis of the agonist-induced responses. This analysis indicated that glutamate is 3.2- and 1.7-fold less potent at hGluN1/hGluN2B(W607C; and N615I) receptors and 2.3-fold more potent at hGluN1/hGluN2B(E657G) receptors than at the WT receptors (**Figure 3A**, **Table 2**). Similar analysis of glycine dose-response suggested that glycine is 2.0- and 1.8-fold less potent at hGluN1/hGluN2B(W607C; and E657G) receptors than at the WT receptors (**Figure 3B**, **Table 2**). Altered glutamate potency in hGluN1/hGluN2B(E657G) receptors and altered glycine potency in hGluN1/hGluN2B(W607C; and E657G) receptors was accompanied by a diminished value of the Hill coefficient indicating on altered degree of cooperativity of the agonists binding to the receptor (Weiss, 1997).

Mutations in the TMD Alter Receptor Desensitization and Decrease Channel Open Probability

To evaluate the effects of mutations in the TMD on NMDAR desensitization, the receptors were activated by a saturating concentration of glutamate (1 mM) in the continuous presence of glycine (30 μM). The analysis of the desensitization—a time-dependent decline of responses (see Equation 2 for definition)—indicated that WT receptors desensitized on average by 16.1% (**Figure 4A**). The desensitization was significantly increased to 72.9% in hGluN1/hGluN2B(V558I) receptors (**Figure 4B**) and was not significantly changed in hGluN1/hGluN2B(L825V) receptors (**Figure 4C**); by contrast, hGluN1/hGluN2B(V618G) receptors desensitized only by 4.1% (**Figure 4D**).

The time course of the desensitization onset of responses induced in the WT and hGluN1/hGluN2B(V558I; W607C; N615I; and L825V) receptors was next analyzed and desensitization (k_d) and (k_r) resensitization rate constants were determined (see Equations 2-4). The desensitization observed in the WT receptor responses was characterized by $k_d = 0.24 \pm 0.08$ s^{-1} ($n = 10$). The value of k_d was significantly increased in hGluN1/hGluN2B[V558I (3.55 ± 0.46 s^{-1}; $n = 7$); and W607C (1.59 ± 0.54 s^{-1}; $n = 4$)] receptor responses (one-way ANOVA, $p < 0.001$; followed by multiple comparisons of the rate constant determined in the mutated receptors vs. the WT; Dunnett's method, $p < 0.050$). The values of the k_d determined in hGluN1/hGluN2B[N615I (0.48 ± 0.14 s^{-1}; $n = 4$); and L825V (0.43 ± 0.16 s^{-1}; $n = 6$)] receptor responses was not significantly different from that determined in WT. WT receptor responses were characterized by $k_r = 1.06 \pm 0.17$ s^{-1} ($n = 10$). The value of the k_r was significantly increased in hGluN1/hGluN2B[W607C (4.79 ± 1.22 s^{-1}; $n = 4$); and N615I (2.61 ± 0.51 s^{-1}; $n = 4$)] receptor responses (one-way ANOVA, $p < 0.001$; followed by multiple comparisons of the rate constant determined in the mutated receptors vs. the WT; Dunnett's method, $p < 0.050$). The values of the k_r determined in hGluN1/hGluN2B[V558I (1.29 ± 0.28 s^{-1}; $n = 7$); and L825V (1.47 ± 0.20 s^{-1}; $n = 6$)] receptors was not significantly different from that determined in WT receptors. Low amplitude of the hGluN1/hGluN2B(V618G) receptor responses precluded detailed analysis of the rate constants characterizing receptor desensitization.

To evaluate the effects of mutations in the TMD on P_o, the WT and mutated receptors were activated by a saturating concentration of glutamate (1 mM) and the rate of channel block by 1 μM MK-801 was fitted to the kinetic model and the P_o determined (see Methods and Equation 5). Using this approach, the P_o of the human WT receptors was determined to be $10.5 \pm 1.3\%$ ($n = 10$) (**Figure 4A**). This value is not different from the P_o determined from the analysis of single-channel of activity induced by 1 mM glutamate in cell-attached patches ($P_o = 10.6 \pm 2.9\%$ ($n = 12$); unpaired t-test, $p = 0.977$) (see Supplementary Figure S4) and, in addition, it agrees well with that determined for rat GluN1/GluN2B receptors (Chen et al., 1999).

PDF-XChange Editor
KOUPIT plnou verzi!
www.pdfxchange.cz

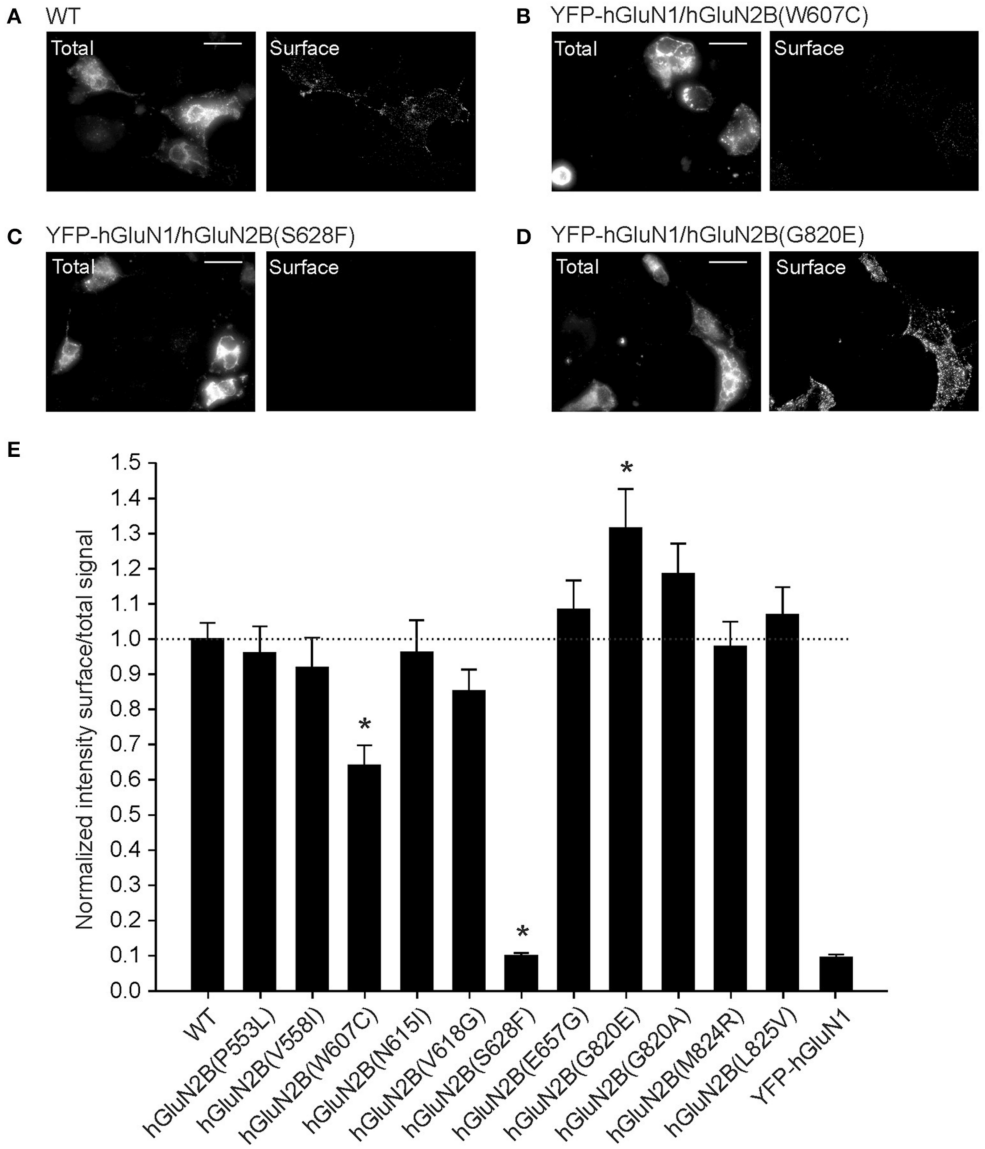


FIGURE 2 | Mutations in the TMD of hGluN2B subunit affect the NMDAR surface expression. **(A–D)** Representative images of the total (left panel) and surface (right panel) pools of YFP-hGluN1 expressed in COS-7 cells. COS-7 cells were transfected with WT **(A)**, YFP-hGluN1/hGluN2B(W607C) **(B)**, YFP-hGluN1/hGluN2B(S628F) **(C)**, and YFP-hGluN1/hGluN2B(G820E) **(D)** receptors. A scale bar in **(A–D)** represents 20 μm. **(E)** An immunofluorescence microscopy was used to determine relative surface-to-total NMDAR levels in COS-7 cells transfected with only YFP-hGluN1 subunit for control (YFP-hGluN1) or both the YFP-hGluN1 and hGluN2B (WT) or mutated hGluN2B subunit. Data show mean ± SEM; $n = 35$ in three experiments. *$p < 0.05$ relative to WT, one-way ANOVA (Multiple comparisons vs. WT-Dunnett's method). For original images see (Supplementary Figures S5–S12).

Superimposed traces indicate that in hGluN1/hGluN2B(V558I; and L825V) receptors, the onset of MK-801 inhibition was decelerated compared to WT receptors (**Figures 4A–C**). The results of the analysis indicated that the P_o decreased from 10.5% in WT receptors to 0.66% in hGluN1/hGluN2B(V558I) and 1.47% in hGluN1/hGluN2B(L825V) receptors. Similar decrease in P_o was observed in hGluN1/hGluN2B(W607C; and V618G) receptors (**Figure 4E**). These data indicate that *de novo* mutations in the TMD alter receptor desensitization and P_o.

Mutations in the Channel Pore Alter Mg^{2+} Inhibition and Single-Channel Amplitude

Structural data indicate that residues hGluN2B(W607; N615; and V618) are part of the NMDAR channel pore. A functionally important feature of NMDARs is the voltage-dependent inhibition by extracellular Mg^{2+}, and several residues located within the ion channel pore have been shown to alter Mg^{2+} sensitivity (Kuner et al., 1996; Kupper et al., 1996; Williams et al., 1998). Fitting the current-voltage relation of WT receptor responses recorded in the presence of 1 mM Mg^{2+} to the

PDF-XChange Editor
KOUPIT plnou verzi!
www.pdfxchange.cz

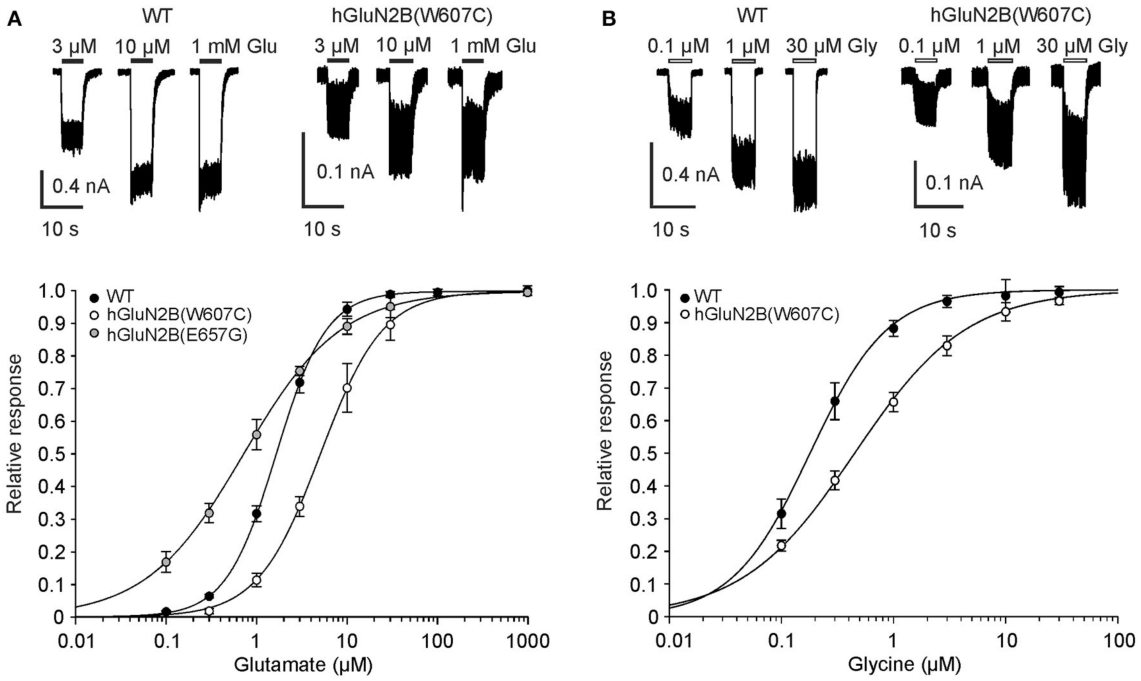


FIGURE 3 | hGluN2B rare variants alter glutamate and glycine potency. **(A)** Representative recordings of responses to 3, 10, and 1,000 μM glutamate applications made in the presence of 30 μM glycine are shown for HEK293T cells expressing WT and hGluN1/hGluN2B(W607C) receptors. Peak concentration-response relationship for glutamate activation of WT, hGluN1/hGluN2B(W607C; and E657G) receptors. **(B)** Representative recordings of responses to 0.1, 1, and 30 μM glycine applications made in the presence of 1 mM glutamate are shown for HEK293T cells expressing WT and hGluN1/hGluN2B(W607C) receptors. Peak concentration-response relationship for glycine activation of WT and hGluN1/hGluN2B(W607C) receptors. Data points in **(A,B)** are averaged values of relative currents form at least five independent measurements. Error bars represent SEM. Values of glutamate and glycine EC_{50}, *h* and *n* are listed in **Table 2**.

TABLE 2 | Summary of the agonist potency data.

Mutation	Glutamate			Glycine		
	EC_{50} (μM)	*h*	*n*	EC_{50} (μM)	*h*	*n*
hGluN2B(WT)	1.6 ± 0.1	1.4 ± 0.1	15	0.22 ± 0.03	1.45 ± 0.11	9
hGluN2B(V558I)	1.6 ± 0.3	1.5 ± 0.2	5	0.22 ± 0.05	1.14 ± 0.05	5
hGluN2B(W607C)	5.1 ± 0.4*	1.3 ± 0.2	5	0.45 ± 0.08*	0.87 ± 0.05*	7
hGluN2B(N615I)	2.7 ± 0.2*	1.2 ± 0.1	5	0.31 ± 0.02	1.41 ± 0.10	5
hGluN2B(V618G)	1.7 ± 0.2	1.2 ± 0.1	5	0.28 ± 0.03	1.43 ± 0.09	5
hGluN2B(E657G)	0.7 ± 0.1*	0.8 ± 0.1*	9	0.39 ± 0.08*	0.97 ± 0.10*	5
hGluN2B(G820A)	1.5 ± 0.3	1.0 ± 0.2	4	0.20 ± 0.09	1.15 ± 0.05	3
hGluN2B(L825V)	1.5 ± 0.1	1.1 ± 0.1	9	0.16 ± 0.01	1.26 ± 0.12	5

The data are expressed as mean ± SEM.
n is the number of cells recorded from.
**p < 0.05; statistical tests on potency were performed on logEC_{50} and logHill compared to the corresponding WT; one-way ANOVA, Tukey post-hoc Dunnett's method.*

Boltzmann function (Equations 6-8) revealed that the affinity for Mg^{2+} in the absence of an electric field ($K_{d(0\ mV)}$) was 5.9 ± 2.3 mM and δ = 0.45 ± 0.07 (*n* = 5) (**Figure 5A**). hGluN1/GluN2B(N615I) receptor responses were only slightly affected by 1 mM Mg^{2+}, and the fit to the Boltzmann function provided unreliable values for both $K_{d(0\ mV)}$ and δ (**Figure 5A**). The responses induced in hGluN1/hGluN2B(W607C; and V618G) receptors were small, precluding detailed analysis of the current-voltage relation. Based on the relative inhibitory effect of 1 mM Mg^{2+} at a holding potential of −60 mV, which decreased from 97 ± 2% (*n* = 5) in WT to 35 ± 3% (*n* = 6) in hGluN1/hGluN2B(W607C), we infer that Mg^{2+} binding within these receptor channels is also altered. The responses induced by hGluN1/hGluN2B(V618G) were small, precluding any reliable analysis of the Mg^{2+} effect. These results agree well with reduced Mg^{2+} block observed in mutated receptors (Lemke et al., 2014).

Next, we aimed to characterize the effect of mutations on the ion permeation employing single-channel recording from outside-out patches. **Figure 5B** shows records of channel activity in outside-out patches recorded in response to the application of 1 mM glutamate in the presence of Mg^{2+}-free extracellular solution at a holding potential of −60 mV (−74 mV after junction potential correction). The mean amplitude of the principal single-channel current was decreased from −4.5 ± 0.1 pA (*n* = 6) in the WT receptors to −2.4 ± 0.1 pA (*n* = 5) for hGluN1/hGluN2B(W607C) receptor channels ($p < 0.001$, compared to WT), −1.8 ± 0.1 pA (*n* = 5) for hGluN1/hGluN2B(N615I) receptor channels ($p < 0.001$, compared to WT), and −3.6 ± 0.1 pA (*n* = 5) for hGluN1/hGluN2B(V618G) receptor channels ($p < 0.001$, compared to WT). These data indicate that mutations in the NMDAR channel pore have opposing effects –an increase in responses due to the reduced Mg^{2+} inhibitory effect and a

PDF-XChange Editor
KOUPIT plnou verzi!
www.pdfxchange.cz

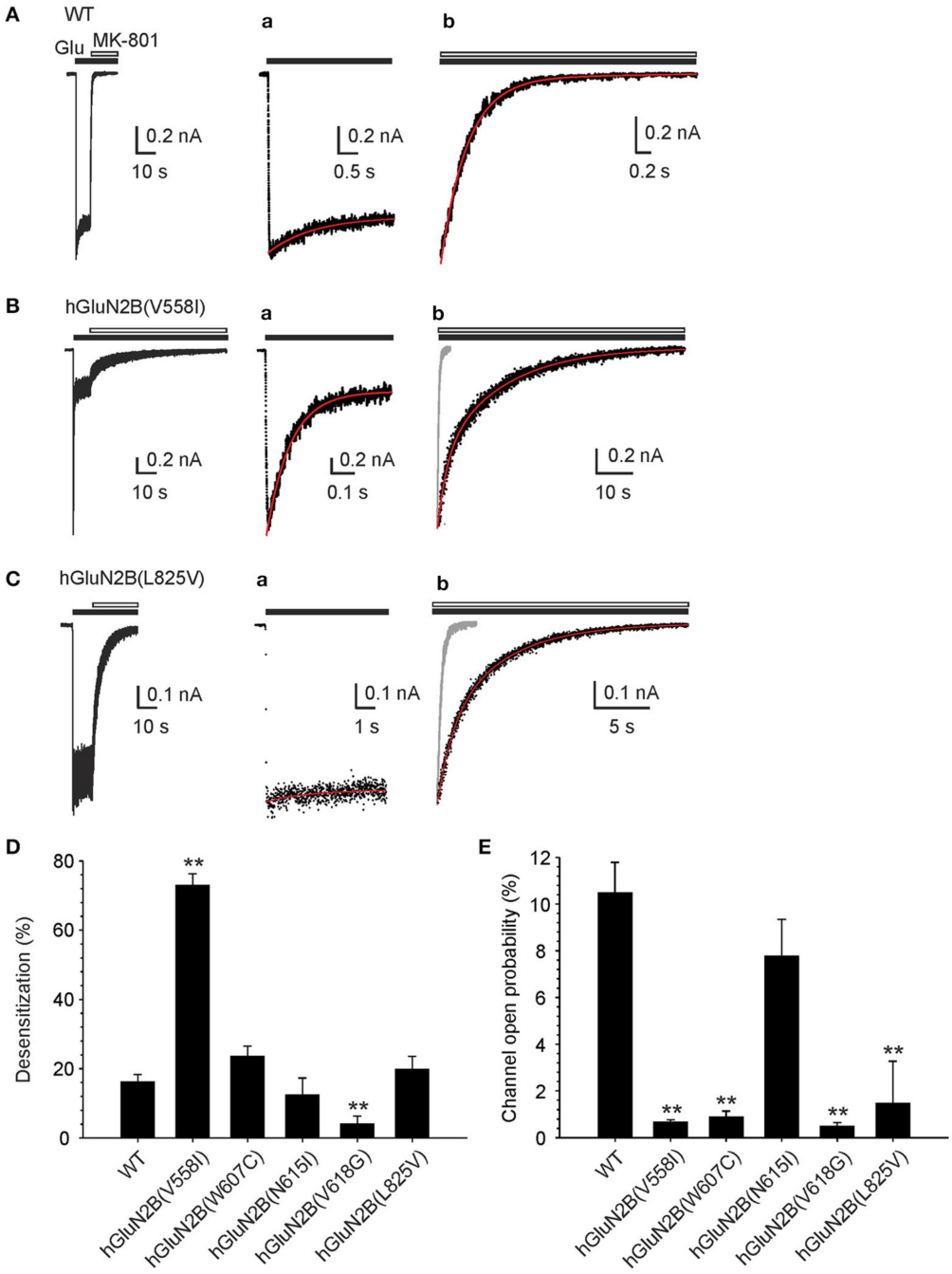


FIGURE 4 | Mutations in the TMD alter receptor desensitization and P_O. **(A-C)** Representative currents induced in WT, hGluN1/hGluN2B(V558I; and L825V) receptors by fast application of 1 mM glutamate (in the continuous presence of 30 μM glycine) and their inhibition by MK-801 (1 μM). **(Aa-Ca)** Show the response to glutamate at an expanded time scale. Desensitization of WT receptors was best described by rate constants $k_d = 0.17\ s^{-1}$ and $k_r = 0.69\ s^{-1}$; desensitization of hGluN1/hGluN2B(V558I) receptors by $k_d = 4.06\ s^{-1}$ and $k_r = 1.12\ s^{-1}$, and desensitization of hGluN1/hGluN2B(L825V) receptors by $k_d = 0.11\ s^{-1}$ and $k_r = 0.83\ s^{-1}$ (indicated by a superimposed red trace). **(Ab-Cb)** Show the onset of MK-801 inhibition on an expanded time scale. The time course of the onset of MK-801 (gray response in Bb and Cb) inhibition was best described by $P_O = 12.2\%$ for WT receptors, $P_O = 0.61\%$ for hGluN1/hGluN2B(V558I) receptors, and $P_O = 1.16\%$ for hGluN1/hGluN2B(L825V) receptors (indicated by a superimposed red trace) (see Methods section for details of the analysis procedure). Graphs show the summary of mean desensitization **(D)** and P_O **(E)** ± SEM (*n*) for WT and mutated receptors. The differences in the mean values of desensitization and P_O determined for the WT and mutated receptors was statistically significant; Kruskal-Wallis one-way ANOVA on Ranks, $p < 0.001$; subsequent Mann-Whitney Rank Sum Test or unpaired *t*-test was used to assess the significance compared to the WT, $^*p = 0.001$–0.05, $^{**}p < 0.001$.

PDF-XChange Editor
KOUPIT plnou verzi!
www.pdfxchange.cz

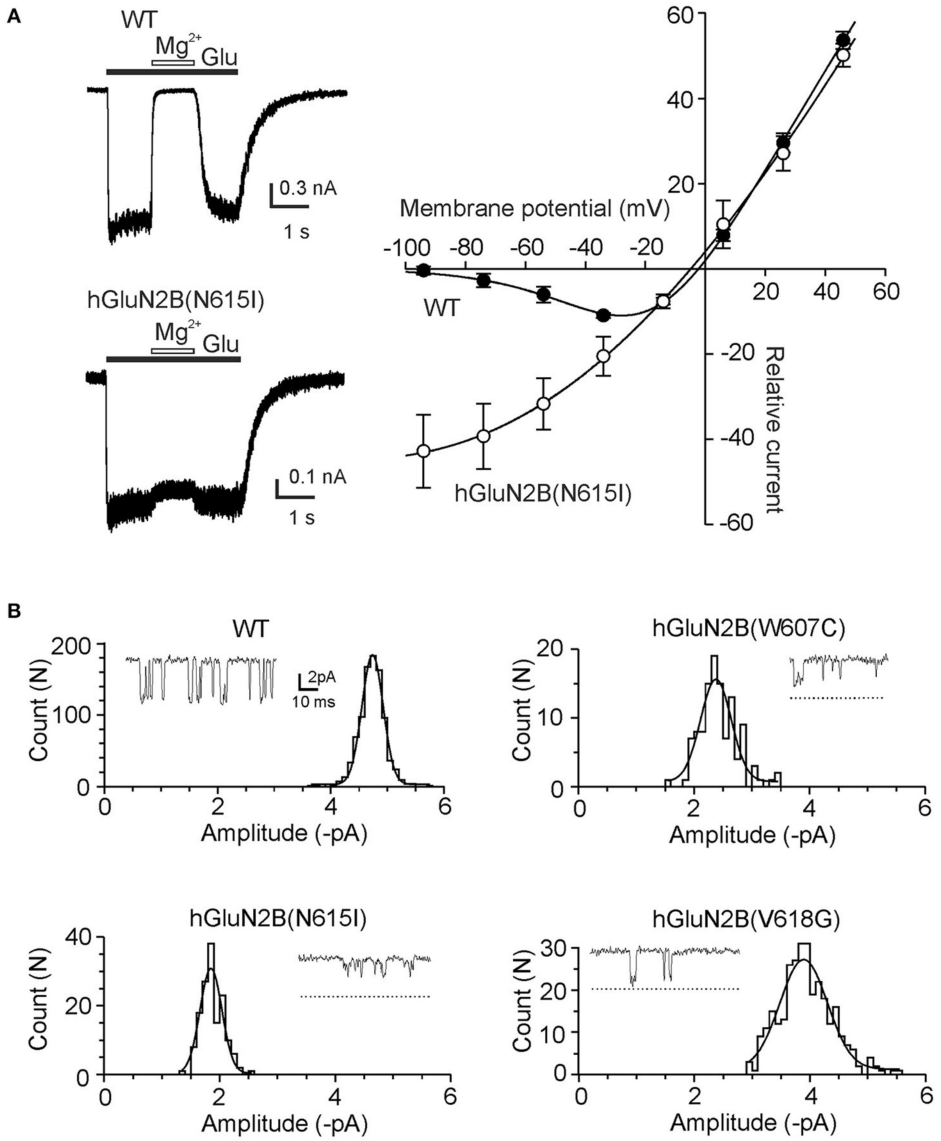


FIGURE 5 | Mutations in the channel pore alter ion permeation. **(A)** Effect of Mg^{2+} on WT and hGluN1/GluN2B(N615I) receptor responses. Whole-cell current responses were induced by 1 mM glutamate in the absence and presence of 1 mM Mg^{2+} at a holding potential of −60 mV. *I-V* relations without Mg^{2+} were fit by a linear equation and normalized to have a slope of 1. Corresponding responses recorded in the presence of Mg^{2+} were normalized and fitted to the Boltzmann equation (Equations 6–8). **(B)** Examples of single-channel openings induced in WT, hGluN1/hGluN2B(W607C; N615I; and V618G) receptors by 1 mM glutamate. Dashed lines show where the current levels identified from the fit to the amplitude distribution for the WT would fall. For individual patches the distribution is shown fitted with a single Gaussian component. Glutamate-induced single-channel currents had mean amplitude: −4.7 pA (WT), −2.4 pA [hGluN1/hGluN2B(W607C)], −1.9 pA [hGluN1/hGluN2B(N615I)], and −3.9 pA [hGluN1/hGluN2B(V618G)].

reduction of responses due to the decrease in the single-channel amplitude; the overall effect will be a function of the membrane potential.

GluN2B(L825V) Mutation Enhances Sensitivity to Endogenous and Synthetic Steroids

Endogenous steroids are potent allosteric modulators of NMDAR activity (Korinek et al., 2011). The sensitivity of the mutant receptors to extracellular PE-S, a steroid that has a positive allosteric and subunit-dependent effect at NMDAR (with preference for GluN2A/B subunits) (Wu et al., 1991; Horak et al., 2006), was evaluated by generating dose-response curves for the potentiation of responses to glutamate. In addition, we analyzed the potentiating effect for AND-hSuc, a more potent synthetic PE-S analog (Krausova et al., 2018). Since the effect of steroids with a potentiating effect at NMDAR is disuse-dependent (Horak et al., 2004), a low concentration of glutamate (1 μM) was used in these experiments. **Figures 6A,B** shows that PE-S and AND-hSuc

PDF-XChange Editor
KOUPIT plnou verzi!
www.pdfxchange.cz

potentiate both the WT and mutated receptors, although to a different extent. Analysis revealed that GluN1/GluN2B(L825V) receptors were significantly more potentiated by a nearly saturating concentration of PE-S (100 μM) than responses induced in the WT and hGluN1/hGluN2B(V558I; W607C; V618G; and G820A) receptors (**Figure 6C**; Kruskal-Wallis one-way ANOVA on Ranks, $p < 0.001$; unpaired *t*-test, $p < 0.001$). Similarly to the effect of PE-S, AND-hSuc (30 μM) potentiated glutamate responses induced in the mutated receptors with a higher potency than in the WT (**Figure 6C**; Kruskal-Wallis one-way ANOVA on Ranks, $p < 0.001$; unpaired *t*-test, $p < 0.001$). GluN1/GluN2B(L825V) receptors were potentiated robustly (1647%) by AND-hSuc. Receptors containing hGluN1 and hGluN2B(V558I; W607C; V618G; or G820A) subunits were potentiated to an extent not significantly different from that determined for the WT receptors (**Figure 6C**; $p = 0.117$–0.412 for PE-S; $p = 0.448$–0.966 for AND-hSuc). Dose-response analysis of the effect of PE-S and AND-hSuc indicated that the increased steroid potentiation of GluN1/GluN2B(L825V) receptors was attributable to the increase in steroid efficacy rather than potency (**Figures 6D,E**).

The time course of the NMDAR responses following brief glutamate application has been suggested to mimic the time course of the NMDAR component of the EPSCs (Lester et al., 1990). To evaluate the effects of steroids on the deactivation time course, we measured current responses induced by a brief (~5 ms) application of 1 mM glutamate to HEK293T cells expressing WT or hGluN1/hGluN2B(L825V) receptors. In the WT receptors, PE-S (100 μM) significantly increased the amplitude of synaptic-like responses and slowed the deactivation (**Figure 6F**, **Table 3**). The deactivation of hGluN1/hGluN2B(L825V) receptors was not significantly different ($p = 0.696$) from that determined for the WT receptors. This agrees well with the prediction made from the simulation of responses to brief glutamate application to NMDARs that have diminished P_o but unaltered glutamate EC_{50} (**Figure 4E**, **Table 2**). In the hGluN1/hGluN2B(L825V) receptors, PE-S (100 μM) significantly increased the amplitude of synaptic-like responses and slowed the deactivation (**Figure 6G**, **Table 3**).

Next, we estimated the relative charge transfer recorded for synaptic-like responses in the presence of PE-S. The charge transfer was calculated as a product of the response amplitude and deactivation time course, and its value increased 3.3-fold for the WT and 3.8-fold for hGluN1/hGluN2B(L825V) receptors when synaptic-like responses were recorded in the presence of PE-S (100 μM) (**Table 3**). Even though this augmentation of synaptic-like responses is prominent, it is not sufficient to compensate for a 7-fold diminution of the synaptic-like response of hGluN1/hGluN2B(L825V) receptors due to their decreased P_o (**Figure 4E**). The increase in the charge transfer was much more robust for synaptic-like responses recorded in the presence of AND-hSuc (30 μM)-its value increased 161-fold for the WT and 180-fold for hGluN1/hGluN2B(L825V) receptors (**Figures 6F,G**, **Table 3**). Estimates indicate that the augmentation of synaptic-like responses is more than sufficient to compensate for a 7-fold diminution of the synaptic-like response of hGluN1/hGluN2B(L825V) receptors when we take into an account their decreased P_o (**Figure 4E**).

Altogether, these results suggest that (i) PE-S and AND-hSuc have a potentiating effect at human WT receptors; (ii) AND-hSuc is a more potent positive allosteric modulator than PE-S; (iii) even though the potentiating effect of steroids at NMDAR is associated with a disuse-dependent mechanism of action, the effect of both PE-S and AND-hSuc was similar at WT and mutated receptors (hGluN1/hGluN2B(V558I; W607G; and V618G) receptors) that have P_o diminished ~10-fold; (iv) hGluN1/hGluN2B(L825V) receptors were potentiated by both steroids more than WT and other mutated receptors; (v) AND-hSuc-induced increase in the charge transfer of synaptic-like responses can compensate for the mutation-induced diminution of P_o in hGluN1/hGluN2B(L825V) receptors; and (vi) an increase in the positive allosteric effect of both steroids at hGluN1/hGluN2B(L825V) receptors is due to an increase in their efficacy rather than potency.

DISCUSSION

The development of next-generation DNA sequencing has given rise to unique data linking patient variants in *GRIN1* and *GRIN2* genes to neurological and psychiatric disorders. While the list of rare variants expands rapidly, the consequences for receptor biogenesis, its structure, function, and pharmacology have been only partially revealed (Yuan et al., 2014; Swanger et al., 2016; Chen et al., 2017; Ogden et al., 2017; Platzer et al., 2017). In this study, we investigated 11 disease-associated rare variants in the GluN2B TMD and found that dysregulation of NMDARs involves multiple mechanisms - altered surface expression, agonist potency, receptor desensitization, probability of channel opening, single-channel currents, Mg^{2+} sensitivity - and their combination. Through functional assessments, we show that loss-of-function variants can be rectified by a pharmacological approach, using PE-S and its synthetic analog AND-hSuc. Impaired surface expression and/or receptor function have important implications that may help to find links connecting genetic variation to disease as well as to understand the role of NMDAR variants in neurodevelopmental disorders (Mcrae et al., 2017).

Mechanisms of hGluN2B(P553L; and V558I) Dysregulation

Crystal structures of the GluN1/GluN2B receptor show that the LBD, the pre-M1 helix, and the M1 helix are structurally coupled, indicating a role in receptor gating (Lee et al., 2014). Conserved residues GluN2B(P553; and V558) are part of the pre-M1 and M1 helix, respectively (Sobolevsky et al., 2009; Karakas and Furukawa, 2014; **Figure 1A**), and despite their physical proximity, the mutation hGluN2B(P553L) rendered the transfected cells virtually glutamate nonresponsive while hGluN2B(V558I) receptors exhibited similar current responses to 1 mM glutamate to the WT, although with a prominent desensitization and a decreased P_o (Supplementary Figure S2, **Figures 4D,E**). Surface expression

PDF-XChange Editor
KOUPIT plnou verzi!
www.pdfxchange.cz

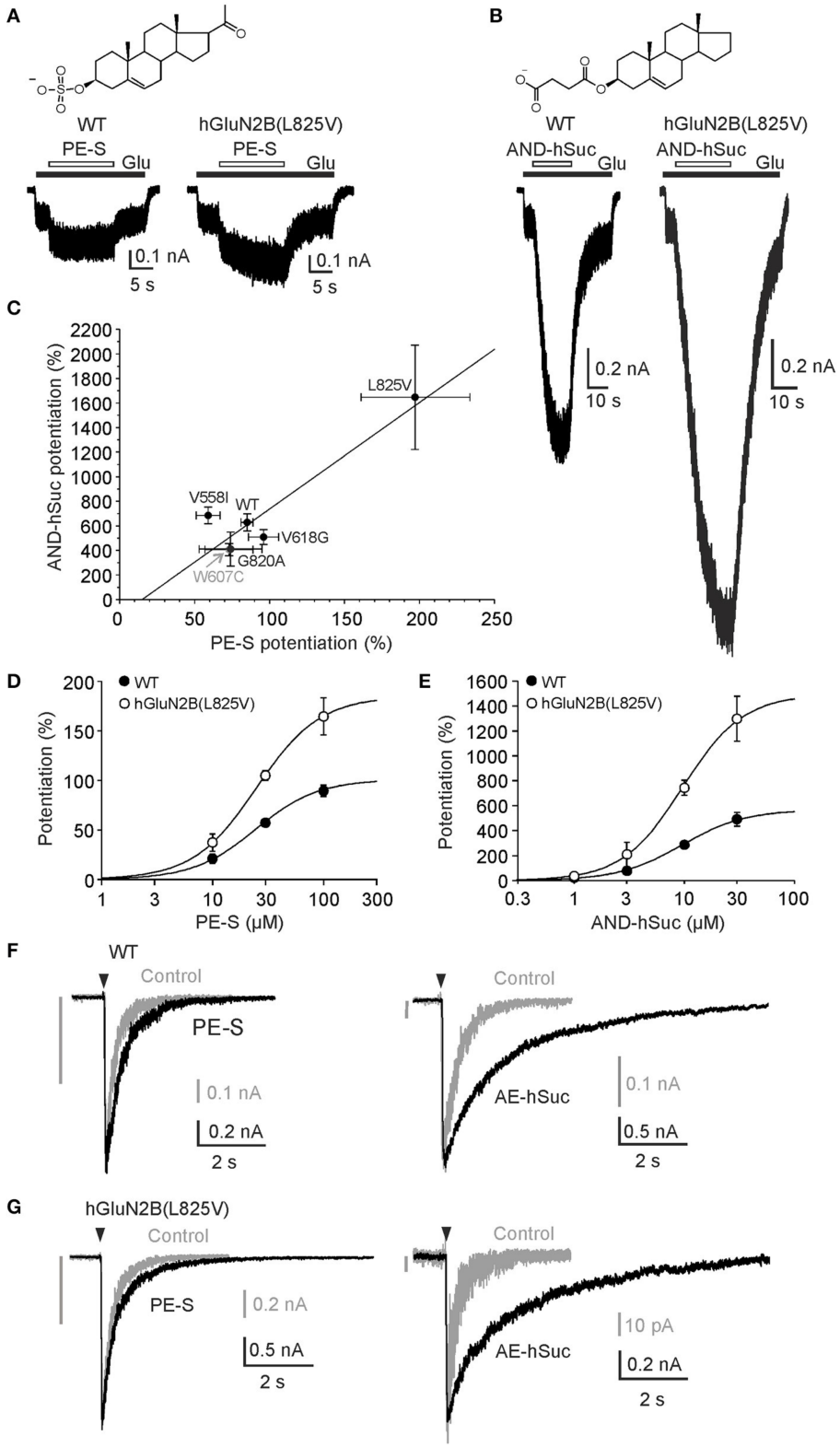


FIGURE 6 | hGluN1/hGluN2B(L825V) has an enhanced sensitivity to steroids. **(A)** Representative responses are shown for WT and hGluN1/hGluN2B(L825V) receptors. PE-S (100 μM) **(A)** and AND-hSuc (30 μM) **(B)** potentiated the WT receptor responses induced by co-application with 1 μM glutamate in the continuous presence of 30 μM glycine to a different extent (by 85% and 575%, respectively). Both steroids potentiated responses induced in hGluN1/hGluN2B(L825V) receptors

(Continued)

PDF-XChange Editor
KOUPIT plnou verzi!
www.pdfxchange.cz

FIGURE 6 | ~2-fold more than in WT receptors. Structure of PE-S **(A)** and AND-hSuc **(B)**. **(C)** Graph shows relative PE-S (100 μM) potentiation ± SEM (n = 5–31) plotted vs. that induced by AND-hSuc (30 μM) ± SEM in the WT and in mutated receptors. Data were fit by a linear regression (Correlation coefficient r = 0.928; p = 0.00764). Concentration dependency for PE-S **(D)** and AND-hSuc **(E)** induced potentiation of WT and hGluN1/hGluN2B(L825V) receptors activated by 1 μM glutamate in the continuous presence of 30 μM glycine. Parameters of the fit (see Equation 9) were for the WT receptors: PE-S induced relative maximal potentiation I_{max} = 101 ± 9%; EC_{50} = 24.3 ± 1.8 μM with h = 1.54 ± 0.08 (n = 7); AND-hSuc I_{max} = 570 ± 57%; EC_{50} = 9.5 ± 1.0 μM; h = 1.50 ± 0.16 (n = 6). In hGluN1/hGluN2B(L825V) receptors: PE-S induced I_{max} =185 ± 50% (p = 0.030 compared to WT); EC_{50} = 24.8 ± 1.2 μM (p = 0.842 compared to WT) with h = 1.52 ± 0.12 (n = 5); AND-hSuc I_{max} = 1492 ± 514% (p = 0.030 compared to WT); EC_{50} = 9.6 ± 2.3 μM (p = 0.961 compared to WT) with h = 1.58 ± 0.36 (n = 6). **(F,G)** Normalized representative current responses of WT and hGluN1/hGluN2B(L825V) receptors induced by brief (5 ms) application of 1 mM glutamate made in the ECS (Control, gray) and in the presence of PE-S (100 μM) or AND-hSuc (30 μM) following steroid pre-application for (>30 s). The vertical gray bar indicates the amplitude of the control response at the same amplitude scale as that recorded in the presence of steroid. See **Table 3** for values and statistics on the steroid effect.

TABLE 3 | Summary of the pharmacological properties for synaptic-like responses.

Receptor		Control	PE-S (100 μM)	Control	AND-hSuc (30 μM)
WT	Potentiation (%)	–	98.7 ± 11.5 (5)	–	924.5 ± 172.7 (5)
	τ (ms)	307 ± 14 (5) †	499 ± 20 (5)‡*	370 ± 35 (5)†	5,961 ± 542 (5)†*
	Deceleration	–	1.63 ± 0.06 (5)	–	16.36 ± 1.44 (5)†
	Charge transfer	–	3.26 ± 0.30 (5)	–	161.4 ± 20.3 (5)
hGluN2B(L825V)	Potentiation (%)	–	140.8 ± 10.8 (5)	–	2,323 ± 121 (5)
	τ (ms)	323 ± 9 (5)†	507 ± 28 (5)‡*	335 ± 29 (5)†	2,467 ± 168 (5)†*
	Deceleration	–	1.57 ± 0.05 (5)	–	7.19 ± 0.59 (5)†
	Charge transfer	–	3.79 ± 0.25 (5)	–	179.7 ± 9.1 (5)

The data are expressed as mean ± SEM (n) is the number of cells recorded from.
$^{*}p < 0.001$ compared to WT; paired t-test.
† τ determined from the single exponential fit.
‡ τ_w determined from the double exponential fit.
Deceleration is defined as $\tau_{steroid}/\tau_{control}$.
Charge transfer is defined as $\tau \times (potentiation/100) + 1$).

of YFP-hGluN1/hGluN2B(P553L) receptors was not altered (**Figure 2E**; however, see Ogden et al., 2017), who show a moderate reduction (by 33%) indicating that minimal current responses to 1 mM glutamate in hGluN1/hGluN2B(P553L) receptors are not due to the lack of surface expression but rather a functional alteration in the receptor. We may hypothesize that the loss of function in hGluN1/hGluN2B(P553L) receptors may be attributed to receptor desensitization since rat GluN1/GluN2A(P552R) receptors, homologous in position to GluN2B(P553), desensitize profoundly (by 98.5%). It is less likely that it is due to altered agonist potency and P_o since rat GluN1/GluN2A(P552R) and rat GluN1/GluN2B(P553R) receptors have the EC_{50} value for both glutamate and glycine decreased in combination with an increased P_o (Ogden et al., 2017). Augmented desensitization of hGluN1/hGluN2B(V558I) receptors agrees well with results of previous experiments with chimeric receptors containing desensitizing GluN2A and non-desensitizing GluN2C subunit, as well as single-point mutations, which have identified the pre-M1 and M1 region as critical for rapid glycine- and Ca^{2+}-independent desensitization of NMDARs (Krupp et al., 1998; Villarroel et al., 1998; Thomas et al., 2006). In addition, this region has been shown to influence P_o of the NMDAR channels (Ogden et al., 2017).

We have employed computational methods to infer the structural consequences of *de novo* missense mutations based on the liganded state with the channel just prior to opening (Vyklicky et al., 2015) as deduced from the available crystal structures of the heterotetrameric GluN1/GluN2B receptor (Furukawa et al., 2005; Karakas and Furukawa, 2014; Lee et al., 2014). In the pre-open liganded state, the pre-M1 helix controls the spacing between M1 and M4 helices. It is also involved in further transmitting the mechanical signal from ligand-induced LBD reorientation through the pore-forming M3 helix to the M1 and M4 helices (**Figure 7A**). Specifically, the hGluN2B(P553) residue interacts weakly with L650 and F653 of the M3 helix. MD simulation further suggests that the hGluN2B(P553L) mutation leads to a formation of a nearly continuous M1 helix as a result of removing the helix-terminating proline residue (**Figure 7B**). The hGluN2B(V558) is mediating an interaction with surrounding hydrophobic residues of M3 helix in the liganded state. The MD simulation suggests that the hGluN2B(V558I) mutation induces stronger interaction of these residues, leading to reorientation of the pre-M1 helix from its horizontal position (**Figure 7C**). As a result, the M1/M4 interaction is weakened.

Mechanisms of hGluN2B(W607C; N615I; and V618G) Dysregulation

Cysteine accessibility to sulfhydryl reagents indicates that conserved residues hGluN2B(W607; N615; and V618) are exposed to the lumen of the NMDAR ion channel (Kuner et al., 1996). Our results show that mutations of these residues underlie multiple effects: hGluN1/hGluN2B(W607C)

PDF-XChange Editor
KOUPIT plnou verzi!
www.pdfxchange.cz

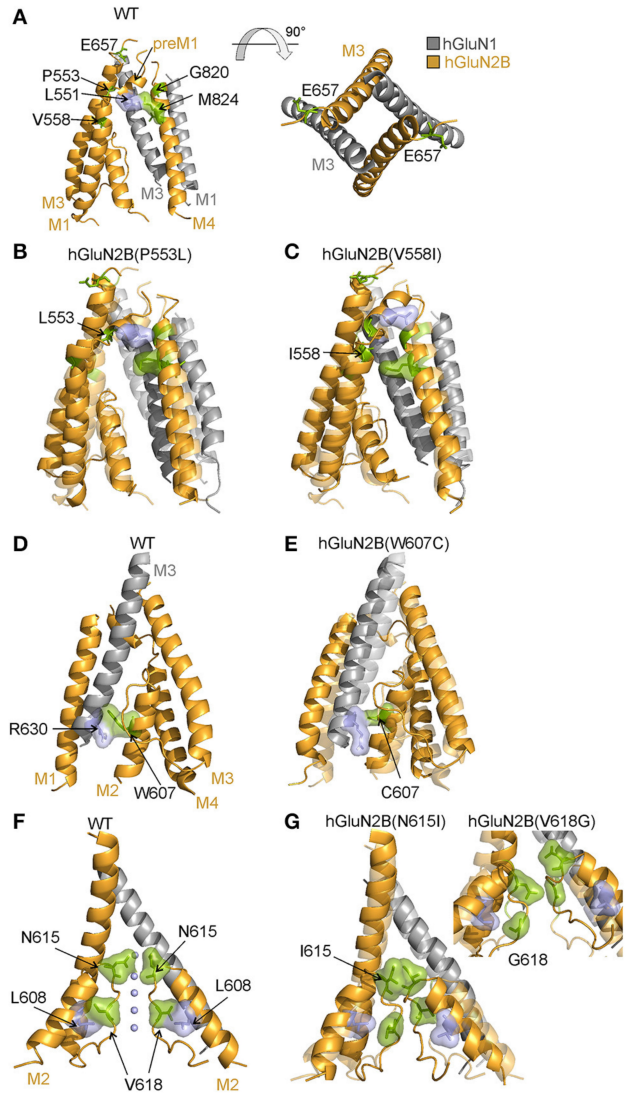


FIGURE 7 | Structural consequences of hGluN2B(P553L; V558I; W607C; N615I; and V618G) mutations. **(A)** Cartoon representation of the homology model of the membrane domain of the WT receptor built from the rat GluN1/GluN2B crystallographic data (Karakas and Furukawa, 2014; Lee et al., 2014) (GluN1 in gray; GluN2B in orange). MD simulation (of the WT receptor) indicates a van der Waals contact between hGluN2B(L551; and M824) that is important for the arrangement of the M1, pre-M1, and M3 helices. On the right, the membrane domains (M3 helices) of the NMDAR channel are viewed from the extracellular side. **(B)** Shows results of MD simulation of the hGluN1/hGluN2B(P553L) (deep colors) and WT receptor (light colors). Comparison of both superimposed models indicates that in hGluN1/hGluN2B(P553L) receptors the helical structure of the pre-M1 is prolonged and as a result contact between hGluN2B(L551; and M824) is disrupted and M1 and M4 helices repositioned. **(C)** Shows results of MD simulation of the hGluN1/hGluN2B(V558I) (deep colors) and WT receptor (light colors). The models indicate that in hGluN1/hGluN2B(V558I) receptors the helical structure of the M1 is prolonged and as a result contact between hGluN2B(L551; and M824) is disrupted and M1 and M4 helices repositioned. **(D,E)** Models of the WT and hGluN1/hGluN2B(W607C) receptors as deduced from the MD simulation. In the WT a van der Waals contact between hGluN2B(R630; and W607) is replaced by a weak contact between hGluN2B(R630) and smaller cysteine in hGluN2B(W607C). This change results

(Continued)

FIGURE 7 | in altered position of the M3 and M2 helices of the hGluN2B subunits. **(F,G)** Shows models of the WT, hGluN1/hGluN2B(N615I; and V618G) channel permeation pathway. The position of ions in the channel of the WT receptor was built from the crystallographic data of the structurally related K+ channel, pdb id 1k4c (Zhou et al., 2001). MD simulation of the WT indicates importance of a van der Waals contact between hGluN2B(L608) and hGluN2B(V618) that allow optimal orientation and precise positioning of the hGluN2B M2 loop in the channel permeation pathway. Permeant ions ($Na^+/K^+/Ca^{2+}$; indicated by blue spheres) interact with polar side chains of hGluN2B(N615) residues and backbone carbonyl groups of hGluN2B(V618). Simulation of the hGluN1/hGluN2B(N615I) receptor indicates that bulky nonpolar isoleucine residue lost the ability to coordinate the ions and occlude the permeation pathway as a result of van der Waals interaction. In addition contact of hGluN2B(L608) and hGluN2B(V618) is disrupted and as a consequence the M2 loop is destabilized with frequent transitions in between diverse conformations of the backbone. Similar destabilization effect is seen in hGluN1/hGluN2B(V618G) receptors.

receptors have a normal or moderately decreased surface expression, a decreased agonist potency, and a decreased P_o; whereas hGluN1/hGluN2B(V618G) have only a decreased P_o (**Figures 2–4**). Similarly to hGluN1/hGluN2B(W607C; and V618G) receptors, hGluN1/hGluN2B(N615I) receptors exhibit reduced responses to 1 mM glutamate (by 72%, see Supplementary Figure S2), although without an obvious change in trafficking and/or the functional parameters studied.

A characteristic feature of the hGluN1/hGluN2B(N615I) receptors was an accelerated rate of recovery from MK-801 inhibition (see Supplementary Figure S1), indicating structural differences in the ion channel pathway between WT and mutated receptors. There is compelling evidence that asparagine residues [GluN1(N616), GluN2A(N614), GluN2B(N615)] and adjacent residues including tryptophan [GluN2A(W606) or GluN2B(W607)] control permeability and block by Mg^{2+} (Williams et al., 1998) and, in addition, GluN2B(N615) controls single-channel conductance (for review see Dingledine et al., 1999). We therefore performed additional experiments to analyze Mg^{2+} block and single-channel currents. In agreement with recent data of Mullier et al. (2017), our analysis showed that Mg^{2+} sensitivity was decreased in hGluN1/hGluN2B(N615I; and W607C) receptors. Since the structural determinants of external Mg^{2+} block are similar to those governing Ca^{2+} permeability through NMDA receptor channels, it is possible that hGluN1/hGluN2B(W607C; N615I; and V618G) receptors may also have altered Ca^{2+} permeability. However, this was not possible to assess reliably due to very small current responses (Supplementary Figure S2). Similarly to Mg^{2+} block, the mean amplitude of the single-channel current was decreased for hGluN1/hGluN2B(W607C; N615I; and V618G) receptor channels.

To infer structural changes induced by mutations in the M2 segment and re-entrant loop, we used our previous model of the TMD with the vestibule open (Vyklicky et al., 2015). The ion filter as well as the lower part of M1, M3, and M4 helices are not changed significantly between the model liganded pre-open and the open state. The used model of the WT NMDAR channel is compatible with previous estimates of the minimum cross-section of the channel permeation pathway

PDF-XChange Editor
KOUPIT plnou verzi!
www.pdfxchange.cz

in the conducting states: 6.0 Å (Vyklicky et al., 1988), 5.5 Å (Villarroel et al., 1995), and ~4.5 × 5.7 Å (Zarei and Dani, 1995), and within the limits proposed for the channel diameter at the level of the activated extracellular vestibule, which was estimated to be 7.3 Å (Villarroel et al., 1995) and 11 Å (Sobolevskii and Khodorov, 2002). The W607 residue is involved in a stacking interaction with hGluN1(R630) residue in the M1 helix, which contributes to a proper arrangement of the M2 helices with respect to their surroundings (**Figure 7D**). MD of mutated model structures indicates that the W607C mutation interferes with this interaction and the relative orientation of the M2 helix (**Figure 7E**). The V618 residue interacting with the L608 contributes to the correct orientation of backbone carbonyl groups within the ion filter (**Figure 7F**). Structural effects of V618G mutation suggest a loss of this orientation, possibly resulting in lower selectivity and efficiency of ion transport (**Figure 7G**). The polar side chain of the N615 residue, homologous to Q586 of AMPAR, serves as the first layer coordinating the ion to be transported. The hGluN2B(N615I) mutation will lead to a change in channel selectivity and ion permeation through the channel (**Figure 7G**).

Mechanisms of hGluN2B(S628F) Dysregulation

Reduced responses to 1 mM glutamate in HEK293T cells transfected with hGluN1/hGluN2B(S628F) receptors (Supplementary Figure S2) correlate with their reduced surface expression (**Figure 2E**, Supplementary Figure S3). hGluN2B(S628) is located at the intracellular segment of the M3 helix and is conserved within the GluN2 family (**Figure 1**). We have shown earlier that amino acid residues within the M3 helix of GluN2B subunit (W635; S645; Y646; and T647) contribute to the regulation of the surface expression of NMDARs and alter the functional properties of NMDARs (Kaniakova et al., 2012). The quality-control at intracellular points is only poorly understood, and it is a matter of speculation whether the defect in surface expression described here for hGluN1/hGluN2B(S628F) receptors involves a mechanism similar to that of other amino acid mutations in the M3 helix or other TMD regions.

Our MD simulation suggests that in the hGluN1/hGluN2B(S628F) receptors, the mutation of a polar and small serine for a larger nonpolar phenylalanine leads to steric hindrance, with the bottom part of the M1 helix altering the quaternary structure of the TMD. This may be the reason why they are offloaded from their trafficking to the cell surface (**Figures 8A,B**).

Mechanisms of hGluN2B(E657G) Dysregulation

Reduced responses to 1 mM glutamate in HEK293T cells transfected with hGluN1/hGluN2B(E657G) receptors with normal surface expression imply that the mutation introduced a severe functional defect (Supplementary Figure S2, **Figure 2E**). Glutamate residue hGluN2B(E657) is conserved within the GluN2, GluA, and GluK family and is part of the linker that connects the LBD and M3 helices. Rearrangement of M3 helices

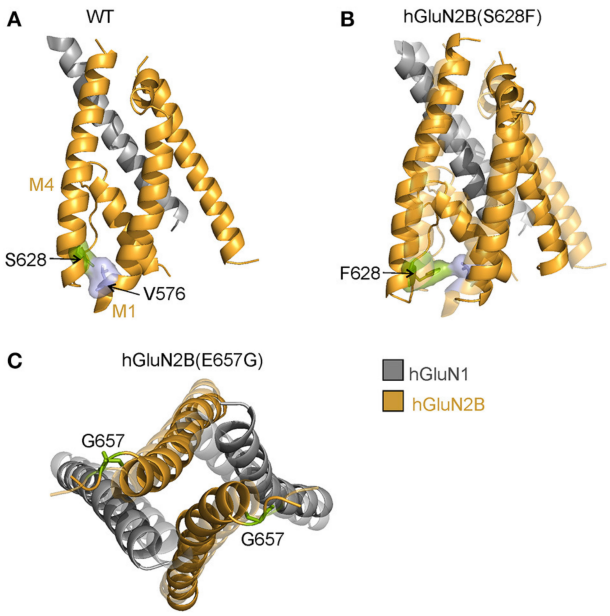


FIGURE 8 | Structural consequences of hGluN2B(S628F; and E657G) mutations. **(A)** Cartoon representation of the homology model of the membrane domain of the WT receptor built from the rat GluN1/GluN2B crystallographic data (Karakas and Furukawa, 2014; Lee et al., 2014) (GluN1 in gray; GluN2B in orange). MD simulation of the WT receptor indicates a series of inter-helical zipper-like contacts spanning along the M1 and M4 helices. The contact between hGluN2B(S628) and hGluN2B(V576) is highlighted. **(B)** According to the MD simulation the hGluN2B(S628F) substitution leads to larger separation of M1 and M4 helices. Contrary to an expected stronger van der Waals interaction with the hGluN2B(V576) across helices the steric effect of larger hydrophobic phenylalanine residue leads to rearrangement of residues along the M4 helix and formation of a chain of van der Waals stabilized M4 residues. **(C)** The MD simulation of hGluN2B(E657G) mutation suggests closing of the ion channel due to a loss of specific interactions along the TMD-LBD hGluN2B linker.

in the activated conformation of the receptor makes the central cavity of the channel accessible to ions, therefore implying a crucial role of the M3-S2 linkers in channel opening (Sobolevsky et al., 2004). Mutations in this region lead to profound alterations of the receptor channel function characterized by diminished P_o and altered transduction of agonist activation to channel opening (Kazi et al., 2014). Missing experimental electron density data in available crystal structures (Karakas and Furukawa, 2014; Lee et al., 2014) does not allow the localization of residues in the linker regions and related structural information is mostly missing, we therefore decided to explore linker structures computationally. Our data indicate that the overall effect of glycine substitution hGluN2B(E657G) on NMDAR gating can be explained by an interaction of specific residues at a site located in the proximity of the M3 helices (**Figures 7A**, **8C**).

Mechanisms of hGluN2B(G820E; G820A; M824R; and L825V) Dysregulation

Reduced responses to 1 mM glutamate observed in HEK293T cells transfected with genes encoding for hGluN1 and hGluN2B(G820A) subunits and a complete loss of responses in

PDF-XChange Editor
KOUPIT plnou verzi!
www.pdfxchange.cz

hGluN1/hGluN2B(G820E; and M824R) receptors are not due to altered surface expression since this was normal or even increased (**Figure 2E**). Small currents in hGluN1/hGluN2B(G820A) receptors precluded detailed functional examination. In contrast, responses to 1 mM glutamate in cells transfected with genes encoding for hGluN1 and hGluN2B(L825V) subunits were not significantly different from those observed in the WT although they had reduced P_o by 86% compared to the WT receptors.

Structurally conserved residues hGluN2B(G820, M824, and L825) (**Figure 1**) are located in mutual proximity in the M4 helix. Several lines of evidence indicate that M1 and M4 helices are located at the periphery of the TMD and seem to have a modulatory role in channel opening and closing, which is primarily mediated by M3 helices that form the central cavity of the channel in the activated receptor (Villarroel et al., 1998; Sobolevsky et al., 2004; Ogden and Traynelis, 2013; Karakas and Furukawa, 2014).The hGluN2B(L825) residue interacts with the F639 from the M1 helix of hGluN1 in the liganded state (**Figure 9A**). The hGluN2B(L825V) mutation leads to a weaker interaction with the hGluN1(F639), although structural effects are inconclusive (**Figure 9B**). MD revealed that hGluN2B(G820) serves as the last residue in the M4 helix, thus allowing the necessary extension of the preceding linker in response to the LBD reorientation. The hGluN2B(G820E; and G820A) mutations remain in the helical context and their side chains interact with the pre-M1 helix, shifting it from its horizontal position and changing the relative positions of M1 and M4 helices (**Figures 9C,D**). In the liganded state, the hGluN2B(M824) residue is involved in an interaction with hGluN2B(L551) of the pre-M1 helix (**Figure 7A**). As a consequence of the hGluN2B(M824R) mutation, the pre-M1 interaction is not formed (**Figure 9E**); this leads to an altered relative position of M1 and M4 helices, which in turn results in inefficient propagation of the mechanical signal from the LBD.

Pharmacology of Mutated Receptors

Therapeutic strategies for the development of new effective drugs for rectifying loss-of-function variants associated with diminution of the receptor P_o may encompass PE-S and its derivatives, since these compounds have a positive allosteric effect that is specifically mediated by the increase in the receptor P_o (Horak et al., 2004; Korinek et al., 2011). Both an endogenously occurring neurosteroid PE-S (Wu et al., 1991;

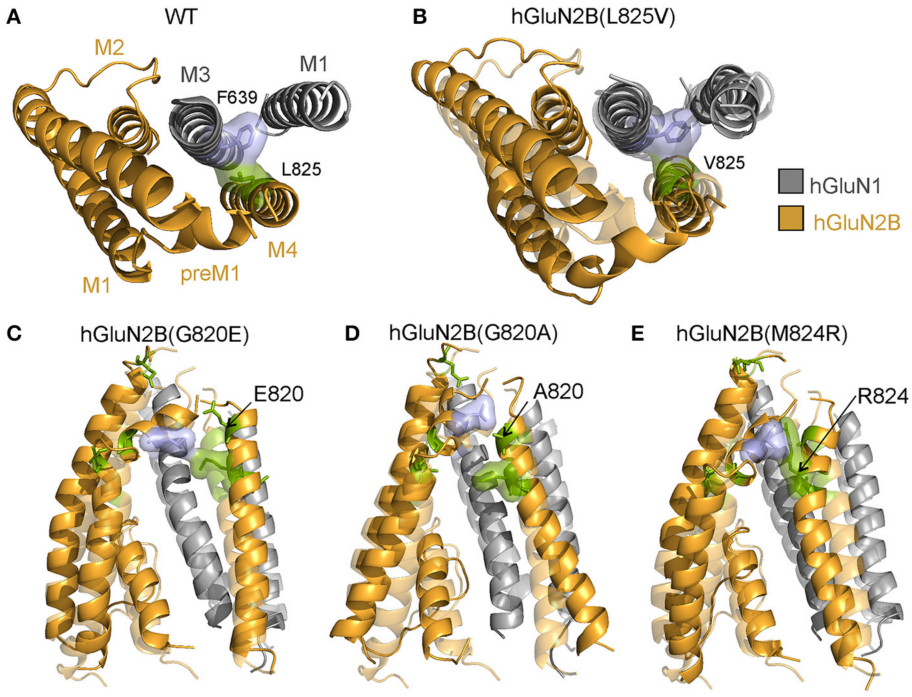


FIGURE 9 | Structural consequences of hGluN2B(L825V; G820E; G820A; and M824R) mutations. **(A)** Cartoon representation of the homology model of the membrane domain of the WT receptor built from the rat GluN1/GluN2B crystallographic data (Karakas and Furukawa, 2014; Lee et al., 2014) (GluN1 in gray; GluN2B in orange). MD simulation of the WT receptor identified a van der Waals contact between hGluN1(F639) and hGluN2B(L825) involved in interaction of hGluN1 M3 helix with the hGluN2B M4 helix**. (B)** The hGluN2B(L825V) substitution for a smaller aliphatic residue leads to weaker van der Waals interaction with the hGluN1(F639) resulting in a slight separation of the interacting helices. However, the structural effects are inconclusive. **(C,D)** MD revealed that hGluN2B(G820) serves as the last residue in the M4 helix thus allowing the necessary extension of the preceding linker in response to the LBD reorientation. The hGluN2B(G820A; and G820E) mutations remain in the helical context and the introduced side chains interact with residues from the pre-M1 helix. This changes the pre-M1 horizontal position as well as relative positions of M1 and M4 helices. **(E)** The hGluN2B(M824) residue is involved in an interaction with hGluN2B(L551) of the pre-M1 helix in the liganded state. The hGluN2B(M824R) mutation prevents the pre-M1 interaction and leads to altered relative position of M1 and M4 helices and consequently to inefficient propagation of the mechanical signal from the LBD.

PDF-XChange Editor
KOUPIT plnou verzi!
www.pdfxchange.cz

Bowlby, 1993) and its more potent synthetic analog AND-hSuc (Krausova et al., 2018) were approximately as effective at WT as at the hGluN1/hGluN2B(V558I; W607C; V618G; and G820A) receptors. Interestingly, both steroids potentiated the amplitude of tonic and synaptic-like responses more profoundly when studied at hGluN1/hGluN2B(L825V) receptors, indicating their prospective use in personalized therapies. It is likely that the augmented potentiating effect for PE-S is not specifically associated with residues at the TMD, since similar increases have been recently shown for receptors mutated in the LBD of the GluN2A subunit (V685G; and D731N) (Swanger et al., 2016).

Functional defects described here in the NMDAR apply for cases in which both alleles in a patient were mutated at exactly the same site. This is expected to be rare, in contrast to heterozygous individuals, who are much more likely to carry only one mutated allele. In this case, the expected genotypic ratio predicts that each neuron will contain 25% of WT receptors, 50% of receptors composed of one hGluN2B subunit mutated and one non-mutated, and 25% of receptors comprised of both hGluN2B subunits mutated.

To build a conception of the degree of the NMDAR defect, we may use as an example the mutation-induced decrease in the receptor P_o (P_o = 10% for the WT and P_o = 1% for receptors with both hGluN2B subunits mutated). Based on the Mendelian laws of inheritance and the law of dominance, we may predict that the overall activity of NMDARs will be diminished, depending on whether the mutation is recessive, independent, or dominant, to 77.5, 55, and 32.5%, respectively, of the activity in the healthy subjects. These calculations indicate that for a full pharmacological rectification of the NMDAR defect, a potentiating effect of 22.5, 45, and 67.5% would be required. Since most neurons express more than one type of GluN2/GluN3 subunits (Monyer et al., 1994), the expected rectifying potentiation effect may be even smaller. However, further studies are required to understand how the degree of NMDAR hypofunction is linked to various clinical symptoms.

AUTHOR CONTRIBUTIONS

VV and LV designed the experiments; VV, BKr, BKy, ML, TS, and MK performed electrophysiological experiments; BKr, SD, and MH performed trafficking experiments; VV, BKr, and LV analyzed the data; JC performed molecular modeling; HC and EK synthetized the steroids; LV wrote the paper.

FUNDING

This work was supported by the Czech Science Foundation: 17-02300S (LV), 16-03913Y (TS); Technology Agency of the Czech Republic: TE01020028 (LV); from Ministry of Health of the Czech Republic: NV15-29370A (LV); ERDF/ESF project PharmaBrain (No. CZ.02.1.01/0.0/0.0/16_025/0007444); Grant Agency of Charles University (GAUK): 880216 (ML), 468217 (SD); Research Project of the AS CR RVO: 67985823; MSM200111601 and BIOCEV–Biotechnology and Biomedicine Centre of Academy of Sciences and Charles University in Vestec, project supported from European Regional Development Fund.

ACKNOWLEDGMENTS

We thank M. Kuntosova for excellent technical assistance, Nikola Bednarova for preparation of mutant receptors, and Kristyna Skrenkova for preparation of YFP-hGluN1 construct.

SUPPLEMENTARY MATERIAL

The Supplementary Material for this article can be found online at: https://www.frontiersin.org/articles/10.3389/fnmol.2018.00110/full#supplementary-material

REFERENCES

Abdrachmanova, G., Teisinger, J., and Vyklicky, L. Jr. (2002). Axotomy-induced changes in the properties of NMDA receptor channels in rat spinal cord motoneurons. *J. Physiol.* 538(Pt 1), 53–63. doi: 10.1113/jphysiol.2001.012794

Adams, D. R., Yuan, H., Holyoak, T., Arajs, K. H., Hakimi, P., Markello, T. C., et al. (2014). Three rare diseases in one Sib pair: RAI1, PCK1, GRIN2B mutations associated with Smith-Magenis Syndrome, cytosolic PEPCK deficiency and NMDA receptor glutamate insensitivity. *Mol. Genet. Metab.* 113, 161–170. doi: 10.1016/j.ymgme.2014.04.001

Akazawa, C., Shigemoto, R., Bessho, Y., Nakanishi, S., and Mizuno, N. (1994). Differential expression of five N-methyl-D-aspartate receptor subunit mRNAs in the cerebellum of developing and adult rats. *J. Comp. Neurol.* 347, 150–160. doi: 10.1002/cne.903470112

Awadalla, P., Gauthier, J., Myers, R. A., Casals, F., Hamdan, F. F., Griffing, A. R., et al. (2010). Direct measure of the de novo mutation rate in autism and schizophrenia cohorts. *Am. J. Hum. Genet.* 87, 316–324. doi: 10.1016/j.ajhg.2010.07.019

Bowlby, M. R. (1993). Pregnenolone sulfate potentiation of N-methyl-D-aspartate receptor channels in hippocampal neurons. *Mol. Pharmacol.* 43, 813–819.

Brooks, B. R., Brooks, C. L. III, Mackerell, A. D. Jr., Nilsson, L., Petrella, R. J., Roux, B., et al. (2009). CHARMM: the biomolecular simulation program. *J. Comput. Chem.* 30, 1545–1614. doi: 10.1002/jcc.21287

Burnashev, N., and Szepetowski, P. (2015). NMDA receptor subunit mutations in neurodevelopmental disorders. *Curr. Opin. Pharmacol.* 20, 73–82. doi: 10.1016/j.coph.2014.11.008

Cais, O., Sedlacek, M., Horak, M., Dittert, I., and Vyklicky, L. Jr. (2008). Temperature dependence of NR1/NR2B NMDA receptor channels. *Neuroscience* 151, 428–438. doi: 10.1016/j.neuroscience.2007.11.002

Chen, N., Luo, T., and Raymond, L. A. (1999). Subtype-dependence of NMDA receptor channel open probability. *J. Neurosci.* 19, 6844–6854.

Chen, W., Shieh, C., Swanger, S. A., Tankovic, A., Au, M., McGuire, M., et al. (2017). GRIN1 mutation associated with intellectual disability alters NMDA receptor trafficking and function. *J. Hum. Genet.* 62, 589–597. doi: 10.1038/jhg.2017.19

Choi, D. W. (1987). Ionic dependence of glutamate neurotoxicity. *J. Neurosci.* 7, 369–379.

Cohen, S., and Greenberg, M. E. (2008). Communication between the synapse and the nucleus in neuronal development, plasticity, and disease. *Annu. Rev. Cell Dev. Biol.* 24, 183–209. doi: 10.1146/annurev.cellbio.24.110707.175235

Colquhoun, D., and Sakmann, B. (1985). Fast events in single-channel currents activated by acetylcholine and its analogues at the frog muscle end-plate. *J. Physiol. Lond.* 369, 501–557. doi: 10.1113/jphysiol.1985.sp015912

de Ligt, J., Willemsen, M. H., van Bon, B. W., Kleefstra, T., Yntema, H. G., Kroes, T., et al. (2012). Diagnostic exome sequencing in persons with severe intellectual disability. *N. Engl. J. Med.* 367, 1921–1929. doi: 10.1056/NEJMoa1206524

PDF-XChange Editor
KOUPIT plnou verzi!
www.pdfxchange.cz

Dingledine, R., Borges, K., Bowie, D., and Traynelis, S. F. (1999). The glutamate receptor ion channels. *Pharmacol. Rev.* 51, 7–61.

Furukawa, H., Singh, S. K., Mancusso, R., and Gouaux, E. (2005). Subunit arrangement and function in NMDA receptors. *Nature* 438, 185–192. doi: 10.1038/nature04089

Hall, B. J., Ripley, B., and Ghosh, A. (2007). NR2B signaling regulates the development of synaptic AMPA receptor current. *J. Neurosci.* 27, 13446–13456. doi: 10.1523/JNEUROSCI.3793-07.2007

Hamdan, F. F., Srour, M., Capo-Chichi, J. M., Daoud, H., Nassif, C., Patry, L., et al. (2014). De novo mutations in moderate or severe intellectual disability. *PLoS Genet.* 10:e1004772. doi: 10.1371/journal.pgen.1004772

Hedegaard, M., Hansen, K. B., Andersen, K. T., Brauner-Osborne, H., and Traynelis, S. F. (2012). Molecular pharmacology of human NMDA receptors. *Neurochem. Int.* 61, 601–609. doi: 10.1016/j.neuint.2011.11.016

Horak, M., Chang, K., and Wenthold, R. J. (2008). Masking of the endoplasmic reticulum retention signals during assembly of the NMDA receptor. *J. Neurosci.* 28, 3500–3509. doi: 10.1523/JNEUROSCI.5239-07.2008

Horak, M., Vlcek, K., Chodounska, H., and Vyklicky, L. Jr. (2006). Subtype-dependence of N-methyl-d-aspartate receptor modulation by pregnenolone sulfate. *Neuroscience* 137, 93–102. doi: 10.1016/j.neuroscience.2005.08.058

Horak, M., Vlcek, K., Petrovic, M., Chodounska, H., and Vyklicky, L. Jr. (2004). Molecular mechanism of pregnenolone sulfate action at NR1/NR2B receptors. *J. Neurosci.* 24, 10318–10325. doi: 10.1523/JNEUROSCI.2099-04.2004

Hu, C., Chen, W., Myers, S. J., Yuan, H., and Traynelis, S. F. (2016). Human GRIN2B variants in neurodevelopmental disorders. *J. Pharmacol. Sci.* 132, 115–121. doi: 10.1016/j.jphs.2016.10.002

Huettner, J. E., and Bean, B. P. (1988). Block of N-methyl-D-aspartate-activated current by the anticonvulsant MK-801: selective binding to open channels. *Proc. Natl. Acad. Sci. U.S.A.* 85, 1307–1311. doi: 10.1073/pnas.85.4.1307

Huganir, R. L., and Nicoll, R. A. (2013). AMPARs and synaptic plasticity: the last 25 years. *Neuron* 80, 704–717. doi: 10.1016/j.neuron.2013.10.025

Jahr, C. E. (1992). High probability opening of NMDA receptor channels by L-glutamate. *Science* 255, 470–472.

Jo, S., Kim, T., Iyer, V. G., and Im, W. (2008). CHARMM-GUI: a web-based graphical user interface for CHARMM. *J. Comput. Chem.* 29, 1859–1865. doi: 10.1002/jcc.20945

Kaniakova, M., Krausova, B., Vyklicky, V., Korinek, M., Lichnerova, K., Vyklicky, L., et al. (2012). Key amino acid residues within the third membrane domains of NR1 and NR2 subunits contribute to the regulation of the surface delivery of N-methyl-D-aspartate receptors. *J. Biol. Chem.* 287, 26423–26434. doi: 10.1074/jbc.M112.339085

Karakas, E., and Furukawa, H. (2014). Crystal structure of a heterotetrameric NMDA receptor ion channel. *Science* 344, 992–997. doi: 10.1126/science.1251915

Kazi, R., Dai, J., Sweeney, C., Zhou, H. X., and Wollmuth, L. P. (2014). Mechanical coupling maintains the fidelity of NMDA receptor-mediated currents. *Nat. Neurosci.* 17, 914–922. doi: 10.1038/nn.3724

Korinek, M., Kapras, V., Vyklicky, V., Adamusova, E., Borovska, J., Vales, K., et al. (2011). Neurosteroid modulation of N-methyl-D-aspartate receptors: molecular mechanism and behavioral effects. *Steroids* 76, 1409–1418. doi: 10.1016/j.steroids.2011.09.002

Krausova, B., Slavikova, B., Nekardova, M., Hubalkova, P., Vyklicky, V., Chodounska, H., et al. (2018). Positive modulators of N-Methyl-D-aspartate receptor: structure-activity relationship study on steroidal 3-hemiesters. *J. Med. Chem.*

Krupp, J. J., Vissel, B., Heinemann, S. F., and Westbrook, G. L. (1998). N-terminal domains in the NR2 subunit control desensitization of NMDA receptors. *Neuron* 20, 317–327. doi: 10.1016/S0896-6273(00)80459-6

Kuner, T., Wollmuth, L. P., Karlin, A., Seeburg, P. H., and Sakmann, B. (1996). Structure of the NMDA receptor channel M2 segment inferred from the accessibility of substituted cysteines. *Neuron* 17, 343–352. doi: 10.1016/S0896-6273(00)80165-8

Kupper, J., Ascher, P., and Neyton, J. (1996). Probing the pore region of recombinant N-methyl-D-aspartate channels using external and internal magnesium block. *Proc. Natl. Acad. Sci. U.S.A.* 93, 8648–8653. doi: 10.1073/pnas.93.16.8648

Kutsuwada, T., Sakimura, K., Manabe, T., Takayama, C., Katakura, N., Kushiya, E., et al. (1996). Impairment of suckling response, trigeminal neuronal pattern formation, and hippocampal LTD in NMDA receptor epsilon 2 subunit mutant mice. *Neuron* 16, 333–344. doi: 10.1016/S0896-6273(00)80051-3

Lazaridis, T. (2003). Effective energy function for proteins in lipid membranes. *Proteins* 52, 176–192. doi: 10.1002/prot.10410

Lee, C. H., Lü, W., Michel, J. C., Goehring, A., Du, J., Song, X., et al. (2014). NMDA receptor structures reveal subunit arrangement and pore architecture. *Nature* 511, 191–197. doi: 10.1038/nature13548

Lek, M., Karczewski, K. J., Minikel, E. V., Samocha, K. E., Banks, E., Fennell, T., et al. (2016). Analysis of protein-coding genetic variation in 60,706 humans. *Nature* 536, 285–291. doi: 10.1038/nature19057

Lelieveld, S. H., Reijnders, M. R., Pfundt, R., Yntema, H. G., Kamsteeg, E. J., de Vries, P., et al. (2016). Meta-analysis of 2,104 trios provides support for 10 new genes for intellectual disability. *Nat. Neurosci.* 19, 1194–1196. doi: 10.1038/nn.4352

Lemke, J. R., Hendrickx, R., Geider, K., Laube, B., Schwake, M., Harvey, R. J., et al. (2014). GRIN2B mutations in West syndrome and intellectual disability with focal epilepsy. *Ann. Neurol.* 75, 147–154. doi: 10.1002/ana.24073

Lester, R. A., Clements, J. D., Westbrook, G. L., and Jahr, C. E. (1990). Channel kinetics determine the time course of NMDA receptor-mediated synaptic currents. *Nature* 346, 565–567.

Lichnerova, K., Kaniakova, M., Skrenkova, K., Vyklicky, L., and Horak, M. (2014). Distinct regions within the GluN2C subunit regulate the surface delivery of NMDA receptors. *Front. Cell. Neurosci.* 8:375. doi: 10.3389/fncel.2014.00375

Lynch, M. A. (2004). Long-term potentiation and memory. *Physiol. Rev.* 84, 87–136. doi: 10.1152/physrev.00014.2003

Mcrae, J. F., Clayton, S., Fitzgerald, T. W., Kaplanis, J., Prigmore, E., Rajan, D., et al. (2017). Prevalence and architecture of de novo mutations in developmental disorders. *Nature* 542, 433-438. doi: 10.1038/nature21062

Mendes, P. (1993). GEPASI: a software package for modelling the dynamics, steady states and control of biochemical and other systems. *Comput. Appl. Biosci.* 9, 563–571. doi: 10.1093/bioinformatics/9.5.563

Mendes, P. (1997). Biochemistry by numbers: simulation of biochemical pathways with Gepasi 3. *Trends Biochem. Sci.* 22, 361–363. doi: 10.1016/S0968-0004(97)01103-1

Mendes, P., and Kell, D. (1998). Non-linear optimization of biochemical pathways: applications to metabolic engineering and parameter estimation. *Bioinformatics* 14, 869–883. doi: 10.1093/bioinformatics/14.10.869

Monyer, H., Burnashev, N., Laurie, D. J., Sakmann, B., and Seeburg, P. H. (1994). Developmental and regional expression in the rat brain and functional properties of four NMDA receptors. *Neuron* 12, 529–540. doi: 10.1016/0896-6273(94)90210-0

Mullier, B., Wolff, C., Sands, Z. A., Ghisdal, P., Muglia, P., Kaminski, R. M., et al. (2017). GRIN2B gain of function mutations are sensitive to radiprodil, a negative allosteric modulator of GluN2B-containing NMDA receptors. *Neuropharmacology* 123, 322–331. doi: 10.1016/j.neuropharm.2017.05.017

Ogden, K. K., Chen, W., Swanger, S. A., McDaniel, M. J., Fan, L. Z., Hu, C., et al. (2017). Molecular mechanism of disease-associated mutations in the Pre-M1 Helix of NMDA receptors and potential rescue pharmacology. *PLoS Genet.* 13:e1006536. doi: 10.1371/journal.pgen.1006536

Ogden, K. K., and Traynelis, S. F. (2013). Contribution of the M1 transmembrane helix and pre-M1 region to positive allosteric modulation and gating of N-methyl-D-aspartate receptors. *Mol. Pharmacol.* 83, 1045–1056. doi: 10.1124/mol.113.085209

Okabe, S., Miwa, A., and Okado, H. (1999). Alternative splicing of the C-terminal domain regulates cell surface expression of the NMDA receptor NR1 subunit. *J. Neurosci.* 19, 7781–7792.

Olney, J. W. (1969). Brain lesions, obesity, and other disturbances in mice treated with monosodium glutamate. *Science* 164, 719–721.

Parsons, M. P., and Raymond, L. A. (2014). Extrasynaptic NMDA receptor involvement in central nervous system disorders. *Neuron* 82, 279–293. doi: 10.1016/j.neuron.2014.03.030

Platzer, K., Yuan, H., Schütz, H., Winschel, A., Chen, W., Hu, C., et al. (2017). GRIN2B encephalopathy: novel findings on phenotype, variant clustering, functional consequences and treatment aspects. *J. Med. Genet.* 54, 460–470. doi: 10.1136/jmedgenet-2016-104509

Rosenmund, C., Feltz, A., and Westbrook, G. L. (1995). Synaptic NMDA receptor channels have a low open probability. *J. Neurosci.* 15, 2788–2795.

PDF-XChange Editor
KOUPIT plnou verzi!
www.pdfxchange.cz

Sali, A., and Blundell, T. L. (1993). Comparative protein modelling by satisfaction of spatial restraints. *J. Mol. Biol.* 234, 779–815. doi: 10.1006/jmbi.1993.1626

Sobolevskii, A. I., and Khodorov, B. I. (2002). Blocker studies of the functional architecture of the NMDA receptor channel. *Neurosci. Behav. Physiol.* 32, 157–171. doi: 10.1023/A:1013927409034

Sobolevsky, A. I., Rosconi, M. P., and Gouaux, E. (2009). X-ray structure, symmetry and mechanism of an AMPA-subtype glutamate receptor. *Nature* 462, 745–756. doi: 10.1038/nature08624

Sobolevsky, A. I., Yelshansky, M. V., and Wollmuth, L. P. (2004). The outer pore of the glutamate receptor channel has 2-fold rotational symmetry. *Neuron* 41, 367–378. doi: 10.1016/S0896-6273(04)00008-X

Soto, D., Altafaj, X., Sindreu, C., and Bayes, A. (2014). Glutamate receptor mutations in psychiatric and neurodevelopmental disorders. *Commun. Integr. Biol.* 7:e27887. doi: 10.4161/cib.27887

Standley, S., Roche, K. W., McCallum, J., Sans, N., and Wenthold, R. J. (2000). PDZ domain suppression of an ER retention signal in NMDA receptor NR1 splice variants. *Neuron* 28, 887–898. doi: 10.1016/S0896-6273(00)00161-6

Swanger, S. A., Chen, W., Wells, G., Burger, P. B., Tankovic, A., Bhattacharya, S., et al. (2016). Mechanistic Insight into NMDA Receptor Dysregulation by Rare Variants in the GluN2A and GluN2B Agonist Binding Domains. *Am. J. Hum. Genet.* 99, 1261–1280. doi: 10.1016/j.ajhg.2016.10.002

Tarabeux, J., Kebir, O., Gauthier, J., Hamdan, F. F., Xiong, L., Piton, A., et al. (2011). Rare mutations in N-methyl-D-aspartate glutamate receptors in autism spectrum disorders and schizophrenia. *Transl. Psychiatr.* 1:e55. doi: 10.1038/tp.2011.52

Thomas, C. G., Krupp, J. J., Bagley, E. E., Bauzon, R., Heinemann, S. F., Vissel, B., et al. (2006). Probing N-methyl-D-aspartate receptor desensitization with the substituted-cysteine accessibility method. *Mol. Pharmacol.* 69, 1296–1303. doi: 10.1124/mol.105.017350

Traynelis, S. F., Wollmuth, L. P., McBain, C. J., Menniti, F. S., Vance, K. M., Ogden, K. K., et al. (2010). Glutamate receptor ion channels: structure, regulation, and function. *Pharmacol. Rev.* 62, 405–496. doi: 10.1124/pr.109.002451

Turecek, R., Vlcek, K., Petrovic, M., Horak, M., Vlachova, V., and Vyklicky, L. Jr. (2004). Intracellular spermine decreases open probability ofN-methyl-d-aspartate receptor channels. *Neuroscience* 125, 879–887. doi: 10.1016/j.neuroscience.2004.03.003

Villarroel, A., Burnashev, N., and Sakmann, B. (1995). Dimensions of the narrow portion of a recombinant NMDA receptor channel. *Biophys. J.* 68, 866–875. doi: 10.1016/S0006-3495(95)80263-8

Villarroel, A., Regalado, M. P., and Lerma, J. (1998). Glycine-independent NMDA receptor desensitization: localization of structural determinants. *Neuron* 20, 329–339. doi: 10.1016/S0896-6273(00)80460-2

Vyklicky, L. Jr., Krusek, J., and Edwards, C. (1988). Differences in the pore sizes of the N-methyl-D-aspartate and kainate cation channels. *Neurosci. Lett.* 89, 313–318. doi: 10.1016/0304-3940(88)90545-9

Vyklicky, V., Korinek, M., Balik, A., Smejkalova, T., Krausova, B., and Vyklicky, L. (2016) "Analysis of whole-cell NMDA receptor currents," in *Ionotropic Glutamate Receptor Technologies*. Neuromethods, Vol. 106, G. Popescu (New York, NY: Humana Press), 205–219.

Vyklicky, V., Krausova, B., Cerny, J., Balik, A., Zapotocky, M., Novotny, M., et al. (2015). Block of NMDA receptor channels by endogenous neurosteroids: implications for the agonist induced conformational states of the channel vestibule. *Sci. Rep.* 5:10935. doi: 10.1038/srep10935

Webb, B., and Sali, A. (2014). Comparative Protein Structure Modeling Using MODELLER. *Curr. Protoc. Bioinformatics* 47, Chapter 5: Unit-5.6 1–32. doi: 10.1002/0471250953.bi0506s47

Weiss, J. N. (1997). The Hill equation revisited: uses and misuses. *FASEB J.* 11, 835–841. doi: 10.1096/fasebj.11.11.9285481

Williams, K., Pahk, A. J., Kashiwagi, K., Masuko, T., Nguyen, N. D., and Igarashi, K. (1998). The selectivity filter of the N-methyl-D-aspartate receptor: a tryptophan residue controls block and permeation of Mg^{2+}. *Mol. Pharmacol.* 53, 933–941.

Wu, F. S., Gibbs, T. T., and Farb, D. H. (1991). Pregnenolone sulfate: a positive allosteric modulator at the N-methyl-D- aspartate receptor. *Mol. Pharmacol.* 40, 333–336.

Yavarna, T., Al-Dewik, N., Al-Mureikhi, M., Ali, R., Al-Mesaifri, F., Mahmoud, L., et al. (2015). High diagnostic yield of clinical exome sequencing in Middle Eastern patients with Mendelian disorders. *Hum. Genet.* 134, 967–980. doi: 10.1007/s00439-015-1575-0

Yuan, H., Hansen, K. B., Zhang, J., Pierson, T. M., Markello, T. C., Fajardo, K. V., et al. (2014). Functional analysis of a de novo GRIN2A missense mutation associated with early-onset epileptic encephalopathy. *Nat. Commun.* 5:3251. doi: 10.1038/ncomms4251

Zarei, M. M., and Dani, J. A. (1995). Structural basis for explaining open-channel blockade of the NMDA receptor. *J. Neurosci.* 15, 1446–1454.

Zhou, Y., Morais-Cabral, J. H., Kaufman, A., and MacKinnon, R. (2001). Chemistry of ion coordination and hydration revealed by a K+ channel-Fab complex at 2.0 A resolution. *Nature* 414, 43–48. doi: 10.1038/35102009

Zhu, X., Petrovski, S., Xie, P., Ruzzo, E. K., Lu, Y. F., McSweeney, K. M., et al. (2015). Whole-exome sequencing in undiagnosed genetic diseases: interpreting 119 trios. *Genet. Med.* 17, 774–781. doi: 10.1038/gim.2014.191

Conflict of Interest Statement: The authors declare that the research was conducted in the absence of any commercial or financial relationships that could be construed as a potential conflict of interest.

Copyright © 2018 Vyklicky, Krausova, Cerny, Ladislav, Smejkalova, Kysilov, Korinek, Danacikova, Horak, Chodounska, Kudova and Vyklicky. This is an open-access article distributed under the terms of the Creative Commons Attribution License (CC BY). The use, distribution or reproduction in other forums is permitted, provided the original author(s) and the copyright owner are credited and that the original publication in this journal is cited, in accordance with accepted academic practice. No use, distribution or reproduction is permitted which does not comply with these terms.

PDF-XChange Editor
KOUPIT plnou verzi!
www.pdfxchange.cz

Journal of Medicinal Chemistry

Article

Cite This: J. Med. Chem. 2018, 61, 4505−4516

pubs.acs.org/jmc

Positive Modulators of the *N*-Methyl-D-aspartate Receptor: Structure−Activity Relationship Study of Steroidal 3-Hemiesters

Barbora Krausova,[†] Barbora Slavikova,[‡] Michaela Nekardova,[‡,§] Pavla Hubalkova,[†,∥] Vojtech Vyklicky,[†] Hana Chodounska,[‡] Ladislav Vyklicky,[†] and Eva Kudova*[,‡]

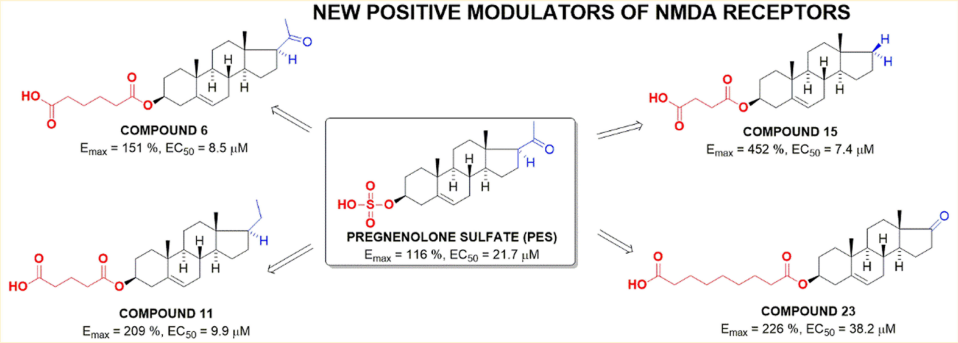
[†]Institute of Physiology of the Czech Academy of Sciences, Videnska 1083, Prague 4, 142 20, Czech Republic

[‡]Institute of Organic Chemistry and Biochemistry of the Czech Academy of Sciences, Flemingovo nam. 2, Prague 6, 166 10, Czech Republic

[§]Faculty of Mathematics and Physics, Charles University in Prague, Ke Karlovu 3, Prague 2, 121 16, Czech Republic

[∥]Third Faculty of Medicine, Charles University in Prague, Ruska 87, Prague 10, 100 00, Czech Republic

Supporting Information



ABSTRACT: Here, we report the synthesis of pregn-5-ene and androst-5-ene dicarboxylic acid esters and explore the structure−activity relationship (SAR) for their modulation of *N*-methyl-D-aspartate receptors (NMDARs). All compounds were positive modulators of recombinant GluN1/GluN2B receptors (EC_{50} varying from 1.8 to 151.4 μM and E_{max} varying from 48% to 452%). Moreover, 10 compounds were found to be more potent GluN1/GluN2B receptor modulators than endogenous pregnenolone sulfate (EC_{50} = 21.7 μM). The SAR study revealed a relationship between the length of the residues at carbon C-3 of the steroid molecule and the positive modulatory effect at GluN1/GluN2B receptors for various D-ring modifications. A selected compound, 20-oxo-pregnenolone hemiadipate, potentiated native NMDARs to a similar extent as GluN1/GluN2A-D receptors and inhibited AMPARs and $GABA_AR$ responses. These results provide a unique opportunity for the development of new steroid based drugs with potential use in the treatment of neuropsychiatric disorders involving hypofunction of NMDARs.

INTRODUCTION

N-Methyl-D-aspartate receptors (NMDARs) are glutamate-gated, calcium-permeable ion channels that are activated during excitatory synaptic transmission and are implicated in various forms of synaptic plasticity,[1] which underlies learning and memory processes.[2] Next-generation genome sequencing allowed identification of mutations in *GRIN* genes encoding for human NMDAR subunits that have been associated with various neurodevelopmental disorders.[3] The analysis of mutated receptors revealed various forms of trafficking and functional defects.[4] Positive allosteric modulators (PAMs) that increase the activity of NMDARs may provide a therapeutic aid for patients suffering from neuropsychiatric disorders where NMDARs hypofunction is thought to be involved, such as intellectual disability,[5] autism spectrum disorder,[6] or schizophrenia.[7]

Neurosteroids are endogenous steroidal compounds that modulate the activity of NMDARs.[8] Despite structural similarity between different neurosteroids, they can exhibit opposite effects at NMDARs, apparently mediated by different molecular mechanisms. The inhibitory effect of neurosteroids on NMDARs is dependent upon a 3α negatively charged substituent and 5β-stereochemistry.[9] This class of neurosteroids is represented by endogenous pregnanolone sulfate (20-oxo-5β-pregnan-3α-yl sulfate, Figure 1A).[10] In contrast, a 3β-negatively charged moiety in combination with Δ^5-stereochemistry (a double bond between C-5 and C-6) favors potentiation of NMDARs.[9a,11] This class of neurosteroids is represented by endogenous pregnenolone sulfate (20-oxo-pregn-5-en-3β-yl sulfate, compound **1**, PES, Figure 1B).[12] PES is an abundantly occurring neurosteroid synthesized de novo in the central nervous system, which exhibits different modulatory effects on several types of

Received: February 15, 2018
Published: April 30, 2018

ACS Publications © 2018 American Chemical Society

DOI: 10.1021/acs.jmedchem.8b00255
J. Med. Chem. 2018, 61, 4505−4516

PDF-XChange Editor
KOUPIT plnou verzi!
www.pdfxchange.cz

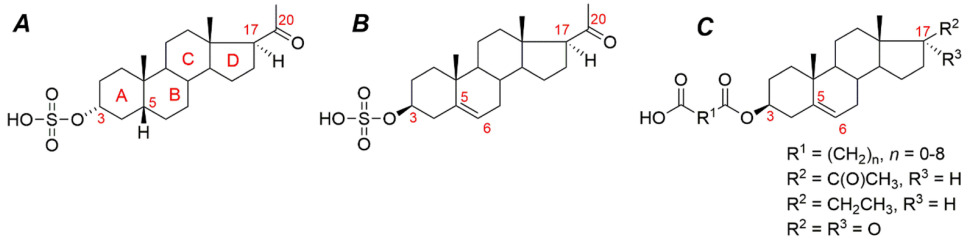
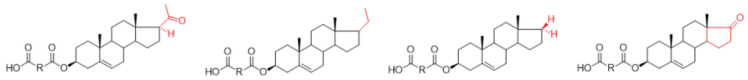


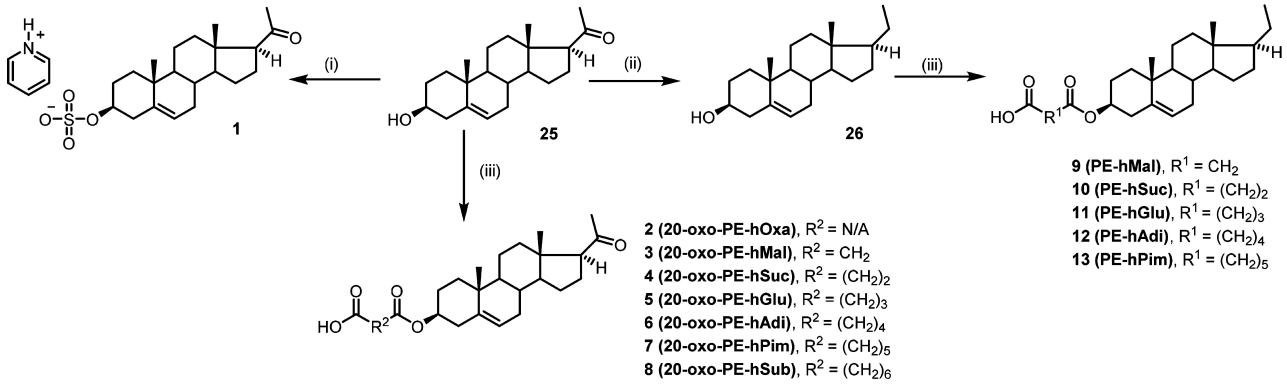
Figure 1. Structure of (A) pregnanolone sulfate, (B) pregnenolone sulfate (**1**, PES), and (C) hemiester analogues of PES.

Table 1. Structures of PES Analogues: Compounds 2−24



C-3 Moiety \ Steroid	20-Oxo-pregn-5-ene compounds	Pregn-5-ene compounds	Androst-5-ene compounds	17-Oxo-androst-5-ene compounds
C_2 (hemiOxalate), R = none	2 (20-Oxo-PE-hOxa)	-	-	-
C_3 (hemiMalonate), R = CH_2	3 (20-Oxo-PE-hMal)	9 (PE-hMal)	14 (AND-hMal)	-
C_4 (hemiSuccinate), R = $(CH_2)_2$	4 (20-Oxo-PE-hSuc)	10 (PE-hSuc)	15 (AND-hSuc)	-
C_5 (hemiGlutarate), R = $(CH_2)_3$	5 (20-Oxo-PE-hGlu)	11 (PE-hGlu)	16 (AND-hGlu)	19 (17-Oxo-AND-hGlu)
C_6 (hemiAdipate), R = $(CH_2)_4$	6 (20-Oxo-PE-hAdi)	12 (PE-hAdi)	17 (AND-hAdi)	20 (17-Oxo-AND-hAdi)
C_7 (hemiPimelate), R = $(CH_2)_5$	7 (20-Oxo-PE-hPim)	13 (PE-hPim)	18 (AND-hPim)	21 (17-Oxo-AND-hPim)
C_8 (hemiSuberate), R = $(CH_2)_6$	8 (20-Oxo-PE-hSub)	-	-	22 (17-Oxo-AND-hSub)
C_9 (hemiAzelate), R = $(CH_2)_7$	-	-	-	23 (17-Oxo-AND-hAze)
C_{10} (hemiSebacate), R = $(CH_2)_8$	-	-	-	24 (17-Oxo-AND-hSeb)

Scheme 1. Synthesis of Pregn-5-ene Derivatives (1−13)[a]



[a]Reagents and conditions: (i) sulfur trioxide−pyridine complex, $CHCl_3$, pyridine; (ii) Zn, TMSCl, MeOH, DCM. (iii) For compound **2**: oxalyl chloride, Et_3N, DCM, DMF. For compounds **3** and **9**: Meldrum's acid, toluene, 80 °C. For compounds **4** and **10**: succinic anhydride, DMAP, pyridine, 110 °C. For compounds **5** and **11**: glutaric anhydride, DMAP, pyridine, 110 °C. For compounds **6** and **12**: adipic acid, EDCI, DIPEA, DMAP, DCM. For compound **7** and **13**: pimelic acid, EDCI, DIPEA, DMAP, DCM. For compound **8**: suberic acid, EDCI, DIPEA, DMAP, DCM.

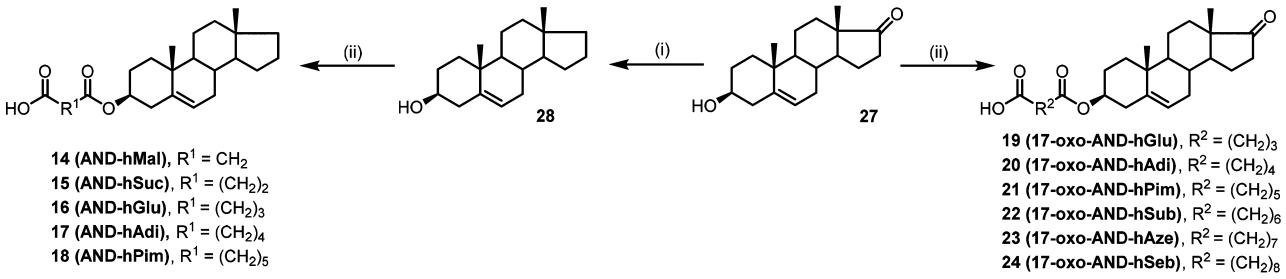
receptors, specifically potentiating the responses elicited by NMDARs[12] while inhibiting currents mediated by γ-amino-butyric acid type A receptors ($GABA_A$Rs),[13] glycine receptors,[14] and α-amino-3-hydroxy-5-methyl-4-isoxazolepropionic acid receptors (AMPARs).[12] A memory enhancement effect after the administration of PES in vivo has been reported.[15]

A structurally distinct class of compounds that act as PAMs of NMDARs, represented by (3-chlorophenyl)(6,7-dimethoxy-1-((4-methoxyphenoxy)methyl)-3,4-dihydroisoquinolin-2(1*H*)-yl)methanone (CIQ), was identified by an extensive study involving 100 000 substances focused on selective action at NMDARs containing GluN2C or GluN2D subunits.[16] The most effective CIQ analogs have EC_{50} values in the submicromolar

DOI: 10.1021/acs.jmedchem.8b00255
J. Med. Chem. 2018, 61, 4505−4516

PDF-XChange Editor KOUPIT plnou verzi! www.pdfxchange.cz

Scheme 2. Synthesis of Androst-5-ene derivatives (14−24)[a]



[a]Reagents and conditions: (i) Zn, TMSCl, MeOH, DCM. (ii) For compound **14**: Meldrum's acid, toluene, 80 °C. For compound **15**: succinic anhydride, DMAP, pyridine, 110 °C. For compounds **16** and **19**: glutaric anhydride, DMAP, pyridine, 110 °C. For compounds **17** and **20**: adipic acid, EDCI, DIPEA, DMAP, DCM. For compounds **18** and **21**: pimelic acid, EDCI, DIPEA, DMAP, DCM. For compound **22**: suberic acid, EDCI, DIPEA, DMAP, DCM. For compound **23**: azelaic acid, EDCI, DIPEA, DMAP, DCM. For compound **24**: sebacic acid, EDCI, DIPEA, DMAP, DCM.

range and induce an approximately 2-fold potentiation of GluN1/GluN2D receptor responses.[17] By replacement of the dimethyl groups on the C-ring with one isopropoxyl group, CIQ analogues can be targeted to the GluN2B subunit.[18] However, the analogue that acts solely at GluN2B subunits exhibits only moderate efficacy and potency (E_{max} = 152%; EC_{50} = 7.2 μM).[18]

The SAR for steroid-based PAMs of NMDARs is only poorly understood and therefore needs to by further characterized, especially in the context of the development of new drug candidates for the prevention and/or treatment of neuropsychiatric disorders and age-related memory deficits.[4,19] Here, we describe a SAR study on hemiester analogues **2**−**24** (Figure 1C and Table 1) with varying lengths of C-3 substituents and different steroidal D-ring modifications, primarily focusing on fine-tuning their modulatory effect on NMDARs. The biological activity of compounds **2**−**24** was evaluated on recombinant GluN1/GluN2B receptors expressed in human embryonic kidney (HEK293) cells. The effect of a selected compound, 20-oxo-pregn-5-ene hemiadipate (**6**), was further analyzed on recombinant GluN1/GluN2A−D receptors, and native NMDARs, AMPARs, and $GABA_A$Rs expressed in hippocampal neurons.

RESULTS AND DISCUSSION

Chemistry. The synthesis of compounds **1**−**13** is summarized in Scheme 1. Compounds **1**−**8** were prepared from commercially available 20-oxo-pregn-5-en-3β-ol (pregnenolone, compound **25**, Steraloids, Newport, RI, USA). Compounds **9**−**13** were prepared from 3β-hydroxy-pregn-5-ene (**26**), which was obtained by the Zn/TMSCl-mediated Clemmensen reduction[20] of pregnenolone **25** (78% yield). Pyridinium salt of pregnenolone sulfate (**1**) was prepared by the treatment of pregnenolone (**25**) with a sulfur trioxide−pyridine complex in $CHCl_3$ (89% yield). Note that compound **1** is not commercially available as is sodium salt and in our experiments exerts better solubility and chemical stability. Compound **2** was prepared by the treatment of pregnenolone **25** with oxalyl chloride in DCM, Et_3N, and DMF (36% yield). Compounds **3** and **9** were prepared by the treatment of **25** and **26**, respectively, with Meldrum's acid in toluene at 80 °C (37% and 32% yield, respectively). Compounds **4**, **10** and **5**, **11** were prepared by the treatment of **25** and **26** respectively with succinic or glutaric anhydride and DMAP in pyridine at 110 °C, yielding hemiesters **4** (52% yield), **5** (51% yield), **10** (43% yield), and **11** (44% yield). Compounds **6**−**8** and **12**, **13** were prepared by the treatment of **25** and **26**, respectively, with adipic, pimelic, or suberic acid, 1-ethyl-3-(3-dimethylaminopropyl)carbodiimide (EDCI), *N*,*N*-diisopropylethylamine (DIPEA), and DMAP in DCM, yielding hemiesters **6** (42% yield), **7** (47% yield), **8** (44% yield), **12** (21% yield), and **13** (35% yield).

The synthesis of compounds **14**−**24** is summarized in Scheme 2. Compounds **19**−**24** were prepared from commercially available 17-oxo-androst-5-en-3β-ol (**27**, Steraloids, Newport, RI, USA). Compounds **14**−**18** were prepared from 3β-hydroxy-androst-5-ene (**28**),[21] which was obtained by the Zn/TMSCl-mediated Clemmensen reduction[20] of compound **27** (75% yield). Compound **14** was prepared by the treatment of **28** with Meldrum's acid in toluene at 80 °C (13% yield). Compounds **15**, **16**, and **19** were prepared by the treatment of **27** and **28** respectively with succinic or glutaric anhydride and DMAP in pyridine at 110 °C, yielding hemiesters **15** (67% yield), **16** (42% yield), and **19** (58% yield). Compounds **17**, **18**, and **20**−**24** were prepared by the treatment of **27** and **28** respectively with adipic, pimelic, suberic, azelaic, or sebacic acid, EDCI, DIPEA, and DMAP in DCM, yielding hemiesters **17** (35% yield), **18** (42% yield), **20** (31% yield), **21** (35% yield), **22** (50% yield), **23** (24% yield), and **24** (27% yield). Although these unoptimized reactions provided low yields of the desired products, we have demonstrated the feasibility of this approach to obtain compounds **14**−**24**.

Biological Activity. To investigate the effect of PES (**1**) and its analogues (compounds **2**−**24**; Figure 1C and Table 1) on the activity of NMDARs, electrophysiological measurements were performed on HEK293 cells that were co-transfected with cDNAs containing genes encoding for the rat GluN1-1a and GluN2B subunits. The degree of modulation (*E*; potentiation/inhibition) for the newly synthesized compounds was determined using the following formula:

$$E = \frac{I_e - I_a}{I_a} \times 100 \quad (1)$$

where I_e is the value of the current amplitude during glutamate and compound coapplication and I_a is the current amplitude value for glutamate application. The degree of potentiation (%) was determined for five compound doses, differing 100-fold in their concentration range, in individual cells, and data were fit to the following equation:

DOI: 10.1021/acs.jmedchem.8b00255
J. Med. Chem. 2018, 61, 4505−4516

PDF-XChange Editor
KOUPIT plnou verzi!
www.pdfxchange.cz

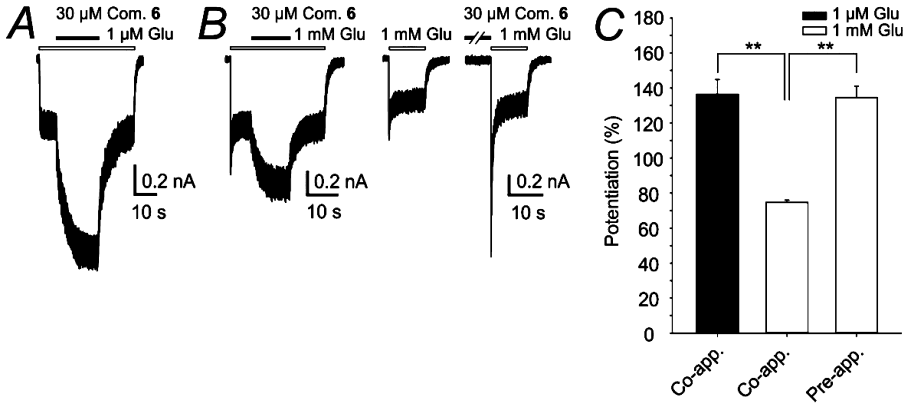


Figure 2. Potentiating effect of compound **6** at GluN1/GluN2B receptors. Examples of traces obtained from HEK293 cells transiently expressing GluN1/GluN2B receptors. (A) Compound **6** (30 μM) was applied simultaneously with 1 μM glutamate (the duration of compound **6** and glutamate application is indicated by filled and open bars, respectively). (B) Compound **6** (30 μM) was either coapplied with 1 mM glutamate (on the left) or preapplied before the receptor was activated by 1 mM glutamate (control and potentiated response on the right). (C) Bar graph shows the degree of potentiation by compound **6** (30 μM) when coapplied with 1 μM glutamate (filled bar), coapplied with 1 mM glutamate (open bar), and preapplied prior to 1 mM glutamate (open bar). Asterisks mark significance at the level of $P \leq 0.001$.

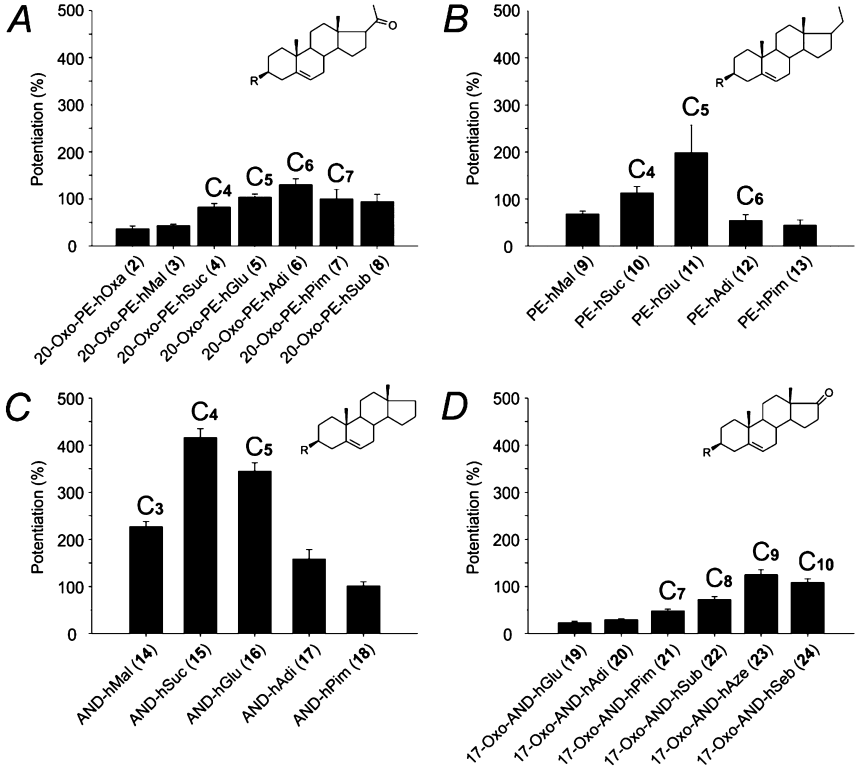


Figure 3. Effect of compounds **2**–**24** on current responses of GluN1/GluN2B receptors. Bar graphs show changes in response to the application of compounds **2**–**24** at a concentration of 30 μM. The numbers above the bars indicate the number of carbons of the particular hemiester moiety. (A) 20-Oxo-pregn-5-en-3β-yl hemiesters. (B) Pregn-5-en-3β-yl hemiesters. (C) Androst-5-en-3β-yl hemiesters. (D) 17-Oxo-androst-5-en-3β-yl hemiesters. Differences in mean values within the structurally related groups (**2**–**8**, **9**–**13**, **14**–**18**, and **19**–**24**) were statistically significant (one way ANOVA; $P < 0.001$).

$$E = \frac{E_{max}}{1 + \left(\frac{EC_{50}}{[compound]}\right)^{h}} \quad (2)$$

where E_{max} is the maximal value of potentiation induced by a saturating concentration of the compound, EC_{50} is the concentration of the compound that produces half-maximal potentiation of the agonist-evoked current, [compound] is the compound concentration, and h is the apparent Hill coefficient.

The results are presented as mean ± SEM, with n equal to the number of studied cells. Unpaired Student's t test was used to perform a statistical comparison between two treatment groups and one-way analysis of variance (ANOVA) for multiple comparisons (unless otherwise stated, a value of $P \leq 0.05$ was used for the determination of significance).

DOI: 10.1021/acs.jmedchem.8b00255
J. Med. Chem. 2018, 61, 4505−4516

PDF-XChange Editor
KOUPIT plnou verzi!
www.pdfxchange.cz

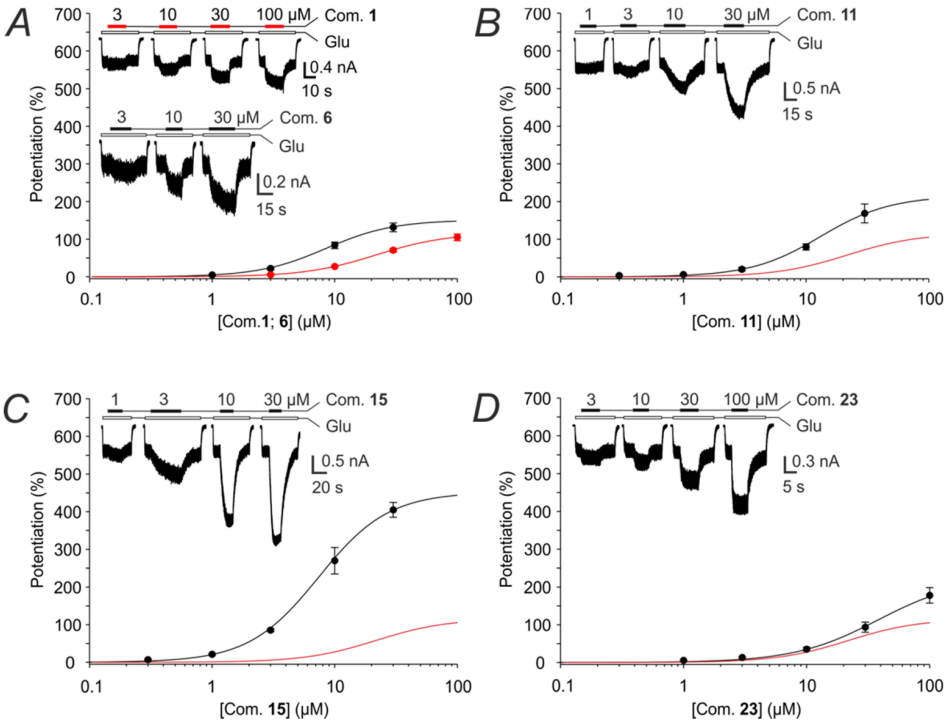


Figure 4. Effect of compounds **1**, **6**, **11**, **15**, and **23** on GluN1/GluN2B receptors. Graphs show the dose−response curves for the effect of the following compounds: (A) PES (**1**; in red) and 20-Oxo-PE-hAdi (**6**), (B) PE-hGlu (**11**), (C) AND-hSuc (**15**), and (*D*) 17-Oxo-AND-hAze (**23**) at GluN1/GluN2B receptors. The red line in (B)−(D) repeats the fitted function for PES (**1**), for comparison. Data points are averaged potentiation values from at least four independent measurements. Error bars represent SEM. The degree of potentiation of glutamate-induced responses recorded in the presence of compounds **1** (3−100 μM), **6** (1−30 μM), **11** (0.3−30 μM), **15** (0.3−30 μM), and **23** (1−100 μM) was determined in individual cells, and data were fitted to the eq 2. Insets show examples of traces obtained from HEK293 cells co-transfected with cDNAs encoding for GluN1-1a and GluN2B subunits. Compounds **1**, **6**, **11**, **15**, and **23** were applied simultaneously with 1 μM glutamate (duration of compound and glutamate application is indicated by filled and open bars, respectively; PES (**1**) in red).

Compounds 2−24 Potentiate Recombinant GluN1/GluN2B Receptor Responses. We have evaluated a relationship between the steroid structure and its modulatory effect on GluN1/GluN2B receptors for compounds **2**−**24**. Figure 2 shows that compound **6** (30 μM) potentiates GluN1/GluN2B receptor responses. The degree of potentiation was affected by the relative timing of compound and glutamate application and dependent on glutamate concentration. The responses induced by 1 μM glutamate were potentiated by 136 ± 8% (n = 10) when compound **6** was coapplied with the agonist. The potentiation was only 75 ± 1% (n = 6) when compound **6** was coapplied with a saturating concentration of glutamate (1 mM). The responses to 1 mM glutamate were potentiated by 134 ± 7% (n = 8) when compound **6** was preapplied prior to glutamate (not significantly different from the potentiation induced at a low concentration of glutamate; unpaired Student's t test, P = 0.398). These results are in agreement with the disuse-dependent effect of PES at NMDARs.[22] In subsequent experiments we used compound coaplication with 1 μM glutamate.

In initial experiments, we analyzed the effect of compounds **2**−**24** at a concentration of 30 μM on GluN1/GluN2B receptors. Figure 3 shows the SAR for the series of 20-oxo-pregn-5-enes (**2**−**8**), pregn-5-enes (**9**−**13**), androst-5-enes (**14**−**18**), and 17-oxo-androst-5-enes (**19**−**24**). The analysis of the potentiating effect indicates that there is an optimal length of the substituents at C-3 in combination with structural modification at C-17 of the steroidal D-ring for acquiring the desired biological effect. Once the 20-oxo substituent of 20-oxo-PE-hAdi (**6**) was removed, the most efficacious PAM was PE-hGlu (**11**), which has a C-3 moiety with five carbons. Analogously, when the steroidal skeleton does not bear the C-17 acyl, the most efficacious PAM was AND-hSuc (**15**), which has a C-3 moiety with four carbons. Such common structural features for compounds **2**−**24** may characterize the pharmacophore of steroidal structural requirements for the optimal potentiating effect at NMDARs. Previously, compounds **2**, **4**, and **5** were found to enhance NMDARs-induced Ca^{2+} accumulation in cultured hippocampal neurons.[9a]

Next, we have performed dose−response analysis for the effect of compounds **1**−**24** on GluN1/GluN2B receptor responses induced by 1 μM glutamate (Figure 4). Fit to eq 2 provided information on the compounds **1**−**24** efficacy and potency. The E_{max} and EC_{50} values for compounds **1**−**24** are shown in Table 2. Compounds **1**−**8** and **21**−**24** were measured up to a concentration of 100 μM and compounds **19** and **20** up to a concentration of 300 μM. Compounds **9**−**18** were measured up to a concentration of 30 μM due to their limited solubility. Our data show that 17 out of 23 newly synthesized compounds had increased efficacy and/or potency at GluN1/GluN2B receptors as compared to endogenous PES (**1**).

The series of 20-oxo-pregn-5-enes (**2**−**8**) exhibits similar values of E_{max} within this structural family (from 93% for the least efficacious compound **2** to 191% for the most efficacious compound 7). In contrast, the EC_{50} values for compounds **2**−**8** differ significantly, with the EC_{50} of the most potent compound **6** (Figure 4A) being up to 6-fold lower (8.5 μM) than that of the least potent compound **2** (48.5 μM). The dose−response

DOI: 10.1021/acs.jmedchem.8b00255
J. Med. Chem. 2018, 61, 4505−4516

PDF-XChange Editor
KOUPIT plnou verzi!
www.pdfxchange.cz

Table 2. Summary of the Dose−Response Analysis Data for the Potentiating Effect of Compounds 1−24 at GluN1/GluN2B Receptor Responses[a]

steroid	E_{max} ± SEM (%)	EC_{50} ± SEM (μM)	h ± SEM	n
PES (**1**)	116 ± 10	21.7 ± 1.6	1.5 ± 0.1	8
20-oxo-PE-hOxa (**2**)	93 ± 25	48.6 ± 12.4*	1.3 ± 0.0	5
20-oxo-PE-hMal (**3**)	108 ± 15	39.8 ± 10.3	1.3 ± 0.1	5
20-oxo-PE-hSuc (**4**)	177 ± 46*	27.6 ± 12.1	1.5 ± 0.2	4
20-oxo-PE-hGlu (**5**)	183 ± 25*	19.0 ± 3.4	1.4 ± 0.1	4
20-oxo-PE-hAdi (**6**)	151 ± 16	8.5 ± 1.0**	1.6 ± 0.1	10
20-oxo-PE-hPim (**7**)	191 ± 63	18.0 ± 7.9	1.4 ± 0.2	5
20-oxo-PE-hSub (**8**)	156 ± 30	19.3 ± 1.7	1.5 ± 0.1	5
one-way ANOVA	P = 0.346	**P < 0.001**	P = 0.494	
PE-hMal (**9**)	71 ± 7*	10.7 ± 0.8**	1.5 ± 0.2	7
PE-hSuc (**10**)	133 ± 19	9.9 ± 5.2*	1.4 ± 0.2	6
PE-hGlu (**11**)	209 ± 22*	9.9 ± 3.7*	1.8 ± 0.3	5
PE-hAdi (**12**)	60 ± 12*	17.2 ± 4.5	1.5 ± 0.4	4
PE-hPim (**13**)	48 ± 11*	26.2 ± 8.1	1.4 ± 0.4	4
one-way ANOVA	**P = 0.002**	P = 0.080	P = 0.820	
AND-hMal (**14**)	236 ± 27**	4.7 ± 1.0**	1.4 ± 0.2	4
AND-hSuc (**15**)	452 ± 46*	7.4 ± 0.4**	1.5 ± 0.1	5
AND-hGlu (**16**)	348 ± 32**	5.2 ± 1.2**	1.7 ± 0.2	7
AND-hAdi (**17**)	191 ± 10**	2.8 ± 0.5**	1.7 ± 0.5	5
AND-hPim (**18**)	109 ± 13	1.8 ± 0.3**	1.8 ± 0.3	4
one-way ANOVA	**P < 0.001**	**P < 0.001**	P = 0.892	
17-oxo-AND-hGlu (**19**)	154 ± 34	151.4 ± 32.7**	1.2 ± 0.1	4
17-oxo-AND-hAdi (**20**)	180 ± 17*	108.9 ± 20.2**	1.4 ± 0.1	7
17-oxo-AND-hPim (**21**)	187 ± 27*	82.4 ± 16.9**	1.2 ± 0.1	7
17-oxo-AND-hSub (**22**)	189 ± 35*	49.1 ± 13.7**	1.4 ± 0.2	5
17-oxo-AND-hAze (**23**)	226 ± 45*	38.2 ± 14.5	1.3 ± 0.2	5
17-oxo-AND-hSeb (**24**)	165 ± 11*	16.1 ± 0.9*	1.6 ± 0.2	5
one-way ANOVA	P = 0.654	**P < 0.001**	P = 0.661	

[a]The degree of potentiation of glutamate-induced responses, recorded in the presence of a given compound at concentrations of 0.3−30 μM (for compounds **9**−**18**), 1−100 μM (for compounds **1**−**8** and **21**−**24**), and 1−300 μM (for compounds **19** and **20**), was determined in individual cells for at least five compound doses, and the data were fitted to the eq 2. Statistical tests on the potency of compounds (**2**−**8**, **9**−**13**, **14**−**18**, and **19**−**24**) were performed on log EC_{50} and log Hill values (one-way ANOVA); $P \leq 0.05$ was used for the determination of significance, as marked in bold. Unpaired Student's t test was used for statistical comparisons of E_{max} and log EC_{50} values for compounds **2**−**24** to PES (**1**: (*) P = 0.001− 0.050; (**) P < 0.001).

analysis of compounds **4**−**7** indicated that at a concentration of 100 μM these compounds potentiated more than predicted from the fit of their potentiating effect at concentrations of 1−30 μM. The potentiating effect induced by these compounds at a concentration of 100 μM was 267 ± 47% (n = 4) for compound **4**, 460 ± 17% (n = 4) for compound **5**, 614 ± 56% (n = 10) for compound **6**, and 458 ± 119% (n = 4) for compound **7**. The reason for this increased potentiation at high compound concentrations is unknown, and we did not analyze it in detail. Augmented potentiation was not observed for compounds **1**−**3** and **8**−**24** (100 μM).

To evaluate the role of the 20-oxo group at the steroid D-ring for biological activity at NMDARs, a series of pregn-5-enes (**9**−**13**) was synthesized. Interestingly, within this structural family, compounds exhibited more than 4-fold difference in the E_{max} values (48% for the least efficacious compound **13** compared to 209% for the most efficacious compound **11**; Figure 4B), with EC_{50} values varying from 9.9 μM for the most potent compound **11** to 26.2 μM for the least potent compound **13**.

Further, we analyzed a series of androst-5-enes (**14**−**18**) lacking a substituent at the position C-17 of the steroidal D-ring. Compound **15** (AND-hSuc) was established as the most efficacious PAM within this structural family with E_{max} value of 452% (Figure 4C), approximately 4.5 times higher than that of the least efficacious compound **18** (109%). In general, compounds **14**−**18** were recognized as the most potent PAMs of all the tested compounds **2**−**24**, with EC_{50} values varying from 1.8 μM for the most potent compound **18** to 7.4 μM for the least potent compound **15** from this series (Table 2). This structural modification led to a significant improvement in potency for all compounds **14**−**18**, suggesting that nonsubstituted D-ring drives the activity of PAM toward stronger potency.

Finally, we tested a series of 17-oxo analogues (**19**−**24**) with 17-oxo group at the steroidal D-ring. 17-Oxo analogues exhibited similar values of E_{max} within this structural family (varying from 154% for the least efficacious compound **19** to 226% for the most efficacious compound **23**; Figure 4D). The potency of compounds **19**−**24** differs significantly, exhibiting up to 9-fold decrease in EC_{50} value for the most potent compound **24** (16.1 μM) compared to the least potent compound **19** (151.4 μM).

Computational Estimate of Physicochemical Properties of Compounds 2−24. Our recent results for steroids with inhibitory action at NMDARs showed the plasma membrane as the route for the steroid to reach its binding site on the receptor.[23] We could speculate that steroids with a potentiating effect, which are structurally similar to the inhibitory ones, may employ the same route. Therefore, we have analyzed the role of lipophilicity in the potency of compounds at NMDARs.

DOI: 10.1021/acs.jmedchem.8b00255
J. Med. Chem. 2018, 61, 4505−4516

PDF-XChange Editor
KOUPIT plnou verzi!
www.pdfxchange.cz

Computational analysis was used to evaluate the lipophilic qualities of compounds **1**–**24**. The relevant physicochemical properties (ΔG_{solv}, log *P*, and log *D* values), which are commonly used for describing the compound lipophilicity,[24] were calculated by quantum mechanics computational methods and with a physicochemical properties predictor.[25] The computational results are summarized in Table S1 (for details see Supporting Information). Compounds **5** and **14** show similar values of log *D* (1.29 and 1.28, respectively). However, the EC_{50} value for compound **5** (19.0 μM) is 4 times higher than for compound **14** (4.7 μM). Similarly, more lipophilic compounds **11** and **22** (log *D* values of 2.47 and 2.42, respectively) show an approximately 5-fold difference in EC_{50} values (Table 2). These results suggest that compound lipophilicity and presumed solubility in the membrane play only a minor role in determining the compound potency and indirectly indicate that potency is more dependent on the specific (structural/binding) interactions between the compound and the NMDAR.

Effect of 20-Oxo-PE-hAdi (6) on Recombinant GluN1/GluN2A–D and Native Receptors. Compound **6** was selected from the library of compounds **2**–**24** for further biological evaluation. To investigate the subunit selectivity of compound **6**, cDNAs coding for the GluN1-1a and GluN2A–D subunits were co-transfected into HEK293 cells. Dose–response analysis for the effect of compound **6** on GluN1/GluN2A–D receptors showed no significant difference in the efficacy and potency at receptors differing in the subunit composition (Table 3).

Table 3. Summary of the Dose–Response Analysis Data for the Potentiation Effect of Compound 6 on Responses of GluN1/GluN2A–D Receptors[a]

receptor	E_{max} ± SEM (%)	EC_{50} ± SEM (μM)	*h* ± SEM	*n*
GluN1/GluN2A	203 ± 43	8.9 ± 1.4	1.7 ± 0.2	7
GluN1/GluN2B	157 ± 16	9.1 ± 1.1	1.7 ± 0.1	8
GluN1/GluN2C	145 ± 39	10.4 ± 3.5	1.7 ± 0.2	6
GluN1/GluN2D	115 ± 9	13.0 ± 1.9	1.7 ± 0.3	5
one-way ANOVA	*P* = 0.363	*P* = 0.520	*P* = 0.997	

[a]The degree of potentiation of glutamate-induced responses recorded in the presence of compound **6** (1–30 μM) was determined in individual cells, and data were fit to eq 2. Statistical tests on the compound **6** potency were performed on log EC_{50} and log Hill values (one-way ANOVA).

Subsequently we compared the effect of compound **6** (30 μM) and PES (100 μM) at recombinant GluN1/GluN2A–D receptors. The results (Figure 5) indicate that compound **6** (30 μM) potentiated all tested subunit compositions of GluN1/GluN2A–D receptors (the degree of potentiation was 192 ± 21% for GluN1/GluN2A, 137 ± 11% for GluN1/GluN2B, 118 ± 17% for GluN1/GluN2C, and 88 ± 11% for GluN1/GluN2D; *n* = 6). PES (100 μM) potentiated GluN1/GluN2A-B receptor responses (107 ± 17% (*n* = 4) for GluN1/GluN2A and 78 ± 4% (*n* = 13) for GluN1/GluN2B) while it inhibited GluN1/GluN2C-D receptor responses (−47 ± 4% for GluN1/GluN2C and −48 ± 3% for GluN1/GluN2D; *n* = 4). This agrees well with the results of previous experiments showing that PES has a dual potentiating and inhibitory action at NMDARs.[22,26] The predominant effect of PES (potentiation of GluN1/GluN2A-B and inhibition of GluN1/GluN2C-D) is the result of different efficacy rather than potency, which is higher for GluN1/GluN2C-D receptors than for GluN1/GluN2A-B receptors.[26] In our experiments we have seen no evidence of a dual effect for compound **6**.

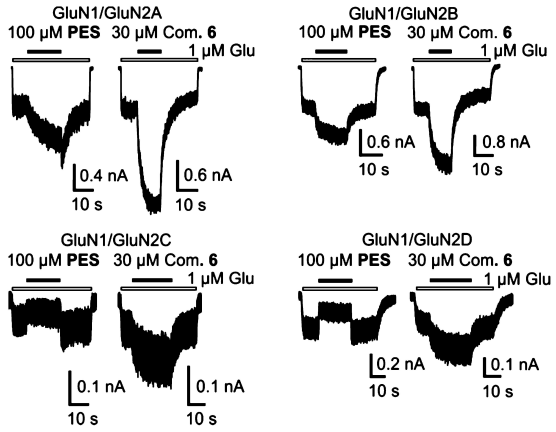


Figure 5. Comparison of the effect of PES and compound **6** on GluN1/GluN2A–D receptor responses. Examples of traces obtained from HEK293 cells transfected with cDNAs encoding for GluN1-1a and GluN2A–D subunits. PES (100 μM) and compound **6** (30 μM) were applied simultaneously with 1 μM glutamate (the duration of the compound and glutamate application are indicated by filled and open bars, respectively).

Native NMDARs expressed in cultured hippocampal neurons were potentiated (138 ± 11%, *n* = 6; Figure 6) by compound **6**

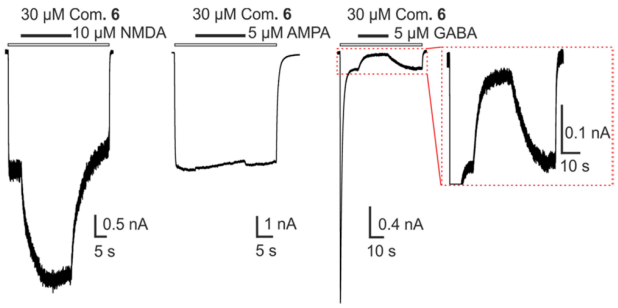


Figure 6. Effect of compound **6** on native NMDARs, AMPARs, and $GABA_A$Rs. Examples of traces obtained from cultured hippocampal neurons. Compound **6** (30 μM) was applied simultaneously with NMDA (10 μM), AMPA (5 μM), and GABA (5 μM) (the duration of compound and agonist application is indicated by filled and open bars, respectively).

(30 μM) to a similar extent as recombinant GluN1/GluN2B receptors (136%; Figure 2A; *P* = 0.824). In contrast to the relatively pronounced potentiating effect of compound **6** on native and recombinant NMDARs responses, compound **6** (30 μM) had only a small inhibitory effect (−7 ± 2%, *n* = 6) on responses induced by selective AMPARs agonist (AMPA 5 μM) recorded in the presence of cyclothiazide (10 μM) for reducing receptor desensitization.[27] Compound **6** (30 μM) inhibited responses induced by 5 μM GABA (−90 ± 2%, *n* = 5). These effects of compound **6** are qualitatively similar to PES effects at native NMDARs, AMPARs, and $GABA_A$Rs.[13,28]

■ CONCLUSIONS

In this study, we examined a library of compounds **2**–**24**, bearing a C-3 hemiester moiety, Δ^5- double bond, and various modifications at position C-17, in order to evaluate their ability

DOI: 10.1021/acs.jmedchem.8b00255
J. Med. Chem. 2018, 61, 4505–4516

PDF-XChange Editor
KOUPIT plnou verzi!
www.pdfxchange.cz

to modulate the activity of NMDARs. The results of our experiments indicate that the C-17 substituent of the D-ring can be structurally modified or fully degraded while maintaining a positive modulatory effect of the steroid. We have also shown that the potentiating effect of these compounds exhibits a dependency on the length of the C-3 substituent for each D-ring modification. The most efficacious and potent modulators, respectively, from all tested compounds (**2**−**24**) were compound **15**, exhibiting the E_{max} value of 452%, and compound **18**, exhibiting the EC_{50} value of 1.8 μM. In addition, we have shown that the selected compound **6** has a subunit-independent effect at recombinant NMDARs, which is similar to that at native NMDARs and has only a minor inhibitory effect at AMPARs. Our data further indicate that compound **6** is an inhibitor of native $GABA_A$Rs. In summary, we conclude that PES analogues modified at the C-3 and/or at the D-ring offer new prospects for further optimization of pharmacological and pharmacokinetic properties of these neuroactive compounds.

EXPERIMENTAL SECTION

Chemistry. General. Melting points were determined with a Hund/Wetzlar micromelting point apparatus (Germany) and are uncorrected. Optical rotations were measured in chloroform using an Autopol IV (Rudolf Research Analytical, Flanders, USA). $[\alpha]_D$ values are given in deg (10^{-1} deg cm^2 g^{-1}). IR spectra were recorded in a Bruker IFS 55 spectrometer (wavenumbers in cm^{-1}). Proton and carbon NMR spectra were measured in a Bruker AVANCE-400 FT NMR spectrometer (400 MHz, 101 MHz) in $CDCl_3$, with tetramethylsilane as the internal standard. Chemical shifts are given in ppm (δ scale). Coupling constants (J) and widths of multiplets (W) are given in Hz. High-resolution MS spectra were performed with a Q-Tof microspectrometer (Waters). Elemental analysis was performed on a PerkinElmer 2400 series II CHNS/O analyzer (USA). Thin-layer chromatography (TLC) was performed on silica gel (ICN Biochemicals). For column chromatography, neutral silica gel 60 μm (Merck) was used. Analytical samples were dried over phosphorus pentoxide at 50 °C/100 Pa. The purity of the final compounds was assessed by a combination of NMR and on the basis of LC−HR-MS analysis or elemental analysis, and the results showed they were greater than 95%.

Biological Activity. Electrophysiological experiments were performed on HEK293 cells transfected with cDNA containing GluN1-1a/GluN2A−D/GFP genes and on cultured hippocampal neurons as described previously.[23a,29] Glutamate-induced responses were recorded at a holding potential of −60 mV. Whole-cell voltage-clamp recordings were made with a patch-clamp amplifier (Axopatch 200B; Axon Instruments. Inc., Foster City, CA) after series resistance (<10 MΩ) and capacitance compensation of 80−90%. For the application of test and control solutions, a microprocessor-controlled multibarrel fast-perfusion system was used, with a time constant of solution exchange around the cells of ∼10 ms. Agonist-induced responses were low-pass filtered at 2 kHz, digitally sampled at 5 kHz, and analyzed with pClamp software version 9.2 (Molecular Devices). Patch pipettes (3−5 MΩ) pulled from borosilicate glass were filled with a Cs^+-based intracellular solution containing the following (in mM): 120 gluconic acid δ-lactone, 15 CsCl, 10 BAPTA, 10 HEPES, 3 $MgCl_2$, 1 $CaCl_2$, and 2 ATP-Mg salt (pH-adjusted to 7.2 with CsOH). Extracellular solution (ECS) contained the following (in mM): 160 NaCl, 2.5 KCl, 10 HEPES, 10 glucose, 0.7 $CaCl_2$, and 0.2 EDTA (pH-adjusted to 7.3 with NaOH). NMDAR responses were induced by 1 μM or 1 mM glutamate (in recombinant receptors) and 10 μM NMDA (native receptors) together with 10 μM glycine. The ECS used for native receptors had the same composition as the ECS used for recombinant receptors. For native NMDAR recordings, ECS additionally contained 10 μM CNQX, 10 μM bicuculline, and 0.5 μM TTX. AMPAR currents were induced with 5 μM AMPA, and the ECS additionally contained 50 μM D-AP5, 10 μM bicuculline, 0.5 μM TTX, and 10 μM cyclothiazide. $GABA_A$R responses were induced with 5 μM GABA and the ECS additionally contained 50 μM D-AP5, 10 μM CNQX, and 0.5 μM TTX. Compound solutions were prepared fresh before each experiment as a stock solution in dimethyl sulfoxide (DMSO). The same concentration of DMSO (1%) was maintained in all test and control extracellular solutions. Experiments were performed at room temperature (21−25 °C).

Experimental Data for Compounds 1−28. General Procedure I: Synthesis of Steroidal Hemiesters from Anhydrides. A mixture of steroid **25**, **26**, **27**, or **28** (1 mmol) and dicarboxylic acid anhydride (6 equiv) was dried overnight at 50 °C. Dry pyridine (12 mL) and DMAP (0.24 equiv) were added. The mixture was heated at 110 °C for 6 h under an inert atmosphere. It was then poured into water and extracted with DCM. Combined organic extracts were washed with brine and dried. Solvents were evaporated, and the residue was purified on a column of silica gel.

General Procedure II: Synthesis of Steroidal Hemiesters from ω-Dicarboxylic Acids. A solution of steroid **25**, **26**, **27**, or **28** (1 mmol) in dry DCM (5 mL) was added under an inert atmosphere to a solution of dicarboxylic acid (2 mmol), EDCI (2 mmol), DIPEA (2 mmol), and DMAP (0.24 equiv) in dry DCM (10 mL) at 0 °C under stirring. The reaction mixture was stirred at room temperature for 18 h. The solvents were then evaporated and the residue was dissolved with DCM, washed with water, dried over sodium sulfate, and concentrated in vacuo. Purification on a column of silica gel gave the desired steroidal hemiester.

20-Oxo-pregn-5-en-3β-yl Sulfate Pyridinium Salt (1, PES). Sulfur trioxide−pyridine complex (318 mg, 2 mmol) was added to a solution of compound **25** (316 mg, 1 mmol) in chloroform (5 mL, P_2O_5 dried and distilled) and dry pyridine (1 drop). The reaction mixture was stirred at room temperature under an inert atmosphere for 6 h. The progress of the reaction was checked by TLC. The reaction mixture was then allowed to stand at −18 °C for 2 h, and the solids were filtered off through a plug of cotton wool. The filtrate was evaporated and dried (25 °C, 100 Pa) for 1 h. The crude material was dissolved in freshly dried chloroform (4 mL), allowed to stand at −18 °C for 2 h, and the solid was filtered off. The filtrate was evaporated, yielding compound **1** (425 mg, 89%): mp 182−184 °C ($CHCl_3$); $[\alpha]_D^{20}$ 18.1 (c 0.3, $CHCl_3$). ^{1}H NMR (400 MHz, $CHCl_3$): δ 0.64 (3H, s, H-18), 1.02 (3H, s, H-19), 2.14 (3H, s, H-21), 2.55 (1H, t, J = 8.9, H-17), 2.65 (1H, ddd, J_1 = 2.3, J_2 = 5.1, J_3 = 13.3, H-4), 4.37 (1H, tt, J_1 = 4.8, J_2 = 11.6, H-3), 5.40 (1H, d, J = 5.2, H-6), 8.02 (2H, m, H-2′ and H-4′, pyridinium), 8.49 (1H, m, H-3′, pyridinium), 9.00 (2H, m, H-1′ and H-5′, pyridinium). ^{13}C NMR (101 MHz, $CDCl_3$): δ 209.7 (C═O), 145.7 (C-1′ and C-5′, pyridinium), 142.5 (C-3′, pyridinium), 140.3 (C-5), 127.2 (C-2′ and C-4′, pyridinium), 122.2 (C-6), 78.9 (C-3), 63.8, 57.0, 50.0, 43.9, 39.3, 38.9, 37.3, 36.6, 31.9, 31.9, 31.7, 28.9, 24.6, 22.9, 21.2, 19.4, 13.3. IR ($CHCl_3$): 1698 (C═O); 1665 (C═C); 1490 (pyridinium); 971, 952 (COS). MS: ESI m/z 395.3 (100%, M − pyH). HR-MS (ESI) m/z: for $C_{21}H_{31}O_5S$ [M − pyH] calcd, 395.18977; found, 395.19906.

20-Oxo-pregn-5-en-3β-yl Hemioxalate (2, 20-Oxo-PE-hOxa).[9a] A mixture of compound **25** (316 mg, 1 mmol), dry DCM (5 mL), triethylamine (0.15 mL), and two drops of previously prepared solution (2 mL of dry DCMDCM and 1 drop of DMF) was added to a cooled (0 °C) mixture of DCM (5 mL) and oxalyl chloride (0.26 mL, 3 mmol). The mixture was allowed to reach 10 °C and then stirred for 2 h under these conditions. 20 mL of water was then added to decompose the excess reagent, and the mixture was stirred for 30 min at room temperature. The organic layer was separated, and ethyl acetate (20 mL) was added to the DCM extract. An aqueous solution of potassium carbonate was then added (10%, 50 mL), the organic layer with undesired byproducts was separated, and then an aqueous solution of HCl was cautiously added to the aqueous layer (1 N, to pH ∼ 4). The crude product was obtained by extraction with ethyl acetate (2 × 25 mL) and dried. Chromatography on a silica gel column (5% methanol in DCM) gave **2** (140 mg, 36%): mp 189−191 °C (ethyl acetate/n-heptane); $[\alpha]_D^{20}$ 6.2 (c 0.3, $CHCl_3$). ^{1}H NMR (400 MHz, $CDCl_3$): δ 0.64 (3H, s, H-18), 1.04 (3H, s, H-19), 2.14 (3H, s, H-21), 2.54 (1H, t, J = 8.9, H-17), 4.81 (1H, m, H-3), 5.43 (1H, m, H-6). ^{13}C NMR (101 MHz, $CDCl_3$): δ 210.4 (C═O), 157.9 (COOH), 157.7 (COO), 138.8 (C-5), 123.4 (C-6), 78.3 (C-3), 63.8 (C-17), 56.9, 49.9, 44.2, 38.8, 37.6, 36.9, 36.7, 31.9, 31.8, 31.7, 27.4, 24.6, 22.9, 21.1, 19.3, 13.3. IR ($CHCl_3$):

DOI: 10.1021/acs.jmedchem.8b00255
J. Med. Chem. 2018, 61, 4505−4516

PDF-XChange Editor
KOUPIT plnou verzi!
www.pdfxchange.cz

1801, 1760, 1699 (C═O); 1672 (C═C); 1192 (C−O). MS: ESI m/z 387.2 (100%, M − 1), 388.2 (24%, M). HR-MS (ESI) m/z: for $C_{23}H_{31}O_5$ [M − 1] calcd, 387.21660; found, 387.21676.

20-Oxo-pregn-5-en-3β-yl Hemimalonate (3, 20-Oxo-PE-hMal). Dry toluene (15 mL) was added to a mixture of compound **25** (316 mg, 1 mmol) and 2,2-dimethyl-4,6-dioxo-1,3-dioxolane (Meldrum's acid, 171 mg, 1.5 mmol). The mixture was heated at 80 °C for 48 h under an inert atmosphere. It was then washed with brine and the solvent was evaporated. Chromatography of the residue on a silica gel column (30−50% ethyl acetate in petroleum ether) gave **3** (149 mg, 37%): mp 166−168 °C (acetone); $[\alpha]_D^{20}$ 10.6 (c 0.2, $CHCl_3$). ^{1}H NMR (400 MHz, $CDCl_3$): δ 0.63 (3H, s, H-18), 1.02 (3H, s, H-19), 2.13 (3H, s, H-21), 2.54 (1H, t, J = 8.8, H-17), 3.42 (2H, s, H-2′), 4.71 (1H, m, H-3), 5.39 (1H, m, H-6). ^{13}C NMR (101 MHz, $CDCl_3$): δ 209.9 (C═O), 169.5 (COOH), 167.4 (COO), 139.3 (C-5), 122.9 (C-5), 76.0 (C-3), 63.8 (C-17), 56.9, 49.9, 44.1, 40.4, 38.9, 37.9, 37.0, 36.7, 31.9, 31.9, 31.7, 27.6, 24.6, 22.9, 21.1, 19.4, 13.3. IR ($CHCl_3$): 1746, 1736, 1725, 1706 (C═O); 1675 (C═C); 1192 (C−O). MS: ESI m/z 357.3 (100%, M − 1 − CO_2), 401.3 (10%, M − 1). HR-MS (ESI) m/z: for $C_{24}H_{33}O_5$ [M − 1] calcd, 401.23335; found, 401.23291.

20-Oxo-pregn-5-en-3β-yl Hemisuccinate (4, 20-Oxo-PE-hSuc).[9a] Compound **4** was prepared according to general procedure I. Starting from compound **25** (251 mg, 0.79 mmol), compound **4** (172 mg, 52%) was obtained as a white solid by column chromatography (30−50% ethyl acetate in petroleum ether): mp 161−163 °C (toluene); $[\alpha]_D^{20}$ +14.3 (c 0.2, $CHCl_3$). ^{1}H NMR (400 MHz, $CDCl_3$): δ 0.63 (s, 3H, H-18), 1.02 (3H, s, H-19), 2.12 (3H, s, H-21), 2.61−2.68 (4H, m, $OOCCH_2CH_2COO$), 4.62 (1H, m, H-3), 5.37 (1H, m, H-6). ^{13}C NMR (101 MHz, $CDCl_3$): δ 209.8 (C═O), 177.0 (COOH), 171.7 (COO), 139.6 (C-5), 122.5 (C-6), 74.5 (C-3), 63.8, 56.9, 50.0, 44.1, 38.9, 38.1, 37.1, 36.7, 31.9, 31.9, 31.7, 29.3, 28.9, 27.8, 24.6, 22.9, 21.1, 19.4, 13.3. IR ($CHCl_3$): 1731, 1716 (C═O); 1671 (C═C). MS: ESI m/z 415.3 (100%, M − 1). For $C_{25}H_{36}O_5$ (416.5) calcd: 72.08%, C; 8.71%, H. Found: 71.85%, C; 8.63%, H.

20-Oxo-pregn-5-en-3β-yl Hemiglutarate (5, 20-Oxo-PE-hGlu).[9a] Compound **5** was prepared according to general procedure I. Starting from compound **25** (316 mg, 1 mmol), compound **5** (219 mg, 51%) was obtained as a white solid by column chromatography (2−5% acetone in DCM): mp 137−139 °C (methanol); $[\alpha]_D^{20}$ 9.1 (c 0.3, $CHCl_3$). ^{1}H NMR (400 MHz, $CDCl_3$): δ 0.63 (3H, s, H-18), 1.02 (3H, s, H-19), 1.96 (2H, p, J = 7.3, H-3′), 2.12 (3H, s, H-21), 2.37 (2H, t, J = 7.3, H-2′), 2.43 (2H, t, J = 7.3, H-4′), 2.54 (1H, t, J = 8.9, H-17), 4.63 (1H, m, H-3), 5.37 (1H, m, H-6). ^{13}C NMR (101 MHz, $CDCl_3$): δ 209.8 (C═O), 177.9 (COOH), 172.4 (COO), 139.7 (C-5), 122.5 (C-6), 74.1 (C-3), 63.8 (C-17), 56.9, 50.0, 44.1, 38.9, 38.2, 37.1, 36.7, 33.6, 32.9, 31.9, 31.9, 31.7, 27.8, 24.6, 22.9, 21.1, 20.0, 19.4, 13.3. IR ($CHCl_3$): 1725, 1711 (C═O); 1655 (C═C); 1417 (C−O). MS: ESI m/z 429.3 (100%, M − 1), 430.3 (30%, M). For $C_{26}H_{38}O_5$ (430.3) calcd: 72.53%, C; 8.90% H. Found: 72.36%, C; 8.89%, H.

20-Oxo-pregn-5-en-3β-yl Hemiadipate (6, 20-Oxo-PE-hAdi). Compound **6** was prepared according to general procedure II. Starting from compound **25** (316 mg, 1 mmol), compound **6** (187 mg, 42%) was obtained as a white solid by column chromatography (2−5% acetone in DCM): mp 135−136 °C (ethyl acetate/n-heptane); $[\alpha]_D^{20}$ 3.0 (c 0.2, $CHCl_3$). ^{1}H NMR (400 MHz, $CDCl_3$): δ 0.63 (3H, s, H-18), 1.02 (3H, s, H-19), 2.12 (3H, s, H-21), 2.28−2.40 (4H, m, H-adipate), 2.53 (1H, t, J = 9.0, H-17), 4.63 (1H, m, H-3), 5.38 (1H, m, H-6). ^{13}C NMR (101 MHz, $CDCl_3$): δ 209.7 (C═O), 178.0 (COOH), 172.8 (COO), 139.8 (C-5), 122.5 (C-6), 73.9 (C-3), 63.8 (C-17), 56.9, 50.0, 44.1, 38.9, 38.2, 37.1, 36.7, 34.3, 33.5, 31.9, 31.9, 31.7, 27.9, 24.6, 24.5, 24.2, 22.9, 21.2, 19.4, 13.3. IR ($CHCl_3$): 1730, 1709 (C═O); 1655 (C═C); 1417 (C−O). MS: ESI m/z 443.3 (100%, M − 1), 444.3 (25%, M). For $C_{27}H_{40}O_5$ (444.3) calcd: 72.94%, C; 9.07% H. Found: 72.71%, C; 9.01%, H.

20-Oxo-pregn-5-en-3β-yl Hemipimelate (7, 20-Oxo-PE-hPim). Compound **7** was prepared according to general procedure II. Starting from compound **25** (316 mg, 1 mmol), compound **7** (215 mg, 47%) was obtained as a white solid by column chromatography (1−10% acetone in DCM): mp 123−125 °C (methanol); $[\alpha]_D^{20}$ 10.1 (c 0.3, $CHCl_3$). ^{1}H NMR (400 MHz, $CDCl_3$): δ 0.63 (3H, s, H-18), 1.02 (3H, s, H-19), 2.12 (3H, s, H-21), 2.26−2.39 (4H, m, H-pimelate), 2.53 (1H, t, J = 8.9, H-17), 4.63 (1H, m, H-3), 5.37 (1H, m, H-6). ^{13}C NMR (101 MHz, $CDCl_3$): δ 209.7 (C═O), 178.5 (COOH), 173.1 (COO), 139.8 (C-5), 122.4 (C-6), 73.8 (C-3), 63.8 (C-17), 56.9, 50.0, 44.1, 38.9, 38.2, 37.1, 36.7, 34.5, 33.7, 31.9, 31.9, 31.7, 28.6, 27.9, 24.7, 24.6, 24.4, 22.9, 21.1, 19.4, 13.3. IR ($CHCl_3$): 1727, 1708 (C═O); 1655 (C═C); 1416 (C−O). MS: ESI m/z 457.3 (100%, M − 1), 458.3 (32%, M). For $C_{28}H_{42}O_5$ (458.3) calcd: 73.33%, C; 9.23% H. Found: 73.05%, C; 9.44%, H.

20-Oxo-pregn-5-en-3β-yl Hemisuberate (8, 20-Oxo-PE-hSub). Compound **8** was prepared according to general procedure II. Starting from compound **25** (316 mg, 1 mmol), compound **8** (208 mg, 44%) was obtained as a white solid by column chromatography (1−10% acetone in DCM): mp 105−107 °C (ethyl acetate/n-heptane); $[\alpha]_D^{20}$ 10.4 (c 0.3, $CHCl_3$). ^{1}H NMR (400 MHz, $CDCl_3$): δ 0.63 (3H, s, H-18), 1.02 (3H, s, H-19), 2.12 (3H, s, H-21), 2.24−2.37 (4H, m, H-suberate), 2.53 (1H, t, J = 9.0, H-17), 4.63 (1H, m, H-3), 5.8 (1H, m, H-6). ^{13}C NMR (101 MHz, $CDCl_3$): δ 209.7 (C═O), 178.6 (COOH), 173.3 (COO), 139.8 (C-5), 122.4 (C-6), 73.7 (C-3), 63.8 (C-17), 56.9, 50.0, 44.1, 38.9, 38.2, 37.1, 36.7, 34.7, 33.9, 31.9, 31.9, 31.7, 28.8, 28.8, 27.9, 24.9, 24.6, 24.6, 22.9, 21.1, 19.4, 13.3. IR ($CHCl_3$): 1728, 1705 (C═O); 1655 (C═C); 1417 (C−O). MS: ESI m/z 471.3 (100%, M − 1), 472.3 (30%, M). For $C_{29}H_{44}O_5$ (472.3) calcd: 73.69%, C; 9.38% H. Found: 73.41%, C; 9.54%, H.

Pregn-5-en-3β-yl Hemimalonate (9, PE-hMal). Compound **9** was prepared in the same manner as compound **3**. Starting from compound **26** (302 mg, 1 mmol), compound **9** (125 mg, 32%) was obtained as a white solid by column chromatography (50% ether in petroleum ether): mp 176−178 °C (methanol); $[\alpha]_D^{20}$ −41.7 (c 0.2, $CHCl_3$). ^{1}H NMR (400 MHz, $CDCl_3$): δ 0.58 (3H, s, H-18), 0.87 (3H, t, J = 7.3, H-21), 1.03 (3H, s, H-19), 3.41 (2H, s, H-2′), 4.67−4.76 (1H, m, H-3), 5.40 (1H, d, J = 4.8, H-6). ^{13}C NMR (101 MHz, $CDCl_3$): δ 169.5 (COOH), 167.4 (COO), 139.2 (C-5), 123.3 (C-6), 76.3 (C-3), 56.2, 53.0, 50.5, 42.0, 40.4, 37.9, 37.9, 37.0, 36.8, 32.1, 31.9, 28.2, 27.7, 24.7, 23.1, 20.9, 19.4, 13.5, 12.5. IR ($CHCl_3$): 1757, 1737, 1718 (C═O); 1670 (C═C); 1409, 1288 (C−O). MS: ESI m/z 387.3 (27%, M − 1), 343.3 (100%, M − 1 − CO_2). HR-MS (ESI) m/z: for $C_{24}H_{35}O_4$ [M − 1] calcd, 387.25408; found, 387.25348.

Pregn-5-en-3β-yl Hemisuccinate (10, PE-hSuc). Compound **10** was prepared according to general procedure I. Starting from compound **26** (302 mg, 1 mmol), compound **10** (145 mg, 43%) was obtained as a white solid by column chromatography (10−30% ethyl acetate in petroleum ether): mp 151−153 °C (methanol); $[\alpha]_D^{20}$ −36.8 (c 0.2, $CHCl_3$). ^{1}H NMR (400 MHz, $CDCl_3$): δ 0.58 (s, 3H, H-18), 0.87 (3H, t, J = 7.3, H-21), 1.02 (3H, s, H-19), 2.58−2.70 (4H, m, $OOCCH_2CH_2COO$), 4.63 (1H, m, H-3), 5.37 (1H, m, H-6). ^{13}C NMR (101 MHz, $CDCl_3$): δ 177.5 (COOH), 171.7 (COO), 139.7 (C-5), 122.9 (C-6), 74.7 (C-3), 56.3, 53.0, 50.6, 42.1, 38.2, 37.9, 37.1, 36.8, 32.1, 32.0, 29.3, 29.0, 28.2, 27.8, 24.7, 23.1, 20.9, 19.4, 13.5, 12.5. IR ($CHCl_3$): 1730, 1716 (C═O); 1670 (C═C); 1290 (C−O). MS: ESI m/z 401.3 (100%, M − 1), 402.3 (30%, M). HR-MS (ESI) m/z: for $C_{25}H_{37}O_4$ [M − 1] calcd, 401.26973; found, 401.26941.

Pregn-5-en-3β-yl Hemiglutarate (11, PE-hGlu). Compound **11** was prepared according to general procedure I. Starting from compound **26** (302 mg, 1 mmol), compound **11** (184 mg, 44%) was obtained as a white solid by column chromatography (1% methanol in DCM): mp 128−130 °C (methanol); $[\alpha]_D^{20}$ −38.7 (c 0.1, $CHCl_3$). ^{1}H NMR (400 MHz, $CDCl_3$): δ 0.58 (3H, s, H-18), 0.87 (3H, t, J = 7.3, H-21), 1.02 (3H, s, H-19), 1.96 (2H, p, J = 7.3, H-3′), 2.37 (2H, t, J = 7.3, H-2′), 2.43 (2H, t, J = 7.3, H-4′), 4.63 (1H, m, H-3), 5.37 (1H, m, H-6). ^{13}C NMR (101 MHz, $CDCl_3$) δ 178.0 (COOH), 172.4 (COO), 139.7 (C-5), 122.8 (C-6), 74.2 (C-3), 56.3, 53.0, 50.6, 42.0, 38.2, 37.9, 37.1, 36.8, 33.6, 32.9, 32.1, 32.0, 28.2, 27.9, 24.7, 23.1, 20.9, 20.0, 19.5, 13.5, 12.5. IR ($CHCl_3$): 1724, 1713 (C═O); 1671 (C═C); 1192 (C−O). MS: ESI m/z 439.3 (100%, M + Na), 440.3 (30%, M + Na + 1). HR-MS (ESI) m/z: for $C_{26}H_{40}O_4Na$ [M + Na] calcd, 439.28189; found, 439.28188.

Pregn-5-en-3β-yl Hemiadipate (12, PE-hAdi). Compound **12** was prepared according to general procedure II. Starting from compound **26** (302 mg, 1 mmol), compound **12** (90 mg, 21%) was obtained as a white solid by column chromatography (0.3−1% methanol in DCM): mp 128−130 °C (methanol); $[\alpha]_D^{20}$ −36.2 (c 0.1, $CHCl_3$).

DOI: 10.1021/acs.jmedchem.8b00255
J. Med. Chem. 2018, 61, 4505−4516

PDF-XChange Editor
KOUPIT plnou verzi!
www.pdfxchange.cz

^{1}H NMR (400 MHz, $CDCl_3$): δ 0.58 (3H, s, H-18), 0.87 (3H, t, J = 7.3, H-21), 1.02 (3H, s, H-19), 2.28−2.34 (4H, m, H-adipate), 4.63 (1H, m, H-3), 5.38 (1H, m, H-6). ^{13}C NMR (101 MHz, $CDCl_3$): δ 178.4 (COOH), 172.8 (COO), 139.8 (C-5), 122.8 (C-6), 74.1 (C-3), 56.3, 53.0, 50.6, 42.0, 38.3, 37.9, 37.1, 36.8, 34.3, 33.5, 32.1, 32.0, 28.2, 27.9, 24.8, 24.5, 24.2, 23.2, 20.9, 19.5, 13.5, 12.5. IR ($CHCl_3$): 1727, 1712 (C═O); 1670 (C═C); 1191 (C−O). MS: ESI m/z 429.3 (100%, M − 1), 430.3 (30%, M). HR-MS (ESI) m/z: for $C_{27}H_{41}O_4$ [M − 1] calcd, 429.30103; found, 429.30063.

Pregn-5-en-3β-yl Hemipimelate (13, PE-hPim). Compound **13** was prepared according to general procedure II. Starting from compound **26** (302 mg, 1 mmol), compound **13** (157 mg, 35%) was obtained as a white solid by column chromatography (10−20% ethyl acetate in petroleum ether): mp 97−99 °C (EtOAc); $[\alpha]_D^{20}$ −38.5 (c 0.2, $CHCl_3$). ^{1}H NMR (400 MHz, CDCl3): δ 0.57 (3H, s, H-18), 0.86 (3H, t, J = 7.3, H-21), 1.01 (3H, s, H-19), 2.23−2.36 (4H, m, H-pimelate), 4.60 (1H, m, H-3), 5.37 (1H, m, H-6). ^{13}C NMR (101 MHz, $CHCl_3$) δ 177.0 (COOH), 173.2 (COO), 139.8 (C-5), 122.7 (C-6), 74.0 (C-3), 56.3, 53.1, 50.6, 42.0, 38.3, 37.9, 37.1, 36.8, 34.5, 33.7, 32.1, 32.0, 28.6, 28.2, 27.9, 24.8, 24.7, 24.5, 23.1, 20.9, 19.4, 13.4, 12.5. IR ($CHCl_3$): 1726, 1712 (C═O); 1671 (C═C); 1257, 1196, 1178 (C−O). MS: ESI m/z 443.4 (100%, M − 1), 444.4 (30%, M). For $C_{28}H_{44}O_4$ (444.6) calcd: 75.63%, C; 9.97% H. Found: 75.25%, C; 9.98%, H.

Androst-5-en-3β-yl Hemimalonate (14, AND-hMal). Compound **14** was prepared in the same manner as compound **3**. Starting from compound **28** (274 mg, 1 mmol), compound **14** (46 mg, 13%) was obtained as a white solid by column chromatography (10−15% acetone in petroleum ether): mp 169−171 °C (ethyl acetate); $[\alpha]_D^{20}$ −53.5 (c 0.3, $CHCl_3$). ^{1}H NMR (400 MHz, $CDCl_3$): δ 0.72 (3H, s, H-18), 1.03 (3H, s, H-19), 3.42 (2H, s, H-2′), 4.73 (1H, m, H-3), 5.40 (1H, d, J = 4.8, H-6). ^{13}C NMR (101 MHz, $CDCl_3$): δ 169.3 (COOH), 167.8 (COO), 139.2 (C-5), 123.3 (C-6), 76.4 (C-3), 54.9, 50.4, 40.7, 40.4, 40.2, 38.7, 37.9, 37.0, 36.8, 32.3, 32.2, 27.7, 25.7, 21.2, 20.6, 19.4, 17.3. IR ($CHCl_3$): 1774, 1736, 1718 (C═O); 1670 (C═C); 1197, 1179, 1160 (C−O). MS: ESI m/z 359.2 (17%, M − 1), 315.2 (100%, M − 1 − CO_2). HR-MS (ESI) m/z: for $C_{22}H_{31}O_4$ [M − 1] calcd, 359.22278; found, 359.22263.

Androst-5-en-3β-yl Hemisuccinate (15, AND-hSuc). Compound **15** was prepared according to general procedure I. Starting from compound **28** (274 mg, 1 mmol), compound **15** (250 mg, 67%) was obtained as a white solid by column chromatography (1% methanol in DCM): mp 159−161 °C (methanol); $[\alpha]_D^{20}$ −63.6 (c 0.1, $CHCl_3$). ^{1}H NMR (400 MHz, $CDCl_3$): δ 0.71 (s, 3H, H-18), 1.02 (3H, s, H-19), 2.56−2.71 (4H, m, $OOCCH_2CH_2COO$), 4.62 (1H, m, H-3), 5.38 (1H, m, H-6). ^{13}C NMR (101 MHz, $CDCl_3$): δ 177.3 (COOH), 171.7 (COO), 139.6 (C-5), 122.9 (C-6), 74.7 (C-3), 54.9, 50.4, 40.7, 40.4, 38.8, 38.2, 37.1, 36.8, 32.3, 32.2, 29.4, 29.0, 27.8, 25.7, 21.2, 20.6, 19.5, 17.4. IR ($CHCl_3$): 1755, 1730, 1717 (C═O); 1672 (C═C); 1176 (C−O). MS: ESI m/z 373.4 (100%, M − 1), 374.4 (28%, M). For $C_{23}H_{34}O_4$ (374.3) calcd: 73.76%, C; 9.15% H. Found: 73.93%, C; 9.25%, H.

Androst-5-en-3β-yl Hemiglutarate (16, AND-hGlu). Compound **16** was prepared according to general procedure I. Starting from compound **28** (274 mg, 1 mmol), compound **16** (165 mg, 42%) was obtained as a white solid by column chromatography (0.2% methanol in DCM): mp 76−78 °C (methanol); $[\alpha]_D^{20}$ −52.0 (c 0.2, $CHCl_3$). ^{1}H NMR (400 MHz, $CDCl_3$): δ 0.71 (3H, s, H-18), 1.02 (3H, s, H-19), 1.95 (2H, p, J = 7.3, H-3′), 2.37 (2H, t, J = 7.3, H-2′), 2.43 (2H, t, J = 7.3, H-4′), 4.63 (1H, m, H-3), 5.38 (1H, d, J = 5.4, H-6). ^{13}C NMR (101 MHz, $CDCl_3$): δ 178.6 (COOH), 172.4 (COO), 139.7 (C-5), 122.8 (C-6), 74.2 (C-3), 54.9, 50.4, 40.7, 40.4, 38.8, 38.3, 37.2, 36.8, 33.6, 33.0, 32.3, 32.2, 27.9, 25.7, 21.2, 20.65, 20.06, 19.5, 17.4. IR ($CHCl_3$): 1725, 1713 (C═O); 1670 (C═C); 1417, 1285 (C−O). MS: ESI m/z 387.3 (100%, M − 1), 388.4 (30%, M). For $C_{24}H_{36}O_4$ (388.3) calcd: 74.19%, C; 9.34% H. Found: 74.23%, C; 9.32%, H.

Androst-5-en-3β-yl Hemiadipate (17, AND-hAdi). Compound **17** was prepared according to general procedure II. Starting from compound **28** (274 mg, 1 mmol), compound **17** (140 mg, 35%) was obtained as a white solid by column chromatography (0.2−0.5% methanol in DCM): mp 86−88 °C (methanol); $[\alpha]_D^{20}$ −52.7 (c 0.2, $CHCl_3$). ^{1}H NMR (400 MHz, $CDCl_3$): δ 0.71 (3H, s, H-18), 1.02 (3H, s, H-19), 2.27−2.41 (4H, m, H-adipate), 4.63 (1H, m, H-3), 5.38 (1H, m, H-6). ^{13}C NMR (101 MHz, $CDCl_3$): δ 178.6 (COOH), 172.8 (COO), 139.8 (C-5), 122.8 (C-6), 74.1 (C-3), 54.9, 50.4, 40.7, 40.4, 38.8, 38.2, 37.2, 36.8, 34.3, 33.6, 32.3, 32.2, 27.9, 25.7, 24.5, 24.2, 21.2, 20.6, 19.5, 17.4. IR ($CHCl_3$): 1728, 1711 (C═O); 1670 (C═C); 1416, 1288 (C−O). MS: ESI m/z 401.3 (100%, M − 1), 402.3 (30%, M). For $C_{25}H_{38}O_4$ (402.3) calcd: 74.59%, C; 9.51% H. Found: 74.54%, C; 9.58%, H.

Androst-5-en-3β-yl Hemipimelate (18, AND-hPim). Compound **18** was prepared according to general procedure II. Starting from compound **28** (274 mg, 1 mmol), compound **18** (174 mg, 42%) was obtained as a white solid by column chromatography (0.2−0.5% methanol in DCM): mp 61−63 °C (methanol); $[\alpha]_D^{20}$ −53.0 (c 0.2, $CHCl_3$). ^{1}H NMR (400 MHz, $CDCl_3$): δ 0.71 (3H, s, H-18), 1.02 (3H, s, H-19), 2.26−2.39 (4H, m, H-pimelate), 2.53 (1H, t, J = 8.9, H-17), 4.63 (1H, m, H-3), 5.37 (1H, m, H-6). ^{13}C NMR (101 MHz, $CDCl_3$): δ 178.8 (COOH), 173.1 (COO), 139.8 (C-5), 122.7 (C-6), 73.9 (C-3), 54.9, 50.4, 40.7, 40.4, 38.8, 38.3, 37.2, 36.8, 34.5, 33.7, 32.3, 32.2, 28.6, 27.9, 25.7, 24.7, 24.4, 21.2, 20.6, 19.5, 17.4. IR ($CHCl_3$): 1725, 1712 (C═O); 1670 (C═C); 1416, 1290 (C−O). MS: ESI m/z 415.3 (100%, M − 1), 416.3 (35%, M). For $C_{26}H_{40}O_4$ (416.3) calcd: 74.96%, C; 9.68% H. Found: 75.04%, C; 9.77%, H.

17-Oxo-androst-5-en-3β-yl Hemiglutarate (19, 17-Oxo-AND-hGlu). Compound **19** was prepared according to general procedure I. Starting from compound **27** (288 mg, 1 mmol), compound **19** (234 mg, 58%) was obtained as a white solid by column chromatography (0.5% methanol in DCM): mp 126−128 °C (methanol); $[\alpha]_D^{20}$ 0.0 (c 0.2, $CHCl_3$). ^{1}H NMR (400 MHz, $CDCl_3$): δ 0.88 (3H, s, H-18), 1.05 (3H, s, H-19), 1.96 (2H, p, J = 7.5, H-3′), 2.38 (2H, t, J = 7.3, H-2′), 2.43 (2H, t, J = 7.3, H-4′), 4.63 (1H, m, H-3), 5.41 (1H, d, J = 5.4, H-6). ^{13}C NMR (101 MHz, $CDCl_3$): δ 221.7 (C-17), 177.7 (COOH), 172.3 (COO), 139.8 (C-5), 122.0 (C-6), 73.9 (C-3), 51.8, 50.2, 47.7, 38.2, 37.0, 36.8, 36.0, 33.6, 32.9, 31.6, 31.5, 30.9, 27.8, 22.0, 20.4, 20.0, 19.5, 13.7. IR ($CHCl_3$): 1731, 1714 (C═O); 1670 (C═C); 1415, 1289 (C−O). MS: ESI m/z 401.3 (100%, M − 1), 402.3 (30%, M). For $C_{24}H_{34}O_5$ (402.2) calcd: 71.61%, C; 8.51% H. Found: 71.47%, C; 8.50%, H.

17-Oxo-androst-5-en-3β-yl Hemiadipate (20, 17-Oxo-AND-hAdi). Compound **20** was prepared according to general procedure II. Starting from compound **27** (288 mg, 1 mmol), compound **20** (130 mg, 31%) was obtained as a white solid by column chromatography (0.5% methanol in DCM): mp 154−156 °C (methanol); $[\alpha]_D^{20}$ 0.0 (c 0.2, $CHCl_3$). ^{1}H NMR (400 MHz, $CDCl_3$): δ 0.88 (3H, s, H-18), 1.05 (3H, s, H-19), 2.28−2.40 (4H, m, H-adipate), 4.63 (1H, m, H-3), 5.38 (1H, m, H-6). ^{13}C NMR (101 MHz, $CDCl_3$): δ 221.1 (C-17), 178.3 (COOH), 172.8 (COO), 140.0 (C-5), 122.0 (C-6), 73.8 (C-3), 51.8, 50.2, 47.7, 38.2, 37.0, 36.8, 36.0, 34.3, 33.6, 31.6, 31.5, 30.9, 27.8, 24.5, 24.2, 22.0, 20.4, 19.5, 13.7. IR ($CHCl_3$): 1731, 1713 (C═O); 1670 (C═C); 1415, 1289 (C−O). MS: ESI m/z 415.3 (100%, M − 1), 416.3 (30%, M). For $C_{25}H_{36}O_5$ (416.3) calcd: 72.08%, C; 8.71% H. Found: 72.09%, C; 8.87%, H.

17-Oxo-androst-5-en-3β-yl Hemipimelate (21, 17-Oxo-AND-hPim). Compound **21** was prepared according to general procedure II. Starting from compound **27** (288 mg, 1 mmol), compound **21** (150 mg, 35%) was obtained as a white solid by column chromatography (0.3−1% methanol in DCM): mp 71−73 °C (methanol); $[\alpha]_D^{20}$ 1.0 (c 0.3, $CHCl_3$). ^{1}H NMR (400 MHz, $CDCl_3$): δ 0.88 (3H, s, H-18), 1.05 (3H, s, H-19), 2.26−2.39 (4H, m, H-pimelate), 4.63 (1H, m, H-3), 5.41 (1H, m, H-6). ^{13}C NMR (101 MHz, $CDCl_3$): δ 221.3 (C-17), 178.6 (COOH), 173.0 (COO), 140.0 (C-5), 122.0 (C-6), 73.7 (C-3), 51.8, 50.3, 47.7, 38.2, 37.0, 36.8, 36.0, 34.5, 33.7, 31.6, 31.5, 30.9, 28.6, 27.8, 24.7, 24.4, 22.0, 20.4, 19.5, 13.6. IR ($CHCl_3$): 1731, 1713 (C═O); 1670 (C═C); 1414, 1285 (C−O). MS: ESI m/z 429.4 (100%, M − 1), 430.4 (30%, M). For $C_{26}H_{38}O_5$ (430.3) calcd: 72.53%, C; 8.90% H. Found: 72.66%, C; 8.97%, H.

17-Oxo-androst-5-en-3β-yl Hemisuberate (22, 17-Oxo-AND-hSub). Compound **22** was prepared according to general procedure II. Starting from compound **27** (288 mg, 1 mmol), compound **22** (220 mg, 50%) was obtained as a white solid by column chromatography (0.5% methanol in DCM): mp 123−125 °C (methanol); $[\alpha]_D^{20}$ 0.0 (c 0.1, $CHCl_3$). ^{1}H NMR (400 MHz, $CDCl_3$): δ 0.89 (3H, s, H-18), 1.05 (3H, s, H-19), 2.25−2.38 (4H, m, H-suberate), 4.61 (1H, m, H-3), 5.41 (1H,

DOI: 10.1021/acs.jmedchem.8b00255
J. Med. Chem. 2018, 61, 4505−4516

PDF-XChange Editor
KOUPIT plnou verzi!
www.pdfxchange.cz

m, H-6). ^{13}C NMR (101 MHz, $CDCl_3$): δ 221.1 (C-17), 178.9 (COOH), 173.2 (COO), 140.0 (C-5), 121.9 (C-6), 73.6 (C-3), 51.8, 50.2, 47.6, 38.2, 37.0, 36.8, 36.0, 34.6, 33.8, 31.6, 31.5, 30.9, 28.8, 28.8, 27.8, 24.9, 24.6, 22.0, 20.4, 19.5, 13.6. IR ($CHCl_3$): 1731, 1712 (C═O); 1680 (C═C); 1248 (C−O). MS: ESI m/z 443.3 (100%, M − 1), 444.3 (35%, M). For $C_{27}H_{40}O_5$ (444.3) calcd: 72.94%, C; 9.07% H. Found: 72.77%, C; 9.18%, H.

17-Oxo-androst-5-en-3β-yl Hemiazelate (23, 17-Oxo-ANDhAze). Compound **23** was prepared according to general procedure II. Starting from compound **27** (288 mg, 1 mmol), compound **23** (110 mg, 24%) was obtained as a white solid by column chromatography (10−15% acetone in petroleum ether): mp 86−87 °C (acetone); $[\alpha]_D^{20}$ 0.8 (c 0.3, $CHCl_3$). ^{1}H NMR (400 MHz, $CDCl_3$): δ 0.88 (3H, s, H-18), 1.05 (3H, s, H-19), 2.25−2.40 (4H, H-azelaic acid ester), 4.61 (1H, m, H-3), 5.40 (1H, d, J = 4.8, H-6). ^{13}C NMR (101 MHz, $CDCl_3$): δ 221.3 (C-17), 178.8 (COOH), 173.3 (COO), 140.1 (C-5), 121.9 (C-6), 73.6 (C-3), 51.8, 50.2, 47.6, 38.2, 37.0, 36.8, 36.0, 34.7, 33.9, 31.6, 31.5, 30.9, 29.0 (2x), 28.9, 27.8, 25.0, 24.7, 22.0, 20.4, 19.5, 13.7. IR ($CHCl_3$): 1731, 1711 (C═O); 1671 (C═C); 1191(C−O). MS: ESI m/z 457.3 (100%, M − 1), 458.3 (32%, M). For $C_{28}H_{42}O_5$ (458.3) calcd: 73.33%, C; 9.23% H. Found: 73.67%, C; 9.39%, H.

17-Oxo-androst-5-en-3β-yl Hemisebacate (24, 17-Oxo-ANDhSeb). Compound **24** was prepared according to general procedure II. Starting from compound **27** (288 mg, 1 mmol), compound **24** (130 mg, 27%) was obtained as a white solid by column chromatography (15% acetone in petroleum ether): mp 96−98 °C (acetone); $[\alpha]_D^{20}$ 0.0 (c 0.3, $CHCl_3$). ^{1}H NMR (400 MHz, $CDCl_3$): δ 0.88 (3H, s, H-18), 1.05 (3H, s, H-19), 2.24−2.37 (4H, m, H-sebacic acid ester), 4.62 (1H, m, H-3), 5.40 (1H, m, H-6). ^{13}C NMR (101 MHz, $CHCl_3$): δ 221.3 (C-17), 178.7 (COOH), 173.4 (COO), 140.1 (C-5), 121.9 (C-6), 73.6 (C-3), 51.8, 50.3, 47.7, 38.2, 37.1, 36.9, 36.0, 34.8, 33.9, 31.6, 31.5, 30.9, 29.1, 29.1, 29.1, 27.8, 25.1, 24.7, 22.0, 20.4, 19.5, 13.7. IR ($CHCl_3$): 1731, 1711 (C═O); 1670 (C═C); 1189, 1178 (C−O). MS: ESI m/z 471.4 (100%, M − 1), 472.4 (35%, M). For $C_{29}H_{44}O_5$ (472.7) calcd: 73.69%, C; 9.38% H. Found: 73.53%, C; 9.43%, H.

3β-Hydroxy-pregn-5-en (26). Trimethylsilyl chloride (62 mL, 0.48 mol) was added dropwise to a stirred mixture of pregnenolone **25** (10 g, 0.03 mol) and zinc powder (52 g, 0.47 mol) in DCM and methanol (1:1, 300 mL) at 0 °C. The reaction mixture was stirred at room temperature. After 18 h, zinc was removed by filtration. The filtrate was poured into an aqueous saturated solution of sodium hydrogen carbonate; the product was extracted with chloroform, washed with 1 M hydrochloric acid, water, and dried over anhydrous sodium sulfate. Evaporation of the solvents yielded 7.5 g (78%) of compound **26**, which was crystallized for further synthesis: mp 133−135 °C (ethyl acetate/n-heptane), lit.:[30] 133−134 °C; $[\alpha]_D^{20}$ −55.3 (c 0.3, $CHCl_3$), [31] −60 (c 2.95, $CHCl_3$). ^{1}H NMR (400 MHz, $CDCl_3$): δ 0.58 (3H, s, H-18), 0.87 (3H, t, J = 7.3, H-21), 1.01 (3H, s, H-19), 3.53 (1H, m, H-3), 5.36 (1H, m, H-6). ^{13}C NMR (101 MHz, $CHCl_3$): δ 140.9 (C-5), 121.8 (C-6), 71.9 (C-3), 56.3, 53.1, 50.7, 42.4, 42.1, 38.0, 37.4, 36.7, 32.1, 32.0, 31.8, 28.2, 24.8, 23.1, 21.0, 19.5, 13.5, 12.5. IR spectrum ($CHCl_3$): 3609, 3462 (OH); 1668 (C═C); 1046 (C−O). MS: EI m/z 302.3 (50%, M), 284.3 (85%, M − H_2O). For $C_{21}H_{34}O$ (302.5) calcd: 83.38%, C; 11.33%, H. Found: 83.22%, C; 11.16%, H.

3β-Hydroxy-androst-5-en (28). Compound **28** was prepared in the same manner as compound **26.**[21] Starting from compound **27** (10 g, 0.03 mol), compound **28** (7.2 g, 75%) was obtained: mp 135−136 °C (ethyl acetate/n-heptane), lit.,[21] (133−134 °C). ^{1}H NMR (400 MHz, $CDCl_3$): δ 0.72 (3H, s, H-18), 1.01 (3H, s, H-19), 3.53 (1H, m, H-3), 5.36 (1H, m, H-6). ^{13}C NMR (101 MHz, $CHCl_3$): δ 140.9 (C-5), 121.9 (C-6), 71.9 (C-3), 55.0, 50.5, 42.4, 40.7, 40.4, 38.8, 37.4, 36.8, 32.3, 32.3, 31.8, 25.7, 21.3, 20.6, 19.6, 17.4.

■ ASSOCIATED CONTENT

Supporting Information

The Supporting Information is available free of charge on the ACS Publications website at DOI: 10.1021/acs.jmedchem.8b00255.

Molecular formula strings for target compounds and some data (CSV)

Computational analysis for compounds **1**−**24** and spectra (PDF)

■ AUTHOR INFORMATION

Corresponding Author

*Phone: +420-220-183-273. Fax: +420-220-183-578. E-mail: kudova@uochb.cas.cz.

ORCID

Eva Kudova: 0000-0001-7131-5948

Author Contributions

Synthesis was done by B.S. and H.Ch. In vitro screening was done by B.K., P.H., and V.V. The computational analysis was done by M.N. The manuscript was written by E.K., L.V., and B.K.

Notes

The authors declare no competing financial interest.

■ ACKNOWLEDGMENTS

This work was supported by the Czech Science Foundation (GACR), Grants 17-02300S and P208/12/G016; Technology Agency of the Czech Republic, Grant TE01020028; Ministry of Health of the Czech Republic, Grant NV15-29370A; ERDF/ESF Project "PharmaBrain", Grant CZ.02.1.01/0.0/0.0/16_025/0007444; CAS, Grant MSM200111601; Grant Agency of Charles University (GAUK), Grant 928216; Research Project of the AS CR RVO, Grant 67985823, RVO Grant 61388963; and BIOCEV, Biotechnology and Biomedicine Centre of the Academy of Sciences and Charles University in Vestec, project supported by the European Regional Development Fund. The authors thank Ben Watson-Jones for language correction.

■ REFERENCES

(1) Citri, A.; Malenka, R. C. Synaptic plasticity: multiple forms, functions, and mechanisms. *Neuropsychopharmacology* **2008**, *33* (1), 18−41.

(2) Collingridge, G. Synaptic plasticity. The role of NMDA receptors in learning and memory. *Nature* **1987**, *330* (6149), 604−605.

(3) (a) Hu, C.; Chen, W.; Myers, S. J.; Yuan, H.; Traynelis, S. F. Human GRIN2B variants in neurodevelopmental disorders. *J. Pharmacol. Sci.* **2016**, *132* (2), 115−121. (b) Burnashev, N.; Szepetowski, P. NMDA receptor subunit mutations in neurodevelopmental disorders. *Curr. Opin. Pharmacol.* **2015**, *20*, 73−82.

(4) Swanger, S. A.; Chen, W.; Wells, G.; Burger, P. B.; Tankovic, A.; Bhattacharya, S.; Strong, K. L.; Hu, C.; Kusumoto, H.; Zhang, J.; Adams, D. R.; Millichap, J. J.; Petrovski, S.; Traynelis, S. F.; Yuan, H. Mechanistic insight into NMDA receptor dysregulation by rare variants in the GluN2A and GluN2B agonist binding domains. *Am. J. Hum. Genet.* **2016**, *99* (6), 1261−1280.

(5) Hamdan, F. F.; Gauthier, J.; Araki, Y.; Lin, D. T.; Yoshizawa, Y.; Higashi, K.; Park, A. R.; Spiegelman, D.; Dobrzeniecka, S.; Piton, A.; Tomitori, H.; Daoud, H.; Massicotte, C.; Henrion, E.; Diallo, O.; S2D Group; Shekarabi, M.; Marineau, C.; Shevell, M.; Maranda, B.; Mitchell, G.; Nadeau, A.; D'Anjou, G.; Vanasse, M.; Srour, M.; Lafreniere, R. G.; Drapeau, P.; Lacaille, J. C.; Kim, E.; Lee, J. R.; Igarashi, K.; Huganir, R. L.; Rouleau, G. A.; Michaud, J. L. Excess of de novo deleterious mutations in genes associated with glutamatergic systems in nonsyndromic intellectual disability. *Am. J. Hum. Genet.* **2011**, *88* (3), 306−316.

(6) (a) Voineagu, I.; Wang, X.; Johnston, P.; Lowe, J. K.; Tian, Y.; Horvath, S.; Mill, J.; Cantor, R. M.; Blencowe, B. J.; Geschwind, D. H. Transcriptomic analysis of autistic brain reveals convergent molecular pathology. *Nature* **2011**, *474* (7351), 380−384. (b) Tarabeux, J.; Kebir, O.; Gauthier, J.; Hamdan, F. F.; Xiong, L.; Piton, A.; Spiegelman, D.;

DOI: 10.1021/acs.jmedchem.8b00255
J. Med. Chem. 2018, 61, 4505−4516

PDF-XChange Editor
KOUPIT plnou verzi!
www.pdfxchange.cz

Henrion, E.; Millet, B.; S2D Team; Fathalli, F.; Joober, R.; Rapoport, J. L.; DeLisi, L. E.; Fombonne, E.; Mottron, L.; Forget-Dubois, N.; Boivin, M.; Michaud, J. L.; Drapeau, P.; Lafreniere, R. G.; Rouleau, G. A.; Krebs, M. O. Rare mutations in N-methyl-D-aspartate glutamate receptors in autism spectrum disorders and schizophrenia. *Transl. Psychiatry* **2011**, *1*, e55.

(7) Gonzalez-Burgos, G.; Lewis, D. A. NMDA receptor hypofunction, parvalbumin-positive neurons, and cortical gamma oscillations in schizophrenia. *Schizophr. Bull.* **2012**, *38* (5), 950−957.

(8) Korinek, M.; Kapras, V.; Vyklicky, V.; Adamusova, E.; Borovska, J.; Vales, K.; Stuchlik, A.; Horak, M.; Chodounska, H.; Vyklicky, L., Jr Neurosteroid modulation of N-methyl-D-aspartate receptors: molecular mechanism and behavioral effects. *Steroids* **2011**, *76* (13), 1409−1418.

(9) (a) Weaver, C. E.; Land, M. B.; Purdy, R. H.; Richards, K. G.; Gibbs, T. T.; Farb, D. H. Geometry and charge determine pharmacological effects of steroids on N-methyl-D-aspartate receptor-induced Ca (2+) accumulation and cell death. *J. Pharmacol. Exp. Ther.* **2000**, *293* (3), 747−754. (b) Stastna, E.; Chodounska, H.; Pouzar, V.; Kapras, V.; Borovska, J.; Cais, O.; Vyklicky, L., Jr Synthesis of C3, C5, and C7 pregnane derivatives and their effect on NMDA receptor responses in cultured rat hippocampal neurons. *Steroids* **2009**, *74* (2), 256−263. (c) Kudova, E.; Chodounska, H.; Slavikova, B.; Budesinsky, M.; Nekardova, M.; Vyklicky, V.; Krausova, B.; Svehla, P.; Vyklicky, L. A New class of potent N-methyl-D-aspartate receptor inhibitors: sulfated neuroactive steroids with lipophilic D-ring modifications. *J. Med. Chem.* **2015**, *58* (15), 5950−5966. (d) Adla, S. K.; Slavikova, B.; Smidkova, M.; Tloustova, E.; Svoboda, M.; Vyklicky, V.; Krausova, B.; Hubalkova, P.; Nekardova, M.; Holubova, K.; Vales, K.; Budesinsky, M.; Vyklicky, L.; Chodounska, H.; Kudova, E. Physicochemical and biological properties of novel amide-based steroidal inhibitors of NMDA receptors. *Steroids* **2017**, *117*, 52−61.

(10) Park-Chung, M.; Wu, F. S.; Farb, D. H. 3 alpha-Hydroxy-5 beta-pregnan-20-one sulfate: a negative modulator of the NMDA-induced current in cultured neurons. *Mol. Pharmacol.* **1994**, *46* (1), 146−150.

(11) Park-Chung, M.; Wu, F. S.; Purdy, R. H.; Malayev, A. A.; Gibbs, T. T.; Farb, D. H. Distinct sites for inverse modulation of N-methyl-D-aspartate receptors by sulfated steroids. *Mol. Pharmacol.* **1997**, *52* (6), 1113−1123.

(12) Wu, F. S.; Gibbs, T. T.; Farb, D. H. Pregnenolone sulfate: a positive allosteric modulator at the N-methyl-D-aspartate receptor. *Mol. Pharmacol.* **1991**, *40* (3), 333−336.

(13) Majewska, M. D.; Mienville, J. M.; Vicini, S. Neurosteroid pregnenolone sulfate antagonizes electrophysiological responses to GABA in neurons. *Neurosci. Lett.* **1988**, *90* (3), 279−284.

(14) Wu, F. S.; Chen, S. C.; Tsai, J. J. Competitive inhibition of the glycine-induced current by pregnenolone sulfate in cultured chick spinal cord neurons. *Brain Res.* **1997**, *750* (1−2), 318−320.

(15) Flood, J. F.; Morley, J. E.; Roberts, E. Memory-enhancing effects in male mice of pregnenolone and steroids metabolically derived from it. *Proc. Natl. Acad. Sci. U. S. A.* **1992**, *89* (5), 1567−1571.

(16) Mullasseril, P.; Hansen, K. B.; Vance, K. M.; Ogden, K. K.; Yuan, H.; Kurtkaya, N. L.; Santangelo, R.; Orr, A. G.; Le, P.; Vellano, K. M.; Liotta, D. C.; Traynelis, S. F. A subunit-selective potentiator of NR2C- and NR2D-containing NMDA receptors. *Nat. Commun.* **2010**, *1*, 90.

(17) Santangelo Freel, R. M.; Ogden, K. K.; Strong, K. L.; Khatri, A.; Chepiga, K. M.; Jensen, H. S.; Traynelis, S. F.; Liotta, D. C. Synthesis and structure activity relationship of tetrahydroisoquinoline-based potentiators of GluN2C and GluN2D containing N-methyl-D-aspartate receptors. *J. Med. Chem.* **2013**, *56* (13), 5351−5381.

(18) Strong, K. L.; Epplin, M. P.; Bacsa, J.; Butch, C. J.; Burger, P. B.; Menaldino, D. S.; Traynelis, S. F.; Liotta, D. C. The Structure-activity relationship of a tetrahydroisoquinoline class of N-methyl-D-aspartate receptor modulators that potentiates GluN2B-containing N-methyl-D-aspartate receptors. *J. Med. Chem.* **2017**, *60* (13), 5556−5585.

(19) Vyklicky, V.; Krausova, B.; Cerny, J.; Ladislav, M.; Smejkalova, T.; Kysilov, B.; Korinek, M.; Danacikova, S.; Horak, M.; Chodounska, H.; Kudova, E.; Vyklicky, L. Surface expression, function, and pharmacology of disease associated mutations in the membrane domain of the human GluN2B subunit. *Front. Mol. Neurosci.* **2018**, *11*, 110.

(20) Xu, S. T.; Toyama, T.; Nakamura, J.; Arimoto, H. One-pot reductive cleavage of exo-olefin to methylene with a mild ozonolysis-Clemmensen sequence. *Tetrahedron Lett.* **2010**, *51*, 4534−4537.

(21) Bazin, M. A.; Travert, C.; Carreau, S.; Rault, S.; El Kihel, L. First synthesis of 7alpha- and 7beta-amino-DHEA, dehydroepiandrosterone (DHEA) analogues and preliminary evaluation of their cytotoxicity on Leydig cells and TM4 Sertoli cells. *Bioorg. Med. Chem.* **2007**, *15* (9), 3152−3160.

(22) Horak, M.; Vlcek, K.; Petrovic, M.; Chodounska, H.; Vyklicky, L., Jr. Molecular mechanism of pregnenolone sulfate action at NR1/NR2B receptors. *J. Neurosci.* **2004**, *24* (46), 10318−10325.

(23) (a) Borovska, J.; Vyklicky, V.; Stastna, E.; Kapras, V.; Slavikova, B.; Horak, M.; Chodounska, H.; Vyklicky, L., Jr. Access of inhibitory neurosteroids to the NMDA receptor. *Br. J. Pharmacol.* **2012**, *166* (3), 1069−1083. (b) Vyklicky, V.; Krausova, B.; Cerny, J.; Balik, A.; Zapotocky, M.; Novotny, M.; Lichnerova, K.; Smejkalova, T.; Kaniakova, M.; Korinek, M.; Petrovic, M.; Kacer, P.; Horak, M.; Chodounska, H.; Vyklicky, L. Block of NMDA receptor channels by endogenous neurosteroids: implications for the agonist induced conformational states of the channel vestibule. *Sci. Rep.* **2015**, *5*, 10935.

(24) (a) Faassen, F.; Kelder, J.; Lenders, J.; Onderwater, R.; Vromans, H. Physicochemical properties and transport of steroids across Caco-2 cells. *Pharm. Res.* **2003**, *20* (2), 177−86. (b) Barton, P.; Davis, A. M.; McCarthy, D. J.; Webborn, P. J. Drug-phospholipid interactions. 2. Predicting the sites of drug distribution using n-octanol/water and membrane/water distribution coefficients. *J. Pharm. Sci.* **1997**, *86* (9), 1034−1039.

(25) (a) Mannhold, R.; Poda, G. I.; Ostermann, C.; Tetko, I. V. Calculation of molecular lipophilicity: State-of-the-art and comparison of log P methods on more than 96,000 compounds. *J. Pharm. Sci.* **2009**, *98* (3), 861−93. (b) Kibbey, C. E.; Poole, S. K.; Robinson, B.; Jackson, J. D.; Durham, D. An integrated process for measuring the physicochemical properties of drug candidates in a preclinical discovery environment. *J. Pharm. Sci.* **2001**, *90* (8), 1164−1175.

(26) Horak, M.; Vlcek, K.; Chodounska, H.; Vyklicky, L., Jr Subtype-dependence of N-methyl-D-aspartate receptor modulation by pregnenolone sulfate. *Neuroscience* **2006**, *137* (1), 93−102.

(27) Patneau, D. K.; Vyklicky, L., Jr.; Mayer, M. L. Hippocampal neurons exhibit cyclothiazide-sensitive rapidly desensitizing responses to kainate. *J. Neurosci.* **1993**, *13* (8), 3496−3509.

(28) Bowlby, M. R. Pregnenolone sulfate potentiation of N-methyl-D-aspartate receptor channels in hippocampal neurons. *Mol. Pharmacol.* **1993**, *43* (5), 813−819.

(29) Vyklicky, V.; Smejkalova, T.; Krausova, B.; Balik, A.; Korinek, M.; Borovska, J.; Horak, M.; Chvojkova, M.; Kleteckova, L.; Vales, K.; Cerny, J.; Nekardova, M.; Chodounska, H.; Kudova, E.; Vyklicky, L. Preferential inhibition of tonically over phasically activated NMDA receptors by pregnane derivatives. *J. Neurosci.* **2016**, *36* (7), 2161−2175.

(30) Huang-Minlon. Reduction of steroid ketones and other carbonyl compounds by modified Wolff-Kishner method. *J. Am. Chem. Soc.* **1949**, *71* (10), 3301−3303.

(31) Barton, D. H.; Miller, E. The application of the method of molecular rotation differences to steroids; concerning u-ergostadienol. *J. Chem. Soc.* **1949**, *27*, 337−340.

DOI: 10.1021/acs.jmedchem.8b00255
J. Med. Chem. 2018, 61, 4505−4516